Twenty Second Edition

Photovoltaics International

THE TECHNOLOGY RESOURCE FOR PV PROFESSIONALS

First Solar Improvements in CdTe module reliability and long-term degradation
Fraunhofer ISE Technologies for mass production of PERC and MWT solar cells
ISFH The role of encapsulants in standard and novel crystalline silicon module concepts
MiaSolé A methodology for testing, characterization and prediction of edge seal performance in PV modules
Mott MacDonald In-field performance of a polycrystalline versus a thin-film solar PV plant in Southeast Asia
ISC Konstanz Cleaning for high-efficiency solar cell processes

Fourth Quarter, December 2013

www.pv-tech.org

Best quality. Highest returns. Hanwha Q CELLS is your premium supplier for high-quality PV solutions.

Hanwha Q CELLS is beating the uncertainty on the solar market with superior product quality and warranties that only a financially secure technology leader can offer.

At its headquarters in Germany, Hanwha Q CELLS operates one of the largest research and development centres in the industry with over 200 scientists and engineers. This allows the company to deliver continuous innovation and top performing technology, particularly in terms of the optimisation of levelised costs of energy and product reliability.

12-YEAR PRODUCT WARRANTY Fully automated manufacturing prevents production-related imperfections. The in-house module test centre requires testing procedures up to three times stricter than those required by the IEC test criteria. Together with the VDE, Hanwha Q CELLS has implemented the most stringent quality assurance programme in the industry – the basis for our warranty promise. The Q CELLS Triple Yield Security also protects against potential-induced degradation (PID), hot-spots and counterfeit products. All of these measures have just one aim: to set new standards in terms of stability and efficiency with the new G3 product generation of solar modules – and as such ensuring the great satisfaction of and high returns for our customers.

TRUST IN GERMAN ENGINEERING

RELATIVE MODULE EFFICIENCY COMPARED TO NOMINAL POWER [%]

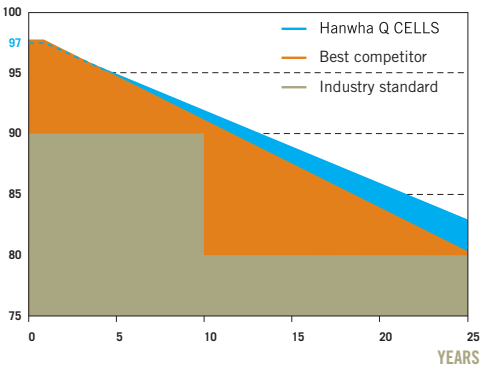

25-YEAR LINEAR PERFORMANCE WARRANTY

Let yourself be amazed by our premium quality now at www.q-cells.com

Q CELLS

Photovoltaics International

Published by:
Solar Media Ltd.,
5 Prescot Street,
London E1 8PA, UK
Tel: +44 (0) 207 871 0122
Fax: +44 (0) 207 871 0101
E-mail: info@pv-tech.org
Web: www.pv-tech.org

Publisher: David Owen

Head of Content: Ben Willis
Deputy Head of Content: John Parnell
Commissioning Editor: Adam Morrison
Sub-Editor: Steve D. Brierley
Senior News Editor: Mark Osborne
Reporters: Andy Colthorpe, Lucy Woods
Editorial Consultant: Graham Anderson
Design: Tina Davidian
Production: Daniel H Brown, Viki Hämmerle

Sales Director: David Evans
Account Managers: Adam Morrison, Graham Davie

Cover image: A First Solar scientist characterizes a thin-film CdTe research cell at the company's R&D facilities in Perrysburg, Ohio, USA.

Image courtesy of First Solar.

Printed by Buxton Press
Photovoltaics International
Twenty Second Edition
Forth Quarter 2013
Photovoltaics International is a quarterly journal published in February, May, August and November.

Distributed in the USA by Mail Right International, 1637 Stelton Road B4, Piscataway, NJ 08854.

ISSN: 1757-1197

USPS Information
USPS Periodical Code: 025 313

Periodicals Postage Paid at New Brunswick, NJ
Postmaster: Send changes to:
Photovoltaics International,
Solar Media Ltd., C/o 1637 Stelton Road, B-4, Piscataway, NJ 08854, USA

Foreword

The period of 'profitless prosperity' in the PV industry is finally at an end. Throughout 2013, despite continued economic woes, the PV industry has continued to expand and finally become a global industry.

Market forecasts indicating that the sector could reach its next 100GW milestone in just the next two years suggest the industry is on the cusp of another period of strong growth. All the signs confirm this is the case, with utilization rates at their highest level since 2010, companies reporting full order books well into next year and the first tentative announcements of factory capacity expansions making the headlines.

Although the really significant capacity expansions that would confirm a full-blooded upswing have yet to materialize, 'effective capacity' in 2014 is highly unlikely to meet end-market demand, should forecasts of 45 to 55GW come true. When the next technology and buy cycle occurs is still a moot point but it's closer than many would have dared to think at the beginning of this year.

The 22nd edition of *Photovoltaics International* will be an indispensible resource as that buy cycle draws nearer. As usual the journal provides a wealth of information on the latest cutting edge innovations in PV technology, covering all the key areas of the supply chain.

In this edition, US thin-film giant **First Solar** gives us an exclusive behind-the-scenes look at the new technologies and processes it is using to improve the reliability of its CdTE PV modules (p. 66). The company also reviews its 'Black' series module construction, which has been designed for harsh conditions to see how new developments have improved the long-term power generating capabilities of its modules.

Meanwhile, researchers from **ISC Konstanz** explore the increasing importance of wafer cleaning in the processing of high-efficiency solar cells (p. 47). Their paper outlines a number of advanced cleaning steps, weighing up the pros and cons of each and suggesting how they can best be integrated into existing fabs.

And the team from **Fraunhofer ISE** explore the options for PERC and MWT cells, two cell technologies that have shown great promise in recent years (p. 39). They look at what productions technologies are becoming available to take these cells from the lab to the fab and into mass production.

Another unforgettable milestone is that the 22nd edition of *Photovoltaics International* marks the fifth year of the publication's launch. It is often difficult to appreciate the extent to which the journal has gone from strength to strength over its half-decade of publication and become so highly respected across the globe. Recent feedback from industry events such as EU PVSEC and PV Taiwan reiterated how the journal's focus on next-generation technology and manufacturing practices is highly sought after and the team's efforts to retain the high standards are truly appreciated by readers.

As the industry enters its next critical growth phase, in which cost-per-watt strategies will depend increasingly on the introduction of new technology on the manufacturing floor, rather than material cost reductions in the past few years, the continued necessity for *Photovoltaics International* is assured.

Ben Willis
Head of Content
Solar Media Ltd

Photovoltaics International

Photovoltaics International's primary focus is on assessing existing and new technologies for "real-world" supply chain solutions. The aim is to help engineers, managers and investors to understand the potential of equipment, materials, processes and services that can help the PV industry achieve grid parity. The Photovoltaics International advisory board has been selected to help guide the editorial direction of the technical journal so that it remains relevant to manufacturers and utility-grade installers of photovoltaic technology. The advisory board is made up of leading personnel currently working first-hand in the PV industry.

Editorial Advisory Board

Our editorial advisory board is made up of senior engineers from PV manufacturers worldwide. Meet some of our board members below:

Gary Yu, Senior Vice President, Operations

Mr. Yu served as Trina Solar's Vice President of Manufacturing since May 2007 and in July 2010 was promoted to the position of Senior Vice President of Operations. Mr. Yu has 17 years' manufacturing management experience in semiconductor-related industries. Before joining Trina Solar, he was Managing Director of Wuxi Lite-On Technology, an LED assembly company based in China. Prior to Wuxi Lite-On Technology, he served as a Director of Manufacturing for 1st Silicon Sdn. Bhd. in Malaysia, prior to which he worked at Macronix International, a semiconductor integrated device manufacturer in Taiwan. Mr. Yu has a master's degree in Industrial Engineering and Management from National Chiao Tung University in Taiwan and a bachelor's degree in Chemical Engineering from Tunghai University.

Takashi Tomita, Senior Executive Fellow, Sharp Solar

Takashi Tomita has been working at Sharp for 34 years and is widely recognised as a fore-father of the solar industry in Japan. He was responsible for setting up Sharp's solar cell manufacturing facilities in Nara and silicon production in Toyama. Takashi's passion for solar power has led him to hold numerous posts outside of his roles at Sharp, including: Vice Representative at the Japan Photovoltaic Industry Association; Committee Member of Renewable Energy Portfolio Standard of METI; Adviser Board Member of Advanced Technology of Nara; Visiting Professor of Tohoku University; Adviser of ASUKA DBJ Partners (JAPAN) and Adviser of Global Catalyst Partners (US).

Dr. Peng Heng Chang, CEO, Motech Industries, Inc.

Dr. P.H. Chang was elected CEO of Motech in March 2010. Dr. Chang has over 30 years of experience in management at multinational technology companies and in-depth knowledge in Materials Engineering. Prior to joining Motech, Dr. Chang was VP of Materials Management and Risk Management, VP of Human Resources and Senior Director of Materials Management at Taiwan Semiconductor Manufacturing Co. (TSMC); VP of Administration at Worldwide Semiconductor Manufacturing Co. and Professor of Materials Science and Engineering at National Chiao Tung University in Hsinchu, Taiwan. Dr. Chang also worked for Inland Steel Co. and Texas Instruments in the US prior to 1990. He received his Ph.D. degree in materials engineering from Purdue University in 1981.

Professor Eicke R. Weber, Director of the Fraunhofer Institute for Solar Energy Systems ISE in Freiburg

Professor Eicke R. Weber is the Director of the Fraunhofer Institute for Solar Energy Systems ISE in Freiburg. Weber has earned an international reputation as a materials researcher for defects in silicon and III-V semiconductors such as gallium arsenide and gallium nitride. He spent 23 years in the U.S. in research roles, most recently as Professor at the University of California in Berkeley. Weber is also the Chair of Applied Physics, Solar Energy, at the University of Freiburg, and during his career has been the recipient of several prestigious awards including the Alexander von Humboldt Prize in 1994, and the German Cross of Merit on ribbon in June 2006.

Dr. Zhengrong Shi, Executive Chairman and Chief Strategy Officer, Suntech

Dr. Zhengrong Shi is founder, CEO and Chairman of the board of directors of Suntech. Prior to founding Suntech in 2001, he was a Research Director and Executive Director of Pacific Solar Pty., Ltd., the next-generation thin-film technology company, before which he was a Senior Research Scientist and leader of the Thin Film Solar Cells Research Group in the Centre of Excellence for Photovoltaic Engineering at the University of New South Wales in Australia. Dr. Shi holds 11 patents in PV technologies and is a much-published author in the industry. His work has earned him such accolades as "Hero of the Environment" (TIME magazine 2007) and "Corporate Citizen of the Year" at the China Business Leaders Awards 2007. A member of the NYSE advisory board, Dr. Shi has a Bachelor's degree in optical science, a Master's degree in laser physics and a Ph.D. in electrical engineering.

Dr. Sam Hong, President and COO of Neo Solar Power

Dr. Hong has more than 30 years of experience working in the solar energy industry. He has served as the Research Division Director of Photovoltaic Solar Energy Division at Industry Technology Research Institute (ITRI), a research organization that serves to strengthen the technological competitiveness of Taiwan, and Vice President and Plant Director of Sinonar Amorphous Silicon Solar Cell Co., which is the first amorphous silicon manufacturer in Taiwan. In addition, Dr. Hong was responsible for Power Subsystem of ROCSAT 1 for the Taiwan National Space Program. Dr. Hong has published three books and 38 journal and international conference papers, and is a holder of seven patents. Dr. Hong was the recipient of Outstanding Achievement Award from the Ministry of Economic Affairs, Taiwan, and was recently elected as chairman of the Taiwan Photovoltaic Industry Association.

Dr. G. Rajeswaran, President and CTO of Moser Baer Photovoltaic Ltd

Raj served as President and CTO of Moser Baer Photovoltaic Ltd. from July 2007 until October 2008, since which time he has been Group CTO for all the Moser Baer business units and holder of the CEO function for launching new businesses. He spent 22 years with Eastman Kodak Company as the Vice President of Advanced Development & Strategic Initiatives, where he managed Kodak's Japan display operations including technology & business development in Japan, Taiwan, Korea and China. He has also served as Vice President and on the board of SK Display Corporation, and worked in technology development with Brookhaven National Laboratory. Raj has a Ph.D., an M.Tech. and a B.E. in electrical engineering. A much-published author, speaker and patent holder, Raj is a member of the Society for Information Display (SID) and has chaired several international conferences in the field of OLEDs.

Contents

SNEC 8th (2014) International Photovoltaic Power Generation Conference & Exhibition

SNEC 2014
PV POWER EXPO
Dialogue & Conference & Exhibition

www.snec.org.cn

180,000sqm	1,800+	5,000+	150,000
Exhibition Space	Exhibitors	Professionals	Visitor Attendances

May 20-22, 2014

Shanghai New International Expo Center

(2345 Longyang Road, Pudong District, Shanghai, China)

member of GLOBAL SOLAR ALLIANCE

Tel: +86-21-64276991 +86-21-33561099

Fax: +86-21-33561089 +86-21-64642653

For exhibition: info@snec.org.cn

For conference: office@snec.org.cn

Fab & Facilities

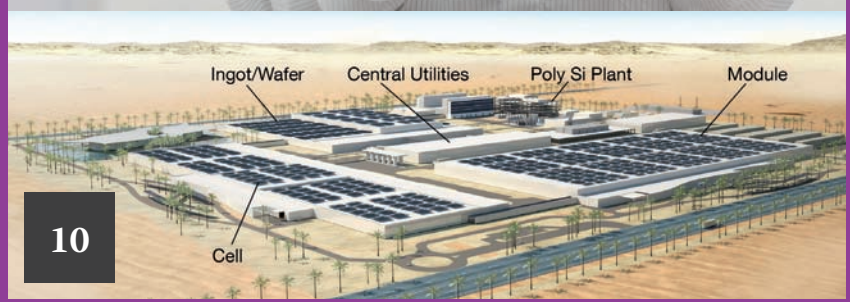

News

China awards accreditation to Trina Solar PV research lab

China's Ministry of Science and Technology has awarded accreditation to Trina Solar's State Key Laboratory of PV Science and Technology. The laboratory researches PV materials, cell and module technologies and system level performance.

Last year the Chinese module manufacturer used the laboratory to successfully develop and launch pilot commercial production of its P-type crystallised silicon Honey Ultra modules, which have a solar cell efficiency of 20.54%. State Key Laboratories are a number of learning institutions in China receiving assistance from the government including funding and administrative support.

China's government has accredited Trina's research lab.

New manufacturing facilities

Mozambique opens first PV production facility

Mozambique has officially opened the country's first PV module production facility. The plant was funded by the Indian government via its Export Import Bank, which provided a US$13 million loan in 2011.

It will produce modules for the local market to boost rural electrification. It is hoped the plant will be able to reduce the cost of solar panels in the country as it looks to boost access to affordable energy.

The facility outside the capital Maputo was opened by Mozambique president, Armando Guebuza. Italian tool manufacturer Ecoprogetti kitted out the plant for Mozambique's Fundo Nacional de Energia (FUNAE).

Brazil's Minas Gerais in line for PV manufacturing plant

The Brazilian state of Minas Gerais is in line to become home to the country's first PV cell and module manufacturing plant.

The state's deputy governor, Alberto Pinto Coelho, made the announcement following a fact finding mission to France's National Solar Energy Institute, INES. In an official statement, Coelho said that in addition to cells and modules, the proposed facility would also produce polysilicon, but gave no further details on this or on its envisaged capacity.

The facility would be built under the state's renewable energy incentive programme launched in August, which offers tax breaks to companies looking to build facilities for factories producing components for renewable energy plants, such as solar modules.

Minas Gerais is looking to make greater use of renewable energy to power its mining industry.

Hanergy to build thin-film plant in Rio Grande

The local government of Rio Grande do Sul has announced that Chinese firm Hanergy plans to build a thin-film solar PV module factory in the Brazilian state. A preliminary agreement was signed in Beijing on 4 December between Hanergy directors, regional Science, Innovation and Technological Development (SCIT) secretary Cleber Prodanov and Susana Kakuta, director of Tecnosinos Technological Park, Sao Leopoldo, where the production line will be built.

In 2012, three firms announced that they would invest around US$377 million in the PV industry in the state of Rio Grande do Sul, including a US$50 million investment by Real Solar into a 240MW PV module factory in Amez, a US$308 million investment by Bacilieri Equipamentos Elétricos into installing around 200MW of capacity across the state of Rio Grande do Sul and around US$19 million invested by Enerbra Indústria e Commercio de Paneis Solar to build PV systems in the state. The planning phase of Hanergy's new module facility will be completed by April 2014.

M+W lands deal to build 70MW solar factory in Argentina

Germany-based construction and engineering company, M+W, has been awarded a contract to construct a 70MW solar module factory with Schmid Group in Argentina.

M+W will be responsible for engineering, project planning, construction and installation of the 70MW PV production plant in San Juan. The Schmid Group is the general contractor, jointly bidding with M+W for the winning tender. Provincial energy

Brazil's Minas Gerais is to host of the country's first PV manufacturing plant.

M+W is to to build a 70MW solar factory in Argentina.

body for San Juan, Energia Provincial Sociedad del Estrado (EPSE), awarded the contract. The factory will be 13,000 square metres and M&W said it would produce monocrystalline silicon-ingot through to the module.

Production is scheduled to start by mid 2015. The modules produced will be used to power gold and copper mining operations and irrigation systems in San Juan.

Expanding production for 2014

JinkoSolar to expand solar module capacity as fully booked into 2014

China's JinkoSolar has said it will expand module capacity to at least 2GW in 2014, due to solar modules sales being virtually fully booked through the first half of the year.

Experiencing one of the strongest financial rebounds amongst its tier one rivals globally in 2013, JinkoSolar is also transforming its business model towards that established by First Solar and SunPower in becoming a full-service PV energy provider (PVEP).

Daqo to double polysilicon production at Xinjiang facility

Daqo New Energy has plans to double polysilicon production at its plant in Xinjiang, China to 12,000MT per annum by the end of 2014.

The company had said in September, 2013 that production at the plant would be increased from 5,000MT to 6,150 MT by the end of 2013. The company was targeting production costs of US$14/kg after making major technology upgrades to the plant in an effort to sell polysilicon at a profit after ASPs fell below production costs in 2012. Polysilicon ASPs have stabilised in 2013 at around US$17/kg.

Spire completes installation of turn-key PV module assembly line in Eastern Europe

PV equipment supplier Spire Corporation said that it had completed the installation of a turn-key module assembly line for an unidentified customer in Eastern Europe. The company said that it was the first of its kind in the region, and would be used to produce modules for large utility-scale installations within the local regional market. Spire is also providing on-going technical support for the training and the production ramp up of the line, which is expected to begin in 2014.

Trina Solar adding 500MW of module capacity via joint venture

Major tier one PV manufacturer, Trina Solar, is to take over operations of tier two module manufacturer, NESL Solartech, and expand capacity to 500MW.

The deal was struck with Chinese conglomerate Yabang Investment Holding Group, owners of NESL Solartech. The new joint venture will be called Changzhou Trina Yabang Solar Energy Co., Ltd. Trina Solar will hold a 51% stake and Yabang Group will have a 49% interest. The facility will be managed by Trina Solar

REC Silicon is to reduce its workforce due to polysilicon uncertainties.

Company news

STR Holdings sales continue to decline as restructuring continues

Specialist encapsulant supplier, STR Holdings, continues to struggle following the loss of its major customer, First Solar, last year, as third quarter sales continued to decline, forcing further plant closures and restructuring efforts.

The company reported third quarter sales of US$6.2 million, down from US$7.8 million in the prior quarter and US$11.2 million in the first quarter of 2013. STR Holdings' revenue decline was approximately 20% sequentially and 73% from the third quarter of 2012. On a year-over-year basis, volume declined in the third quarter of 2013 by approximately 64%.

Mothballed Hoku plant to go back under hammer

Hoku's abandoned polysilicon plant in Pocatello City, Idaho is to be re-auctioned with bidding starting at US$5 million.

The plant, which was never completed, was sold to principal contractor JH Kelly for US$5.273 million. The company says it is still owed US$25 million for its work.

The sale was subsequently blocked by the bankruptcy court which said the sale had not met the terms it had previously set out. A piecemeal auction attracted bids totalling just US$4.78 million. A live auction for the entire plant was due to take place on-site after *Photovoltaics International* went to press, according to documents lodged with the court. A fair market value of US$6.25 million-US$35 million has been placed on the site. Hoku invested more than US$600 million in the facility. The company has filed for Chapter 7 bankruptcy and owes an estimated US$1 billion.

REC Silicon reduces workforce due to polysilicon uncertainties

REC Silicon is to reduce its workforce by approximately 60 across all locations, with immediate effect. Polysilicon ASPs have remained at low levels throughout 2013, after falling massively (50% per annum) over the previous two-years, due to overcapacity and weaker end market growth.

US-based polysilicon producers are also being impacted by anti-dumping duties imposed on them by the Chinese government as part of an effort to support domestic polysilicon producers,

Module manufacturer asola is to resume production.

decimated by prices falling below production costs and many shuttering operations.

Module manufacturer asola to resume production

German module manufacturer asola is to resume production at its facility in Erfurt. The company was purchased by Chinese capacitor manufacturer STGCON in June and has since undergone restructuring.

Early signs indicated that module production would be outsourced from Germany to Croatia as the business shifted it focus to project development, storage and specialist installs such as car ports.

The move into storage systems alongside PV modules has been confirmed. The restructuring at asola saw it become part of TUSAI Holding along with STGCON and the electric vehicle charging firm American TellusPower.

Thin-film facilities

Nanosolar Germany relaunched as Smartenergy Renewables Deutschland

The German arm of Nanosolar, the US based thin-film company which closed in July this year, was relaunched at the beginning of November as Smartenergy Renewables Deutschland.

In addition to providing support to existing Nanosolar customers, for which there are reserves of Nanosolar's modules, Smartenergy Renewables Deutschland said it would focus on building integrated PV (BIPV) modules and also intends to become an independent power producer. The company announced its intention to expand workforce to support its ramping up of production and of services offered. Smartenergy Renewables Deutschland owns a highly automated ISO certified module factory in Luckenwald, Germany.

The company will be producing utility cSi modules as well as BIPV modules, which it aims to make available from 2014. The company's utility modules which are cSi based glass-glass construction have an output of between 290Wp and 300Wp, to be used initially on Smartenergy Renewables Deutschland's own PV projects.

Hanergy to make payouts to thin-film subsidiary

Hanergy Solar is set to receive significant investment from its parent company as it prepares to ramp up its thin-film production capacity.

In a statement to the Hong Kong stock exchange, Hanergy Solar announced that it had agreed a payment schedule for the next round of payments from its parent company. It will receive an installment of HK$500 million (US$64.5 million) in December and another of the same size in January next year with the remaining HK$587.8 million (US$75.8 million) to be paid during February 2014.

Changing global market and technology trends – new challenges for PV manufacturing strategies and facility concepts

Klaus Eberhardt & **Peter Csatáry**, M+W Group, Stuttgart, Germany

ABSTRACT

The PV manufacturing and technology hubs established over the past decade will change at an accelerated pace through the globalization of solar power installations. This development will be most pronounced in regions with high solar radiation, where grid parity can be achieved without subsidies. It can therefore be expected that parts of manufacturing within the PV added-value chain will also be established in new markets, such as South America, Africa, the Middle East and Asia. This trend will also stimulate these economies by the generation of new employment opportunities in the advanced technology sector. During the development of a new business plan, the key factors to resolve include the optimum manufacturing size and the extent to which upstream integration, from module manufacturing to poly Si, will be competitive. This paper addresses technology trends and strategic considerations for optimally selecting a PV manufacturer's strategy for each region, the determinants for centralized versus decentralized manufacturing, and the impact of these on fab and facilities concepts. Furthermore, the dependence of manufacturing capacity on fab and facility cost, as well as on the energy demand for individual manufacturing steps along the value chain, is discussed and compared.

Introduction

Since 2011 the PV industry has been plagued by an oversupply, with worldwide manufacturing capacity in 2013 totalling approximately 60GWp versus a significantly lower demand of approximately 38GWp. This has fuelled rapid price erosion for PV panels/modules and has resulted in strong market consolidation, since many manufacturers have had to sell their products at or below cost. As a consequence, investment in new equipment and manufacturing facilities has generally been low, and, even today, some idle manufacturing capacity is still available. Wherever possible, such capacity will first be upgraded and ramped up before new manufacturing plants are constructed.

The low prices have fuelled demand in new markets and countries looking to implement PV energy at competitive costs, even without the dependence on subsidies. From 2015 onwards it is expected that the gap between production capacity and PV installations will narrow considerably as demand accelerates. Low spot market prices cause older manufacturing lines to become obsolete with respect to technology and equipment, with the result that they are unable to remain competitive. Furthermore, emerging new geographical markets and regions are developing policy-

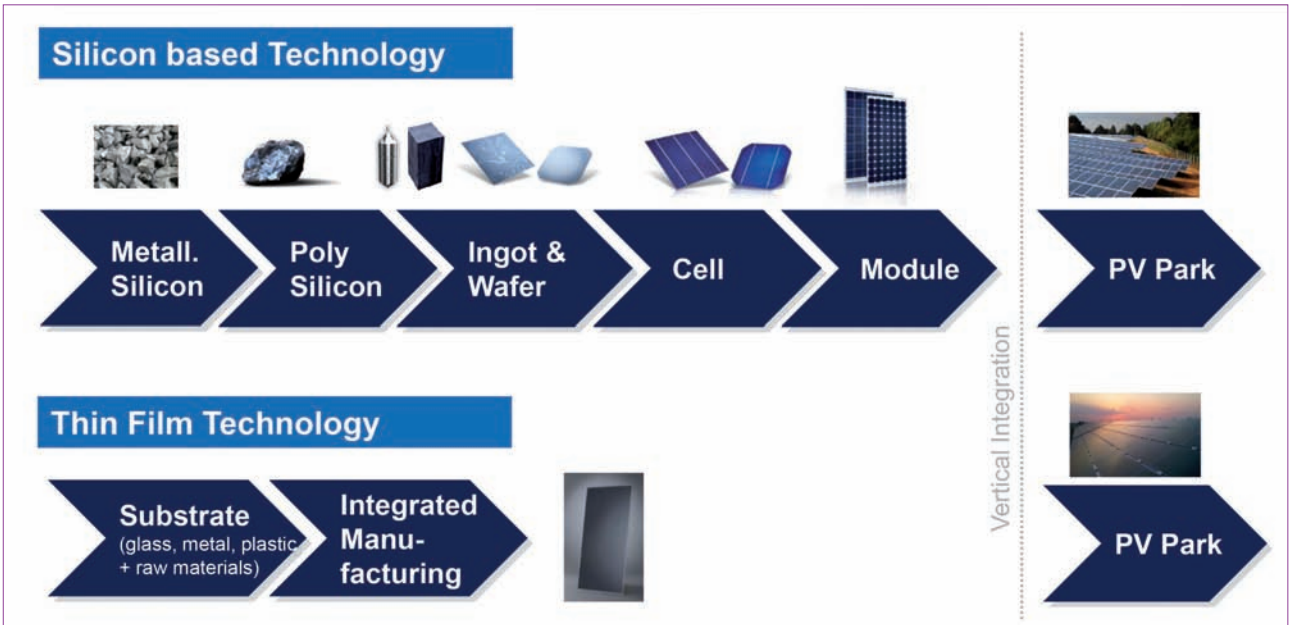

Figure 1. PV added-value chain for c-Si and thin-film technologies.

driven strategic roadmaps to start up domestic manufacturing facilities and the necessary infrastructure to support local employment.

It is therefore only a matter of time until new manufacturing facilities will start to develop globally. Total PV industry spending is expected to increase from $2.3bn in 2013 to $4.34bn by 2015 [1]. This forecast corresponds with market reports [2] as well as internal information at M+W Group. Because of massive competition, only cost-efficient facilities with leading-edge technologies will be economically viable, in line with the constant downward drift for PV panel/module prices, and also paving the way for a reduction in the overall balance of system (BOS) investment costs.

> "Because of massive competition, only cost-efficient facilities with leading-edge technologies will be economically viable."

This paper addresses the challenges and key criteria for cost-effective PV fab design resulting from these predicted developments. The key questions from a fab and facility point of view are the most economic size, the choice of the location, the clustering of particular parts of the PV added-value chain in a certain location, and how to facilitate cost-effective manufacturing. The authors have investigated the value chain based on crystalline silicon (c-Si) with respect to specific investment for fabs and facilities between 100 and 600MWp/annum. Furthermore, the specific energy demand for each manufacturing step is highlighted, since significant differences exist, with a corresponding impact on the operating costs. The advantages of local manufacturing are also evaluated from a macroeconomic point of view by estimating the workforce necessary to operate a PV manufacturing facility, as well as the positive effect on job creation within the support and supply industries. Finally, a set of recommendations for the location and state-of-the-art design for future, cost-effective PV fabs and facilities is provided.

The PV added-value chain

PV modules based on c-Si currently dominate the market. These technologies are characterized by well-defined manufacturing steps as shown in Fig. 1.

Traditionally, most manufacturers commence operations with module manufacturing and continue upstream integration to cell, and even wafer and ingot, manufacturing. Even when co-located on one site, this approach results in independent, decentralized facilities with relatively high maintenance and operational costs, since potential synergies cannot be optimally utilized. Poly Si manufacturing is dominated by companies active in the chemical industry, and, up to now, only a few PV manufacturers operate their own poly Si plants.

PV thin-film technologies are based on CdTe, CIGS or amorphous/micromorphous silicon. All three thin-film technologies share the following features:

- Manufacturing is based on glass substrates.
- Production lines are fully integrated.
- Finished modules exit the line as end products.

Thin-film technologies address specific applications and will grow with the market if the panel efficiency exceeds 14–15% at a specific cost level. For the remainder of this paper, the focus will be on c-Si-based technology since it represents approximately 90% of the entire market.

Technology trends

In order to track the PV price learning curve to and below 0.5€/Wp [3], it is essential to implement new technologies with the aim of reducing costs. The trend is the introduction of high-efficiency solar modules with conversion efficiencies exceeding 20%: high-efficiency modules have the additional benefit that the BOS costs

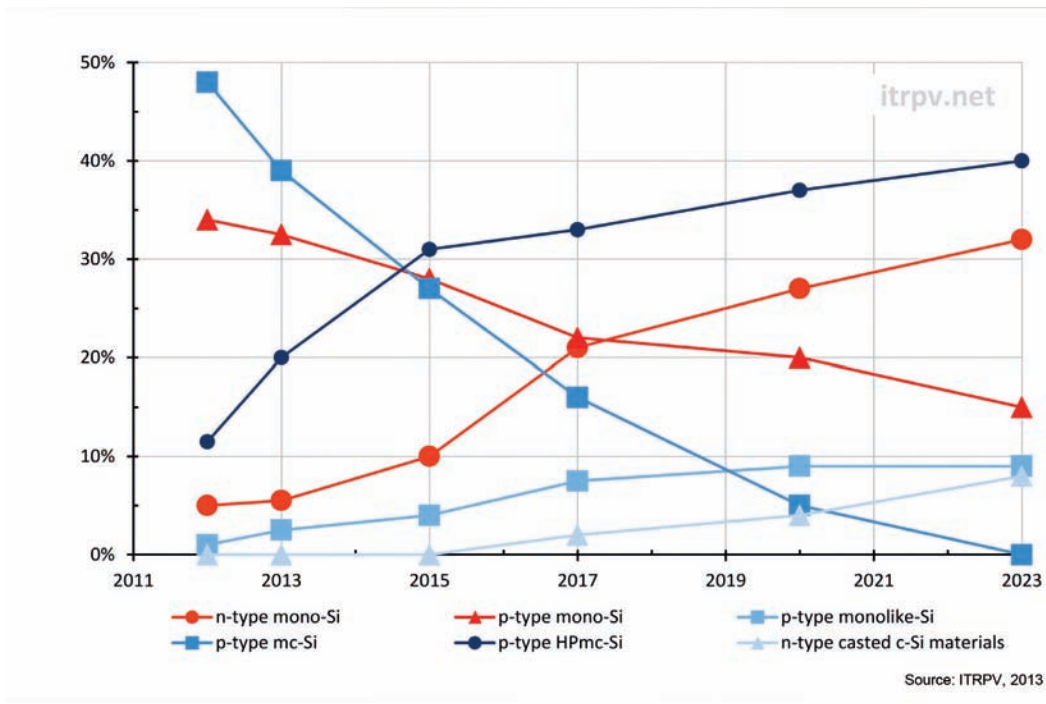

Figure 2. Expected relative market share for cast and mono-Si materials [4].

per Wp also decrease, since less module area is required per Wp. Various new and/or additional process steps have been developed in order to reach or exceed the 20% efficiency level. To date, this has been an incremental evolution rather than a paradigm shift to new and revolutionary technologies. The challenge is that both the investment and the operational costs for any new technology should be minimized, with a target cost level for a finished module at or below 0.5€/Wp.

The International Technology Roadmap for Photovoltaic (ITRPV) forecasts that n-type monocrystalline silicon will increase its market share to 30% in 2023 [4], whereas today's predominant technology, p-type multicrystalline silicon (mc-Si), will sharply decrease, as outlined in Fig. 2.

SunEdison has commercialized a continuous Czochralski (CZ) crystal pulling process [5]; furthermore, diamond sawing (versus traditional wire sawing) will increase its market share. Various cell technologies based on n-type Si are available, including heterojunction with intrinsic thin layer (HIT), commercialized by Panasonic [6], and interdigitated back contact (IBC), commercialized by SunPower [7]. The status and future of industrial n-type silicon solar cells is addressed by Kopecek et al. [8]. Various companies have started pilot manufacturing of passivated emitter and rear cell (PERC) solar cells based on p-type wafers. A recent technology overview of process flows is described by Dullweber et. al [9].

A frequent question is whether the upcoming new technologies will have a significant impact on the design of the building and facilities. Current investigations have shown that such new technologies will have little effect on ingot manufacturing, but more pronounced impacts on the wafer and cell lines, since different manufacturing steps with various new process gases and chemicals will be required.

As a first example, diamond sawing will result in a reduction in slurry handling and disposal systems. Second, HIT technology does not require a high temperature diffusion process step; in addition, this technology also requires a reduced number of process operations. Therefore, both the overall electrical power demand as well as the total manufacturing area could decrease, resulting in a reduction in both investment and operating costs. Moreover, new types of screen-printing metal pastes are necessary, which influence the supply and disposal of the respective chemicals. Some process steps will also require a higher level of cleanliness: the specifications for deionized water, chemicals and gases, as well as the need for local cleanrooms, must therefore be reviewed.

All of these factors need to be taken into consideration when designing new and cost-effective manufacturing facilities, in order to ensure adequate space allocation, appropriate supply and disposal of process-related utilities, optimized logistics and the 'just clean enough' approach.

Scaling effects and integration

The last intensive investment cycle in the PV manufacturing industry (2006 to 2008) resulted in the current global overcapacity. During that period, some manufacturers planned to develop new greenfield sites with manufacturing capacities approaching the GWp/annum scale. So far, very few GWp facilities have been built on a single site. Since the PV industry is rapidly maturing, and new capacities are being planned right now, the question is whether an integrated facility on a GWp scale remains an economically feasible approach.

Several possibilities exist for driving down investment as well as running costs for PV manufacturing facilities, as highlighted in Fig. 3.

The PV manufacturer, as well as its equipment and technology suppliers, has the strongest influence with regard to technology and process tool selection. The PV manufacturer, in conjunction with the design/build contractor (EPC) of the building and facilities, can control scaling effects and the degree of integration. Value engineering (VE) steps evaluated during the early design phases can potentially produce the largest decrease in overall investment cost. The authors compared scaling factors for the manufacturing and gross building areas of a 100MWp/annum with a 600MWp/annum cell manufacturing line [10]. From a cost point of view, and if adequate land is available, it is generally recommended to select a single-level building concept, since multi-level

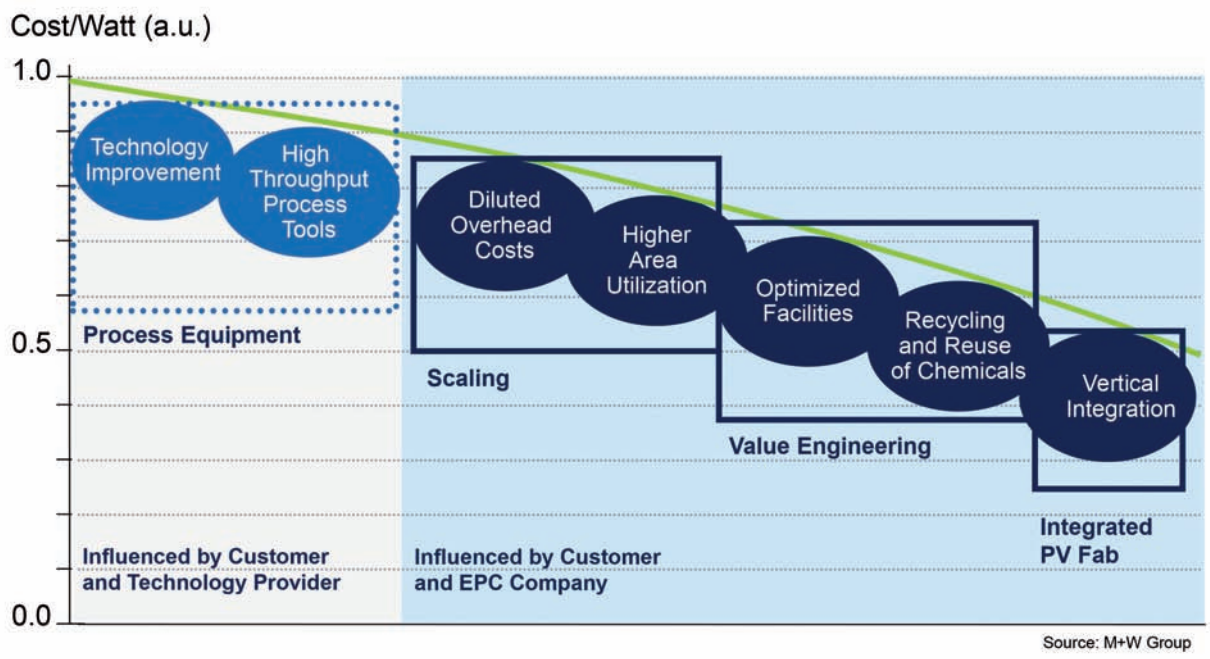

Figure 3. Elements for driving down costs within the PV added manufacturing chain.

buildings take longer to construct, and the complexity of internal logistics and automation requirements become increasingly challenging.

> "It is generally recommended to select a single-level building concept."

The impact of the integration of different added-value steps (ingot to module) by various manufacturing capacities is shown in Fig. 4, consisting of benchmark investments for the building and the facilities for co-located ingot-to-module manufacturing complexes with annual manufacturing capacities ranging from 100 to 600MWp.

The most pronounced decline in specific investment occurs between an annual manufacturing capacity of 100 and 200MWp. From 200 to 600MWp/annum the trend continues, but starts to flatten. Above an annual capacity of 600MWp, the authors conclude that a further significant decrease in the specific costs for the building and facilities will not occur for a number of reasons, primarily driven by the increase in overall footprint of the single manufacturing building, where special measures for fire protection in accordance with local codes and regulations may have to be considered. In addition, the volume for make-up and exhaust air increases, thereby increasing the length and diameters of ducts; the specific power consumption of the larger fans also increases as a result of higher pressure drops. These additional measures can completely cancel the potential savings to be gained in manufacturing through further scaling.

Another key question is whether the entire manufacturing process along the PV added-value chain should be integrated and in close vicinity to the end market, or if the decentralized approach could be more cost-effective.

If the proximity to a market and the shipping times become important factors, module manufacturing should be close to the market and the capacity should not be larger than what the local or regional markets can absorb. Other factors – such as the availability of skilled labour, supply chain and cost of utilities – should also be taken into account. The predominant operational cost for the utilities is electrical power. The energy demand for a 600MWp/annum reference PV manufacturing facility was investigated: the results for the specific energy demand (MWh/annum) for poly Si, (mono-) ingot/wafer, cell and module manufacturing are illustrated in Fig. 5.

A poly Si manufacturing plant was included for completeness, the figures being based on an assumed conversion ratio of 5g of silicon per Wp of capacity. Since different technologies are utilized for the various steps, the specific energy demand can vary slightly from the depicted values. It is evident that poly Si and ingot/wafer plants require the highest energy supply on a per MWp basis, primarily driven by the hydrochlorination, CVD deposition and ingot-growing steps, all of which are energy-intensive operations. Consequently, it will be challenging for such manufacturing steps to competitively produce poly Si in regions with relatively high energy costs. The impact of energy costs is less pronounced for cell manufacturing and even less critical for module manufacturing, which suggests locating cell and module manufacturing facilities with small- to medium-size capacities (200 to 600MWp/annum) close to the end-user market. Poly Si and ingots can only be manufactured in a cost-effective manner in countries with relatively low energy costs; in these operations, capacities can be higher (10.000t/annum or above 1GWp/annum, respectively) in order to benefit from potential scaling effects.

Localization of PV manufacturing

To date, the largest markets for module installation have been in Europe, and most manufacturing capacity has been built in Asia. PV installations are expected to shift from Europe to the Americas, Asia and the Middle East/North Africa in the near future. In parallel, the overall market is predicted to grow to 56GWp in 2016 (Fig. 6).

To maintain sustainable growth in the long term, solar power cannot depend on local subsidies or feed-in tariffs to achieve grid parity. Consequently, new cost-effective manufacturing facilities will be required as the supply and demand

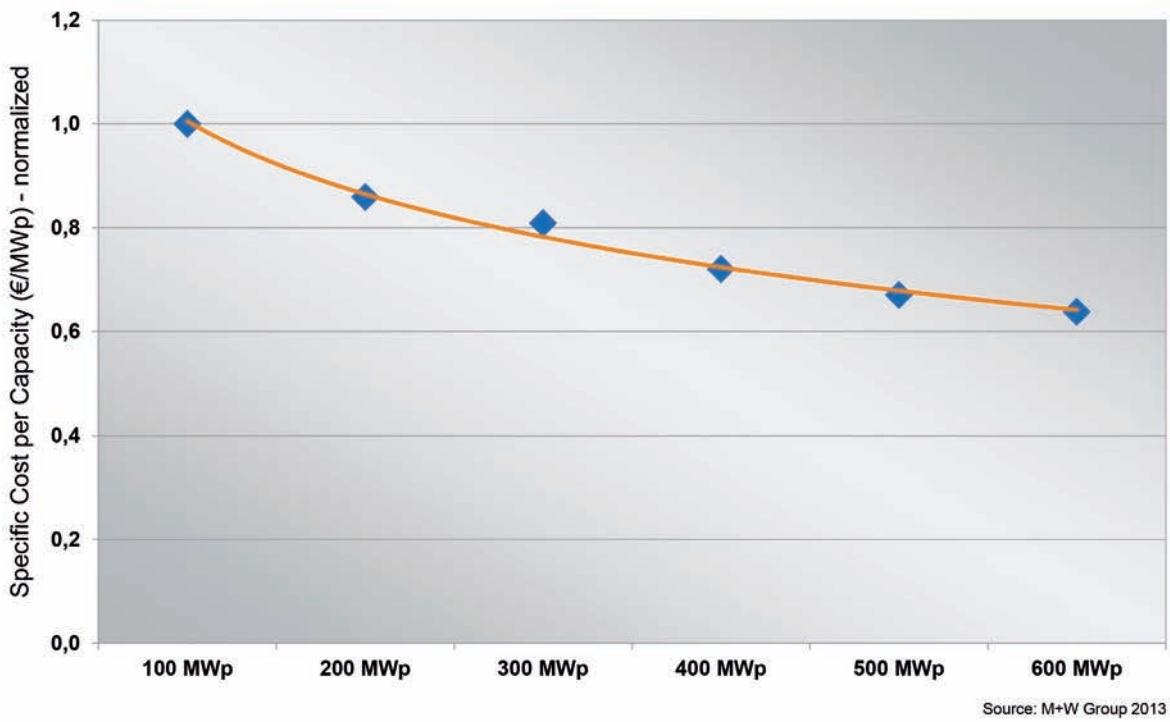

Figure 4. Specific fab and facility investment for ingot/wafer, cell and module manufacturing by capacities.

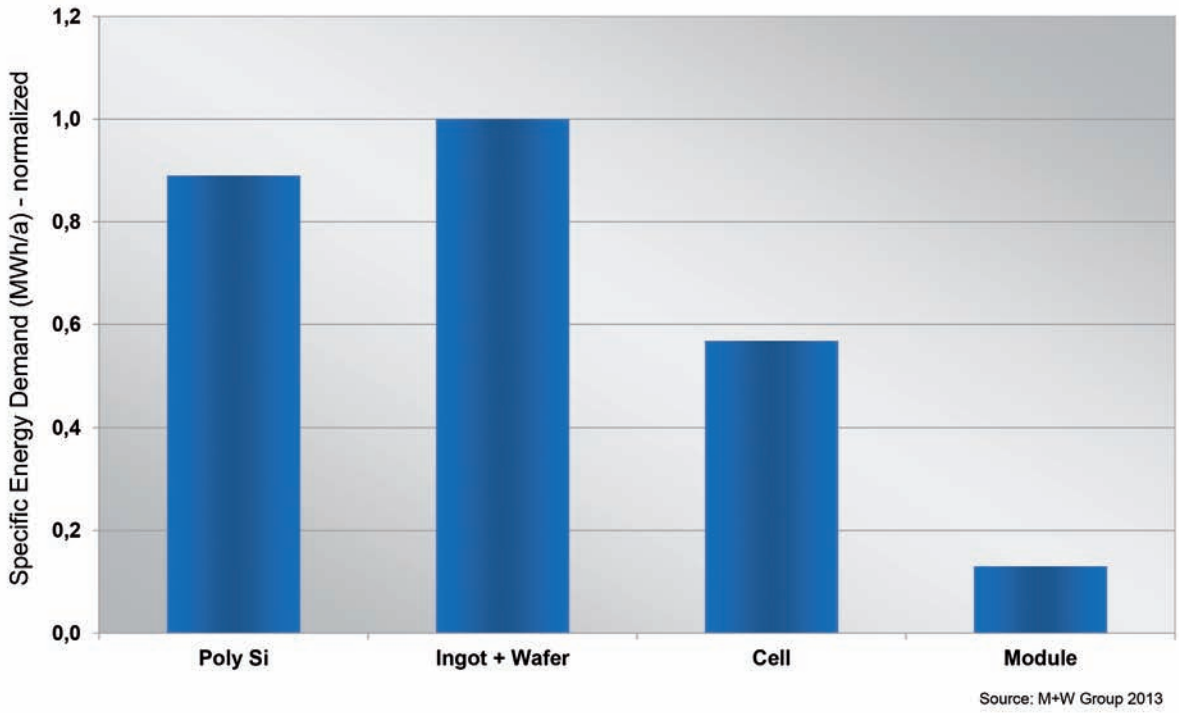

Figure 5. Normalized specific energy demand in MWh/annum for poly Si to module manufacturing.

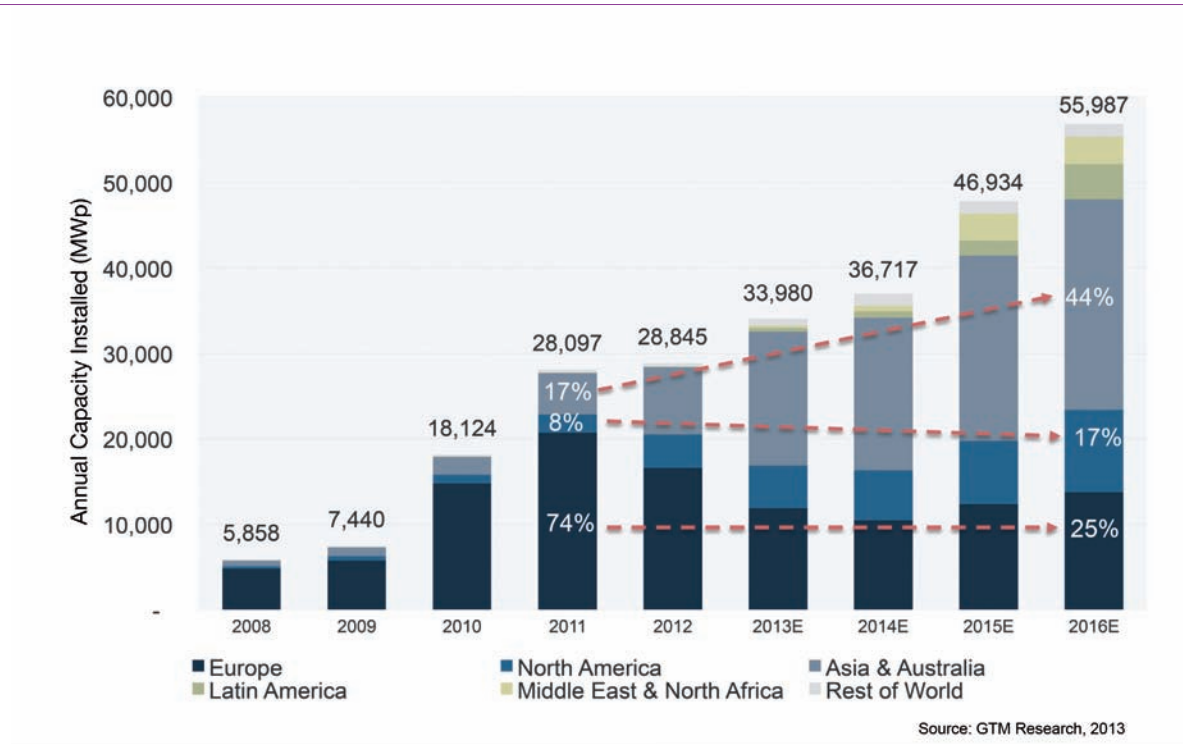

Figure 6. Global PV installations: 2008–2016E [11].

curves converge, and PV manufacturers will need to evaluate new site locations. As previously discussed, energy costs are a key decision-making criterion, particularly for poly Si and ingot/wafer manufacturing, but another important site selection consideration exists that relates to macroeconomic requirements at national level.

Through local PV manufacturing, countries will become less dependent on fossil energy and generate numerous employment opportunities for a broad range of skill sets. The job creation aspect is not limited to the manufacturing site itself, but also applies to the related service and supply industries. As a rule of thumb, 15 new jobs per MWp annual capacity are required for an integrated poly Si to module manufacturing facility: 9000 people must therefore be hired to operate a 600MWp/annum plant around the clock. In addition, there is a leverage factor of approximately two to three for job creation in the service and supply industries, as well as in the downstream sector for PV power plants. The diverse types of support function required for a PV production plant in terms of R&D, education centres and the service and supply industries are shown in Fig. 7.

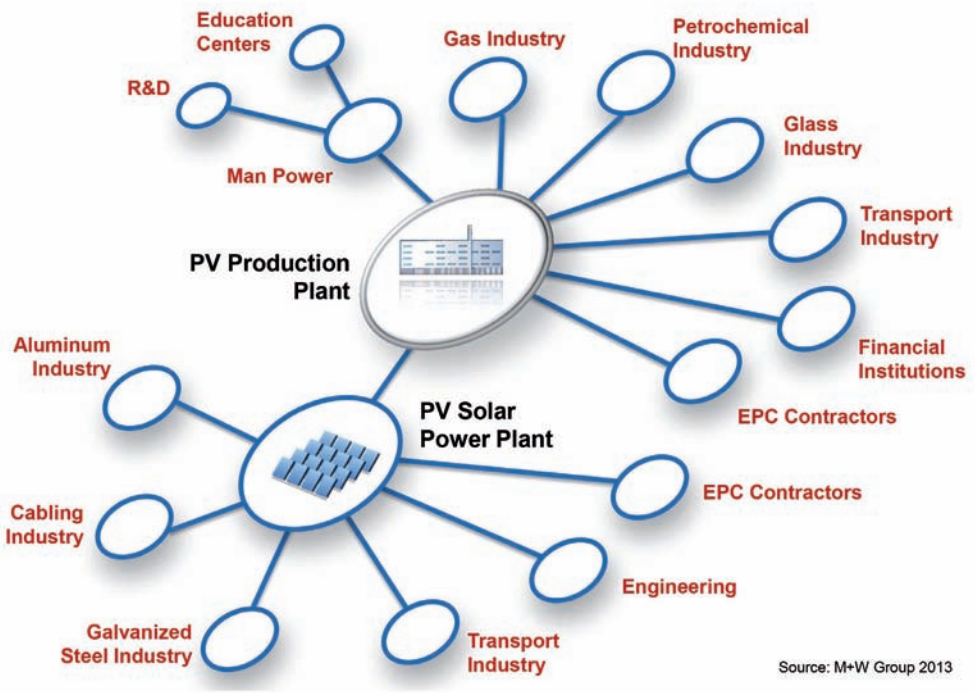

Figure 7. Job creation opportunities for PV manufacturing and solar installations including the entire supply chain.

This also explains why a number of countries with high growth rates in solar installations are eager to set up local manufacturing for single parts, or even for the entire added-value chain. An important consideration in the case of closed markets is that the price of modules and related BOS costs could increase. To establish a new industry in conjunction with the creation of employment opportunities, a national incentive plan acts as a useful catalyst, but only for a limited period in order to allow the local industry to become competitive during the ramp-up of production.

Future trends

Process technology advancements will remain one of the most important factors in driving down manufacturing costs of PV modules. Because of the expansion of the global PV markets in different climatic conditions, the optimal selection of cell and module process technologies should be considered on a case-by-case basis. For this reason, the authors do not anticipate the dominance of one mainstream technology, but rather the co-existence of a suite of different technologies. Incremental steps will occur to increase module efficiency and drive down cost. From an EPC company's perspective, it will be important, during the engineering of such a fab, to design the facilities to precisely match the requirements of the process and manufacturing technology. Seamless integration of process and facility technologies is key to achieving these targets without oversizing the facility systems for each individual production technology.

> "Reducing the investment and running costs will be of utmost importance to fully utilize potential synergies."

Reducing the investment and running costs, particularly for integrated facilities co-located on one site, will be of utmost importance to fully utilize potential synergies. M+W Group has experienced requests for either centralized and integrated or decentralized manufacturing complexes, depending on an inquiry's origin. The recycling of water and certain process gases and chemicals will become cost-effective for GWp/annum-scale facilities: as previously discussed, the cost of electrical energy and the potential market's size are key drivers for such decisions. A state-of-the-art concept for a fully integrated PV manufacturing facility from poly Si to module on a GWp/annum scale has been recently developed by M+W Group and its partners, and is illustrated in Fig. 8.

As depicted, a central facility plant serves the individual process steps with main utilities, with specific utilities located within the respective manufacturing buildings. The poly Si manufacturing plant is adjacent to the ingot/wafer building. Wafers are transferred to the cell deposition building, followed by module assembly and final storage/shipping. By utilizing synergies for the utility supply and disposal systems, investment as well as running costs can be significantly reduced. Such facilities will most likely be implemented in countries with low energy costs and sufficient market demand.

Countries with relatively high energy costs or limited markets (below 400MWp/annum) will primarily follow the trend towards the construction of local cell and module manufacturing plants. Scenario planning should focus on potential future needs in order to be flexible for expansion in case of short-term market growth. Specific factory planning employed at an early stage during site assessment/selection and site master planning can mitigate potential surprises later on.

Conclusions

The PV manufacturing industry will resume its growth after the recent downturn and intensive consolidation. From a fab and facility perspective, the key questions are:

- What should be the optimum manufacturing capacity?
- How much process integration should be implemented?
- Where will the new facility be built?

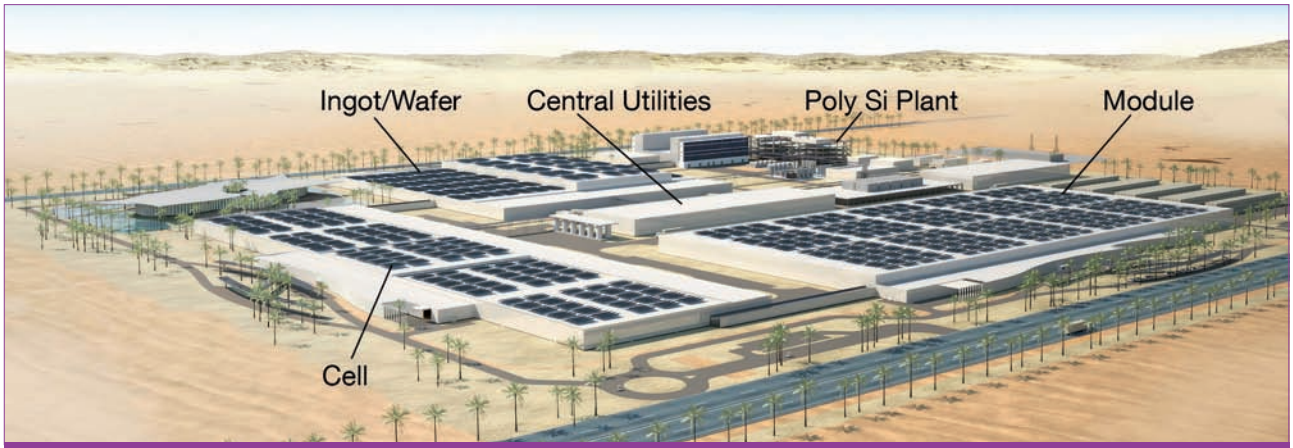

Figure 8. Concept for a fully integrated PV manufacturing line.

- How should the facility be designed to ensure cost-effective operation?

The authors have addressed the specific cost per manufacturing capacity within the PV added-value chain, as well as the specific energy demand for each of the production steps. A minimum production capacity of 200MWp/annum is recommended for cost-effective manufacturing. Increasing the production capacity from 200 to 600MWp/annum will further result in specific operational reductions, but to a lesser degree. From a fab and facility perspective, for production capacities above 600MWp/annum, the effect on specific production cost reduction decreases further.

> "A minimum production capacity of 200MWp/annum is recommended for cost-effective manufacturing."

The degree of integration will be influenced by the local cost of electrical energy. In regions with high energy costs, it will be challenging to operate poly Si and ingot/wafer plants in a cost-effective manner because of their high energy demand. It can therefore be concluded that central poly Si and ingot/wafer plants with capacities exceeding 1GWp/annum will be situated in locations with competitively low energy costs. The location of future cell and module facilities near to the end-user market should be considered, since this approach offers numerous benefits, not only from a cost perspective, but also from a macroeconomic point of view, with direct employment creation and the development of the associated service and supply industries.

Acknowledgements

The authors wish to thank numerous colleagues within the Global Technology Services (GTS) division at M+W Group for their support and valuable discussions.

References

[1] Campos, J.-F.L. 2013, "IHS boosts capital spending forecast as market conditions improve", Press Release, November 11th [http://www.isuppli.com/Photovoltaics/News/Pages/IHS-Boosts-Solar-Capital-Spending-Forecast-as-Market-Conditions-Continueto-Improve.aspx].

[2] NPD Solarbuzz 2013, "PV markets quarterly report", July.

[3] Fraunhofer ISE 2012, "Photovoltaics report", December 11th, pp. 41–42.

[4] SEMI PV Group Europe 2013, "International technology roadmap for photovoltaic (ITRVP): Results 2012", 4th edn (March) [http://www.itrpv.net/Reports/Downloads/].

[5] Kearns, J. & Li, B. 2013, "Progress in n-type monocrystalline silicon for high efficiency solar cells", *Photovoltaics International*, 21st edn, pp. 34–37.

[6] Panasonic 2013, "Panasonic HIT solar cell achieves world's highest conversion efficiency of 24.7% at research level", Press Release, February 12th.

[7] SunPower 2011, "20% efficiency maximum system output reduced installation cost", Document 001-65754 RevA.

[8] Kopecek, R. & Libal, J. 2013, "The status and future of industrial n-type silicon solar cells", *Photovoltaics International*, 21st edn, pp. 52–60.

[9] Dullweber, T. et al. 2013, "Emitter technology options for industrial PERC solar cells with up to 20.3% conversion efficiency", *Photovoltaics International*, 21st edn, pp. 44–51.

[10] Rauter, G. et al. 2009, "Scaling challenges for PV manufacturing facilities", *Photovoltaics International*, 5th edn, pp. 14–23.

[11] GTM Research 2013.

About the Authors

Klaus Eberhardt is the technology manager for photovoltaics at M+W Group. He has many years' experience in the PV industry, and successfully started up the PV business at M+W in 2000. With his technology know-how and strategic and operational skills, as well as international experience in marketing and product development, he supports M+W Group's customers in the PV industry on a global scale. Klaus received his diploma in electrical engineering as well as his Ph.D. from the University in Stuttgart.

Peter Csatáry is head of the Global Technology Services group at M+W Group, which focuses on the technology-driven market and concept development for process and manufacturing technology, including energy management and environmental engineering. He has been with the company since 1989, and has co-authored numerous papers and publications in the PV and semiconductor industries. Peter received a B.Sc. in mechanical engineering and an M.Sc. in industrial engineering from the University of the Witwatersrand, South Africa.

Enquiries

Klaus Eberhardt
M+W Germany GmbH
Lotterbergstr. 30
70499 Stuttgart
Germany

Email: klaus.eberhardt@mwgroup.net

Materials

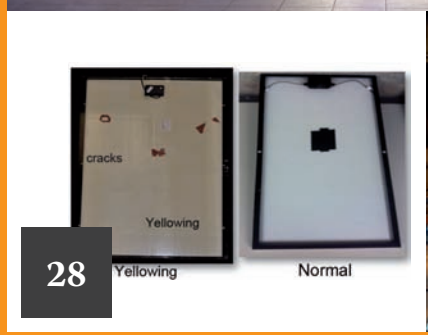

News

Europe to impose 42.1% anti-dumping duties on Chinese solar glass firms

The EU is to apply a 42.1% anti-dumping duty on Chinese solar glass manufacturers, according to a document published in the organisation's official journal. The new levies came into effect on 28 November. The investigation was announced in February this year with a parallel anti-subsidy inquiry following in April. Companies that cooperated with the EU investigation will be charged slightly lower rate of 38.4%, with Henan Yuhua given the lowest rate of 17.1% to reflect its smaller dumping margin. Hehe Group was given a 32.3% levy and Xinyi Group a 39.3% rate. The EU believes that the duties could allow manufacturers that ceased production due to price pressure from an influx of low-cost Chinese solar glass to begin again.

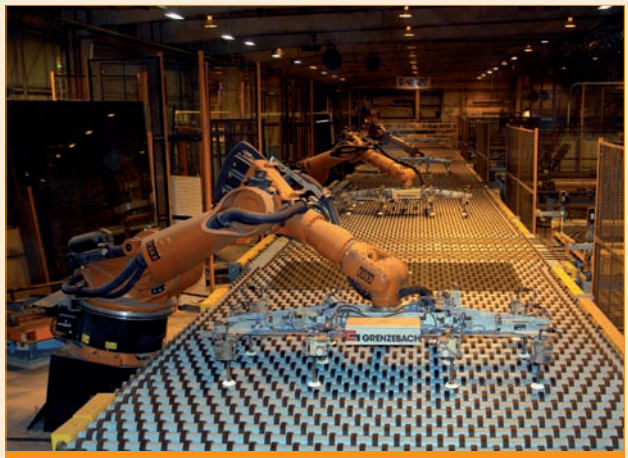

Europe is to impose 42.1% anti-dumping duties on Chinese solar glass firms.

Polysilicon probe

China extends EU polysilicon probe by six months

China's Ministry of Commerce (MOFCOM) has said it will extend a probe into imports of solar-grade polysilicon from Europe by six months.

MOFCOM cited the complex nature of the case, in its decision to prolong the investigation. China's probe into imported polysilicon was instigated after the US and European Union launched investigations into alleged dumping of cut price modules into those markets by Chinese manufacturers.

In July China said it would impose duties on imported polysilicon from the US and South Korea, but did not make a decision on imports from Europe as the wider trade dispute with the EU was at its peak at the time. This broader dispute was resolved, but China has said its investigation into European polysilicon is still ongoing and will run until May 2014.

Research and Development

Heraeus solar products launch drive after R&D expansion

Citing the fast pace of material developments for PV manufacturing, Heraeus' Photovoltaics Business Unit is expanding its silver paste R&D capabilities at its site in West Conshohocken, Pennsylvania.

The company said that it would be hiring more R&D specialists, while expanding the lab infrastructure at Conshohocken. However, this would be undertaken in tandem with the relocation of R&D members of other Heraeus sites to Conshohocken.

The collaboration with its Application and Technical Service Centers located in China, Taiwan, Korea, Japan, Singapore and Germany are unaffected by the consolidation of R&D activities and were said to benefit from the faster product cycle-times planned.

SERIS and FHR Anlagenbau agree coatings collaboration

The Solar Energy Research Institute of Singapore (SERIS) and Germany-based FHR Anlagenbau have announced a collaboration to develop high-performance Transparent Conductive Oxide (TCO) coatings.

The coatings are used in a number of PV module technologies including CdTe, CIGS and amorphous silicon and advanced high-performance silicon wafer solar cell technologies such as hetero-junction solar cells.

The team is looking to reduce or eradicate the use of many of the scarce, toxic and expensive materials currently used for the development of TCOs.

Wafer supply

PV Crystalox expects slightly higher solar wafer shipments

Wafer producer PV Crystalox Solar has said it expects shipments to be at the high end of its mid-year guidance of 160-180MW.

The company, which is still operating at very low utilization rates, noted that it continued to operate in cash conservation mode, while reducing production costs, quality improvement programmes and inventory management.

As the company had long-term polysilicon purchasing agreements, it has been re-selling polysilicon due to

SERIS and FHR Anlagenbau have agreed to collaborate on developing coatings.

PV Crystalox expects slightly higher solar wafer shipments.

ingot production cuts. However, PV Crystalox noted that wafer and polysilicon inventories by the end of 2013 were expected to be significantly lower than it started with at the beginning of the year. The company had shipped 79MW of wafers in the first half of 2013, up from 61MW in the same period a year ago. Revenue was €28.6 million, down from €32.6 million in the first-half of 2012. The company had reported a loss of €0.9 million.

Trendforce: Return to wafer supply contracts

Tightening supply of quality solar wafers due to booming demand for PV modules could see the return of contract trading by wafer producers, according to market research firm, EnergyTrend. Strong wafer demand in the fourth quarter is expected to continue into the first quarter of 2014 as demand in China, Japan and other key markets grows, impacting the ability of wafer suppliers to keep up with demand especially for high-efficiency wafers used for residential markets.

EnergyTrend, a division of Taiwan-based TrendForce, said that smaller wafer producers with better technology had primarily returned to full production and been able to raise prices, a trend is said could continue. Demand for mainstream multicrystalline wafers remains unabated, with prices since October 2013 increasing by 5%, EnergyTrend said. As a result, wafer manufacturers were said to be considering short-term contract trading.

GCL Poly warns of demand outstripping supply

China's largest polysilicon and solar wafer producer, GCL-Poly Energy, has said that continued high manufacturing utilisation rates at customer facilities meant its production supply could not meet with market demand.

The company reported polysilicon production volume for the first three quarters of 2013 had been approximately 35,531MT, representing an increase of approximately 8.1% compared with 32,864MT over the prior-year period.

Production improved slightly in the third quarter, reaching approximately 13,550MT. The company said it sold approximately 12,490 MT of polysilicon for external customer wafer production in the first three quarters of 2013, representing an increase of approximately 29.2% compared with 9,669 MT over the same period of last year.

However, external polysilicon sales in the third quarter were approximately 4,018MT, a 511.6% increase over sales in the third quarter of 2012, when production was being rapidly scaled down as overcapacity saw polysilicon prices dip to record low (US$15/kg) in the fourth quarter. GCL-Poly said polysilicon ASPs had remained flat through the year at US$17/kg.

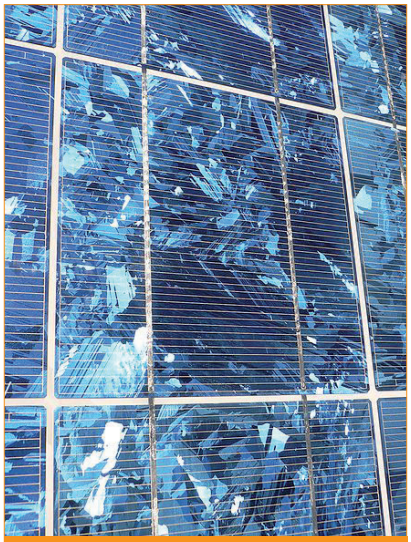

Polysilicon and wafer costs set to drop to record low, says Solarbuzz.

Materials market forecasts

Solarbuzz: Polysilicon and wafer costs set to drop to record low

Manufacturing costs for tier one integrated polysilicon and PV wafer makers are set to hit a record low of US$0.20 per watt in 2014, according to analysis by NPD Solarbuzz.

The market research firm said that although the predicted 6% fall in costs next year will not equal the average 16% decrease they have seen annually since 2008, a hugely competitive market will continue to spur manufacturers to drive down costs.

According to Solarbuzz, manufacturers are relocating their polysilicon operations to areas with low electricity costs and replacing manufacturing capacity using the so-called Siemens manufacturing process with fluidised bed reactor (FBR) plant. Solarbuzz said manufacturers had reported being able to cut costs using FBR to less than US$10 per kilogram.

Lux Research: Materials market to grow 9% a year

The market for PV materials will grow at 9.2% annually till 2018, according to new a new report by Lux Research.

Despite oversupply issues pushing down prices of polysilicon, other materials that present an opportunity to drastically increase module efficiency can be sold at a premium. Lux claims that materials for solar modules have enjoyed rising profit margins since 2009, with the exception of glass and polysilicon.

Some gases, metals, polymers and process chemicals and solvents are achieving double digit profits. The study found that encapsulants, backsheets and metallisation pastes were delivering high profits and making a big impact on module efficiency.

New orders

Centrotherm booked new orders totalling €163.2 million in revised accounting period

The centrotherm Group was able to secure new orders totalling €163.2 million during its restructuring period through October 2012 and May 2013.

New orders booked included €123.2 million within its silicon segment, which accounted for the majority of backlog. The company did not provide expected shipment schedules on its order intake.

The company said it had also received new orders in its photovoltaics and semiconductors segment, totalling €35.4 million, while centrotherm also received new orders totalling €4.5 million in its thin-film and customized systems segment, reflecting the industry-wide collapse in production equipment capital spending due to overcapacity.

Total order backlog to 31 May 2013 stood at €305.7 million, down from over €500 million when the company last produced full quarterly financial reports.

The company had recently suffered the cancellation of a €255 million order from CEEG in Algeria, which had been included in its order backlog from the first quarter 2012 reporting period. Sales for the period were therefore significantly down on previous years at just €69.2 million, compared to €149.2 million during the first nine months of 2012.

GT Advanced Technologies heads downstream with Apple sapphire supply deal

Iconic consumer electronics firm, Apple, is investing US$578 million in a new manufacturing plant to be operated by GT Advanced Technologies (GTAT), creating 700 jobs in Arizona, US.

Leveraging its technology in making sapphire substrate equipment, GTAT and Apple have signed a multi-year sapphire materials agreement that will contribute around 80% of 2014 revenue, highlighting the continued weakness of the upstream PV materials market.

GTAT reported third quarter revenue declined significantly to US$40.3 million including US$28.6 million in polysilicon, US$4.4 million in photovoltaic, and US$7.3 million in sapphire. However, the company also reported that approximately US$18 million of revenue in the quarter was related to the company terminating an outstanding order for TCS equipment used in polysilicon production and booking the non-refundable deposit.

PVA TePla wins order from PV customer on back of improving bookings

Crystal growing equipment specialist, PVA TePla, has said it has seen an increase in new orders, including an order from the PV industry.

The company reported financial results for the first nine months of 2013, noting new orders had reached €65.3 million, up from €42.2 million in the same period a year ago.

In its Solar Systems segment, PVA TePla reported orders worth €7.8 million, compared to just €1 million in the previous year period, noting that it had recently received an order for crystal-growing systems from a solar module manufacturer based in Asia.

However, for the first nine months, consolidated sales revenue reached of €46.5 million, down from €83.7 million in the prior-year period.

Source Apple

Apple is investing in a new sapphire plant to be operated by GT Advanced Technologies.

Product Reviews

EVASA

High electrical resistivity encapsulant from EVASA offers PID-free solution

Product Outline: EVASA has developed a new series of PV module encapsulants that have high electrical resistivity, which prevents potential-induced degradation (PID) effects. 'Solarcap PID FREE' encapsulant was said to have been tested by different independent laboratories resulting in demonstrable losses below 2%.

Problem: Potential-induced degradation (PID) is believed to be caused by the leakage of current from a solar cell, due to negative charge carriers that would normally flow from the cell surface to the back contact. Moisture penetration and high module voltages are thought to create the current discharge and module performance loss.

Solution: Solarcap PID FREE encapsulant is designed to provide structural support, electrical insulation, protection and transparency for c-Si PV modules. Their high level of thermal stability of the encapsulant is said to be a result of the elimination of residual tensions during manufacturing, avoiding shrinkage of the material during the lamination process. The cycle time may change according to the laminator, module design, temperature and targeted crosslinking degree, however typical cycles work at temperatures from 150 to 155 degrees Celsius and times of around 14 minutes, with a gel content >85%.

Applications: C-Si solar cell/module encapsulant providing PID free results.

Platform: EVASA Solarcap materials, including Solar Total Transmission (>91%) that are protected against degradation and yellowing. Comprise of a very high gel content (>87%) and adhesion properties of (>85 N/cm), with less than 1% shrinkage.

Availability: September 2013 onwards.

Dow Corning

Dow Corning's silicone-based ECA designed for MWT cell designs

Product Outline: Dow Corning's silicon-based, next-generation Electrically Conductive Adhesive (ECA) 'PV-5802' will be used in Tianwei New Energy's Metal Wrap Through (MWT) module production line, developed by ECN of the Netherlands. PV-5802 is said to provide improved electrical properties and stability, enhancing the electrical performance, reliability and durability of MWT modules.

Problem: Conductive adhesives are used to attach and make electrical contact between the current carrying ribbons, busbars and back contact sheets of the cells. Degradation in the interconnect may affect current carrying capacity. Conductive adhesives capable of withstanding stresses in a PV module with minimal degradation over a 20-plus year product life cycle are required.

Solution: Dow Corning's PV-5802 new silicone-based ECA has been developed for the MWT module technology. It was said to have demonstrated excellent conductivity and production yield in tests on Tianwei's MWT production line. The MWT modules using PV-5802 had cell-to-module power loss of less than 0.4%. Full area module efficiencies reached 16.8 %, for multi-crystalline silicon modules. In ageing tests, the modules showed very low degradation: 0% loss after 300 thermal cycles (between 40 and 85 degrees Celsius), and 0.2% loss after 1,500 hours in damp heat conditions (85 degrees Celsius, 85 % relative humidity).

Applications: PV back contact module manufacturing such as IBC as well as MWT solar cells.

Platform: The PV-5802 ECA has an Ag filler content below 60% but maintains a conductivity after curing below 1 mOhmcm. It is flexible over a wide range of temperatures, which enables stress-relief and is beneficial for durability.

Availability: Currently available.

Freiberg Instruments

Freiberg Instruments PIDcon bench top metrology solution replaces mini-modules and climate chambers

Product Outline: Freiberg Instruments new potential induced degradation (PID) control device (PIDcon) was designed for solar cells and encapsulation films based on the knowledge of Fraunhofer CSP, in order to combine the advantages of established test procedures, while replacing the need for mini-modules and climate chambers.

Problem: Failures of crystalline silicon solar modules under the influence of high system voltage were first reported in 2010. Affected solar cells show an extreme drop of the shunt resistance, an effect termed potential induced degradation (PID). Until now PID tests are principally conducted at modules. Manufacturing of modules and climate chamber testing require considerable expenses for materials, equipment and work.

Solution: The Freiberg Instruments' PIDcon allows routine quality control of standard production solar cells, test of new production processes, material or layer variations and qualification for various solar cell technologies as well as evaluation of impact from various module set ups. The PIDcon device reproduces a typical module stack on the surface of solar cell test samples. The sample undergoes the same voltage stress as in conventional module tests. Also glass sheets or polymer encapsulants can be tested with respect to their specific PID susceptibility when PID-sensitive cells are used.

Applications: PID test procedure for solar cells and module components (glass, polymer sheets).

Platform: PIDcon size: 300x350x208 mm. Sample size: 156x156 mm (125x125 mm option), standard two or three busbar cells, others on request. Adjustable temperature up to 100 degrees Celsius, typical measurement condition 60 degrees Celsius.

Availability: Currently available.

Impact of silver powder grain size and inorganic additives on the performance of front-side pastes

Stefan Körner, **Kathrin Reinhardt**, **Uwe Partsch** & **Markus Eberstein**, Fraunhofer IKTS, Dresden, Germany

ABSTRACT

This paper presents the results of a study of the influence of silver powder particle size and inorganic additives on sintering and electrical performance of a PV front-side metallization paste. Three different silver powder grain sizes were used in sample front-side pastes. Also examined is the effect of using four different inorganic additives determined by their redox potential. Solar cells produced using the sample pastes were electrically characterized, and selective etch-backs and FESEM investigations were performed to correlate electrical performance with the glassy interface between the metallization and the silicon wafer. In the absence of additives, the highest efficiencies were obtained with the medium silver grain size. If the inorganic species has an oxidizing nature, the mass transport of silver in the glass phase can be enhanced. However, the etch process at the wafer surface is also improved by a greater quantity of silver oxide in the flowing glass. It is shown that if the oxidizing capacity of the additive is too powerful, the electrical performance is negatively influenced. Moreover, the impact of additives is highly dependent on the silver particle size.

Introduction

The metallization step is one of the key processes in the manufacturing of crystalline solar cells: glass-containing silver pastes are usually screen printed and fired in a rapid thermal process (RTP). During the firing step, the glass dissolves the silver and flows viscously onto the silicon wafer. The silver-containing glass melt reacts with the silicon nitride layer (anti-reflective coating – ARC), which is thereby removed; during the temperature peak and cooling ramp, the silver precipitates at the interface [1–3]. It was recently reported [4] that the overall contact formation kinetics of a front-side silver metallization can be divided into two independent but strongly interacting single kinetic phenomena: 1) the phase transport kinetics and mass transport of silver in the silver paste; and 2) the reaction kinetics at the wafer surface. The phase transport kinetics are determined by the sintering behaviour of the silver powder, the glass chemistry and its viscosity, and the silver oxidation and dissolution in the glass phase. The reaction kinetics at the wafer surface are determined by the etching process of the silicon nitride and the P-doped silicon, as well as by the formation of silver precipitations during thermal treatment. Both these processes are dependent on the oxygen partial pressure [5,6]; one way of changing the oxygen partial pressure at the interface is to use a paste containing an inorganic additive.

> "One way of changing the oxygen partial pressure at the interface is to use a paste containing an inorganic additive."

This paper reports the investigation of the influence of silver particle size and inorganic additives on the sintering and electrical performance of the metallization paste. In particular, three different silver powder grain sizes were used to examine the phase transport kinetics, and four different inorganic compounds varying in their redox behaviour were chosen to affect the reaction kinetics at the interface. Three of the compounds have an oxidizing influence, and one of them exhibits a reducing characteristic. Given the redox potential and the related oxygen partial pressure in the interface region during firing, the silver dissolution (and thus the silver mass transport) in the glass should be influenced: the amorphous interlayer should therefore contain different quantities of silver precipitations. To examine this concept, the electrical performance of the solar cells was studied.

Experimental

For the study, sample pastes without additives were first formulated using three silver powders (Technic Inc.) which differ in particle size distribution (Table 1) and will be referred to as coarse, medium and fine. The pastes contain 95 vol% silver powder and 5 vol% glass frit. A lead-oxide- and bismuth-oxide-free frit with a particle size of d_{50} = 1.5µm was employed as the glass frit.

Next, sample pastes were formulated with (95–x) vol% silver, 5 vol% glass and x vol% inorganic additive. The inorganic additives included in the pastes were utilized as received from the supplier; Table 2 shows the redox behaviour of each additive. In order that the additives would be activated before and during silver densification, they were chosen for their thermal decomposition property in the

	Coarse	Medium	Fine
PSD [µm]	1.3–3.2	0.6–1.9	0.4–1.0

Table 1. Particle size distribution (PSD) of silver powders used.

Additive	Redox behaviour	
A	oxidation	++
B	oxidation	+
C	reduction	+++
D	oxidation	+++

Table 2. Additives used, categorized according to their redox behaviour.

temperature range 200–600°C. This property should have a significant effect on the oxygen partial pressure in the paste: the silver dissolution, the penetration of the ARC, and the possible etching process of the wafer surface during RTP should therefore be influenced.

As an organic vehicle, all the pastes include 5 wt% ethyl cellulose, which was dissolved in dibutyl phthalate and terpineol. All raw materials were mixed using a standard procedure and then homogenized on a three-roll mill (EXAKT 120E). The pastes were characterized by means of hot stage microscopy (HSM), and screen printed on multicrystalline silicon wafers (68Ω/sq. emitter, 2" × 2"): a layout with one busbar and 22 fingers was chosen. Firing takes place at different peak temperatures in an infrared belt furnace, and the efficiency and serial resistance of the resulting solar cell were measured using a custom-built set-up at Fraunhofer IKTS, Dresden.

To study the microstructure at the interface of the metallization and the silicon wafer, FESEM (field emission scanning electron microscopy) images (Carl Zeiss NVision40) were captured for investigating a correlation between paste recipe, interface microstructure and electrical data. The quantity and distribution of silver in the glassy interface was adjusted by selectively etching back the silver metallization layer using nitric acid (65%, 7 min, 70°C). An FESEM investigation was performed after each etch-back step.

Results

The sintering behaviour, as recorded by HSM, of dried paste samples having different silver grain sizes is shown in Fig. 1. With decreasing silver particle size, the sinter onset occurs at a temperature of about 275°C, compared with 350°C for the coarser paste. The paste with the coarse powder shows a maximum densification at about 600°C. After sinter onset, between 300 and 350°C, the medium powder exhibits a higher sinter rate than at higher temperatures, and above 350°C, the sinter rate is comparable with that of the coarse silver powder; the maximum densification is reached at about 550°C. The paste with the fine silver powder yields a sinter onset at the lowest temperature; moreover, the shrinkage behaviour differs from that of the other two pastes, an effect that has already been reported in the literature [7]. The maximum densification of the fine powder is not as high as that of the other two pastes.

Fig. 2 shows the efficiencies and

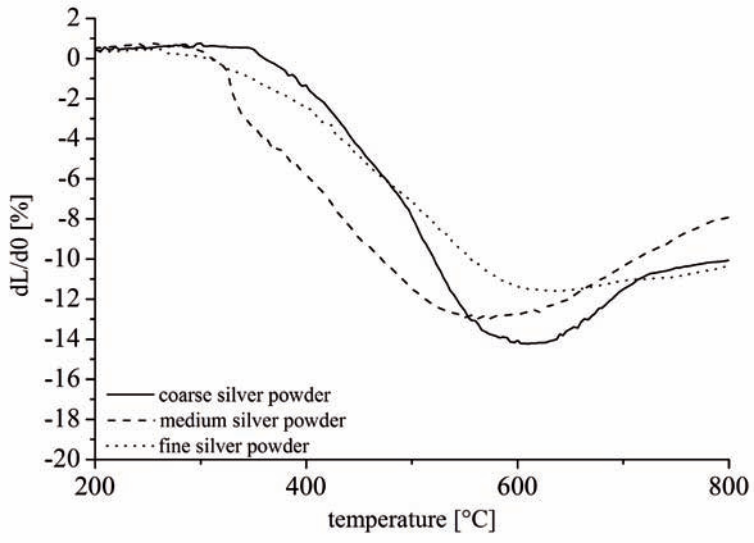

Figure 1. Sintering behaviour of pastes with different grain sizes as a function of temperature at a heating rate of 10Kmin^{-1}, recorded by HSM and normalized to 55% green density.

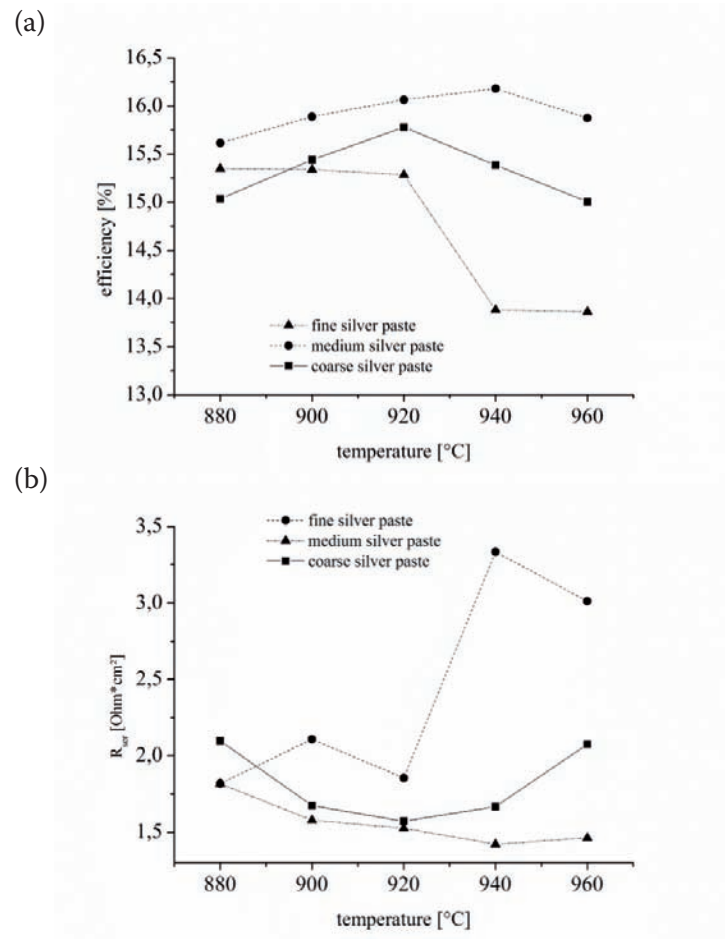

Figure 2. Dependency of efficiency (a) and serial resistance (b) of the three pastes on peak firing temperature.

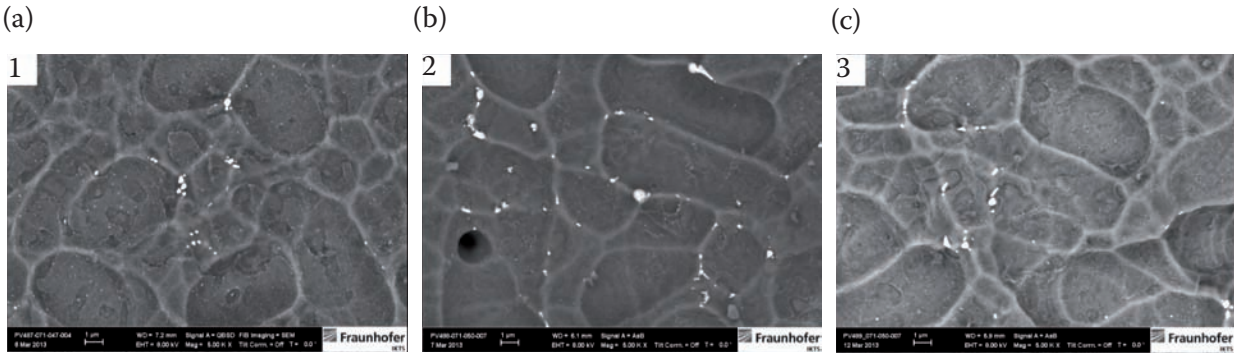

Figure 3. Wafer surface, showing the glassy interfaces after selective etch-back of the silver metallization using nitric acid: (a) paste with coarse silver powder; (b) paste with medium silver powder; (c) paste with fine silver powder.

serial resistances of the solar cells obtained with the three pastes as a function of the peak temperature during firing. The sample paste with the medium silver powder demonstrates the most stable and highest efficiency in the complete process window, reaching above 16%; in contrast, the serial resistance is the lowest of the three in the full peak firing temperature range.

"The sample paste with the medium silver powder demonstrates the most stable and highest efficiency in the complete process window."

The coarse silver paste shows a clear maximum efficiency at 920°C, but this is somewhat lower than the efficiencies obtained for the medium powder. The serial resistance of the coarse silver paste also reaches a clear minimum at 920°C, which is close to that of the medium silver paste.

The fine silver paste exhibits a narrow process window between 880 and 920°C; efficiencies above 15% can be achieved in this temperature range, whereas at higher temperatures the efficiency decreases dramatically. From the EHM measurements, the electrical characteristics show good correlation with the sintering behaviour. The efficiencies and serial resistances obtained from the fine silver powder at lower temperatures are similar to those of the coarse silver paste, and at higher peak firing temperatures both these characteristics deteriorated. The medium powder, however, demonstrates a different behaviour.

Fig. 3 shows the glassy interface after selective etch-back of the silver metallization fingers. Both of the wafer surfaces 1 (Fig. 3(a)) and 2 (Fig. 3(b)) are glazed with a thin, almost homogeneous glass film. In principle, two types of silver precipitations occur at the interface in the frame of this study. The first type is referred to as *colloids*, which are very small in size (<< 1µm) and statistically spread over the whole wafer surface. The second type is referred to as *nuggets* – these are somewhat bigger (0.5–1µm) and located at the silicon texture edges. At the same firing peak temperature, the amount and type of silver precipitation varies with the silver particle size used.

In the case of the coarse silver paste, the interface layer contains many silver colloids which are spread over the whole surface (Fig. 3(a)). In contrast, the interface of the medium

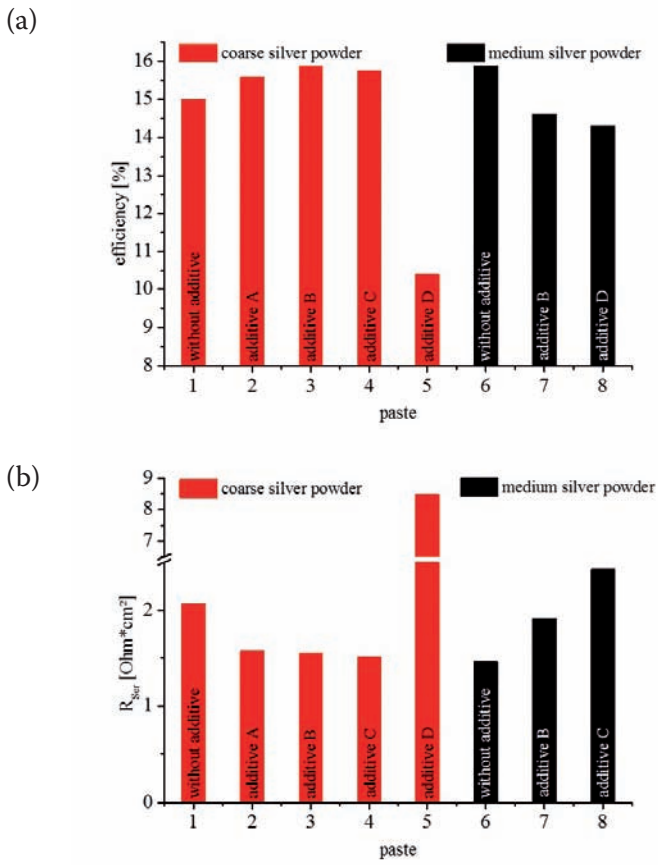

Figure 4. Efficiency (a) and serial resistance (b) of pastes with inorganic additives at a peak firing temperature of 960°C.

silver powder paste shows fewer silver colloids spread over the wafer surface in the glass phase (Fig. 3(b)). Furthermore, they are not as big as those for the coarse silver paste; however, there are more nuggets at the texture edges of the silicon. Again in good correlation with HSM and efficiency, the fine silver powder (Fig. 3(c)) exhibits almost the same type, amount and distribution of silver precipitation in the thin glass film as the coarse silver paste. For the highest peak firing temperature, the amount of silver dissolved in the glass frit should therefore be approximately the same.

In terms of the electrical characteristics and the appearance of the interface, the results of the fine and coarse silver powders are similar. With this in mind, the inorganic additives are put in the pastes with coarse and medium silver powders only.

The influence of the different additives on cell performance as a function of the silver powder particle size used is shown in Fig. 4. In the case of the coarse silver powder paste (red bars), an improvement in cell performance for all additives except the last one can be seen. The two oxidizing additives A and B show an improvement in cell performance of 0.6 and 0.9% in comparison with the reference case without additive. With the reducing additive C, a gain of 0.8% is obtained, yielding an efficiency of 15.8%. This result is in the range of the best efficiency reached with the medium silver powder without additive. By contrast, the strongest oxidizing additive D results in a decrease in efficiency of about 4.5%. Different reasons are assumed for this deterioration and will be discussed later.

The two most effective additives were introduced into the medium silver paste. Fig. 4 shows the influence of the inorganic additives B and C on the efficiency at 960°C peak firing temperature (black bars). A decrease in efficiency is obtained for both additives: additive B lowers the cell performance by about 1.3%, while additive C decreases the efficiency by about 1.5%.

Fig. 5 compares the glassy layers on the wafer surfaces after selective etch-back of the coarse silver metallization. A significant change in silver precipitations at the interface compared with Fig. 3(a) is evident. With oxidizing additive A Fig. 5(a)), the glass layer becomes more inhomogeneous than in the case of the reference state: the silver precipitations differ in quantity and type. The colloids are much smaller than for the pastes without additives, while the nuggets at the texture edges have increased in size and number.

With additive B (Fig. 5(b)) the colloids have almost disappeared, but there is a greater number of silver nuggets, and their size is smaller, than for additive A. In the case of both additives, there are nuggets as large as those for the reference paste; however, there are much bigger ones adjacent to these at the grain boundaries.

Additive D is the strongest of the investigated additives with an oxidizing characteristic. This can be clearly seen at the interface between the silver metallization and the wafer surface: the glass layer is rough and contains a lot of big silver nuggets. Not only are these nuggets to be found at the grain boundaries, but they also spread over the entire surface. In areas without nuggets, there are many colloids.

The change in the redox behaviour of the inorganic additive when additive C is used results in a complete change in appearance of the wafer surface. The glassy layer is similar to that in the no-additive and the homogenous additive B cases. With the reducing additive C, there are (as with additive A) fewer colloids than with the pure glass-

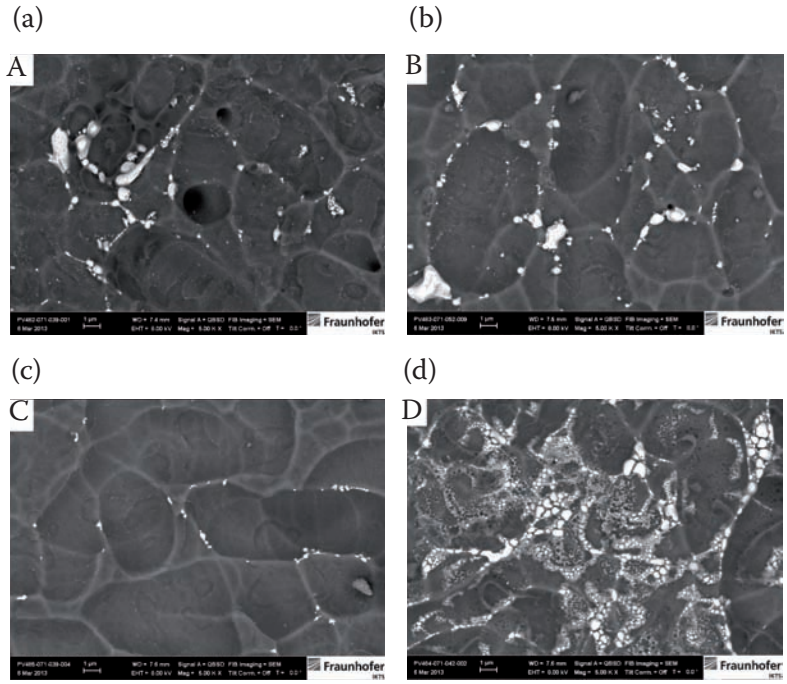

Figure 5. Wafer surface after selective etch-back of the coarse silver metallization using nitric acid. The glassy interface shown contains silver precipitations, which differ in quantity and type depending on the inorganic additive used: (a) additive A; (b) additive B; (c) additive C; (d) additive D.

containing silver powder. Nevertheless, at the grain boundaries of the silicon wafer there are more nuggets, which are rather small in size compared with those obtained with other two oxidizing species, but comparable to those for the reference state.

Discussion

The paste with the medium silver powder demonstrates the most stable and highest efficiency (Fig. 3(b)) in the temperature range 880–960°C: this is related to the sinter kinetics of the silver powder, as seen in Fig. 1. During heating, the medium powder maintains a larger surface for a longer time, which promotes the dissolution of silver under oxidation in the glass frit. More silver can therefore be dissolved in the glass, which promotes etching of both the ARC layer and the silicon surface, as well as boosting the number of silver precipitations in the glassy interface between the silver bulk and the silicon wafer; this in turn improves the electrical contact, which is reflected in the resistance measurements. The serial resistance of the medium silver powder yields lower, and much more stable, values over the whole firing temperature range than the other two silver powders. For both coarse and fine silver powders, the contact and serial resistances are slightly higher than those for the medium silver powders.

Since the coarse silver powder has a smaller surface than the medium powder, less silver is transported to the silicon surface. The fine silver powder may sinter at first to coarser particles and then behave similarly to the coarse silver powder. This effect was also found by Hilali et al. [7], who correlated sintering kinetics with paste performance: if the particle size is too small, cell performance decreases.

> "The amount and type of silver precipitation at the wafer surface can be influenced by the use of inorganic additives."

Fig. 5 illustrates that the amount and type of silver precipitation at the wafer surface can be influenced by the use of inorganic additives, in comparison to a pure glass-containing coarse silver paste. If the inorganic species has an oxidizing characteristic, the amount of silver located in the glassy interface is increased, which can be explained by the thermal behaviour of the additives during RTP. During heating-up of the wafer, the additive begins to decompose, and free oxygen is produced, forming a micro-atmosphere with increased partial pressure in the paste's microstructure. The increasing oxygen partial pressure supports the dissolution of silver as silver oxide in the glass phase. This process can start at a temperature as low as approximately 330°C [8].

Fig. 5 also shows that, with increasing oxidizing power of the additives (A, B and D), the glass layer at the wafer surface becomes more inhomogeneous. This might be due to the improved silver oxide dissolution in the paste glass, and to the related enhanced etching capability. The contact formation depends on the ratio between etching and silver precipitation at the interface. With slightly increased oxidation potential, additive A has a slightly higher serial resistance than additive B. Nevertheless, the use of an additive which oxidizes the surface too strongly (such as additive D) has a negative effect on cell performance: the reason for this is the degradation of the emitter. If the amount of silver oxide becomes too high, the etching of the surface of the wafer can be too strong, and thus the penetration can be too deep. As a consequence, the emitter becomes damaged and cell performance is decreased, which in turn results in an increasing serial resistance. The results show that, in general, inorganic additives do not work – a successful outcome depends upon an interaction between different factors, such as the grain sizes or temperatures used.

Surprisingly, the greatest improvement in cell performance can be achieved with the reducing additive C (Fig. 4). Compared with the paste without any additive, the amount of silver at the interface is almost the same. The reason for this is the unchanged oxygen partial pressure during RTP, and thus the silver dissolution in the glass frit is not affected.

If the silver particle size is reduced, the inorganic additives no longer yield an improvement in efficiency (Fig. 4 – black bars): cell performance is reduced compared with the medium silver paste. A decreased efficiency and an increased serial resistance are obtained. This is related to the optimized sintering behaviour of the medium silver paste and the supplementary effect of the additives: the additives enhance the reaction kinetics at the wafer surfaces. Because

of the aligned silver powder and glass frit, the use of additives results in an acceleration of the reaction kinetics that is too high at the interface, so that the etch depth can become to deep, and damage to the emitter can occur. Matching the size of the silver particles with the influence of the additives is therefore important.

Conclusion

The influence of silver powder particle size and inorganic additives on sintering and electrical performance of a paste was investigated; for the study, three different silver powders were mixed with 5 vol% glass. The phase transport kinetics, as well as the reaction kinetics at the interface, were found to be influenced by the silver powder grain size used. The medium silver powder provided the highest surface for the longest time, so the silver dissolution and transport onto the silicon surface was enhanced. The coarse silver powder had a smaller surface and the silver transport was not as good as for the medium grain size. This aspect correlated with the electrical performance of the solar cells obtained.

> "It is important that the silver powder and the redox potential of the additives are matched."

If the inorganic species has an oxidizing nature, the mass transport of silver in the glass phase can be enhanced. However, the etch process at the wafer surface is also improved by a greater quantity of silver oxide in the flowing glass. If the oxidizing capacity of the additive is too powerful, the electrical performance is negatively influenced. The impact of additives, however, is dependent on the silver particle size, so it is important that the silver powder and the redox potential of the additives are matched.

Acknowledgement

The authors are grateful for the financial support from the Sächsische AufbauBank for the 'KOMET' project (No. 1000694198).

References

[1] Ballif, C. et al. 2003, "Silver thick-film contacts on highly doped n-type silicon emitters: Structural and electronic properties of the interface", *Appl. Phys. Lett.*, Vol. 82, No. 12.

[2] Schubert, G. 2006, "Thick film metallisation of crystalline silicon solar cells", Ph.D. thesis, University of Konstanz.

[3] Hong, K.-K. et al. 2009, "Mechanism for the formation of Ag crystallites in the Ag thick-film contacts of crystalline Si solar cells", *Sol. Energy Mater. Sol. Cells*, Vol. 93, pp. 898–904.

[4] Eberstein, M. et al. 2012, "Sintering and contact formation of glass containing silver pastes", *Energy Procedia*, Vol. 27, pp. 522–530.

[5] Cho, S.-B. et al. 2010, "Role of the ambient oxygen on the silver thick-film contact formation for crystalline silicon solar cells", *Curr. Appl. Phys.*, Vol. 10, pp. S222–S225.

[6] Huh, J.-Y. et al. 2011, "Effect of oxygen partial pressure on Ag crystallite formation at screen-printed Pb-free Ag contacts of Si solar cells", *Mater. Chem. Phys.*, Vol. 131, pp. 113–119.

[7] Hilali, M. et al. 2006, "Effect of Ag particle size in thick-film Ag paste on the electrical and physical properties of screen printed contacts and silicon solar cells", *J. Electrochem. Soc.*, Vol. 153, No. 1, pp. A5–A11.

[8] Heinz, M. & Stiebing, M. 2013, "Modellierung der Nanopartikelbildung in Gläsern durch Kombination von optischer Spektroskopie und Röntgenkleinwinkelstreuung", *Proc. 87. Glastechnische Tagung*, Bremen, Germany.

About the Authors

Stefan Körner is a Ph.D. student at TU Dresden. He received his diploma in chemistry in 2012 from Chemnitz University of Technology, for which he carried out research, in cooperation with Leibniz IOM (Leipzig), on gold nanoparticles for biochemical applications. He currently works at Fraunhofer IKTS in Dresden in the thick-film technology and photovoltaics group, where he is investigating the contact formation between front-side metallization and multicrystalline silicon.

Kathrin Reinhardt is a Ph.D. student in materials science at TU Dresden. She received her diploma (FH) in chemical engineering from the University of Applied Sciences Dresden in 2006, and since then has been working in the thick-film technology and photovoltaics group at Fraunhofer IKTS. She began her Ph.D. at IKTS in 2010, on the topic of the relationships between rheological properties and deposition behaviour of highly filled suspensions.

Uwe Partsch studied electrical engineering at the Technical University of Dresden and received his Ph.D. in 2002 in the field of LTCC sensors. After working as a project and group leader in the area of LTCC integrated microsystems and multilayer ceramic fuel cells, he was appointed head of the Hybrid Microsystems department at Fraunhofer IKTS.

Markus Eberstein studied materials science with a special focus on glass at TU Berlin, and received his Ph.D. in 2001 in the field of microelectronics materials from the BAM Federal Institute for Materials Research and Testing, Berlin. He is currently the manager of the thick-film technology and photovoltaics group at Fraunhofer IKTS. The focal points of his research are structure–properties relationships of glass and ceramic thick-film materials, sintering kinetics, and dielectric and optical properties, as well as laser structuring of glass and ceramics.

Enquiries

Dr.-Ing. Markus Eberstein
Group Manager Thick Film Technology and Photovoltaics
Fraunhofer Institute for Ceramic Technologies and Systems IKTS
Winterbergstr. 28
01277 Dresden
Germany

Tel: +49 351 2553-7518
Fax: +49 351 2554-265
Email:
markus.eberstein@ikts.fraunhofer.de
Website: http://www.ikts.fraunhofer.de

The importance of backsheet quality for PV module longevity

Carrie Xiao, PV Tech China, translated by Huangye Jiang

ABSTRACT

Certain PV modules have begun showing signs of yellowing, a consequence of backsheet deterioration. This phenomenon can impact on power plant performance and safety, and is emerging as a potential problem waiting to happen with low-cost modules. This paper explores the key attributes of backsheets and assesses the relative benefits of the different types of backsheet on the market and the materials used in them. The different tests undertaken for backsheets are reviewed, and arguments are put forward for the requirement of a standardized testing regime for this crucial module component.

Introduction

Setting: a solar plant in Europe. The owner walks to the edge of the plant, and finds the PV modules are exhibiting a yellowish colour instead of the expected bright silver (see Fig. 1). Why had these supposedly good-quality modules changed colour? The owner queries the supplier, who replies: "It's perfectly normal – it's just like when people get tanned after long hours of sunbathing, no matter how much suncream they apply."

This does not relieve the owner's worries, so the supplier replaces the batch of modules that are most severely affected by the yellowing condition. In a subsequent analysis of the faulty modules, the source of the yellowing becomes clear: a key encapsulation material – the backsheet.

> "The appearance of yellowing of a module is a forewarning of cracking."

"For the most part, the appearance of yellowing of a module means a reduction in its transparency, and at the same time it is a forewarning of cracking," says David Li, sales manager of PV backsheet specialty products at Honeywell. "Backsheet yellowing is a widespread phenomenon, mostly found in areas of strong sunshine, such as Spain. The use of non-UV-proof EVA and backsheets leads to accelerated ageing; the module then takes on a yellowed appearance, affecting its lifetime."

Mr. Wei, the product manager at HT-SAAE (Shanghai Aerospace Automobile Electromechanical Co., Ltd.), has visited several plants in Europe, and confirms that many operators have encountered similar problems.

Conrad Burke, DuPont PV Solution's marketing director, bluntly warns: "Backsheets play an essential role in protecting modules; they are the electrical insulator between the modules and the surrounding environment. Defective modules could result in major disasters, cause unexpected power attenuation and compromise safety. Such a huge consequence may have a damaging effect on brand reputation, and even endanger human lives, and the issue needs to be given sufficient attention."

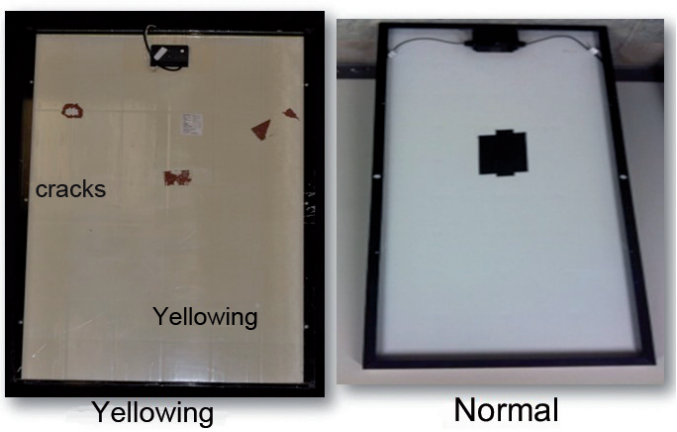

Figure 1. Yellowing and cracking of a PV module.

Ensuring the safety of modules and plants

Similarly to human beings, modules need to fight against ageing from UV. The light-induced degradation (LID) of modules must be reduced in order for them to keep running for 25 years. Consider the suncream analogy: the PV backsheet is the 'suncream' for a module – its quality therefore determines the module's ability to fight against UV and exposure.

Since most modules will be located in an outdoor environment, it is well known that UV, moisture, high or low temperatures, chemical gases, sand particles and various other external conditions will affect them. This is the reason why these conditions all feature in the tests of module components and materials. As a module's outer protection, a backsheet needs to be versatile in terms of its function.

Burke says: "In order to protect modules for 25 years, backsheets need to possess three key characteristics: weather resistance, mechanical strength and adhesion strength. At the same time, these three characteristics must be optimally balanced."

David Li explains: "Of the three key characteristics, weather resistance mainly consists of UV proofing, and the resistance to hydrolysis, high/low temperatures (temperature difference between day and night) and sand abrasion. These resistance properties could support a module's suitability for use in different geographic and climatic environments around the world. For example, in desert areas, which are sandy and hot, good backsheets could endure the physical abrasion from sand and other external sharp objects; in some fire-prone areas, fluoropolymer film-based backsheets could prevent fires and reduce safety concerns."

Mr. Wu, a technical consultant at Krempelm, adds: "Good backsheets should protect cells from the

surrounding environment, thus ensuring a high efficiency, and providing everlasting insulation protection."

Good-quality backsheets provide not only protection but also insulation: they prevent water vapour getting inside modules. Water penetration accelerates the degradation of ethylene-vinyl acetate (EVA) and the corrosion of conductive materials, thus impacting on cell efficiencies, lowering module power and even causing electricity leakage in the long term. All of these things could affect the power output of a module, as well as being potential hazards. Further studies have shown that a higher water vapour transmission rate in backsheets could lead to the acceleration of potential-induced degradation (PID).

Knowing the backsheet: material is the key

The quality of a backsheet is determined by its key material and by the structure of the materials used in it. DuPont categorizes backsheets into three basic types – double fluoropolymer, single fluoropolymer and non-fluoropolymer – and also defines many sub-categories within them. For the sake of simplicity, the market follows the two general categories of fluoropolymer and non-fluoropolymer.

> "The quality of a backsheet is determined by its key material and by the structure of the materials used in it."

David Li from Honeywell notes: "As a result of the severe squeezing of costs in recent years, backsheet companies have become very ambiguous about the fine line between fluoropolymer and non-fluoropolymer, because if a product contains some fluorine plastic, it could be deemed as fluoropolymer from a certain point of view. Nowadays, some backsheet coatings are claimed to be fluoropolymer, but the specific amount of fluoropolymer content is not known."

After considering all the information available, PV Tech observes the following categorization:

- First category: traditional fluoropolymer film-based compound backsheet (such as TPT, TPE, KPK, KPE, single-side THV).
- Second category: PET-like non-fluoropolymer backsheet.
- Third category: fluoride-coated backsheet.

Of these three types, the first is already in production and being used in the industry, which means it is more reliable and traditional; suppliers in this category include DuPont, Taiflex, 3M, Arkema, Honeywell, Toyo Aluminium, and Cybrid from China. It is noteworthy that DuPont and Arkema do not manufacture backsheets, but only the essential materials used in them: DuPont has its branded fluoropolymer products – Tedlar PVF film – and Arkema supplies Kynar PVDF film. Honeywell and 3M, however, are involved in the entire fluoropolymer supply chain. More details can be found in Table 1.

Why fluoropolymer films?

"Because good-quality fluoropolymer films resist ageing from external UV, backsheets made from these materials are not affected very much by UV, and the products have better resistance to the weather," explains David Li. "Whether a backsheet will last for 25 years depends on the molecular structure of its key materials. A fluoropolymer is made through high-temperature melting, after which high polymers form a complete film that is not easy to damage."

Regarding non-fluoropolymer PET – or polyester – backsheets in the second category, whose usage has been increasing in recent years, Li says the early products had a guaranteed lifetime of only 10–15 years – and that was just for rooftop use, where conditions are not so harsh. "Later, PET material manufacturers made some improvements, such as adding in some anti-UV reagents in order to delay the harm by UV rays to some extent; however, that process could not change the nature of polyester materials. Nowadays, Japan has extended its requirement for module lifetime to 20 years, leading to many Japanese module manufacturers changing their choices for backsheets."

It has been reported that non-fluoropolymer PET backsheets yellow after ageing by UV light and are prone to the risk of delaminating cracks. However, the manufacturing companies in the second backsheet category – such as Toray from Japan and Coveme – have different ideas. They believe that PET backsheets benefit from a low cost and are easy to process, while offering high adhesion between the layers and therefore having few problems with appearance.

There is only one issue on which compound backsheets suppliers and PET non-fluoropolymer backsheets suppliers agree – a problem which concerns fluoropolymer-coated backsheets: current backsheets coated with fluorocarbon ethyl vinyl ether (FEVE) are formed by chemical cross-linking, resulting in a relatively sharp mechanical form and poor wear-resistance properties, which makes them unsuitable for plants in west China, where there are strong winds and large amounts of sand.

FEVE-coated materials form a layer with a lower mechanical strength on the PET surface; thermal expansion and contraction may cause plastic materials to crack, and in certain areas where there are huge temperature differences and high humidity, backsheets easily become detached. In spite of that, PV newcomer Fuji Film has introduced a new backsheet product. One of the company's executive officers, Yoshihisa Goto, says its new backsheet enhanced by a glue-free coating employs two patent technologies which the company has used in camera films: one is enhanced PET-based film-manufacture technology, and the other is glue-free-coating precision-moulding technology. Goto also says: "The new backsheets use enhanced PET (hydrolysis resistant) at the backsheet interface instead of adhesive. These PET materials are UL certified for long-term usage under high temperatures (RTI values at 130°C), and are 250μm thick." Compared with traditional compound TPE backsheets, Fuji believes that, even after accelerated ageing tests, its backsheet products have the benefits of still maintaining the same power efficiency, the same water vapour transmission rate, the same breakdown voltage, and the same high weather resistance and safety levels.

Jiangsu Serphim Energy has employed Fuji Film's new backsheets. Peng Jin, CTO of Serphim, says the company tested many different backsheets last year and finally chose Fuji's material for the modules it later sold to Europe; the megawatt amount has now reached double digits.

As for fluoropolymer backsheets, their development and success have a close relationship with the whole market. In previous years, when the PV market was flourishing because of strong demand for PV backsheets in China, fluoropolymer films, especially DuPont's Tedlar PVF films, were in short supply. In response, companies came up with solutions for backsheets that do not use fluoropolymer films, but instead use fluoropolymer coatings on PET films; such backsheets have not only made it easier for companies who want to dabble in the backsheet industry, but also resulted in lower prices. At the time of writing, Jolywood and UM Technologies were the main suppliers of fluoropolymer-coated backsheets.

Backsheet type	Material structure	Company	Role	Price
I. Fluoropolymer film-based compound backsheets	*Double-side fluoropolymer* ①TPT Tedlar PVF/PET/Tedlar PVF ②Double-side PVDF PVDF/PET/PVDF (KPK) *Single-side fluoropolymer* ①TPE Tedlar PVF/PET/Tie Layer ②Single-side PVDF PVDF/PET/Tie Layer (KPE) ③Single-side ECTFE ECTFE/PET/Tie Layer ④Single-side THV THV/PET/EVA ……	DuPont	Fluoropolymer films supplier; the only supplier of Tedlar PVF, bought by Tailflex (Tailflex Solmate), SFC and Kempel for their compound backsheets. (T stands for DuPont Tedlar; DuPont states that only the backsheets using DuPont Tedlar PVF are truly TPT and TPE backsheets.)	High, with a 5–10% fluctuation range within the category Products from different suppliers have different characteristics
		Arkema	Fluoropolymer films supplier, providing Kynar PVDF fluoropolymer films; the K in KPK stands for Arkema Kynar PVDF.	
		Honeywell	The entire production chain of fluoropolymer films (Honeywell PowerShield ECTFE fluoropolymer films, backsheets).	
		Toyo Al	Backsheet supplier – procures the PVDF.	
		3M	Fluoropolymer films and backsheets (THV), currently selling a few non-fluoropolymer backsheets.	
		Krempel	Backsheet supplier – procures films from Arkema and DuPont.	
		Isovoltaic	Began with fluoropolymer backsheets, and has now turned to other materials.	
		Cybrid	Backsheet supplier – recently supplied KPF backsheets, with fluoropolymer films purchased from Arkema and SKC (Cybrid states that it could choose multi-materials, including PVF); sells a few PET backsheets.	
		Lucky Films	Backsheet supplier – procures fluoropolymer films.	
II. PET/partial PET non-fluoropolymer backsheets	PET polyester backsheets PET/PET/Tie Layer HPET Hydrolysis-resistant polyester HPET/HPET/Tie Layer	Coveme	Backsheet supplier – procures PET.	Medium, with fluctuation
		Toray	Material supplier, providing PET and backsheets.	
III. Coating-base and other backsheets	Coating/PET/Coating (Jolywood and UM use FEVE; LG uses PVDF) Coating/PET/Tie layer (Fujifilm)	Jolywood	Backsheet supplier.	Low
		UM	Backsheet supplier (HFF).	
		Fujifilm	Backsheet supplier.	Medium
		LG	Backsheet supplier.	Low
	PA/PA/PA nylon structure and other new materials	Isovoltaic	Backsheet supplier.	Low

Table 1. Backsheet types and some of the main material suppliers (the backsheet quality varies).

Which standards and tests are the most sensible?

Although there is some debate about which types of backsheet perform best, the distinction between them is becoming blurred. Each category has its suppliers and their supporters, who are trying to convince their customers to have confidence in and employ their products. Since there is currently no unified standard or recognized testing, all backsheet products could find their own breeding ground.

In relation to actual outdoor conditions, backsheet products need to be tested with respect to six aspects: UV light, temperature, humidity, environmental corrosion, electrical insulation and physical protection. It is believed that the current international standards are several years behind, failing to keep up with backsheet requirements. The tests for backsheets are normally done along with module testing, and the current criterion is IEC 61730, during which only the partial discharge property is tested.

To highlight the property advantages of a particular brand, there are numerous other tests on the market. "There are tests from certifying organizations, but the testing methods are not unified and overly promote a single performance indicator; new products are being introduced all the time, but only one or two of them have proven long-term outdoor usage experience. Currently, Krempel leads the march of progress in standardizing IEC backsheet criteria," Mr. Wu from Krempel tells *Photovoltaics International*.

"Some emerging companies have underlined the advantages of their products by performing tests that are several times more punishing than those in IEC testing," says Dr. Fu Bo, R&D director at DuPont (China). "However, the point is whether these tests are sensible. Some tests are called 'accelerated ageing tests' and are carried out under the conditions of PCT60-90hr (121°C/100%/2atm); a temperature of 121°C, however, is not appropriate for testing outdoor ageing – it should instead be considered to be 'destructive testing'.

"The purpose of testing is not to damage the products under extreme unusual conditions, but rather to expose

them to close-to-outdoor conditions and simulated actual application environments, which is in accordance with the testing requirements of accelerated ageing conditions, but is lacking from current certification processes. The current certification tests for backsheets overstate the hydrothermal ageing tests but understate the UV ageing tests. There is no need to perform so many hours of hydrothermal ageing tests."

> "The current certification tests for backsheets overstate the hydrothermal ageing tests but understate the UV ageing tests."

Dr. Fu identifies a number of tests that would be useful for backsheets, one of which is a long-term UV ageing test. "In order to achieve 25 years' lifetime, backsheets need to undergo 275kWh/m^2 UV exposure for a desert environment, or 171kWh/m^2 for a milder climate. This test could single out those materials that are unable to resist UV ageing, and could reveal the potential risks of yellowing and cracks," he says.

A second regime would be a comprehensive ageing test, in which backsheet materials are tested against UV, temperature, humidity and multi-stress ageing in environments that resemble actual outdoor conditions. A third would be a sequence ageing test – for this a backsheet is subjected to thermal cycles after UV exposure. "This method could better simulate the impact of temperature differences between day and night, as well as between seasons, after the effects of outdoor ageing have taken their toll," says Dr. Fu. His final proposal is a test for conditions such as sand abrasion and chemical corrosion in environments characteristic of, for example, seashores, livestock sheds and industrial cities.

The current IEC certification tests do not include a UV ageing test or a weather-resistance test: the UV light intensity used in the IEC certification tests only equates to 70 days' outdoor exposure, and there is no requirement for such tests for the back side of a module. To solve this problem as soon as possible, many material suppliers, such as Krempel and DuPont, are discussing the need for a revision of the IEC standards for backsheets. Revising standards, however, takes time, and during the period of revision it is entirely up to the individual companies whether or not they act in accordance.

Costs determined by the technical roadmap

Since no single standard exists and there are lots of confusing tests, the market in PV backsheet production is increasingly being overrun by local companies. With production being localized, competition has flourished in recent years and, along with international top-tier material suppliers, many domestic backsheets companies are emerging.

Every backsheet company makes its own choices of materials and product structures; the market has therefore been flooded with a multitude of backsheet products. The immediate result of this has been a turbulent market and chaotic pricing. It is known that the price battle between backsheet companies is extremely fierce, with prices ranging from RMB10/m^2 to RMB30/m^2 (approximately US$1.64–4.92/m^2). On top of that, there is a tremendous variation in quality. Although the market in backsheets has been broken into, the actual essential materials are not something every company is capable of possessing because of large technical obstacles, and consequently these materials are mostly controlled by international suppliers.

Costs are determined by the technical roadmap, and therefore prices will vary. The first category, fluoropolymer backsheets, has the highest prices: 10 to 15% higher than PET backsheets, and the prices vary within the category. As for fluoropolymer-coated backsheets, the prices of some of the new types are relatively low. Within the three categories there are different price groups, and hence pricing gaps: the difference in costs is therefore magnified. Under pressure to reduce costs, manufacturers have brought down the price of fluoropolymer backsheets over the last few years. Some manufacturers have reduced the thickness of the

Conditions	Times	Testing Items	Measuring Units	Testing Standards	Results		
					●	●	●
Outer Layer UVA	>3000h	Yellowing (Junction Box Side)	Δb*	ASTM E308	≥2	<2	<1
	>3000h	Elongation	% Loss	ASTM D882	≥80%	<80%	<50%
Outer Layer UV - Xenon	5000h	Inner Layer Stability	n/a	Visual	Cracked	Slightly Cracked	Good
Damp Heat	1000h	EVA Adhesion	% Loss	ASTM D903 (180 deg) ASTM D1876 (t-peel)	≥50% or Break	<50%	<20% or Glass Peel
	1000h	Elongation	% Loss	ASTM D882	≥80%	<80%	<50%
Thermal Exposure	Varies	Inner Layer Softening Temp.	°C	JIS K7196	n/a	<170	>170
Initial	0h	Coefficient of Thermal Expansion (MD, TD)	(μm/C*m)	Internal	≥100 (MD or TD)	<100 (MD or TD)	<50 (MD or TD)
Outdoor Performance	Varies	Years Used in PV Backsheet*	Years	n/a	<20	n/a	≥20

TEST/PROPERTY DETAIL

Damp Heat: 85°C, 85% RH.
UVA: 70°C, QUV 340 nm, 1.2 W/m²-nm at 340 nm, continuous.
Xenon: ASTM G155 cycle 7A (modified), Xenon .55 W/ m²-nm at 340 nm, daylight filter, 65 BPT, continuous, no water spray.
CTE: -40°C tp 85°C.
*For non-TPT™ backsheets, numbers shown are based on commercial introduction from Photon 2011 Survey.

Figure 2. Testing and valuation standards for PV backsheets suggested by DuPont.

fluoropolymer films in response to price declines; if the reduction is beyond a reasonable range, however, it could have a huge impact on backsheet quality.

"I do not agree in cutting costs by cutting back on the amount of material used in products. Nowadays, the whole industry remains competitive through reducing, and just as with 'white goods' the trend is a vicious cycle," says Mr. Wu from Cybrid. Costs should be cut by technology innovation, he believes, highlighting Cybrid's newly developed Flursoskin technology, an upgrade of the KPE products.

Mr. Wu goes on to say that KPE products were developed and patented by Cybrid in 2010, and first used by Trina Solar and later by other backsheet companies. During their use, however, problems emerged, including poor UV resistance, which prevented the KPE film from playing its protective role in addition to other roles of the product in the long term.

In the area of domestic backsheet production, along with Cybrid and HIUV, another company – Jiangsu Gorichen New Materials – has begun to manufacture backsheets; its FPE backsheet film has passed CPVT (National Centre of Supervision and Inspection on Solar Photovoltaic Products Quality) tests. It is said that Gorichen's backsheet oriented itself as a fluorine-based compound backsheet, employing PVDF materials from KUREHA, whose PVDF materials have a proven track record of almost 30 years as a fluorine weather-resistant layer in certain applications.

According to Lux Research, the current demand for materials used in crystalline silicon modules is the largest market opportunity, with US$23.8bn expected to be reached by 2018. Backsheets, non-EVA laminations, metallization coatings and anti-reflection coatings for module glasses are the specific areas having innovation initiatives and being key to product quality. It is this market opportunity that is attracting ever more material suppliers, such as the entry of Fuji Film into the solar industry. Newcomers will further agitate this specific niche of the market, and downstream module manufacturers and plant operators will need to pay particular attention to it.

Backsheet usage by companies

The diversification of backsheets has a direct impact on the downstream industry: module companies can now choose from many different backsheet suppliers.

According to research published in *Photovoltaics International*, most mainstream module manufacturers – including Yingli, CSUN, Canadian Solar, JA Solar, Suntech, Renesola, Tianwei, HT-SAAE and Sunowe – currently choose compound backsheets, whose market share was 68% in 2011–2012, followed by PET backsheets with 20%. Fluoropolymer-coated backsheets accounted for 7%, with the remainder at 5%.

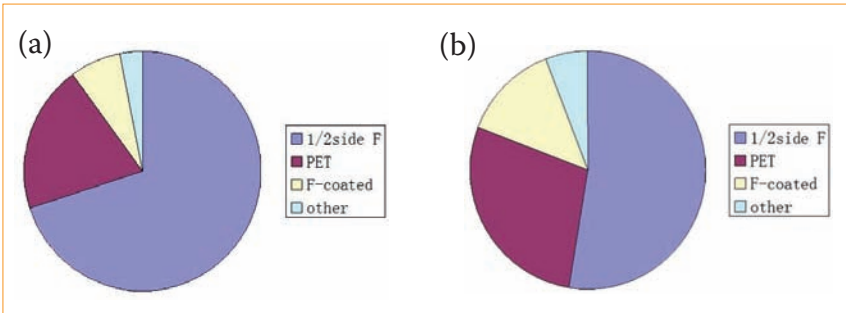

Figure 3. Market share trends for different backsheets: (a) 2011; (b) 2012.

As indicated by data, the market share of PET backsheets rose significantly in 2012 because of the influence of the market and pricing. Other large companies – including Trina Solar, Hareon Solar and Talesun – have turned to PET non-fluoropolymer backsheets for some of their products and also to the fluoropolymer-coated backsheets: as a consequence, the market share of compound backsheets has declined (see Fig. 3). According to feedback from module manufacturers, the type of backsheet they choose relates, to some extent, to the market they are supplying. Moreover, backsheets in the different categories demonstrate different results in the various certification tests, and sometimes a certain property is the key criterion for a specific market.

Another crucial factor affecting the change in market share is price. In recent years a vicious cycle of buying has become apparent among Chinese module manufacturers because of the pressure to rapidly cut costs. They probe into the materials used by their competitors and compare prices with fellow companies; this information is then used as the rationale for buying materials. As mentioned above, the three categories of backsheet have three price ladders; in particular, compound backsheets are much more expensive than those in the other two categories, so it is not difficult to understand why backsheets of poorer quality and thus higher risk might be used.

Conclusions: precautionary action

If the condition of backsheets and other key components and materials is taken into account, it is expected that within a few years, there could be an explosion of issues with modules as they present with the kinds of problem outlined at the beginning of this paper. Parts of China, for example Qinghai, are considered high risk areas for backsheets because of the strong UV light, dry air and huge temperature differences, all of which could be fatal to backsheets, which might begin to suffer from cracking.

Many plant operators are beginning to pay serious attention to the problem. Some of the major power companies in China, for example, have specified that Tedlar PVF TPT backsheets be used by module suppliers for deployment in western China. Despite the high price per square metre, backsheets that are able to endure an outdoor usage of 25 years will, in the longer term, have an ROI that is still higher than that achievable with other backsheets.

But the rest of the industry needs to remember that PV plants are long-term capital projects, requiring huge investment and a long ROI period. PV manufacturers should not, for the sake of a better bidding price, cut corners and carelessly rush out key components of the plant. How long PV plants made of such components will last could have a direct impact on the development of the entire PV industry.

> "When problems are reported, it is already too late – for a plant designed to run for 25 years, precautionary action is far more important."

In the case of the PID phenomenon, no one cared about it until reports of problems in plants emerged and brought the issue into the spotlight. But when problems are reported, it is already too late – for a plant designed to run for 25 years, precautionary action is far more important.

Cell Processing

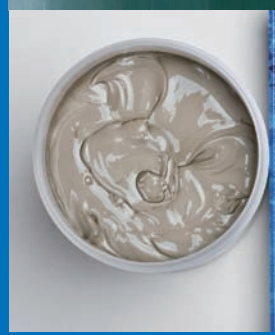

News

Yingli Green details long-term cell efficiency roadmap to 2020

Yingli Green Energy has provided a window into its longer-term cell efficiency roadmap to 2020, having previously only provided its solar cell roadmap to include planned development to the end of 2015. The chart also included higher cell efficiency targets for commercial-scale production of multicrystalline cells compared to previous guidance. The roadmap chart projects commercial-scale p-type multicrystalline cell efficiencies from 17.6% in 2013 to 19% in 2020. Lab-based efficiencies of multicrystalline cells would be only 1% higher (20%) by 2020, consistently closing the gap between lab and real world fab production cells, which stood at almost 2% difference in 2012. In 2011, Yingli Green reported an average cell conversion efficiency rate of 19.0% on PANDA production lines, which used N-Type wafers and a record cell conversion efficiency rate of 20.0% on the PANDA trial production line. The new roadmap for PANDA cells continues a steady trajectory of improvements for both lab and fab-based cells through 2015. Significant improvements are being planned in the 2016/17 timeframe, although the biggest gains are expected during 2020 when efficiencies of the PANDA cell are targeted are reaching 23% in commercial production. Again, lab to fab differences would have narrowed to just 1%.

Yingli Green has published a roadmap setting out its cell efficiency plans to 2020.

Cell efficiencies

Spectrolab sets new world record for solar cell efficiency

Spectrolab has set a new solar cell efficiency world record for a non-concentrated solar cell of 38.8% and in doing so has beaten the company's own previous record of 37.8%, set in April. Best known for supplying multi-junction solar cells and panels for concentrated photovoltaic (CPV) applications, satellites and spacecraft, Spectrolab developed the new cell from Boeing semiconductor bonding technology. The cell could be used on high power spacecraft and unmanned aerial vehicles. The record 38.8% conversion efficiency has been verified by the US Department of Energy via its National Renewable Energy Laboratory in Colorado. Research analysts Lux Research predicted last year that by 2022, Spectrolab cells could reach 50% efficiency. Spectrolab is part of Boeing Defense, Space and Security.

AVACO unveils new buffering layer to enhance conversion efficiency AVACO, a specialist manufacturer of sputtering (PVD) vacuum deposition equipment and atomic layer deposition (ALD) equipment, has announced the development of a new concept buffer layer deposition for photovoltaic cells. By using its atomic layer deposition (ALD) process, AVACO claims to have improved energy conversion efficiency to approximately 30% higher than the conventional CIGS solar cell that uses Cds for the buffer layer.

Imec and Meco present high-efficiency i-PERC-type silicon solar cells

Belgian nanoelectronics research centre imec and semiconductor plating equipment supplier Meco presented its high-efficiency i-PERC-type silicon solar cells at EU PVSEC. On show was a large area (156mm x 156mm) cell with Nickel/Copper plating on the front contacts that the companies claim has achieved an average efficiency of 20.5% and a maximum efficiency of 20.7%. The cells were processed on imec's solar cell pilot line using Meco's inline plating tool to deposit the Ni/Cu front contacts.

The metallization process of the Ni/Cu stack included Ultraviolet (UV) laser ablation, sequential in-line plating of the metal layers and contact annealing. The resulting i-PERC solar cell achieved an average efficiency of 20.5% on more than 100 cells with a very low standard deviation of only 0.1% and an average fill factor of 80%, validating the high quality of the front contacts.

Cost reduction

DEK Solar and ISFH use 'Dual Print' process to achieve silver cost less than US$0.01 per Wp

Having continued to optimise its latest 'Dual Print' stencils and screens to provide fine-line front side silver contacts, DEK Solar, in conjunction with the Institute for Solar Energy Research Hamelin (ISFH) has reduced metallization silver cost to below US$0.01 per Wp, while achieving a 20.2% cell efficiency on a PERC solar cell. The work utilised ISFH's PERC cells and DEK Solar's Eclipse metallization platform as well as its Dual Print screens and stencils and optimized frontside silver metallization pastes from Heraeus.

Spectrolab has set a new record for non-concentrated cell efficiency.

Previous work has resulted in 19.8% cell efficiencies with only 67.7mg of Ag per wafer. Increasing paste quantity by only 7mg resulted in the record conversion efficiencies, according to the company.

3M backside busbar tape reduces silver paste requirements

3M Renewable Energy has launched its latest backside busbar tape, '4706' which allows manufacturers to eliminate silver-based backside busbars.

The tape can be bonded to aluminium pastes, commonly used on the back surface of crystalline solar cells, and provides reliable, low-resistance electrical contact comparable to backside silver busbars, providing potential to improve absolute efficiency by approximately 0.2%, according to the company.

The tape is a copper foil tape coated with a high-performance heat-curable adhesive on one side, with preliminary tests demonstrating a stable long-term electrical performance in damp heat and thermal cycling.

Heraeus develops customised back-side tabbing paste for Taiwan market

The Heraeus Photovoltaics Business Unit has launched a customised back-side tabbing paste, especially developed for the Taiwan market. The PV materials specialist said that the back-side tabbing paste, 'SOL203T', exhibited 15% less paste and 25% less silver usage per cell while maintaining the required adhesion.

The company also noted that its front-side paste, 'SOL9610M', offered improved overall performance and continued to gain strong market acceptance in Taiwan. Heraeus said that it also demonstrated a 1% improvement in efficiency over previous generations of pastes for n-type solar cells with the combination of SOL9350 and SOL9610 Series for the p+ and n+ wafer surfaces respectively.

Hanwha SolarOne reduces silver paste consumption by 45%

With its evolutionary E-STAR II cell in production, Hanwha SolarOne said that upgrades enabled a silver paste consumption reduction of up to 45%, while improving cell conversion efficiencies by 0.2 to 0.25%.

Through its 'Project EStarII' production enhancement strategies, the module manufacturer says it is aiming to lower production costs, improve cell efficiencies, enhance product features and improve quality and yield. Hanwha SolarOne's capacity has remained unchanged for two years at 800MW for ingot and wafer production and 1.3GW for cell production.

The company has a nameplate capacity for modules of 1.5GW, compared to rivals that mostly have capacity of 2GW and higher. The company has however reduced labour costs with a shift to fully-automated processes that have also improved product quality consistency as well as using thinner glass and thin frames to reduce BOM costs.

Heraeus has developed a back-side tabbing paste for Taiwan market.

DuPont improves lightly doped emitter performance with frontside silver paste

DuPont Microcircuit Materials has enhanced the performance of its 'Solamet' PV18x series frontside silver metallisation materials for monocrystalline wafers employing enhanced Lightly Doped Emitters (LDEs).

Providing optimised LDE performance was said to be "a strong differentiator" for PV cell producers as Solamet PV18A demonstrated efficiency gains with finer lines and lower laydown than previous iterations. DuPont noted that it was also developing diffusion recipes in-house aimed at boosting cell efficiencies beyond 19.3% already demonstrated on monocrystalline wafers that use the lasted PV18A silver paste.

Company news

Neo Solar Power posts rising profits on increased demand for solar cells and modules

Neo Solar Power (NSP) has reported that accumulated net profits for the first nine months of 2013 reached NT$200 million (US$6.8 million) as demand, higher ASPs and high utilisation rates continued.

Following the merger with DelSolar earlier in the year, NSP reported third quarter revenue (including Del Solar module sales) of NT$6,386 million (US$216 million), a 57% increase quarter-on-quarter.

The company noted that demand was increasing from customers in Japan, United States, and China, as well as in emerging markets. In the third quarter, NSP raised NT$4.1 billion to support liquidity requirements and capacity expansions.

However, the company said that it would be undertaking retro-fit and upgrades to existing manufacturing lines to cautiously add needed capacity to meet market demand.

Centrotherm booked new orders totalling €163.2 million in revised accounting period

The centrotherm Group secured new orders totalling €163.2 million (US$222 million) during its restructuring period between October 2012 and May 2013. New orders booked included €123.2 million (US$167.7 million) within its silicon segment, which accounted for the majority of backlog. The company did not provide expected shipment schedules on its order intake. The company said it had also received new orders in its photovoltaics and semiconductors segment totalling €35.4 million (US$48.2 million) and received new orders totalling €4.5 million (US$6.11 million) in its Thin Film & Customized Systems segment. Centrotherm noted that due to its restructuring efforts it had liquidity of around €110.0 million (US$149.8 million) as of 21 October 2013, enabling it to continue operations and investment in R&D in anticipation of a recovery in equipment purchases from the PV industry.

Uptick in interest but no orders from solar manufacturers for BTU International

BTU International has reported third quarter net sales of US$12.0 million, down 15.7% compared to US$14.2 million in the preceding quarter, as little sales activity was generated from the PV sector. Management noted that despite downstream PV demand growth, customers had yet to place orders as utilisation rates continued to increase.

The company also reported higher than expected losses of US$5.1 million in the third quarter of 2013. BTU International said that it expected revenue in the fourth

quarter in the US$13.5 million to US$14.5 million range but added that gross margins would continue to be affected by under absorption factory utilisation, due to the absence of solar customer demand.

Applied Material's results positive but solar division scales back

Applied Materials has reported positive results while also revealing that it has diverted resources away from its solar operations. The company plans to merge with Tokyo Electron next year and the company's executives indicated that its solar division is becoming less of a priority. In 2013 the company reduced solar spending by about US$120 million and reallocated dollars from solar to semi and from overheard to products. The saving in spending on solar plus US$40 million in overhead savings has been put into R&D programmes within SSG [the company's advanced chip group]. Applied Materials' Energy and Environmental Solutions (EES) group, which houses the solar division saw sales slide by 59% to US$173 million.

R&D news

Hanwha Q CELLS qualifies Aurora's Decima CD inline metrology tool

After an extensive evaluation period, Hanwha Q CELLS has qualified for production purposes the use of ACT Aurora Control Technologies inline Decima CD metrology tool. Hanwha Q CELLS has also installed a Decima system at its advanced production facility in Germany, according Aurora, which was said to be in operation for monitoring cell quality during cell processing. Aurora said that it would continue to work with Hanwha Q CELLS in a development partnership to further advance the Decima technology and its applications.

IHS raises capital spending forecast amid PV industry demand and high utilisation rates

Global capital spending in the PV industry is expected to increase at a higher rate than previously expected, argues market research firm IHS. Higher end market demand and severely restricted CapEx over the last two-years has seen manufacturers up and down the supply chain experience higher utilisation rates, which will fuel a recovery in capital spending in 2014 and through 2015, IHS said.

PV producers are expected to spend in the region of US$3.3 billion on expanding capacity to meet demand, a 42% increase over 2013 spending, and higher than IHS' previous forecast of spending increasing 37% next year. IHS also expects strong CapEx increases in 2015, rising 32% from 2014 to reach US$4.3 billion - a major upgrade from the market research firm's previous forecast of only 5% growth over 2014. However, IHS continues to believe that the current outsourcing trend is simply a fad, in contrast to rival market research firm, NPD Solarbuzz.

UNSW to lead major Asian-based solar cell manufacturer R&D initiative

Professor Stuart Wenham at the University of New South Wales (UNSW) is leading a new PV cell processing initiative with many of the largest Asia-based cell manufacturers to improve silicon quality and cell performance. Wenham said that most of the largest cell manufacturers in China, Taiwan, Korea and Singapore would collaborate with UNSW on a hydrogen passivation process with modified production equipment intended to boost silicon quality and potential boost cell efficiencies at low cost.

Around 10 large cell manufacturers have signed up to the R&D programme, which will also include collaboration with key equipment suppliers from Europe. Unlike a typical university-led next-generation technology, initial implementation of the new process is being fast tracked.

Product Reviews

3M Renewable Energy

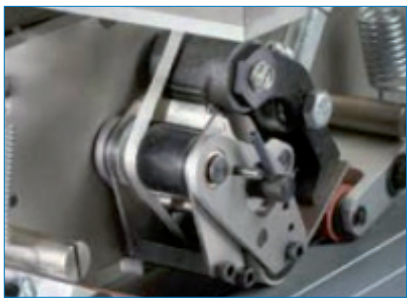

3M backside busbar tape reduces silver paste requirements

Product Outline: 3M Renewable Energy has launched its latest backside busbar tape, '4706', which allows manufacturers to eliminate silver-based backside busbars, enabling cost savings and protecting against the volatility of silver prices.

Problem: The reduction in silver paste consumption has been a key driver in solar cell processing cost reduction strategies. Replacing conventional deposition techniques that require long heat and cure cycles could reduce processing time and material usage.

Solution: The 4706 backside busbar tape can be bonded to aluminium pastes, commonly used on the back surface of crystalline solar cells, and provides reliable, low-resistance electrical contact comparable to backside silver busbars, providing potential to improve absolute efficiency by approximately 0.2%, according to the company. The 4706 tape can be incorporated into existing manufacturing processes with an automated tape bonder. The fast-curing thermoset adhesive enables high productivity to match typical cell manufacturing processes. These cells can be inter-connected using standard tabbing and stringing operations in typical panel manufacturing.

Applications: Crystalline silicon backside busbars.

Platform: The 4706 tape is a copper foil tape coated with a high-performance heat-curable adhesive on one side, with preliminary tests demonstrating a stable long-term electrical performance in damp heat and thermal cycling.

Availability: October 2013 onwards.

Heraeus

Heraeus offers metallization pastes for n-type solar cells with improved line uniformity and aspect ratio

Product Outline: The Heraeus Photovoltaics Business Unit has launched a new family of pastes for the metallization of bifacial n-type solar cells. The new SOL9350 Series is claimed to enable increased cell efficiency and improved printability.

Problem: N-type monocrystalline solar cells offer the highest potential conversion efficiencies, however the metallization process using screen printing and the firing furnace through technique can limit the open circuit voltage (VOC) of such cell types. Metallization pastes used to contact boron emitters have the most impact on the cell VOC.

Solution: The SOL9350 Series is said to represent the latest generation of Ag-Al conductor pastes for contacting boron emitters for high-efficiency n-type solar cells. Processing improvements include excellent flooding and low bleeding for easier handling. The performance improvements of the paste in turn help to print finger lines with improved line uniformity and aspect ratio. The SOL9350 Series can print through narrower finger line openings and provide high line uniformity. This in conjunction with lower contact resistances and minimized cell damaging is claimed to provide the highest performance for high-efficiency n-type solar cells.

Applications: Bifacial n-type solar cells.

Platform: The Heraeus Photovoltaics Business Unit offers a package of pastes for bifacial n-type solar cells: for p+ wafer surfaces as well as for n+ surfaces. Their current recommendations for n-type solar cells are the Ag-Al conductor SOL9350 Series for p+ emitter in conjunction with the Ag conductor SOL9610 Series or lower Ag content SOL9300 Series for the Back Surface Field (BSF).

Availability: September 2013 onwards.

SoltaBond

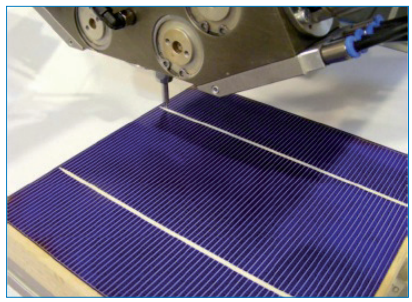

SoltaBond provides electrically conductive adhesives to reduce costs in c-Si PV modules

Product Outline: SoltaBond has developed a variety of optimized conductive adhesives. By carefully matching the adhesive properties to different surfaces, these new adhesives, such as 'SB 1227' are especially suitable for the variety of new cell concepts, such as back contact, heterojunction thin cells, or Cu-galvanic cells, and allow for cost reductions.

Problem: Due to pricing pressures there is strong interest in bringing new cell concepts to the market with higher conversion efficiencies. However these cell concepts require new contacting technologies as opposed to conventional soldering that must also be cost competitive.

Solution: SB 1227 reliably bonds to TCO and low temperature screen print paste used on Heterojunction cells. Fast cure adhesive versions allow processing temperatures as low as 100°C, which are claimed to considerably reduce the thermal stress and have been successfully tested on 40µm thin wafers. Such low temperature adhesives are also especially suitable for back contact cells, as they substantially remove the bow effects. SoltaBond adhesives are said to provide improved bond strength on silicon nitride and therefore allow for removal of screen printed busbars. The removal of busbars makes it possible to use stencil printing instead of screen printing, which leads to reduced finger width and higher aspect ratio.

Applications: Conductive adhesives for c-Si back contact, heterojunction cells, or Cu-galvanic cells.

Platform: SoltaBond conductive adhesives form reliable bonds to electroplated Ni/Ag or Ni/Cu fingers.

Availability: Currently available.

Technologies for mass production of PERC and MWT solar cells

Sebastian Mack, **Benjamin Thaidigsmann**, **Elmar Lohmüller**, **Andreas Wolf**, **Florian Clement**, **Marc Hofmann**, **Ralf Preu** & **Daniel Biro**, Fraunhofer Institute for Solar Energy Systems (ISE), Freiburg, Germany

ABSTRACT

Over the last few years several technologies have been investigated with the aim of reducing recombination in emitters and at passivated surfaces. Because of its high efficiency potential, the passivated emitter and rear cell (PERC) design is of interest to both cell manufacturers and R&D institutes all over the world. Another cell design of interest is the metal wrap-through (MWT) solar cell, where the absence of front busbars leads to reduced shading. The MWT technology, especially when combined with rear-surface passivation, has the potential to significantly decrease the cost of ownership of today's solar cells. This paper gives an overview of the current status of the production technology for the fabrication of PERC and MWT-PERC solar cells, as well as a summary of recently published papers in this field.

Introduction

Since the initial work of Blakers in 1989 [1], many research institutes, universities and R&D departments have reported on progress in surface passivation, simplified process sequences and novel technologies targeted at an industrial fabrication of high-efficiency p-type passivated emitter and rear cell (PERC) structures [2,3]. Whereas the front side of PERC-type cells, and of standard H-pattern silicon solar cells with an aluminium back-surface field (Al-BSF), is identical, the former feature a dielectrically passivated rear surface with local contacts. A different solar cell structure that addresses changes in the front contact layout is the metal wrap-through (MWT) concept [4], in which the external busbar contacts are moved from the front to the rear, resulting in reduced shading. To benefit from reduced shading, only one additional process step – namely via drilling – is necessary for combining MWT with PERC [5] to yield high-efficiency MWT-PERC structures.

Since both MWT and PERC structures attract increased market attention owing to their high conversion efficiencies, this offers the possibility for increased €/Wp module prices and yet potentially reduced system cost with these premium products.

In recent years solar cell and equipment manufacturers have suffered from massive overcapacity in the PV market. The resulting decrease in the cost of solar modules wiped out margins and led to several companies leaving the PV business. The dramatic fall in price of solar modules has only recently slowed, let alone stopped. An increasing book-to-bill ratio of equipment vendors indicates that there might be some light at the end of the tunnel. Some forecasts anticipate increased equipment orders in 2014 for new production lines or for the retrofitting of existing ones.

This paper presents a brief overview of the different equipment that might be included in these lines for the fabrication of PERC and MWT-PERC solar cells; an update of recently published papers is also given. The scope of the paper is limited to solar cells fabricated from p-type silicon wafers; for an overview of n-type technology, the reader is referred to a recent article by Kopecek and Libal [6].

Solar cell structures

Fig. 1(a) shows a schematic cross section of a standard p-type Al-BSF solar cell with a full-area aluminium rear contact; an industrial p-type PERC solar cell with a passivated rear side and local contacts is shown in Fig. 1(b). The front side – namely the texture, emitter, anti-reflective coating (ARC) and front grid – of both solar cell structures is identical and may feature a selective emitter (SE).

Fig. 2 (top) shows the most prominent MWT structures without and with rear-surface passivation. In an attempt to further streamline the process sequences and reduce cost, new structures that omit the emitter on the rear and/or in the via have been developed (Fig. 2, middle and bottom): these have been proposed for BSF solar cells by Weiwei [7], and

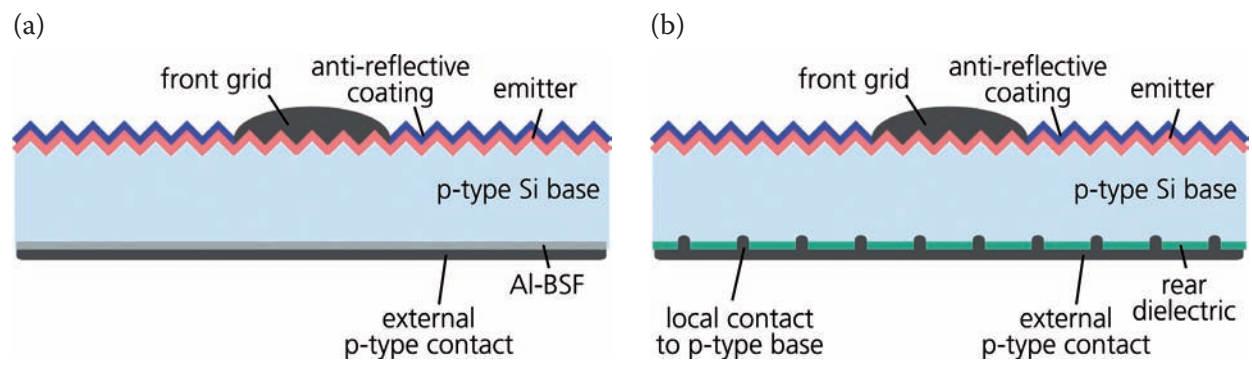

Figure 1. Schematic cross section of (a) a standard p-type Al-BSF solar cell, and (b) an industrial p-type PERC solar cell with local contacts.

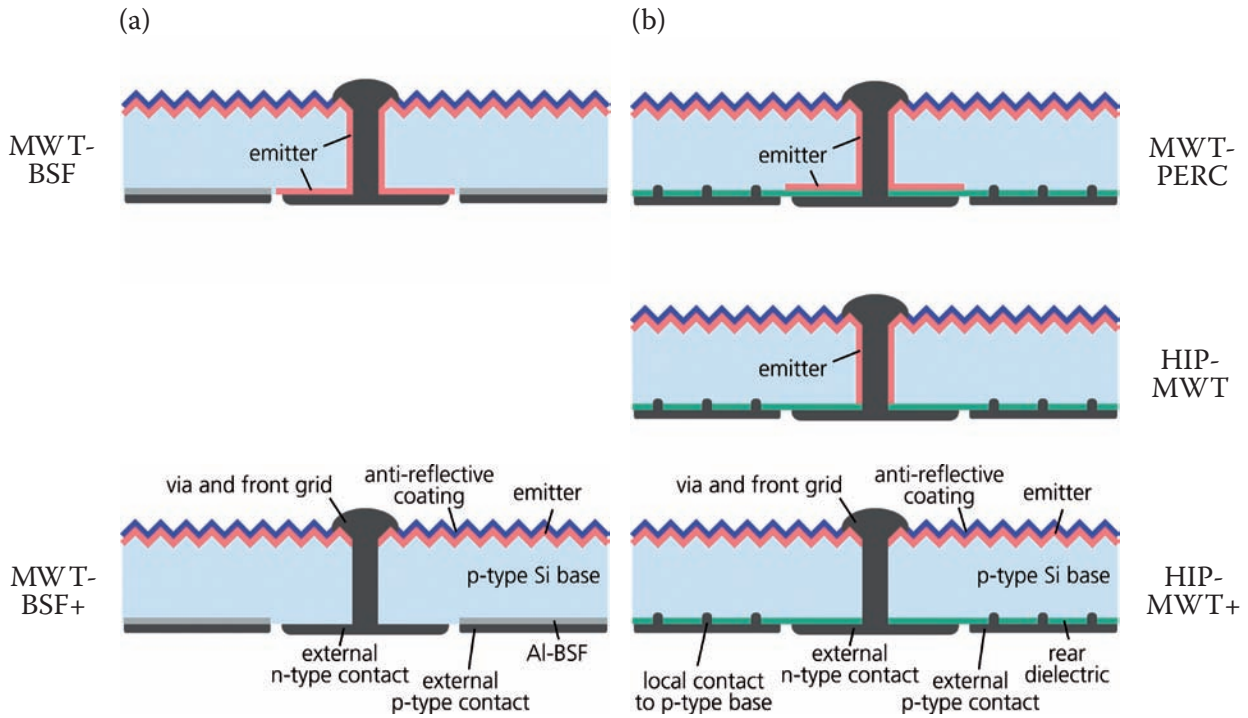

Figure 2. Overview of various MWT structures for p-type silicon wafers (a) without and (b) with rear-surface passivation. MWT-BSF+ denotes a simplified MWT-BSF structure without via and rear emitter, as proposed by Weiwei [7]. The high-performance MWT (HIP-MWT) approach [8] is a simplified version of the conventional MWT-PERC structure without rear emitter. A further simplified structure, without even a via emitter, is referred to as HIP-MWT+ [9].

for MWT solar cells with rear-surface passivation (MWT-PERC) [10] by Thaidigsmann (HIP-MWT+) [9,11]. Apart from the adapted contact layout, all other technologies known from Al-BSF or PERC fabrication sequences – for example emitter diffusion, selective emitter formation or surface passivation – can also be applied to MWT solar cells.

> "In principle, it is straightforward to integrate MWT cell fabrication into existing p-type Al-BSF or PERC production lines."

In principle, it is straightforward to integrate MWT cell fabrication into existing p-type Al-BSF or PERC production lines. The only additional process step is the drilling of vias [5], typically by a laser process, for example after surface passivation. Via metallization is then performed during the printing of the rear solder pads, using an adequately formulated via paste. As a result, retrofitting of production lines for conventional H-pattern solar cells is becoming more and more attractive – the front-end process sequence is the same as for H-pattern solar cells. It has recently been shown that some issues arising from the rear n-type contact might be overcome by omitting the via and rear emitter in these structures [9,11], which has been corroborated by the work of other authors [7,12]. The most important topic for future investigations is the long-term reverse-bias stability. Preliminary results indicate the existence of via pastes which do not show increasing leakage current after reverse loading [13,14]. Regarding reverse-bias stability, MWT solar cells without a rear emitter even offer the promising possibility of an integrated bypass diode functionality at no extra cost – its implementation only requires a specially adapted via paste composition [15]. From the point of view of the authors, solutions to all MWT-technology-related issues exist. An overview of the status of MWT solar cells and module technology can be found in the literature [9,16].

Several technologies that may be implemented for the fabrication of high-efficiency PERC or MWT devices will be discussed next.

Technologies

Emitter formation

As both p-type Al-BSF and PERC solar cells feature a phosphorus-doped emitter, advances in emitter formation are not solely limited to PERC solar cells. However, as rear-surface passivation leads to a lower overall recombination rate than for Al-BSF solar cells (and thus a higher open-circuit voltage), PERC solar cells especially benefit from low-recombination emitters. Furthermore, calculations show that, for industrial-type high-efficiency PERC solar cells, the recombination in the emitter region forms the largest contribution to the total [17], which highlights the necessity for process improvements in this field.

Because of its robustness and simplicity, atmospheric pressure diffusion of $POCl_3$ in tube furnaces is still the workhorse for emitter formation in the silicon solar industry. One quartz boat typically holds 200 to 250 wafers; back-to-back loading or the use of half-pitch boats is known to further increase throughput. An evolution of this process is low-pressure $POCl_3$ diffusion [18], which is considered to yield improved homogeneity over the wafer and boat, with boat capacities of 500 to 1000 wafers.

Recently, ion-implanted emitters have also come into the spotlight [19,20] owing to their precise junction control and low dark saturation current densities. The latter characteristic also results from thin thermal-oxide passivation layers that are grown during the required high-temperature step for crystal damage annealing and dopant activation. Another advantage of ion implantation is the elimination from the process chain of the phosphosilicate glass (PSG) layer removal and edge-isolation steps. Both atmospheric and low pressure diffusion, as well as ion implantation, are already up and running in production.

Methods for selective emitter formation include laser doping from PSG [21], the application of a dopant paste [22], and etch-backs of highly doped emitters, either by the activation of an etching paste [23] or in a liquid [24] or a gas phase [25]. Selective emitters, however, have lost some of their attraction, owing to the ability of the newest silver paste generations to also contact lightly doped emitters, with phosphorus surface concentration of $1 \cdot 10^{20}$ to $2 \cdot 10^{20} cm^{-3}$. If, in the race for the highest efficiencies, phosphorus surface concentrations below $10^{20} cm^{-3}$ and high-quality surface passivation layers are used, selective emitters can still demonstrate notable advantages over homogeneous emitters [17] because of improved shielding of contact recombination, which results in a higher open-circuit voltage.

> "Selective emitters can still demonstrate notable advantages over homogeneous emitters."

For further information on phosphorus emitters, the reader is referred to the article by Dullweber et al. [26].

Rear-surface passivation

A major difference between Al-BSF and PERC solar cells is the existence of a dielectrically passivated rear side, as indicated in Fig. 1. For decades the thermal oxidation of silicon has been the standard technology in the semiconductor industry for the passivation of n- or p-doped surfaces; it was also used in the first PERC cell by Blakers et al. [1]. The very good passivation quality of the thermal oxide layers results from the growing of the dielectric in the wafer at high temperatures (700°C < T < 1050°C) in an atmosphere containing O_2 or H_2O gas; this yields very low interface trap densities and a low density of fixed *positive* charge at the Si/SiO_2 interface ($Q_f < 5 \cdot 10^{11} cm^{-2}$). The positive charge depletes or weakly inverts the p-type surface. Recently, several institutes have applied thin thermal oxide layers grown at 800°C < T < 900°C for rear-surface passivation [27,28]. A promising synergic approach is the combination of ion implantation and thermal oxidation for rear-surface passivation into a single process sequence [29,30].

Nevertheless, most institutes and companies currently report on the use of Al_2O_3 passivation layers for achieving low surface recombination velocities on lightly doped p-type surfaces. The excellent passivation quality results from a high density of fixed *negative* charge at the Si/Al_2O_3 interface ($|Q_f| > 3 \cdot 10^{12} cm^{-2}$), which leads to an accumulation of majority carriers at the interface. High-throughput production equipment for these layers is available from several manufacturers: it mainly relies on atomic layer deposition (ALD) [31], plasma-enhanced chemical vapour deposition (PECVD) [3,32] or atmospheric pressure CVD (APCVD) [33]. Since very low surface recombination velocities have been reported with all technologies [34–36], the technology of choice might be a question of cost, material consumption, homogeneity, throughput and uptime rather than conversion efficiency.

In contrast to this, SiN_x layers with a refractive index n > 2.4

Company/Institute	Cell type	Front side	Rear side passivation	η [%]	V_{oc} [mV]	j_{sc} [mA/cm^2]	FF [%]
Hyundai (2013, [2])	LCO, Cz-Si		ALD Al_2O_3	20.1	650	39.0	79.2
Sunrise (2013, [3])	LCO, Cz-Si		PECVD Al_2O_3	20.3*	658	39.0	79.2
imec (2013, [27])	LCO, Cz-Si	Thermal SiO_2	Thermal SiO_2	20.1*	650	38.8	79.8
ISFH (2013, [19])	LCO, Cz-Si	Ion-implanted emitter + thermal SiO_2	ALD Al_2O_3	20.0	659	38.7	78.3
ISFH (2013, [25])	LCO, Cz-Si	Gas phase etched-back emitter	ALD Al_2O_3	20.3*	660	38.3	80.3
Q-Cells (2011, [51])	LFC, mc-Si			19.5*	652	38.9	76.7
Q-Cells (2011, [51])	LFC, Cz-Si			20.2*	652	38.9	79.9
ISE (2013, [52])	LFC, cast-mono	Thermal SiO_2	Thermal SiO_2	19.8*	654	39.0	77.6
Schott (2012, [53])	LCO, Cz-Si		MW-PECVD	21.0*	664	39.9	79.2

* Independently confirmed by Fraunhofer ISE CalLab PV Cells.

Table 1. Published results for 156mm p-type PERC solar cells with screen-printed contacts.

and SiO_xN_y passivation layers [37] make use of a high density of fixed *positive* charge at the interface ($Q_f > 2 \cdot 10^{12} cm^{-2}$). These layers drive the surface into a state of strong inversion, which leads to surface recombination velocities similar to those for Al_2O_3 layers. SiN_x layers are typically deposited at intermediate temperatures using PECVD technology in a direct or remote plasma configuration; however, when these layers are applied for rear-surface passivation in p-type PERC solar cells, inversion layer shunting [38] must be prevented.

In general, all rear passivation layers are formed with a thickness of around 5 to 20nm, followed by the deposition of other dielectric capping layers for improved optics and surface passivation, as well as for preventing alloying of the screen-printed aluminium layers through the passivation layers [2,39]. In some approaches, the deposition of the passivation and capping layer takes place in the same system, with the aim of reducing cost.

It should be added that a rear-surface conditioning process is typically carried out before surface passivation, to prevent the formation of a rear texture [19] or, at least, to partly remove it [12,28,29]. In some process flows, rear polishing is implemented in the wet chemical edge-isolation step [25,31].

Contact formation

A second difference between Al-BSF and PERC solar cells is the metallization fraction of the rear side. Whereas Al-BSF solar cells feature a fully metallized and contacted rear surface, PERC solar cells feature only local contacts. To the authors' knowledge, only two approaches for local contacting are currently in production. The first approach makes use of laser-fired contact (LFC) technology, in which a laser locally alloys the rear point contacts through the passivation layer after contact firing [40]. The second approach is the local contact opening (LCO) concept [41], in which the rear passivation layers are locally opened by laser ablation or etching pastes before aluminium metallization and local contact alloying during contact firing. Several contact layouts have been reported, for example point, line or dash contacts.

The large majority of silicon solar cells fabricated throughout the world feature screen-printed contacts; however, in the race to achieve reduced shading, lower series resistance values and reduced silver consumption, other approaches are under investigation.

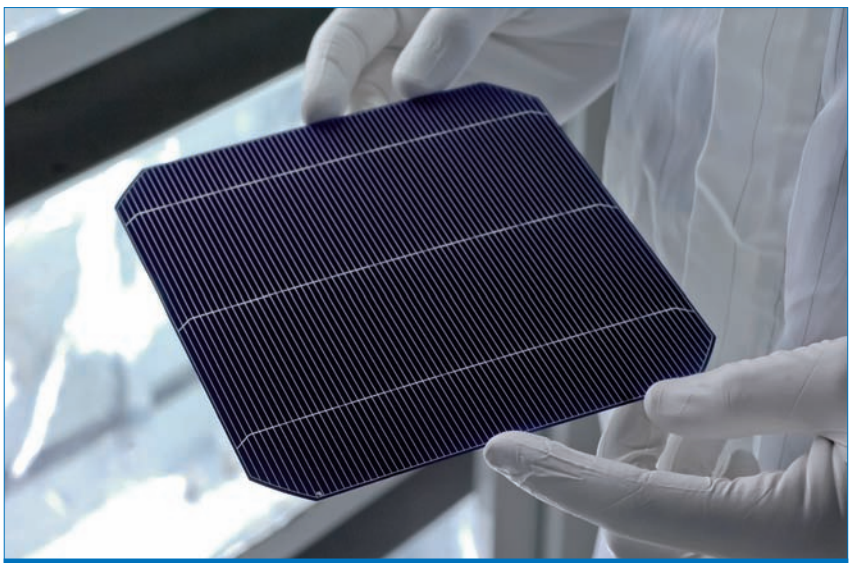

Figure 3. Photograph of a 156mm Cz-Si HIP-MWT solar cell fabricated at Fraunhofer ISE.

To the authors' knowledge, print-on-print and dual print (printing of silver fingers and non-contacting busbars in two process steps using different silver pastes) are already up and running in production lines, whereas stencil printing, inkjet printing [42] and flexographic printing [43] of a metal paste have not yet been implemented in industrial manufacturing.

Two other approaches aim at eliminating the front busbars, similarly to the MWT approach. Both the 'SmartWire' [44] and the 'Multi Busbar' [45] approaches use a metal net applied perpendicularly to the silver finger grid in order to directly contact each silver finger. Compared with the MWT approach, the drawbacks are higher shading values and the necessity to still guide the interconnector from the front of a solar cell to the rear of the adjacent cell, which makes module assembly more complex.

Company/Institute	Cell type	Cell area [cm^2]	Comment	η [%]	j_{sc} [mA/cm^2]	V_{oc} [mV]	FF [%]	j_{-12V} [mA/cm^2]
Kyocera (2008, [56])	MWT-BSF, mc-Si	233	RIE texture	18.3*	37.2	626	78.5	
ECN (2012, [57])	MWT-BSF, mc-Si	243		17.9	36.4	632	77.8	
Bosch (2011, [58])	MWT-BSF, Cz-Si	-	Selective emitter (SE)	19.4				
Canadian Solar (2013, [7])	MWT-BSF+, cast-mono Si	243	SE	19.6	39.0	639	78.7	2.45
Fraunhofer ISE (2011, [5])	HIP-MWT, mc-Si	243	PECVD-Al_2O_3	18.2*	36.9	637	77.3	2.55
Fraunhofer ISE (2011, [59])	MWT-PERC, FZ-Si	149	SE, thermal SiO_2, dispensed front grid	20.6*	39.9	661	78.3	4.65
Fraunhofer ISE (2012, [60])	HIP-MWT, mCz-Si	239	SE, thermal SiO_2, stencil-printed front grid	20.2*	39.2	661	78.0	2.75
Fraunhofer ISE (2012, [61])	HIP-MWT+, FZ-Si	149	SE, thermal SiO_2	20.3*	39.2	664	78.1	4.71
Canadian Solar (2013, [12])	Sim. HIP-MWT+, Cz-Si	239	Average values, SE, ALD Al_2O_3	20.6	40.0	661	77.9	

* Independently confirmed

Table 2. Published MWT solar cell results for p-type silicon wafers (mCz denotes magnetic-field-assisted Cz growth).

For MWT solar cells there is no stress on the front contacts during soldering: this promotes the use of very thin silver fingers with reduced contact adhesion requirements, formed (for example) by dispensing [46] or direct plating technology. Industrial solutions for the in-line annealing of contacts are already available [47].

Solar cell results

The implementation of a dielectrically passivated rear side with local contacts leads to an increase in conversion efficiency of 0.5 to 1.0% abs. compared with solar cells with a full-area Al-BSF rear contact, as reported by several authors [48–50]. Table 1 lists a selection of recently published results for large-area p-type PERC solar cell results with screen-printed contacts. From this table it is evident that, on Cz-Si, conversion efficiencies exceeding 20% have been achieved using several approaches. High-quality surface passivation layers and emitters yield open-circuit voltages of 660mV and short-circuit current densities close to 39mA/cm^2. Moreover, Table 1 indicates the remarkable progress achieved in the fabrication of high-quality multicrystalline and cast-mono wafers, which demonstrate open-circuit voltages above 650mV and conversion efficiencies approaching 20%.

The highest conversion efficiencies of PERC solar cells have in the past been reported by R&D groups at universities and research institutes. In the last few years, with solar cell manufacturing growing into a multi-billion dollar market, most companies have established their

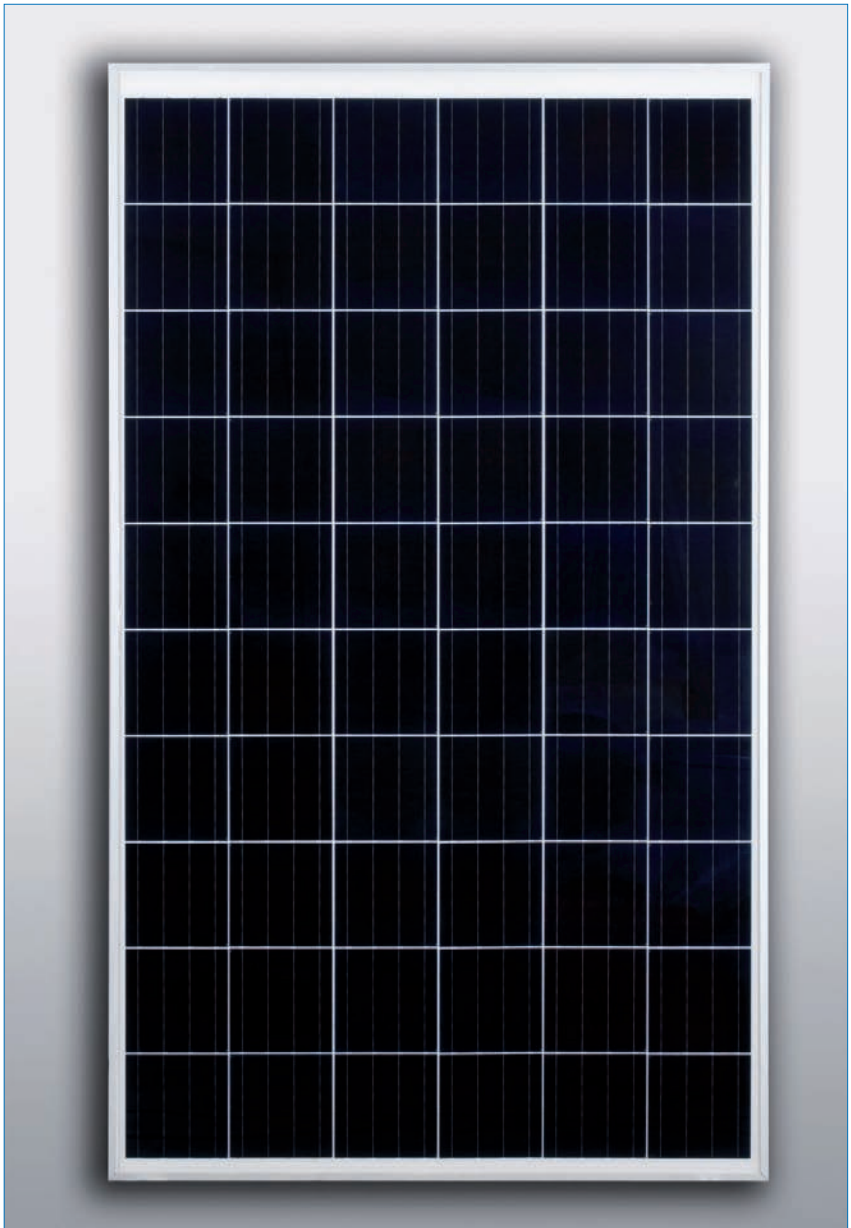

Figure 4. Photograph of a 60-cell HIP-MWT module with an output power of 277Wp (independently confirmed by Fraunhofer ISE CalLab PV Modules).

own R&D departments alongside their conventional production line business. Supported by the process fine-tuning that is possible when processing thousands of wafers per hour, industrial manufacturers now seem to have achieved at least the same conversion efficiency level for industrial-type PERC solar cells: indeed, at the EU PVSEC conference in Paris in 2013, several cell and production equipment manufacturers reported pilot-line and production conversion efficiencies of above 20% on Cz-Si.

"MWT technology allows an efficiency gain of up to 0.5% abs. compared with H-pattern solar cells."

Fig. 3 shows a photograph of a 156mm-size p-type Cz-Si HIP-MWT solar cell from Fraunhofer ISE. As reported by several authors, MWT technology allows an efficiency gain $\Delta\eta$ of up to 0.5% abs. compared with H-pattern solar cells [5,54,55]. A selection of recently published representative MWT results, both from industry and institutional research, is listed in Table 2. Very high conversion efficiencies of up to 19.6% [7] without and 20.6% [59] with rear-surface passivation have been reported. A calculation based on realistic assumptions of specific process improvements reveals that stable conversion efficiencies beyond 21% on p-type monocrystalline silicon wafers are possible with MWT-PERC-type structures [62].

Although several companies have been working on MWT technology [63,64], the concept has not yet been brought into mass production; this shortcoming is attributed to the lack of an economically feasible module interconnection technology in the past. Foil-based approaches [65] have been commercialized [66], but it has not been until now that competitive prices have been announced by producers of suitable structured backsheets. Owing to its reliability, cost effectiveness and similarities to conventional module interconnection, ribbon-based interconnection [67] is also the centre of interest for equipment manufacturers [68]. Together with industry partners [68], ISE has successfully demonstrated the ribbon-based module integration of HIP-MWT+ solar cells into a 60-cell demo module with an output power of 277Wp (see Fig. 4).

"MWT solar modules are expected to be widely available within the next few years."

Conclusions

This paper has summarized the current status of p-type PERC and MWT-PERC technology and solar cells. Several technologies were discussed that might be included in the newest generation of production lines for manufacturing high-efficiency PERC and/or MWT-PERC solar cells; the latest published cell results for both of these structures were summarized. Whereas solar modules fabricated from PERC solar cells are already commercially available, which underlines the maturity of this product, MWT – and particularly MWT-PERC – solar cells have not yet made the transition to high-volume production, although only one additional process – the drilling of vias – is required to make the benefits of reduced shading accessible. This is attributed to the lack of an economically feasible module interconnection technology in the past. Since all cell-related issues seem to have been resolved and production equipment is currently ready for use, MWT solar modules are expected to be widely available within the next few years.

References

[1] Blakers, A.W. et al. 1989, "22.8% efficient silicon solar cell", *Appl. Phys. Lett.*, Vol. 55, pp. 1363–1365.

[2] Shin, H.-N.-R. et al. 2013, "Characterization of aluminium-metallization compatibility of dielectric capping layers for the development of rear-passivated silicon solar cells", *Proc. 28th EU PVSEC*, Paris, France.

[3] Tjahjono, B.S. et al. 2013, "Optimizing CELCO solar cell technology in one year of mass production", *Proc. 28th EU PVSEC*, Paris, France.

[4] van Kerschaver, E. et al. 1998, "A novel silicon solar cell structure with both external polarity contacts on the back surface", *Proc. 2nd WCPEC*, Vienna, Austria, pp. 1479–1482.

[5] Thaidigsmann, B. et al. 2011, "HIP-MWT – A new cell concept for industrial processing of high-performance metal wrap through silicon solar cells", *Proc. 26th EU PVSEC*, Hamburg, Germany, pp. 817–820.

[6] Kopecek, R. & Libal, J. 2013, "The status and future of industrial n-type silicon solar cells", *Photovoltaics International*, 21st edn, pp. 52–60.

[7] Weiwei, Y. et al. 2013, "19.6% cast mono-MWT solar cells and 268 W modules", *IEEE J. Photovolt.*, Vol. 3, pp. 697–701.

[8] Thaidigsmann, B. et al. 2011, "HIP-MWT: A simplified structure for metal wrap through solar cells with passivated rear surface", *Energy Procedia*, Vol. 8, pp. 498–502.

[9] Thaidigsmann, B. et al. 2013, "P-type MWT solar cells: Current status and future expectations", *Proc. 28th EU PVSEC*, Paris, France.

[10] Dross, F. et al. 2006, "Impact of rear-surface passivation on MWT performances", *Proc. 4th WCPEC*, Waikoloa, Hawaii, USA, pp. 1291–1294.

[11] Mack, S. et al. 2013, "Technology for mass production of >20% efficient p-type silicon solar cells", *Proc. 28th EU PVSEC*, Paris, France.

[12] Wu, J. et al. 2013, "Research status of 2nd generation metal wrap through solar cells at Canadian Solar Inc.", *Proc. 28th EU PVSEC*, Paris, France.

[13] Lohmüller, E. et al. 2013, "Via pastes for MWT silicon solar cells" [submitted for publication in *IEEE J. Photovolt.*].

[14] Spribille, A. et al. 2013, "Wet chemical single-side emitter etch back for MWT solar cells with Al-BSF and challenges for via paste selection", *Proc. 28th EU PVSEC*, Paris, France.

[15] Thaidigsmann, B. et al. 2013, "Characterization and modeling of screen-printed metal insulator semiconductor tunnel junctions for integrated bypass functionality in crystalline silicon solar cells", *J. Appl. Phys.*, Vol. 113, pp. 214502.

[16] Lohmüller, E. et al. 2012, "Current status of MWT silicon solar cell and module technology", *Photovoltaics International*, 17th edn, pp. 75–81.

[17] Jäger, U. et al. 2013, "Benefit of selective emitters for p-type silicon solar cells with passivated surfaces", *IEEE J. Photovolt.*, Vol. 3, pp. 621–627.

[18] Mühlbauer, M. et al. 2011, "Industrial low-pressure phosphorus diffusion for high performance and excellent uniformity", *Proc. 26th EU PVSEC*, Hamburg, Germany, pp. 2028–

2030.
[19] Dullweber, T. et al. 2013, "Ion-implanted PERC solar cells with Al_2O_3/SiNx rear passivation", *Energy Procedia*, Vol. 38, pp. 430–435.
[20] Hieslmair, H. et al. 2013, "Industrial advanced cell designs by ion implantation", *Proc. 28th EU PVSEC*, Paris, France.
[21] Jäger, U. et al. 2009, "Selective emitter by laser doping from phosphosilicate glass", *Proc. 24th EU PVSEC*, Hamburg, Germany, pp. 1740–1743.
[22] Antoniadis, H. 2009, "Silicon ink high efficiency solar cells", *Proc. 34th IEEE PVSC*, Philadelphia, Pennsylvania, USA, pp. 650–654.
[23] Zhu, R., Wang, X. & Zhang, L. 2012, "A new solution of forming selective emitter with etch back technology", *Proc. 27th EU PVSEC*, Frankfurt, Germany, pp. 1870–1872.
[24] Lauermann, T. et al. 2009, "Insect: An inline selective emitter concept with high efficiencies at competitive process costs improved with inkjet masking technology", *Proc. 24th EU PVSEC*, Hamburg, Germany, pp. 1767–1770.
[25] Hannebauer, H. et al. 2013, "Gas phase etch back – A new selective emitter technology for high-efficiency PERC solar cells", *Proc. 28th EU PVSEC*, Paris, France.
[26] Dullweber, T. et al. 2013, "Emitter technology options for industrial PERC solar cells with up to 20.3% conversion efficiency", *Photovoltaics International*, 21st edn, pp. 44–51.
[27] Choulat, P. et al. 2013, "Cost effective dry oxidation for emitter passivation: A key step for high efficiency screen-printed p-type PERC solar cells", *Proc. 28th EU PVSEC*, Paris, France.
[28] Mack, S. et al. 2010, "Towards 19% efficient industrial PERC devices using simultaneous front emitter and rear surface passivation by thermal oxidation", *Proc. 35th IEEE PVSC*, Honolulu, Hawaii, USA, pp. 17–21.
[29] Mack, S. et al. 2012, "Synergistic use of ion implant annealing processes for thermal oxide rear surface passivation", *Proc. 27th EU PVSEC*, Frankfurt, Germany, pp. 875–878.
[30] Lai, J.-H. et al. 2011, "High-efficiency large-area rear passivated silicon solar cells with local Al-BSF and screen-printed contacts", *IEEE J. Photovolt.*, Vol. 1, pp. 16–21.
[31] Sastrawan, R. et al. 2013, "Implementation of a multicrystalline ALD-Al_2O_3 PERC-technology into an industrial pilot production", *Proc. 28th EU PVSEC*, Paris, France.
[32] Dullweber, T. et al. 2012, "High-efficiency industrial-type PERC solar cells applying ICP AlO_x rear passivation layer", *Proc. 27th EU PVSEC*, Frankfurt, Germany, pp. 672–675.
[33] Kübler, C. 2012, "SCHMID's APCVD machine proves itself in the manufacturing of PERC cells with an efficiency of 20.74%", Press Release, September 24th.
[34] Saint-Cast, P. et al. 2009, "Very low surface recombination velocity on p-type c-Si by high-rate plasma-deposited aluminum oxide", *Appl. Phys. Lett.*, Vol. 95, pp. 151502.
[35] Black, L.E., Provancha, K.M. & McIntosh, K.R. 2011, "Surface passivation of crystalline silicon by APCVD aluminium oxide", *Proc. 26th EU PVSEC*, Hamburg, Germany, pp. 1120–1124.
[36] Dingemans, G. et al. 2009, "Stability of Al_2O_3 and Al_2O_3/a-SiNx:H stacks for surface passivation of crystalline silicon", *J. Appl. Phys.*, Vol. 106, pp. 114907/114901–114904.
[37] Münzer, K.A. et al. 2012, "Centaurus solar cell technology in production", *Proc. 27th EU PVSEC*, Frankfurt, Germany, pp. 666–671.
[38] Dauwe, S. et al. 2002, "Experimental evidence of parasitic shunting in silicon nitride rear surface passivated solar cells", *Prog. Photovolt.: Res. Appl.*, Vol. 10, pp. 271–278.
[39] Woehl, R. et al. 2010, "Firing stable passivation layers for the front and rear side of high efficiency n-type back-contact back-junction solar cells", *Proc. 25th EU PVSEC*, Valencia, Spain, pp. 2272–2276.
[40] Schneiderlöchner, E. et al. 2002, "Laser-fired rear contacts for crystalline silicon solar cells", *Prog. Photovolt.: Res. Appl.*, Vol. 10, pp. 29–34.
[41] Agostinelli, G. et al. 2005, "Local contact structures for industrial PERC-type solar cells", *Proc. 20th EU PVSEC*, Barcelona, Spain, pp. 942–945.
[42] Jesswein, R. et al. 2013, "Process optimization of single step inkjet printed front contacts for industrially fabricated solar cells leads to an efficiency gain of 0.3%abs with consumption of less than 60mg silver", *Proc. 28th EU PVSEC*, Paris, France.
[43] Lorenz, A. et al. 2013, "Flexographic printing – High throughput printing technology for fine line seedlayer printing", *Proc. 28th EU PVSEC*, Paris, France.
[44] Carstensen, I. 2013, "Meyer Burger's revolutionary SmartWire connection technology significantly lowers photovoltaic production costs and boosts PV system energy yield by 10%", Press Release, February 11th.
[45] Braun, S. et al. 2013, "The multi-busbar design: An overview", 4th Metalliz. Worksh. Contact. Si Sol. Cells, Konstanz, Germany.
[46] Pospischil, M. et al. 2013, "Process development for a high-throughput fine line metallization approach based on dispensing technology", 4th Metalliz. Worksh. Contact. Si Sol. Cells, Konstanz, Germany.
[47] Mack, S. et al. 2011, "High capacity inline annealing for high efficiency silicon solar cells", *Proc. 26th EU PVSEC*, Hamburg, Germany, pp. 1089–1093.
[48] Wu, J. et al. 2013, "Application of ion implantation emitter in PERC solar cells", *Proc. 39th IEEE PVSC*, Tampa, Florida, USA.
[49] Wolf, A. et al. 2010, "Pilot processing of 18,6% efficient rear surface passivated silicon solar cells with screen printed front contacts", *Proc. 25th EU PVSEC*, Valencia, Spain, pp. 1391–1395.
[50] Schultz, O. et al. 2008, "Thermal oxidation for crystalline silicon solar cells exceeding 19% efficiency applying industrially feasible process technology", *Prog. Photovolt.: Res. Appl.*, Vol. 16, pp. 317–324.
[51] Engelhart, P. et al. 2011, "Q.ANTUM – Q-Cells next generation high-power silicon solar cell & module concept", *Proc. 26th EU PVSEC*, Hamburg, Germany, pp. 821–826.
[52] Schwab, C. et al. 2013, "Evaluation of cast mono silicon material for thermal oxide passivated solar cells", *Energy Procedia*, Vol. 40, pp. 611–617.
[53] Lachowicz, A. et al. 2012, "NO_x-free solution for emitter etch-back", *Proc. 27th EU PVSEC*, Frankfurt, Germany, pp. 1846–1850.
[54] Clement, F. et al. 2009, "Industrially feasible multi-crystalline metal wrap through (MWT) silicon solar cells exceeding 16% efficiency", *Solar*

Energy Mater. & Solar Cells, Vol. 93, pp. 1051–1055.
[55] Meyer, K. et al. 2010, "Novel MWT cell design on monocrystalline silicon wafers", *Proc. 25th EU PVSEC*, Valencia, Spain, pp. 1774–1777.
[56] Nakatani, N. et al. 2007, "High efficiency multicrystalline silicon back-contact solar cells", *Tech. Digest 17th Internat. PVSEC*, Fukuoka, Japan, pp. 401–403.
[57] Lamers, M.W.P.E. et al. 2012, "17.9% metal-wrap-through mc-Si cells resulting in module efficiency of 17.0%", *Prog. Photovolt.: Res. Appl.*, Vol. 20, pp. 62–73.
[58] Meyer, K. et al. 2011, "MWT cells with Al-BSF on Cz silicon with efficiencies up to 19.4%", *Proc. 26th EU PVSEC*, Hamburg, Germany, pp. 981–988.
[59] Lohmüller, E. et al. 2011, "20% efficient passivated large-area metal wrap through solar cells on boron-doped cz silicon", *IEEE Electron Dev. Lett.*, Vol. 32, pp. 1719–1721.
[60] Thaidigsmann, B. et al. 2012, "The path to industrial production of highly efficient metal wrap through silicon solar cells", *GREEN*, Vol. 2, pp. 171–176.
[61] Lohmüller, E. et al. 2012, "Evaluation of via pastes for p- and n-type metal wrap through (MWT) solar cells", *Proc. 27th EU PVSEC*, Frankfurt, Germany, pp. 590–595.
[62] Thaidigsmann, B. et al. 2012, "Loss analysis and efficiency potential of p-type MWT-PERC solar cells", *Solar Energy Mater. & Solar Cells*, Vol. 106, pp. 89–94.
[63] van der Heide, A., Gribenski, D. & Szlufcick, J. 2009, "Industrial fabrication of multi-crystalline MWT cells with interconnection flexibility of 16.5% efficiency", *Proc. 24th EU PVSEC*, Hamburg, Germany, pp. 942–945.
[64] Augustin, L.M. et al. 2011, "Mass production and field performance of durable metal-wrap-through integrated back contact foil based 'Sunweb' modules", *Proc. 26th EU PVSEC*, pp. 3113–3116.
[65] Bultman, J.H. et al. 2003, "Fast and easy single step module assembly for back-contacted C-Si solar cells with conductive adhesives", *Proc. 3rd WCPEC*, Osaka, Japan, pp. 978–982.
[66] Späth, M. et al. 2008, "First experiments on module assembly line using back-contact solar cells", *Proc. 23rd EU PVSEC*, Valencia, Spain, pp. 2917–2921.
[67] Eitner, U., Eberlein, D. & Tranitz, M. 2012, "Interconnector-based module technology for thin MWT cells", *Proc. 27th EU PVSEC*, Frankfurt, Germany, pp. 3461–3464.
[68] Spribille, A. et al. 2013, "HIP-MWT: Our approach for high performance ribbon based back contact MWT modules with low CTM losses", *Proc. 7th SNEC Internat. PV Power Gen. Conf.*, Shanghai, China.

About the Authors

Sebastian Mack has a diploma degree in physics from the University of Jena and received his Ph.D. from the University of Konstanz, Germany. For his doctoral thesis, carried out at Fraunhofer ISE, he investigated thermal oxidation processes for industrial high-efficiency PERC solar cells. Sebastian is currently a postdoctoral researcher in the Thermal Processes / Passivated Solar Cells group at Fraunhofer ISE.

Benjamin Thaidigsmann studied physics at the University of Tübingen, Germany, and finished his diploma thesis on a quantum efficiency analysis of crystalline silicon solar cells at Fraunhofer ISE in 2009. He received his doctoral degree in 2013 for his work on the development and characterization of MWT silicon solar cells with surface passivation. Benjamin is currently head of the Industrial Cell Structures team at Fraunhofer ISE.

Elmar Lohmuller studied physics at the University of Tübingen, Germany, and received his diploma degree in 2010. For his diploma thesis, he worked on the development of p-type MWT-PERC silicon solar cells at Fraunhofer ISE. Elmar is now working towards his Ph.D., focusing on the development of n-type MWT solar cells.

Andreas Wolf studied physics at the Technical University of Darmstadt and at the KTH Royal Institute of Technology in Stockholm. He received his Ph.D. from the Leibniz University of Hanover in 2007. Andreas is head of the Thermal Processes / Passivated Solar Cells group at Fraunhofer ISE.

Florian Clement received his Ph.D. in 2009 from the University of Freiburg, and heads the MWT Solar Cells / Printing Technology group at Fraunhofer ISE. Florian's research focuses on the development of highly efficient pilot-line-processed MWT solar cells, as well as on the development and evaluation of printing technologies.

Marc Hofmann received a diploma degree in electrical engineering from the University of Applied Sciences Koblenz, Germany, and a Ph.D. degree in physics from the University of Konstanz, Germany, for his research on surface conditioning and passivation of crystalline silicon by plasma processes. Marc is head of the Plasma Technology / Passivated Solar Cells group at Fraunhofer ISE.

Ralf Preu received a diploma degree in physics in 1996 from the University of Freiburg, Germany, and a Ph.D. degree in electrical engineering in 2000. He also has a diploma degree in economics, which he was awarded by the University of Hagen in 2003. Ralf is director of the PV Production Technology and Quality Assurance division at Fraunhofer ISE.

Daniel Biro studied physics at the University of Karlsruhe, Germany, and at UMASS Amherst, USA, later completing his Ph.D. at the University of Freiburg in 2003. Daniel coordinated the design and ramp-up of the Fraunhofer ISE production technology lab PV-TEC and is now head of the High Temperature and Printing Technology / Industrial Solar Cell Structures department.

Enquiries

Fraunhofer Institute for Solar Energy Systems (ISE)
Heidenhofstrasse 2
79110 Freiburg
Germany

Tel: +49 (0) 761 4588 0
Email: info@ise.fraunhofer.de
Website: www.ise.fraunhofer.de

Cleaning for high-efficiency solar cell processes

Florian Buchholz & **Eckard Wefringhaus**, International Solar Energy Research Center Konstanz (ISC Konstanz), Germany

ABSTRACT

This paper discusses the role of wafer cleaning in solar cell processing, and addresses its increasing importance with the introduction of new process steps for manufacturing high-efficiency solar cells. The requirements for cleaning before several process steps, in relationship to the solar cell production sequence, are discussed: front-end-of-the-line (FEOL) cleaning needs to reduce metal surface concentrations by several orders of magnitude (residues from wafer sawing), while back-end-of-the-line (BEOL) cleaning needs to reduce mostly process-induced contamination, which tends to be much lower. A ten-step roadmap for process integration and optimization of new cleaning processes from lab to fab is suggested, which is based on process analytics and simple bath-lifetime simulations. A number of advanced cleaning steps are identified and their suitability for solar cell mass production is examined. The influence of the different input variables is demonstrated, with a focus on feed and bleed settings. Finally, the need for constant monitoring of cleaning baths is highlighted, and a device developed by Metrohm for cost-effective on-site monitoring of metallic contamination is discussed.

Role of wafer cleaning in solar cell processing

'Clean' wafer surfaces in wafer-based silicon solar cell processing are required before high-temperature steps, such as diffusion and thermal oxidation and surface passivation (PECVD, ALD, etc.). The reason for this is that metallic impurities have a detrimental effect on the lifetime of photo-generated carriers. Metallic species act as recombination centres when they penetrate into the bulk, which can happen during high-temperature processes (vulnerability is high notably during thermal oxidation). High diffusivity and solubility in silicon in particular have been reported for iron, copper and nickel [1]. Furthermore, metal impurities can increase the surface recombination velocity [2,3] by increasing the defect density of the interface; they may also lead to leakage currents [4] and may result in junction breakdown [5]. A recent study of the impact of the most common contaminants on solar cell performance when present in silicon solar cells was presented by Coletti et al. [6].

In the following text the importance of efficient and tailored cleaning for high-efficiency processes will be stressed. The main sources of metallic contamination will be addressed, several cleaning-bath mixtures will be discussed and a guide to the successful introduction of new cleaning processes from the process engineering and process analytical side will be given.

> "Metallic impurities have a detrimental effect on the lifetime of photo-generated carriers."

The main source of metallic contamination in solar cell manufacturing is the as-cut wafer, which introduces significant amounts of metal impurities that are on its surface. The conventional slurry-based sawing process leaves traces of the sawing wire itself on the surface. As the sawing wire is usually made of a brass- or copper-coated steel wire, the highest measured values of surface contamination are those of copper and iron. Extensive work on the impact of iron and copper contamination on silicon device manufacturing has been carried out [7,8]. However, the contamination level may differ from supplier to supplier (see Table 1), as different wires are available on the market [9,10]. The classical slurry-based sawing process with SiC particles is increasingly being replaced by fixed abrasive diamond-wire sawing [11]. The diamond-wire sawing process is reported to reduce surface contamination [10]; however, copper – a fast-diffusion impurity – is replaced by nickel –another fast-diffusing species – which is found to be especially harmful in near-surface regions [6].

Another source of metal contamination is solar cell process induced. The alkaline etching solution (KOH/NaOH based) – as used for alkaline texturing, saw damage etch or the removal of porous silicon after acidic texturing – cannot be purified the same way as acids; moreover, the high pH value reduces the solubility of metal species and leads to increased wafer surface contamination [9]. The same phenomenon has been observed for non-optimized cleaning solutions that reach critical metallic contamination loads [12].

The metallic impurity sources discussed so far can be considered more or less constant and predictable to a certain extent (as long as the sawing conditions do not differ from batch to batch or the cleaning baths do not encounter critical

Manufacturer	Surface concentration (c_{SF}) [E10 atoms/cm^2]						
	Al	Cr	Cu	Fe	Mn	Ni	Ti
A	600	10	2400	4300	60	210	60
B	2300	30	< 2	680	7	20	210
C	120	10	15600	5200	30	20	100

Table 1. Metallic surface concentration on wafers from different manufacturers [9].

conditions). Defective equipment as the contamination source is less common and more unpredictable, but can have a detrimental effect on the device yield. Although most of the parts in etching machines are made of PP, PVDF or even PFA, there may be unexpected corrosion of wires, screws or other metal parts that are still in use in these machines. This slow deterioration is accelerated by corrosive vapours that are emitted from the etching baths (HCl vapour in particular is known to be extremely corrosive to any metal parts [13, p. 70]).

Contamination from dust in an industrial environment may also occur [1] – a topic that has not been addressed much in solar cell manufacturing, perhaps because it has not yet been perceived as a problem. With cell efficiencies increasing, however, dust contamination may become a problem in the future. While some manufacturers already use advanced and costly clean-room equipment, this is certainly not the standard. In general, unforeseeable and unexpected contamination especially needs to be detected as early as possible in order to prevent yield losses and, potentially, a lengthy and costly search for the source of the problem. So, apart from output-quality monitoring, thorough process monitoring is recommended; how this can be realized will be addressed in the last section of this paper.

Increasing relevance of cleaning for high-efficiency solar cell processes

With the introduction of new process steps, the requirements of wafer cleaning must be re-evaluated. While the phosphorus diffusion process, with its ability to getter metal impurities [14], is relatively robust against surface contamination [15], the same thing may not be said about boron emitter diffusion for n-type junction formation [4,16]. Nevertheless, acceptable gettering efficiencies have recently been demonstrated for boron emitter diffusion [17]. Several process steps – for example, thermal oxidation, passivation with aluminium oxide (Al_2O_3) [18], and deposition of doped amorphous silicon for heterojunction solar cells [19] – are well known for requiring very clean surfaces and also defined surface conditioning. In general, as the efficiency of solar cells increases, through either new process steps or optimization of existing processes, the influence of single steps may become dominant: the losses that have so far been minor will no longer be covered up by factors such as material quality or poorly optimized steps. A good explanation for this phenomenon is given by Glunz [20], who compares process optimization with fixing a 'leaky bucket', as presented in his keynote speech at the 27th EUPVSEC in Frankfurt in 2012. The optimization and further development of the whole process therefore includes the optimization and/or exchange of cleaning steps.

Large batch / inline processing vs. single wafer handling

Wafer-cleaning technology has a long history in CMOS fabrication [21,22]. To obtain good yields in CMOS fabrication on an ultra-large integration scale, extremely clean surfaces are crucial. Up to several hundred process steps are required for the assembly of microchips, such as CPUs, so that even the smallest amounts of contamination on the wafer surface may lead to device failure and a drastic reduction in yield. Accordingly, process experience has been built up over a long time in this field. At first glance, it seems to be a good idea to draw upon that set of tools and use similar process sequences. However, wafer throughput numbers of the two industries differ by about two orders of magnitude: in solar cell fabrication, up to several thousand wafers per hour are produced, a quantity that large semiconductor factories might not even attain in a week [23]. Consequently, the process specifications are very different.

Highly efficient cleaning sequences, such as the best-known reference procedure, developed by Kern et al. [24] at the *Radio Corporation of America* (and hence called the RCA cleaning sequence), might be suitable for research and development applications but not for mass production of solar cells. The number of steps of the standard clean 1 (SC-1) and standard clean 2 (SC-2) is high, and these steps require high temperatures and long process times, which massively influence cost of ownership.

Another cleaning sequence that is in use in research labs (which is the process of record – POR – at ISC Konstanz), and also borrowed from IC manufacturing, is SPM (sulphuric-acid hydrogen-peroxide mixture) based [25]. However, this sequence cannot be introduced into solar cell mass processing, because the highly corrosive solution enriches water as it oxidizes the surface of the wafers, and hence dilutes itself, so as a result the bath has to be frequently replaced [13, p. 73].

Even in semiconductor manufacturing, the need for simplification has been recognized, and some approaches – the introduction of ozone-based cleaning solutions, for example – have also been published [26]. Some of these alternatives are discussed below. It should be stressed here that, if CMOS processes are to be mimicked for solar cell mass production, thorough testing as regards their suitability and cost effectiveness is required.

From lab to fab

In order to implement new process steps in existing solar cell production lines that are assumed to require advanced cleaning, the following ten-step scheme is suggested.

1. Choose a suitable test structure.
2. Test whether pre-existing industrial cleaning can replace the laboratory cleaning sequence.
3. Evaluate the optimization potential of the industrial process.
4. Choose a 'new', advanced cleaning procedure.
5. Collect input variables for the mass production simulation (by process analytics).
6. Simulate bath ageing.
7. Artificially age the bath, and test the cleaning efficiency.
8. If not suitable, try optimization.
9. Integrate the new process step into the process sequence.
10. Monitor the bath and surface concentrations.

To optimize costly pilot-line testing, the authors suggest working with a simple (e.g. Excel based) cleaning-bath simulation tool, and processing analytical methods in combination with artificial bath ageing to obtain information about mass production suitability.

Since the processing of complete solar cells (at least on a lab scale) is time and resource consuming, it is usual for simplified test structures to be used to obtain the relevant information (**1**). Common test structures for process optimization are symmetrical minority-carrier lifetime samples, which can be used for qualitative and quantitative

comparisons of the influence of different process conditions on electrical solar cell properties. In order to gain a more complete picture, cell precursor structures can be fabricated (performed as shown in Fig. 1) and measured by QSS-PC. The implied V_{oc} values obtained in this way yield valuable information about losses due to recombination that is induced by metallic impurities. The advantage of this kind of structure is that metallization losses, often the dominant losses in cell voltage due to metallization–silicon interface recombination [27], are left out of the picture, and the smaller factors, such as cleanliness, become more evident.

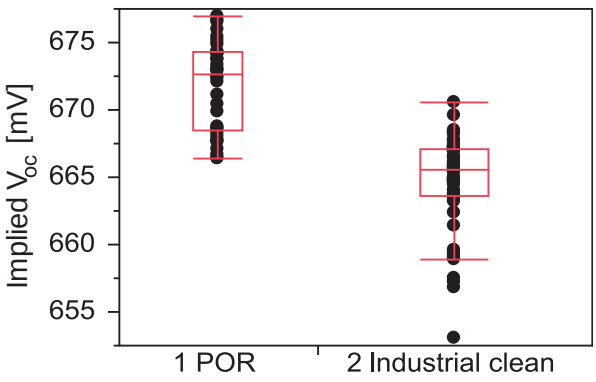

Figure 1. Implied V_{oc} of BiSoN precursor structures (solar cells without metallization), as measured by QSS-PC.

Is advanced cleaning really necessary?

An example of the need for new, advanced cleaning procedures is given in Fig. 1; for this, N-type BiSoN solar cell precursors were manufactured. ISC Konstanz's baseline process for bifacial n-type solar cells using only standard industrial process equipment and screen-printing metallization achieves up to 20% energy conversion efficiency, as reported by Edler et al. [27] at this year's EU PVSEC in Paris. In this experiment the current POR for pre-diffusion cleaning – a time- and chemical-consuming lab-only cleaning sequence for both the boron and phosphorus diffusion – was replaced by a standard industrial HCl+HF cleaning sequence (**2**): in consequence, a loss in implied V_{oc} of almost 10mV was recorded.

Sometimes, however, existing cleaning procedures may be optimized without the need to replace them (**3**). It has been suggested that the cleaning efficiency of an HCl step increases with lower HCl concentration [28]; in turn, the dosing volume can be increased in order to reduce bath contamination load, and moreover the net chemical consumption can be reduced. This approach, however, is unlikely to work with surfaces that are highly contaminated (especially by copper), such as after initial saw damage removal or alkaline texturing. Furthermore, potential organic residues will not be removed. An alternative, which might also help, is the addition of complexing agents: one example is SX-E, which will increase the solubility of metallic species, as reported by Treichel et al. [29].

Available cleaning-bath solutions and procedures for advanced cleaning

When the optimization of existing cleaning baths is not possible, a new, more advanced cleaning sequence needs to be chosen (**4**). Good cleaning efficiencies are ensured when cleaning solutions with a high oxidizing potential are used (possible examples are listed below). Oxidizing solutions can prevent the outplating of noble metal species (most notably copper) on the silicon surface. Furthermore, they can remove the organic contamination that remains on the surface as a result of wafer sawing or from texturing additives used for cleaning the incoming wafers or for post-texturing cleaning. In most cases a final HF dip is used to remove the sacrificial oxide layer from the surface in order to render the surface hydrophobic. It might be worth considering the use of a mixture of diluted HF and diluted HCl here, to prevent copper plating (copper has a low solubility in HF and a strong tendency for outplating [19]). Between the cleaning bath and the oxide removal step, wafers need to be rinsed in deionized water, to reduce water consumption – usually rinsing cascades are used for this. If a hydrophilic surface is required, ozonated water may be used as the last cleaning step.

> "Good cleaning efficiencies are ensured when cleaning solutions with a high oxidizing potential are used."

When oxidizing cleaning solutions are used to clean highly doped regions, etching of the surface can occur and a change in sheet resistance may be observed, which has to be taken into consideration. Moldovan et al. [30] showed that this effect can be used to advantage for a controlled emitter etch-back in ozone-based cleaning solutions. The following (incomplete) list is a collection of advanced cleaning solutions that have been suggested or designed for use in solar cell processing.

- SC-1 (only)
- SC-2 (only)
- H_2O/O_3
- HF/O_3
- HCl/O_3 or combination of HCl and HF
- SELURIS clean
- SX-E

The listed cleaning solutions are divided into three groups. The first group is simply the split-up RCA process sequence. Typically, SC-1 consists of ammonia (NH_3OH) and hydrogen peroxide (H_2O_2); it has excellent particle removal performance and will also remove organic contamination. SC1, however, is less effective in removing metallic impurities (especially at higher bath contamination loads, since H_2O_2 decomposition is catalyzed by metallic species). A less costly alternative is a mixture of NaOH with H_2O_2, often referred to as pseudo SC-1 (pSC-1); the major disadvantage of this is the need for thorough H_2O_2 control, as too low a concentration will increase the etch rate significantly, so that polishing of the surface may occur.

The SC-2 cleaning solution is a mixture of HCl and H_2O_2, and reportedly has a very good cleaning efficiency for metallic impurities [13]; however, the H_2O_2 decomposition at low pH-values is catalyzed by Cl^- ions. A lengthy discussion and summary of SC-1 and SC-2 can be found in Reinhardt et al. [13]. In general, (p)SC-1 and SC-2 require high temperatures for best performance: 70–80°C is suggested. The H_2O_2 consumption at these temperatures is high, so – in the authors' opinion – neither of these cleaning solutions is suitable for transfer to solar cell mass production.

The second group – ozone-based cleaning solutions – seems to be more promising. The oxidizing species O_3 is usually dissolved with a contacting membrane and has a relatively short half-lifetime in solution, which simplifies disposal. Once purchased, ozone-generating equipment operates at a relatively small running cost [31,32]. Ozone-based cleaning solutions usually work with low acid concentrations (or even with no added acid) [30,33], so chemical consumption for feed and bleed processing is low. Heating is not required, and higher ozone solubility is achieved using lower temperatures [34].

The last group comprises two commercially available additives, both based on biologically degradable complexing agents. SELURIS C by BASF is the main component of an alkaline cleaning mixture with H_2O_2 and water. With this recipe, low H_2O_2 decomposition and (hence) low H_2O_2 consumption have been claimed [35,36]. The SX-E approach by Sunsonix is not really a stand-alone solution but an additive that can be mixed with any existing cleaning solution, boosting its efficiency [29,37].

A critical factor related to the introduction of new processes, especially with new machines, is the ability to monitor the reagent concentration, most importantly when one or more components are consumed during the process, as in the case of H_2O_2. Monitoring can be a simple operation, especially with a small number of ingredients (e.g. monitoring by titration), but can be complex when there are multiple ingredients involved. Nevertheless, monitoring reagent concentrations is crucial for cost-effective processing, as a waste of expensive chemicals, or the loss of cleaning efficiency through a slowly changing bath make-up, can be avoided.

> "Monitoring reagent concentrations is crucial for cost-effective processing."

Simulation of cleaning-bath lifetime

To determine the connection of throughput and initial contamination level with cleaning-bath performance (**5+6**), a simple Excel-based simulation tool can be used: in combination with analytical methods, this enables one to obtain detailed information about process requirements, process stability and cleaning mechanisms. The variables used in this simulation are summarized in Fig. 2.

Surface contamination needs to be measured before and after cleaning. In this study the data for surface contamination was collected using the sandwich-etch extraction method to dissolve surface and near-surface metallic species, as described by Buchholz et al. [9], and measurements were then carried out by ICP-MS. The advantage of this method is that sampling can be performed on site to avoid risk of contamination during transportation; moreover, virtually all kinds of wafer surface in silicon solar cell processing can be measured. Using these measurements, the first simulations can be run by inputting bath size, throughput, and feed and bleed settings. The bath volume is usually kept constant independently of the dosage and carry-over from the previous bath by an overflow. The more information that is available, the more accurately the simulation will work. Variables that can be added are, for example, background contamination levels (of a new cleaning bath), certificates of analysis of the

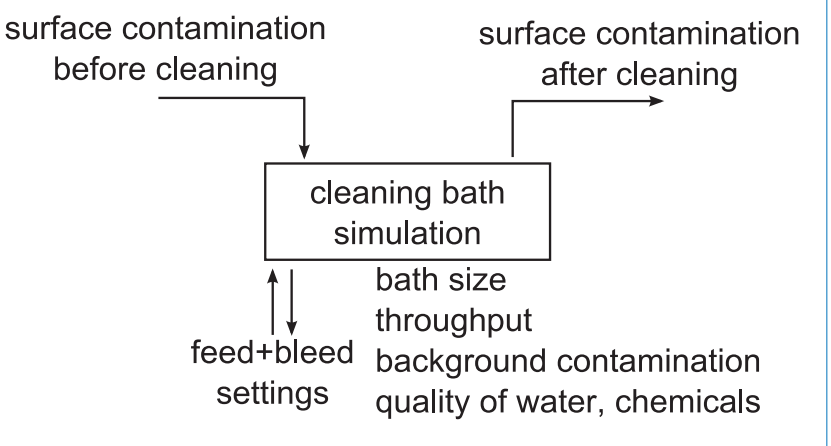

Figure 2. Schematic of the cleaning-bath simulation tool.

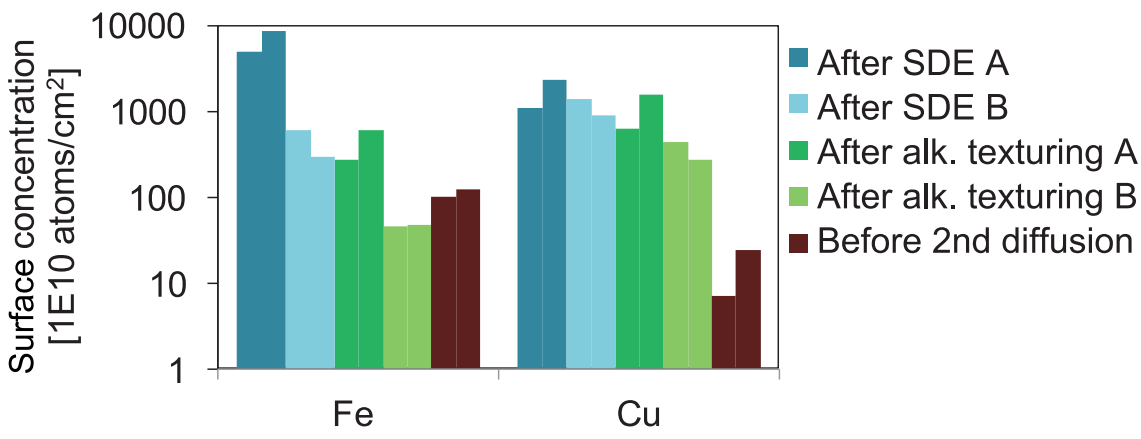

Figure 3. Iron and copper surface concentrations after saw damage etch and alkaline texturing (FEOL) on two different days, as well as before the second diffusion (BEOL), in the aforementioned BiSoN process (two measurements for each sampling point).

as-delivered chemicals, water purity levels, and carry-over from the previous bath (usually rinsing water).

Fig. 3 illustrates the significant variations in surface contamination of iron and copper at different steps in the process chain: cleaning at different stages of the process (front end of the line, FEOL, vs. back end of the line, BEOL) therefore needs to be assessed differently.

The impact of different initial surface concentrations on the bath contamination load, according to the simulation in this study, can be observed in Fig. 4; similar clean surfaces after cleaning, independently of the initial level, and the same process set-up (200L cleaning bath, 1mL/wafer is replenished), are assumed. Under constant feed and bleed conditions, with a constant intake of metal surface contamination, the contamination load of a cleaning bath will eventually reach equilibrium. It is evident from Fig. 4 that different conditions, such as a variation in initial contamination, can significantly alter the etch bath conditions. What has not been taken into account here is that the cleaning efficiency may be reduced by the enrichment of the specific species in the bath: critical concentrations need to be determined experimentally.

Experimental determination of critical concentrations / artificial bath ageing

Before the introduction of a new cleaning sequence into the process sequence, the cleaning bath can be artificially aged (**7+8**) in order to avoid actual large-scale production. Different feed and bleed scenarios should be tested (see Fig. 6), so that the most cost-effective scenario (with sufficiently high cleaning power) can be chosen. Cleaning-bath ageing is most easily realized by spiking lab-scale cleaning baths, for example by using atomic absorption spectrometry (AAS) single-element standard solutions. An example of the combination of cleaning-bath simulation and testing for process suitability in the case of two different cleaning solutions (HF/O_3 and SELURIS) is given in Fig. 5, as presented by Buchholz et al. [12] at this year's EU PVSEC.

The first graph (top left Fig. 5) shows the enrichment according to an enrichment simulation with similar parameters to those used in the simulation in Fig. 4: 500E10 atoms/cm^2 of copper (red curve) and 1000E10 atoms/cm^2 of copper (blue curve) were used as initial contamination levels. The second graph (top centre Fig. 5) shows the cleaning efficiency of a spiked cleaning bath (0ppb, 5ppb, 305ppb): a reduced copper removal efficiency was found for the HF/O_3 bath spiked with 305ppb of copper, while in the case of SELURIS there was no sign of cleaning efficiency reduction. To check whether critical concentrations had been reached, symmetrical lifetime samples were processed using the following process sequence. The as-cut wafers were textured using KOH/RENA monoTEX. The wafers were then cleaned using different cleaning procedures, and different copper contamination levels were obtained by spiking these cleaning solutions. Next, the wafers were diffused using BBr_3 in a tube diffusion furnace, and both sides were passivated using a silicon oxide-nitride passivation stack.

The implied V_{oc} values with different copper contamination levels are plotted in the third graph (top right Fig. 5). Only a small loss in implied V_{oc} is expected from the reduced cleaning efficiency. However, the first two data points already show a statistically significant decrease in implied V_{oc} for symmetrical minority-carrier lifetime samples of ~2mV. To be on the safe side (especially when expecting higher initial surface

contamination), an increase in feed and bleed volume would be advisable for the HF/O_3 process step, resulting in curves similar to those in Fig. 6: an increase from 1mL per wafer to 5mL per wafer reduces the cleaning-bath load considerably. If such modifications are to be implemented, the cost of additional chemical consumption and disposal of used cleaning solution needs to be taken into account. With very low HF concentrations, it might actually be a feasible option for improving the cleaning performance of such a cleaning-bath solution.

Monitoring of cleaning-bath quality

The importance of monitoring impurity concentrations was stressed earlier. On the one hand, cleaning baths can be optimized and controlled to ensure cost-effective processing (**10**); on the other hand, unexpected failures, such as defective equipment, can be detected at an early stage. Analytical technology, however, is often very costly, and/or it may take several days for the results to come back, as samples need to be sent to an analytical laboratory. ICP-MS analysis of wafer surfaces may easily cost up to several hundred or even thousand Euros. Nevertheless, for process analytics and process optimization, this technique cannot very easily be replaced, as it provides a quantitative analysis of many elements simultaneously, with a very low limit of detection. When such samples are required, such as for the above-described introduction of new cleaning processes, a thorough planning of experiments is strongly advised.

Analytical technology, however, is not really suitable for the constant monitoring of cleaning and/or rinsing baths. It is for this reason that Deutsche Metrohm Prozessanalytik and ISC Konstanz have developed and tested a photospectroscopic method which uses the colour of metal complexes to determine the level of contamination by iron and copper, the two most common metallic impurities; it has so far been tested and optimized for diluted HF, HCl (0.05–3%) and water. The complete method is incorporated into a fully automated Metrohm ProcessLAB. The entire sample preparation procedure is managed by a liquid-handling module that is controlled by tiamo (the Metrohm software for titration, control of the modules and data handling), in which the data is also processed and stored. Before and after each analysis stage, the entire system cleans itself automatically. The calibration of the system is performed by adding specific amounts of an iron/copper mixture to a blank solution. The method developed can be used to constantly monitor the quality of the process and of the cleaning baths: early detection of harmful enrichment or contamination from defective equipment is therefore possible. The system also allows the monitoring of most of the baths in use before the critical (i.e. high-temperature or passivation) steps, and may be used as a platform for the development of techniques for additional elements and cleaning baths [38].

> "Fundamental knowledge about cleaning-bath performance and the input variables is crucial for efficient and cost-effective cleaning in solar cell mass production."

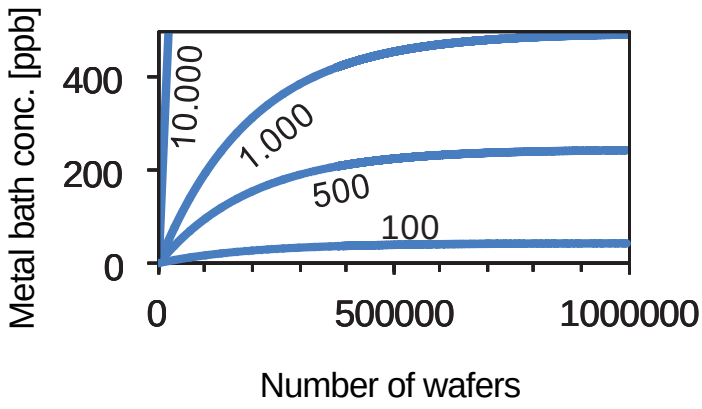

Figure 4. Simulated cleaning-bath concentration vs. wafer throughput, assuming different surface concentrations (10E10–100E10 atoms/cm²) of the to-be-cleaned wafers.

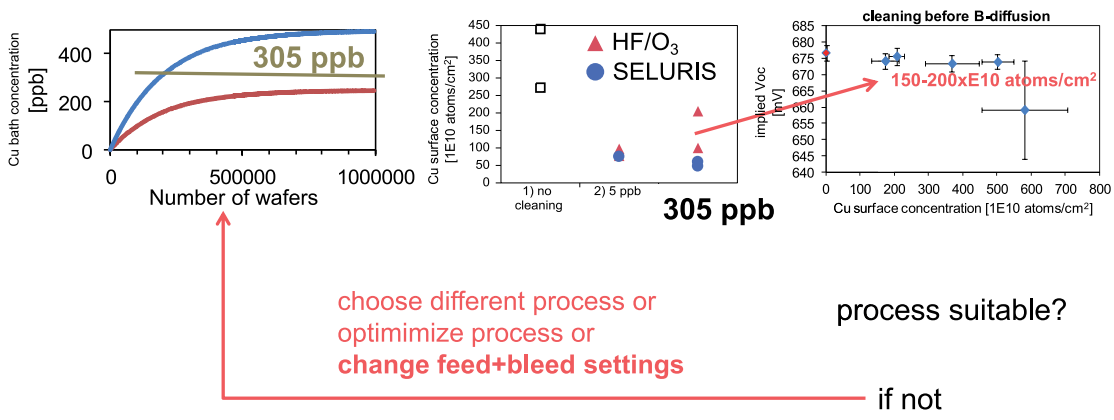

Figure 5. Process assessment of the suitability of two different cleaning baths for FOEL cleaning before boron diffusion (graphs taken from Buchholz et al. [12]).

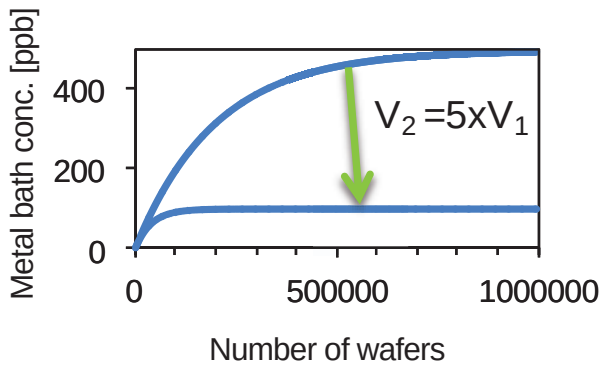

Figure 6. Simulated cleaning-bath concentration vs. wafer throughput: feed and bleed volume at high throughputs is five times as high.

Conclusion

The relevance of wafer-cleaning technology for high-efficiency solar cell processes has been summarized in this paper. O_3-based cleaning appears to be promising; there are, however, other highly efficient cleaning solutions available. Fundamental knowledge about cleaning-bath performance and the input variables, such as metallic surface contamination, is crucial for efficient and cost-effective cleaning in solar cell mass production. A ten-step scheme for the introduction of new process steps into existing lines and/or new solar cell lines has been proposed, with a focus on feed and bleed parameters. FEOL cleaning in particular is highly demanding, as the contamination from the wafer surface can vary from batch to batch. In-line analytical facilities are recommended in order to assure the quality and maintain high yields, especially when unexpected contamination occurs.

Acknowledgement

This work was partially funded by the German Federal Ministry of Education and Research (BMBF) under Contract No. 0355F0335I (xμ-Zelle).

References

[1] Graff, K. 1995, *Metal Impurities in Silicon-Device Fabrication*, Berlin: Springer-Verlag.

[2] Macdonald, D. 2005, "Impact of nickel contamination on carrier recombination in n- and p-type crystalline silicon wafers", *Appl. Phys. A: Mater. Sci. Process.*, Vol. 81, No. 8, pp. 1619–1625.

[3] Zhong, L. et al. 1992, "Dependence of lifetime on surface concentration of copper and iron in silicon wafers", *Appl. Phys. Lett.*, Vol. 61, No. 9, pp. 1078–1080.

[4] Macdonald, D. et al. 2005, "Impact of Cr, Fe, Ni, Ti and W surface contamination on diffused and oxidised n-type crystalline silicon wafers", *Proc. 20th EU PVSEC*, Barcelona, Spain, pp. 627–630.

[5] Breitenstein, O. et al. 2011, "Understanding junction breakdown in multicrystalline solar cells", *J. Appl. Phys.*, Vol. 109, No. 7, pp. 071101–071110.

[6] Coletti, G. et al. 2011, "Impact of metal contamination in silicon solar cells", *Adv. Funct. Mater.*, Vol. 21, No. 5, pp. 879–890.

[7] Istratov, A.A. et al. 2000, "Iron contamination in silicon technology", *Appl. Phys. A: Mater.*

Sci. Process., Vol. 70, No. 5, pp. 489–534.
[8] Istratov, A.A. et al. 2002, "Physics of copper in silicon", *J. Electrochem. Soc.*, Vol. 149, No. 1, pp. G21–G30.
[9] Buchholz, F. et al. 2011, "Measurement and impact of surface transition metal contamination of textured multicrystalline silicon wafers", *Proc. 26th EU PVSEC*, Hamburg, Germany, pp. 1187–1190.
[10] Schweckendiek, J. et al. 2013, "Cleaning in crystalline Si solar cell manufacturing", *Solid State Phenom.*, Vol. 195, pp. 283–288.
[11] Bidiville, A. et al. 2009, "Diamond wire-sawn silicon wafers – from the lab to the cell production", *Proc. 24th EU PVSEC*, Hamburg, Germany.
[12] Buchholz, F. et al. 2013, "Comparison of wafer cleaning procedures for high efficiency n-Type Solar Cells", *Proc. 28th EU PVSEC*, Paris, France.
[13] Reinhardt, K.A. et al. 2011, *Handbook of Cleaning for Semiconductor Manufacturing – Fundamentals and Applications*, Hoboken, NJ, and Salem, MA: John Wiley & Sons, Inc. – Scrivener Publishing LLC.
[14] Bentzen, A. et al. 2006, "Gettering of transition metal impurities during phosphorus emitter diffusion in multicrystalline silicon solar cell processing", *J. Appl. Phys.*, Vol. 99, p. 093509.
[15] Buchholz, F. et al. 2012, "Metal surface contamination during phosphorus diffusion", *Energy Procedia*, Vol. 27, pp. 287–292.
[16] Macdonald, D. et al. 2006, "Effect of gettered iron on recombination in diffused regions of crystalline silicon wafers", *Appl. Phys. Lett.*, Vol. 88, No. 9, pp. 092103–092105.
[17] Phang, S.P. et al. 2011, "Direct comparison of boron, phosphorus, and aluminum gettering of iron in crystalline silicon", *J. Appl. Phys.*, Vol. 109, No. 7, p. 073521.
[18] Rothschild, A. et al. 2012, "Impact of surface preparation prior to ALD-Al_2O_3 deposition for PERC type solar cell", *Proc. 27th EU PVSEC*, Frankfurt, Germany, pp. 1974–1977.
[19] Danel, A. et al. 2012, "HF last passivation for high efficiency a-Si/c-Si heterojunction solar cells", *Solid State Phenom.*, Vol. 187, pp. 345–348.
[20] Glunz, S. 2007, "High-efficiency crystalline silicon solar cells", *Adv. in OptoElec.*, p. 97370 [available online at http://www.researchgate.net/publication/235706671_Overview_of_High_Efficiency_cSi_Solar_Cell_Developments_in_Research_and_Production].
[21] Reinhardt, K.A. et al. 2008, *Handbook of Silicon Wafer Cleaning Technology*, Norwich, UK: William Andrew Inc.
[22] Kern, W. 1993, *Handbook of Semiconductor Wafer Cleaning Technology: Science, Technology, and Application*, Park Ridge, NJ: Noyes.
[23] Leachman, R.C. et al. 1996, "Benchmarking semiconductor manufacturing", *IEEE Trans. Semicon. Manufac.*, Vol. 9, No. 2, pp. 158–169.
[24] Kern, W. et al. 1970, "The RCA-clean", *RCA Review*, Vol. 31, p. 197.
[25] Meuris, M. et al. 1995, "The IMEC clean – A new concept for particle and metal removal on Si surfaces", *Solid State Technol.*, Vol. 38, No. 7, p. 109.
[26] Heyns, M. et al. 1999, "Advanced cleaning strategies for ultra-clean silicon surfaces", *Proc. 6th Intl. Symp. Electrochem. Soc.*, pp. 2–15.
[27] Edler, A. et al. 2011, "Improving screen printed metallization for large area industrial solar cells based on n-type material", *Energy Procedia,* Vol. 8, pp. 493–497.
[28] Anttila, O.J. et al. 1992, "Metal contamination removal on silicon wafers using dilute acidic solutions", *J. Electrochem. Soc.*, Vol. 139, No. 6, pp. 1751–1756.
[29] Treichel, H. et al. 2011, "Removal of trace metals using a biodegradable complexing agent", *Photovoltaics International*, 5th edn, pp. 81–93.
[30] Moldovan, A. et al. 2013, "Combined ozone/HF/HCI based cleaning and adjusted emitter etch-back for silicon solar cells", *Solid State Phenom.*, Vol. 195, pp. 305–309.
[31] Gottschalk, C. et al. 2004, "Using dissolved ozone in semiconductor cleaning applications", *Micro*, Vol. 22, No. 2, pp. 81–84.
[32] Bergman, E. et al. 2001, "Process and environmental benefits of HF-ozone cleaning chemistry", *Solid State Technol.*, Vol. 44, No. 7, p. 115.
[33] Bergman, E.J. et al. 2001, "Pre-diffusion cleaning using ozone and HF", *Solid State Phenom.*, Vol. 76, pp. 85–88.
[34] De Smedt, F. et al. 2001, "The application of ozone in semiconductor cleaning processes: The solubility issue", *J. Electrochem. Soc.*, Vol. 148, p. G487.
[35] Moldovan, A. et al. 2013, "A novel approach to high performance and cost effective surface cleaning for high efficiency solar cells", *Proc. 28th EU PVSEC*, Paris, France.
[36] Ferstl, B. et al. 2013, "Investigation on wet chemical solutions performing pre-diffusion and pre-passivation cleans in next generation PERC-type silicon solar cells", *Proc. 28th EU PVSEC*, Paris, France.
[37] Bohling, D. et al. 2010, "Crystalline silicon solar cell efficiency improvement by advanced cleaning technology", *Proc. NSTI Nanotech*, Anaheim, California, USA, pp. 704–707.
[38] Buchholz, F. et al. 2013, "Spectrophotometric monitoring of iron and copper contamination of cleaning baths for solar cell processing", *Proc. 28th EU PVSEC*, Paris, France.

About the Authors

Florian Buchholz studied chemistry and English at the University of Konstanz and the University of Technology in Sydney from 2003 to 2010. From July 2008 to November 2009 he worked as a research assistant at ISC Konstanz, where he was responsible for wet chemical processes and process analysis. Since 2010 he has been working towards his Ph.D. at ISC Konstanz, investigating metal contamination in solar cell processing, and is currently employed in the quality management department.

Dr. Eckard Wefringhaus is one of the founding members and a member of the Board of ISC Konstanz, and has been a member of the staff since 2006. As director of the quality management department, he is responsible, along with his team, for the supply of infrastructure and machines and for the continuous improvement of standard processes. His current research topics include wet chemical texturing, polishing and edge isolation of silicon wafers.

Enquiries

International Solar Energy Research Center Konstanz e.V.
Rudolf-Diesel-Str. 15
D-78467 Konstanz
Germany

Tel: +49 (0) 7531-36 18 3-553
Fax: +49 (0) 7531-36 18 3-11

Email: florian.buchholz@isc-konstanz.de
Website: http://www.isc-konstanz.de

Characterization of damage and mechanical strength of wafers and cells during the cell manufacturing process

Ringo Koepge[1], **Frank Wegert**[2], **Sven Thormann**[2] & **Stephan Schoenfelder**[1]

[1]Fraunhofer Center for Silicon Photovoltaics CSP, Halle; [2]Hanwha Q CELLS GmbH, Bitterfeld-Wolfen, Germany

ABSTRACT

Minimizing the breakage rate of silicon wafers and cells during production has been one of the key issues for reliable and productive solar cell manufacturing. However, the root causes of damage or breakage, as well as the mechanical characteristics of manufacturing processes, are not completely understood. In the study described in this paper the change in mechanical strength and the damaging of wafers and cells was analyzed in an industrial cell manufacturing line in order to detect critical process steps and handling operations in certain processes such as etching, diffusion, screen printing and firing. An analysis and discussion of damage sources is presented which offers more insight than the conventional study of breakage rate that is mostly performed by cell manufacturers. In a systematic experimental study, 19 different locations in the production line were investigated. The mechanical strength of 800 wafers or cells at different points in the cell line was subsequently determined using the four-line bending test and the statistical parameters for the Weibull distribution. It was discovered that dramatic changes in strength occur at different process steps because of the change in defect structure; there were also found to be several positions at which no further damage was detected. This method of investigation can therefore be used as a fingerprint of a cell line in respect of yield and breakage rates. Individual processes can be identified that indicate high damage potential, although the actual breakage could occur in a subsequent process step.

Introduction

Crystalline solar cell technology still dominates the PV market [1,2]. The production of silicon solar cells, however, needs to be improved with regard to the cost of their manufacture. On the one hand, a higher use of automation and higher throughput for faster processes can decrease these costs. On the other hand, the thickness of wafers has been reduced to 180µm or 160µm in the last few years because the material is still a dominant cost factor [3]; moreover, new cell concepts demand even thinner wafers to achieve high cell efficiencies [3]. As a result of the use of advanced automation with higher throughputs and lower wafer thicknesses, the wafers are subjected to higher static or dynamic loads, and thus they are more susceptible to damage or fracture.

As reported in the literature, investigations regarding the influence of cell processing steps have mostly focused on the damage-etching and texturing steps at the beginning of the cell manufacturing process [4–10]. Evidently, the damage from the wire sawing process is removed by etching, and the strength of the wafers consequently strongly increases, depending on the chosen texturing process or etch depth. Other researchers have investigated in more detail the metallization process at the end of the cell manufacturing procedure [11,12]. While texturization and metallization are very important process steps, other process or handling steps are largely neglected. There seem to exist only a few documented analyses (for example Chen et al. [13] and Micciche et al. 14]) which deal with a sequence of process steps and their influence on the damage and strength of wafers. More recently, there have been detailed investigations regarding damage to wafers caused by handling operations: these investigations show that grippers deform wafers and cause tensile stress fields. Tensile stresses can lead to the failure of a wafer if a critical defect, mainly a critical crack length, in the wafer is put under load [15]. A statistical evaluation of different gripper techniques showed that handling causes damage to wafers, but the level of damage can vary depending on the gripper technology used [16]. Furthermore, it was found that impact loading on the wafer edges can be harmless if the combination of wafer thickness and impact load is below a critical value [17]. In summary, detailed information is available about the influence of individual process steps on the mechanical wafer strength or damage, but there is only a limited understanding so far regarding the influence of the handling steps. Thus, it is difficult to predict wafer damage and strength during the entire cell manufacturing process, and analyses of the complete process line are necessary.

> "A crucial consideration for breakage is not only the damage but also the critical load."

The root causes of the damage or breakage of wafers, however, during cell manufacturing are not completely understood, especially in the handling steps. It is important to note that in brittle materials, such as silicon wafers, a crucial consideration for breakage is not only the damage (cracks, notches, etc.) but also the critical load. Damage and breakage can therefore occur at different stages in cell manufacture. Furthermore, it is insufficient to analyze just the breakage rate. A quantitative and systematic method is required for measuring the intensity of damage and for detecting critical steps in a process line. In combination with ordinary or random root causes, such a quantitative method would provide information about systematic influences on wafer strength as a part

Material	multicrystalline
Dimension	156mm × 156mm (±0.5mm)
Thickness	200µm (±20µm)

Table 1. General properties of extracted wafer samples.

of the statistical process control (SPC) along the cell manufacturing line.

This paper presents an analysis of wafer strength at each position in a cell production line. A variable fracture strength can be related to specific process steps or the handling operation. On the basis of these results, any damage to wafers in previous process steps can be observed and correlated to the observed breakage rate.

Sample extraction

Wafers and solar cells were taken out of the Hanwha Q CELLS' cell manufacturing line at 19 different positions. Each wafer and cell was then analyzed regarding their breakage behaviour to correlate the mechanical properties of the wafers with the actual process step.

The substrates were taken out of one production slot; their specific properties are summarized in Table 1. The chosen cell production line was fully automated for a classic Al-BSF cell process cycle, consisting of the main process steps shown in Fig. 1.

Between the process machine steps the wafer substrates were handled by belt magazines and slot carriers using soft handling and robots. No touching and handling of the substrate by operators occurred anywhere along the entire manufacturing line. The material was extracted by hand before and after every process machine, starting with as-cut wafers in the standard original polystyrene transport box. During and after the extraction no wafer was broken until the four-point bending test was performed. The extracted material was stored carefully in separate boxes on which the transport and sawing direction was marked for the mechanical analysis.

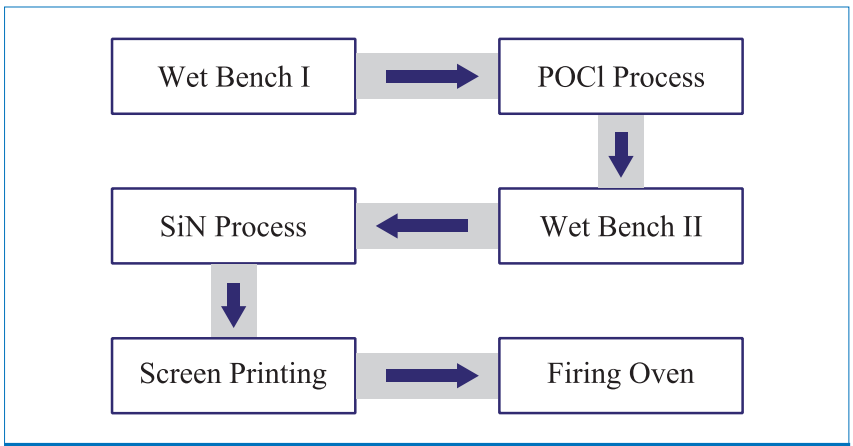

Figure 1. Typical process steps in an actual manufacturing line.

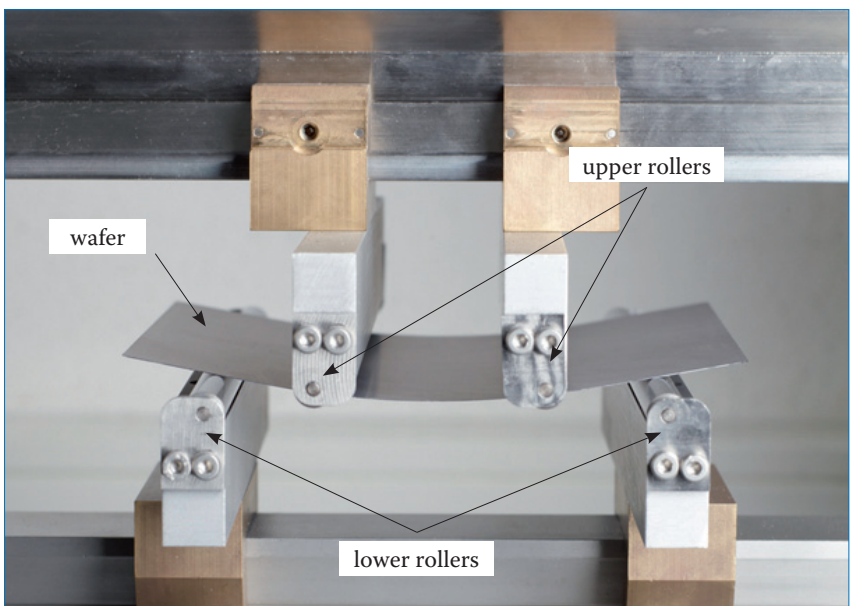

Figure 2. The four-point bending test principle for silicon wafers and cells.

Damage analysis

In order to investigate the damage of the wafers after the handling and process steps, non-destructive or destructive methods can be applied. The resolution of micro-crack detection systems, however, is too low to identify relevant critical cracks (which are in the micrometre range), and a manual analysis by optical and infrared microscopy can be very time consuming. The damage was therefore measured indirectly by wafer strength [6,18,19]; these methods are similar to standard methods for other materials (see, for example, the DIN Standard [20]). Since the strength of a brittle material is defined by the largest defect in the stress field of the loaded wafer/cell, the changes in defect type and size can be determined by measuring the material strength. A statistical approach is therefore used, namely the Weibull distribution [21], which indirectly represents the defect distribution and requires no detailed information about the defect type. Statistical parameters can then be compared for different process steps, and the significance of changes can be analyzed. To ensure reliable results, it is necessary to evaluate 30 to 50 wafers/cells for each position in the process line.

The wafer strength was measured using a four-line bending test, which is more commonly known as the 'four-point bending test' [20]. The set-up is shown in Fig. 2: a parallel set of loading and support rollers bend the wafer uniaxially until the wafer breaks. The fracture force and fracture deflection are derived from the force-deflection charts resulting from the experiments. The set-up geometry consisted of a load span of l = 110mm between the lower rollers and b = 55mm between the upper rollers; the rollers had a diameter of 10mm and were covered by a polymer tape to reduce contact pressure. In this investigation the wafers were placed on the experimental set-up with the sawing direction parallel to the rollers for wafers at process positions P1 to P7 (see Fig. 5). For wafers at positions P8 onwards, a reliable detection of the sawing direction was not possible. The wafer direction can therefore vary within a single batch. After screen printing, the busbars were aligned in parallel to the rollers. The sunny side of the wafers and cells was placed in the constant tensile stress field within

the inner rollers for the four-point bending test. A strength reference was determined by testing two batches of untreated wafers, in both parallel and perpendicular orientations with the sawing direction. The reference represents the mechanical preconditions of the wafers at the beginning of the manufacturing process.

The four-point bending tests were performed on a ZWICK 1445 universal testing machine. The force was measured by a 500N load cell, and the deflection was measured by the position of the machine truss. The mean thickness of every wafer was measured by the weight in order to take into account thickness variations within the batch. The fracture stress was determined by the finite-element (FE) method based on parametric 3D shell models, which considers large deflections of the wafers and contact behaviour between the rollers and the wafer (see Fig. 3(c)). For solar cells with metallization, extended layer shell models were used to calculate a fracture stress of silicon, as described in Kaule et al. [22]; the mean thickness and the resulting fracture force and deflection from the experiment were used as input data for the FE models. The fracture stress was defined as the maximum first-principal stress in the silicon wafer.

The Weibull distribution [21] was used for a statistical evaluation of the fracture stresses of every batch. This distribution function is based on weakest-link theory and is commonly used for brittle materials such as silicon: the two function parameters are the characteristic fracture stress σ_θ, at which 62.3% of all samples fail, and the Weibull modulus m, which represents the scattering. The Weibull parameters, estimated by the maximum-likelihood estimation, as well as the confidence bounds, were determined in accordance with the ASTM standard [23].

Experimental results

The results of the strength and damage analyses are given in the following sections, beginning with a presentation of the experimental data, followed by the statistical parameters. The fracture stresses of every wafer were calculated by considering the thickness and fracture deflection using the FE model. Interestingly, while performing the experiments there was no breakage of wafers or cells due to process or handling steps. Thus, it is important that the invisible damage caused in the manufacturing process is analyzed by strength tests.

> "It is important that the invisible damage caused in the manufacturing process is analyzed by strength tests."

The force-deflection curves were first compared with those derived from the FE model (Fig. 3(a) and (b)). The slopes of the curves represent the stiffness of the wafers; the thickness of the wafer and its variation dominate the variation in stiffness, i.e. the variation in slope. There were only small deviations in mean thickness, which can be seen by the small scattering of the slopes within the batch (Fig. 3(a)). In Fig. 3(b) a comparison of an experimental and simulated data curve is shown: the two data sets are in close agreement, so it can be assumed that the experimental procedure of the four-point bending test was performed correctly and that the model sufficiently represents the mechanical behaviour and the fracture stress. On the basis of these data, the

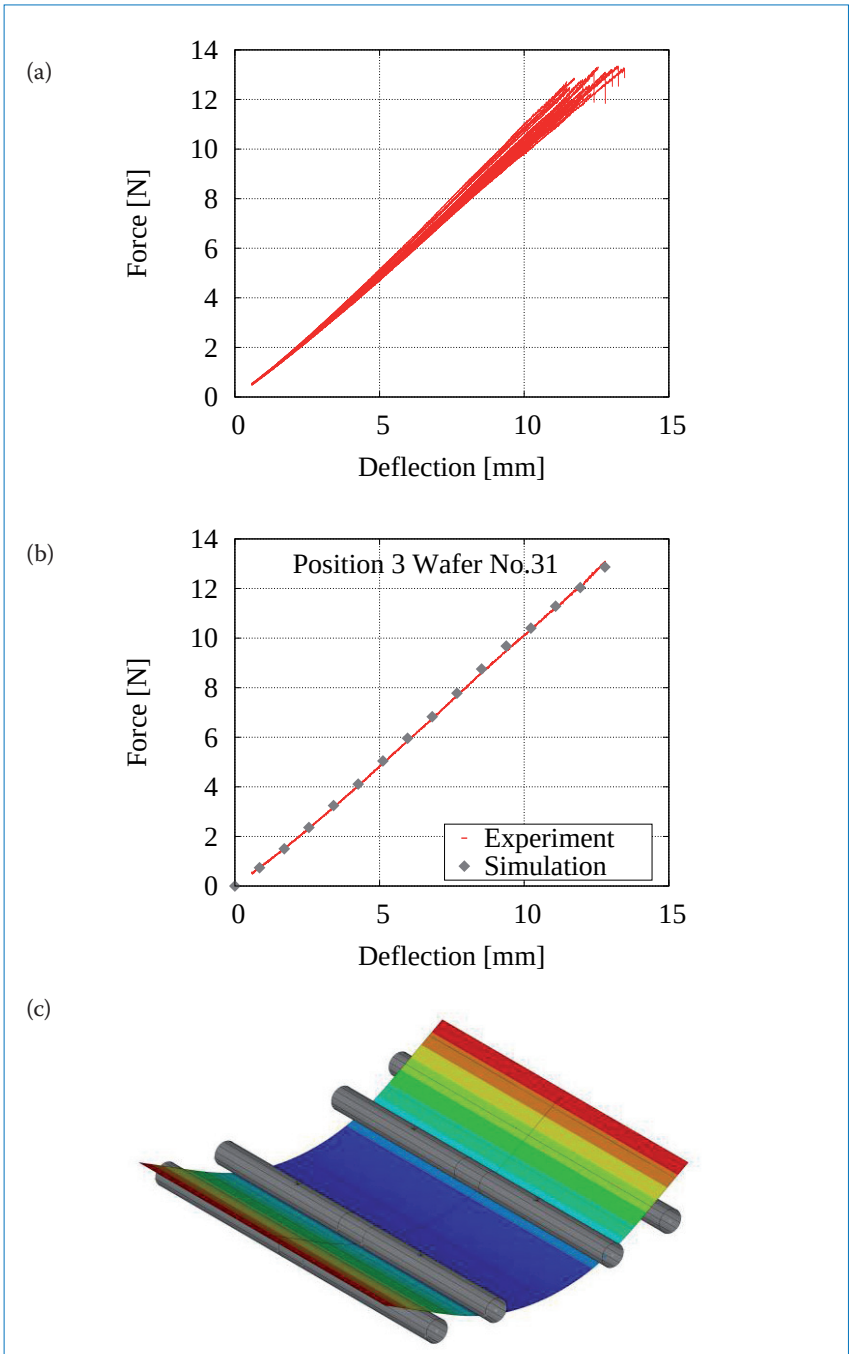

Figure 3. Force-deflection curves from the four-point bending test, and the FE model image: (a) mechanical behaviour of wafers taken from manufacturing position P3; (b) comparison of experimental and simulated data points (wafer no. 31 at P3); (c) calculated deflection of the silicon wafer subjected to four-point bending.

fracture stresses were calculated using the FE model (Fig. 3(c)).

Fig. 4 shows example strength distributions and Weibull plots for the reference batches, i.e. the initial mechanical strength of the wafers used. The distribution of the detected fracture stresses at the beginning (Fig. 4(a) and (b)) and at each extraction position is adequately represented by a Weibull distribution (Fig. 4(c)). Thus, in the following, only the characteristic fracture stress (σ_θ) and the Weibull modulus (m) are used to characterize the mechanical properties of each wafer batch (see Table 2). For the reference batch P1, no significant difference between the characteristic fracture stresses regarding the loading direction could be observed. When the wafers were loaded in parallel and perpendicularly to their sawing direction, 63.2% of the tested wafers failed at tensile stresses of 144.2MPa and 146.2MPa, respectively. In contrast, the Weibull modulus is significantly different. The scattering of fracture stresses depends on the wafer orientation during the four-point bending test. In this case the scattering was higher for wafers that were tested perpendicularly to their sawing direction. Thus, the confidence bound ranges of the characteristic strength and the Weibull modulus must be considered if a comparison is made with data from a subsequent production process.

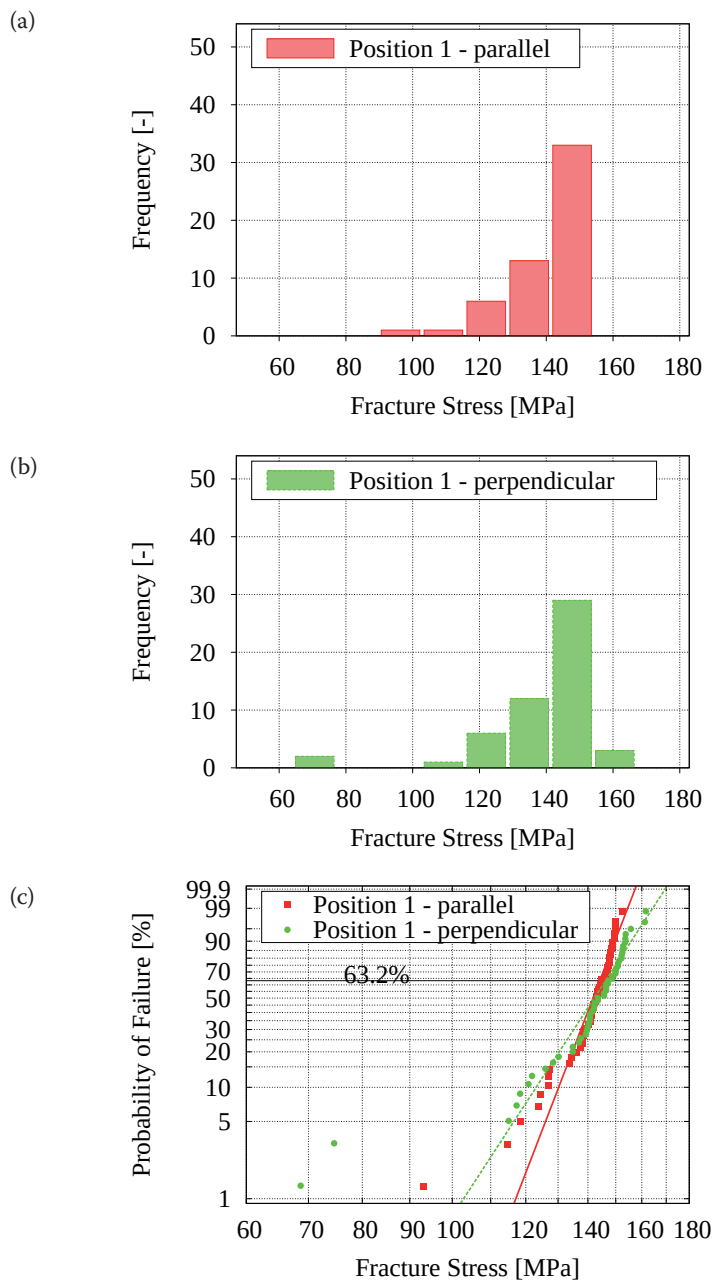

Figure 4. Distribution of fracture stresses of untreated reference wafers: (a) histogram of fracture stresses (parallel to sawing direction); (b) histogram of fracture stresses (perpendicular to sawing direction); (c) Weibull diagram of reference wafers parallel and perpendicular to the sawing direction.

The characteristic fracture stresses and Weibull moduli are summarized in Table 2 for all wafer and cell extraction positions. The strength behaviour for some batches of wafers and cells exhibits significant differences between the characteristic fracture stresses and the Weibull moduli. The significance is rated by the confidence bounds, which may overlap (no significant difference in strength and damage) or may not overlap (significant difference in strength and damage).

A visualization of the characteristic fracture stresses and Weibull moduli vs. the extraction positions in the process line is presented in Fig. 5; the first two bars of P1 and their confidence bounds represent the reference values. It can be clearly seen that there is an initial increase to 199MPa in the characteristic fracture stress after the first etching process, while the Weibull modulus remains within the range of the confidence bounds of the reference parallel and perpendicular batches. The Weibull modulus depends on the loading direction, which cannot be assured for all tested wafers and cells. Thus, similar scattering of the fracture stresses for subsequent process steps can be expected to lie within the range of the reference batches for a Weibull modulus m between 13 and 22. Differences in the Weibull modulus were, however, observed and interpreted between individual extraction positions.

The next stage of increase in fracture stress σ_θ was observed after the diffusion process (batch P7): the characteristic fracture stress rises up to 208MPa. The final increase in σ_θ was determined after a handling operation (batch P14), with the characteristic fracture stress reaching its maximum of about 218MPa after deploying the silicon nitride mounting device. Almost at the end of the manufacturing line, after firing the cell contacts, a decrease of σ_θ to 198MPa was measured. In summary, four processes were detected that showed a significant change in the characteristic fracture stress, but overall the strength of a wafer was increased by about 34% during the process line until the wafer became a complete solar cell.

Extraction position	σ_θ [MPa]	m [-]
P1[1]	144.2 (142.6…145.8)	22.1 (18.0…25.8)
P1[2]	146.2 (143.5…149.0)	13.1 (10.7…15.3)
P2	142.4 (139.9…145.0)	18.5 (13.9…22.5)
P3	198.8 (194.8…202.8)	16.4 (12.4…20.0)
P4	194.0 (190.9…197.2)	21.0 (15.7…25.6)
P5	204.2 (200.1…208.4)	16.7 (12.5…20.3)
P6	193.6 (187.9…199.5)	11.9 (8.8…14.7)
P7	207.6 (202.5…212.9)	13.5 (10.1…16.5)
P8	214.1 (210.9…217.4)	22.1 (16.6…26.9)
P9	206.9 (201.6…212.5)	12.9 (9.7…15.7)
P10	208.2 (205.8…210.6)	29.4 (22.0…35.8)
P11	206.1 (200.7…211.7)	12.6 (9.4…15.3)
P12	196.7 (189.3…204.4)	8.8 (6.6…10.7)
P13	205.0 (199.3…210.9)	11.9 (8.9…14.5)
P14	218.0 (213.5…222.7)	15.9 (11.9…19.4)
P15	218.8 (214.6…223.1)	17.2 (12.9…21.0)
P16	212.9 (207.1…218.9)	12.1 (9.1…14.8)
P17	212.4 (208.2…216.8)	16.7 (12.5…20.3)
P18	197.5 (192.1…203.2)	12.2 (9.1…15.0)
P19	193.9 (190.1…197.7)	17.3 (13.0…21.1)

[1] rollers parallel to saw marks
[2] rollers perpendicular to saw marks

Table 2. Characteristic fracture stresses, Weibull moduli and 90% confidence bounds (in parentheses) of wafer batches at every extraction position (P1 = reference batch).

"Overall the strength of a wafer was increased by about 34% during the process line."

Strengthening and damaging of wafers

The results demonstrated that the strengthening and damaging of silicon wafers due to the manufacturing process can be measured by a statistical characterization of wafer strength. The estimated statistical parameters showed significant differences, and clear trends were visible in the experimental data. Various observations will now be discussed in detail.

The possibility of damaging a wafer exists at many positions in the manufacturing line, as highlighted by Fig. 5: for instance, the characteristic fracture stress increases and decreases between positions P3 and P9 as a result of two etching processes and one diffusion process. Although it was not possible to detect significant differences between manufacturing positions, a trend could be seen. The variation in the Weibull modulus during the manufacturing process confirmed this effect, because a change in this value correlates to a change in the defect distribution. In particular, the Weibull modulus tends to decrease from extraction positions P4 to P6. This means that

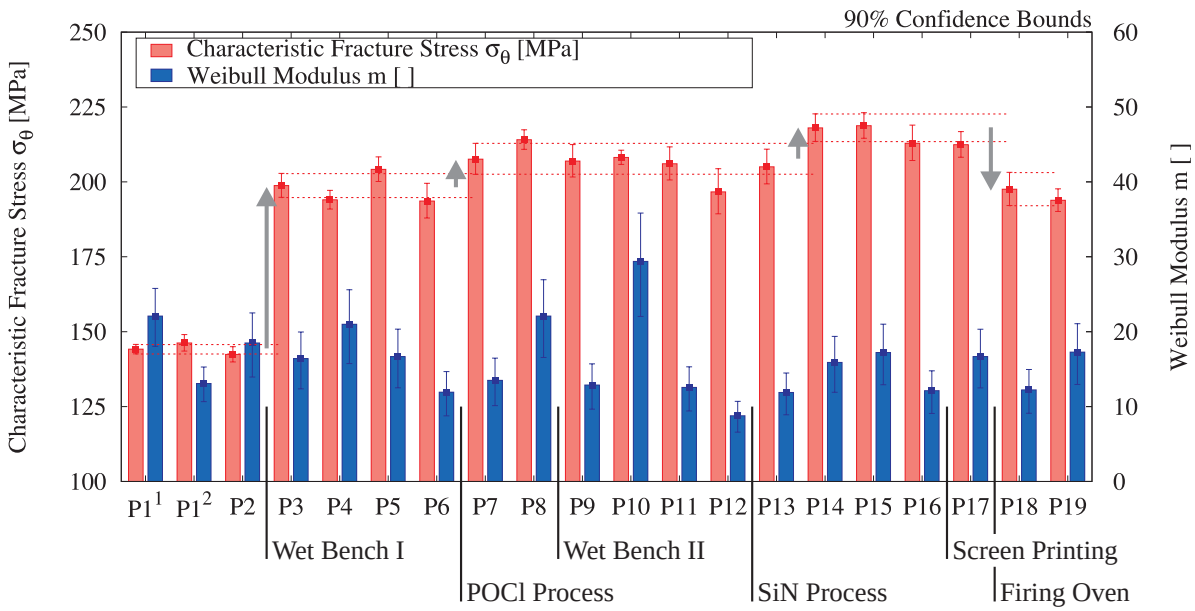

[1] rollers parallel to saw marks
[2] rollers perpendicular to saw marks

Figure 5. Distribution of characteristic fracture stresses (σ_θ) and Weibull moduli (m) at all cell line extraction positions.

an effect is present that changes the fracture stress distribution without a significant shift in the characteristic fracture stress. It is important to note that after the strengthening by POCl diffusion (P7 onwards), the fracture stresses remained nearly constant until P13. A significant departure from the confidence bounds of the Weibull modulus was observed between extraction positions P9 and P10, which is a handling step only. As a result of handling, the defect structure may change, causing a higher scattering of the fracture stress by having no effect on the characteristic fracture stress.

The observed wafer strengthening trend between extraction positions P12 and P14 featured a rising characteristic fracture stress and an increasing Weibull modulus; the deposition of SiN, as well as several handling steps, takes place at these positions. As the Weibull modulus increases, the scattering of the fracture stress of strength wafers decreases because of a narrower defect distribution. The rising characteristic fracture stress, however, is more difficult to explain. This effect represents a strengthening of the wafers due to handling only in these process steps. Currently, there are two hypotheses. First, the SiN process is assumed to strengthen the wafers similarly to the POCl process, but random damage situations during processing and handling in the line caused different defect distributions for the extracted batches P12–P14. Therefore, wafers from P14 might show less of this random damage than those from P12 and P13, which would result in higher fracture stress values. Second, similar strengthening effects due to handling have been seen before [16]. Handling operations could therefore affect the strength of wafers in a positive way. However, the reasons are assumed to be the intrinsic material effects in silicon as a result of cycling [16]; these effects are not yet fully understood and further research is necessary.

In summary, the highest strengthening of the wafers was observed after the first etching and texturing process. This effect is well known and can be correlated with a change in the surface damage intensity of the wafers. Damage such as small cracks caused by wire sawing vanish, and the tips of larger cracks become blunted [6,7,10]. The POCl diffusion process also changes the surface properties. High-temperature processes and the presence of oxygen strengthen the silicon by the formation of a silicon oxide layer in the crack, thus closing it [24,25]. In this case an increase in the characteristic fracture stress is much smaller than if cracks are removed, as in the etching process.

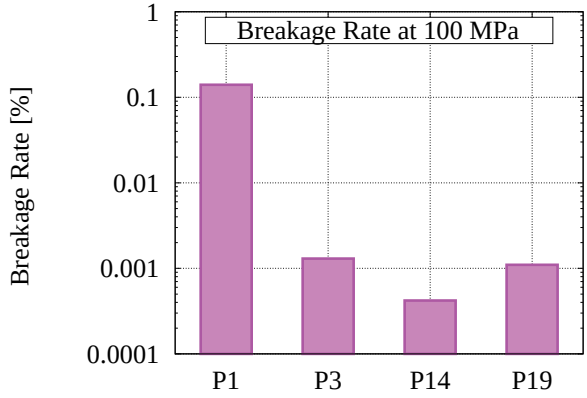

Figure 6. Predicted breakage rate of wafers extracted at different stages of the manufacturing process, for a chosen load of 100MPa (prediction based on determined statistical strength parameters).

The final strengthening effect takes place at position P14, after a handling operation. In the previous section different hypotheses were mentioned regarding this effect, which requires further analysis. The final process step is firing of the contacts, from P17 to P18. A high-temperature process causes internal mechanical stresses in the material because of a thermal expansion mismatch between the silicon and the contacts on the front and back sides. This causes a bowing of the solar cell [11,26], and the residual stresses can reduce the strength of the cell. The residual stress fields due to bowing are tensile stresses on the sunny side of the solar cell. Since this side was tested in the experiments, the drop in fracture stresses most likely results from these residual tensile stresses, which lower the load capability and the strength. Further damage in the firing process step, however, may also contribute to the lower strength of solar cells. Nevertheless, the solar cell in this inspected cell line increases in strength by 34% compared with a virgin as-cut silicon wafer. Although all of the strengthening and damaging effects could similarly be found in other cell lines, these results represent the strength fingerprint of the cell manufacturing line.

Breakage rate estimation

A breakage rate can be estimated on the basis of the fracture stresses of all the wafers and cells used in this investigation. In practice, only the weakest wafers are of interest because they fail first. Thus, for the estimation the focus will be on only the lower end of the fracture stresses of each strength distribution. Fig. 6 shows the probability of failure or estimated breakage rate for an assumed load of 100MPa (neglecting the strength size effect): such a load could be caused by a handling or process step during the manufacturing process. It can be seen that the untreated wafers at the beginning of the production line have the highest probability of failure (0.1%). After the etching step, the breakage rate decreases to approximately 0.0013%, reaching a minimum of less than 0.00042% after the unloading of the SiN mounting device, at position P14. Compared with an untreated as-cut wafer, the breakage rate of a finished solar cell is very low: for a load of 100MPa, the probability of failure decreases during manufacturing to 0.0011% (a factor of 25). Solar cells are therefore mechanically more reliable than as-cut wafers.

It should be borne in mind that the damage potential determined by a breakage rate estimation represents the systematic influence of the manufacturing line on strength and breakage. It can thus be interpreted as a fingerprint of the cell line.

The estimated breakage rate does not represent the total wafer breakage in the line. The real breakage rate is always the sum of the systematic and random damage which causes breakage. If the number of systematic causes (from the Weibull analysis in this paper) is known, as well as the total amount of wafer breakage (resulting from the statistical process control), the contributions of systematic and random damage sources can be determined in order to optimize individual process or handling steps or to benchmark technical improvements in a production process.

Conclusion

A crucial task in solar cell manufacturing is the reduction of the breakage rate in order to achieve a reliable and efficient production process. This paper has presented a way to analyze the damage potential of individual procedures as well as entire manufacturing process lines. With the help of focused systematic mechanical testing and a statistical analysis of wafer strength, a critical process step can be detected and the breakage rate can be estimated. There are three significant strengthening or damaging steps in a solar cell manufacturing line:

1. The first and major process step is the etching and texturing process, which increases the characteristic fracture stress by 40%.

2. Subsequent process steps, such as POCl diffusion, cause a small strengthening increase of 4%.

3. After the cell contacts are fired, the strength decreases by 9%; the final strength of a solar cell, however, is increased by about 34% in comparison to that of the as-cut wafer at the beginning.

> "The variation in the Weibull parameters is important for identifying a change in damage distribution of the wafers during the manufacturing process."

The variation in the Weibull parameters is important for identifying a change in damage distribution of the wafers during the manufacturing process: different trends were observed, which need to be analyzed in more detail to gain a more comprehensive understanding of the impact on defects and the strength associated with individual process steps. Moreover, the statistical Weibull analysis has to be compared with data from the statistical process control in order to enlarge the database and to identify the critical steps in a manufacturing process.

Acknowledgements

The authors are grateful for the financial support from the Federal Ministry of Education and Research within the Spitzencluster Solarvalley Mitteldeutschland in the 'xμ-Zellen II' project (FhG CSP Contract No. 03SF0399D, Q CELLS Contract No. 03SF0399A). Special thanks are given to F. Kaule (Fraunhofer CSP) for the strength evaluation for solar cells.

References

[1] EuPD Research 2011, "PV Thin Film Industry Guidebook".

[2] EuPD Research 2012, "European PV InstallerMonitor 2012/2013".

[3] SEMI PV Group Europe 2013, "International technology roadmap for photovoltaic (ITRVP): Results 2012", 4th edn (March) [available online at http://www.itrpv.net/Reports/Downloads/].

[4] Orellana Pérez, T. et al. 2009, "Increase in mechanical strength of as-cut mono-crystalline silicon wafers by alkaline etching process", *Proc. 24th EU PVSEC*, Hamburg, Germany.

[5] Schneider, A. et al. 2003, "Mechanical wafer stability enhancements and texturing effects of remote downstream plasma etching", *Proc. 3rd World Conf. PV Solar Energy Conv.*, Osaka, Japan.

[6] Barredo, J. et al. 2007, "The influence of different surface treatments on the mechanical strength of silicon wafers", *Proc. 22nd EU PVSEC*, Milan, Italy.

[7] Behnken, H. et al. 2004, "Influence of saw damage etching on the mechanical stability of multi-crystalline wafers", *Proc. 19th EU PVSEC*, Paris, France.

[8] Coletti, G. et al. 2006, "Mechanical strength of silicon wafers depending on wafer thickness and surface treatment", *Proc. 21st EU PVSEC*, Dresden, Germany.

[9] Funke, C., Wolf, S. & Stoyan, D. 2009, "Modeling the tensile strength and crack length of wire-sawn silicon wafers", *J. Solar Energy Eng.*, Vol. 131, pp. 011012-1–011012-6.

[10] Stefancich, M. et al. 2001, "Mechanical effects of chemical etchings on monocrystalline silicon for photovoltaic use", *Solar Energy Mater. & Solar Cells*, Vol. 69, pp. 371–377.

[11] Kohn, C. et al. 2009, "Influence of the metallization process on the strength of silicon solar cells", *Proc. 24th EU PVSEC*, Hamburg, Germany.

[12] Popovich, V.A., Janssen, M. & Bennett, I.J. 2011, "Breakage issues in silicon solar wafers and cells", *Photovoltaics International*, 12th edn, pp. 49–57.

[13] Chen, C.P., Royal, E.L. & Klink, H. 1980, "Effect of production processes on the fracture strength of silicon solar cells", *Proc. 14th IEEE PVSC*, San Diego, California, USA.

[14] Micciche, B., Dingle, B. & Meisser C. 2006, "Understanding the causes for cell breakage during the cell interconnecting process – Part I", *Proc. 21st EU PVSEC*, Dresden, Germany.

[15] Brun, X.F. & Melkote, S.N. 2009, "Analysis of stresses and breakage of crystalline silicon wafers during handling and transport", *Solar Energy Mater. & Solar Cells*, Vol. 93, pp. 1238–1247.

[16] Koepge, R. et al. 2011, "The influence of transport operations on the wafer strength and breakage rate", *Proc. 26th EU PVSEC*, Hamburg, Germany.

[17] Kaule F., Koepge, R. & Schoenfelder, S. 2012, "Damage and breakage of silicon wafers during impact loading on the wafer edge", *Proc. 27th EU PVSEC*, Frankfurt, Germany, pp. 1179–1184.

[18] Schoenfelder, S., Bohne, A. & Bagdahn, J. 2007, "Comparison of test methods for strength characterization of thin solar wafer", *Proc. 22nd EU PVSEC*, Milan, Italy, pp. 1636–1640.

[19] Bohne, A., Schoenfelder, S. & Bagdahn, J. 2008, "The influence of wire sawing process on mono- and multicrystalline silicon wafers", *Proc. 23rd EU PVSEC*, Valencia, Spain.

[20] STANDARD DIN EN 843-1 (2008), "Advanced technical ceramics – Mechanical properties of monolithic ceramics at room temperature – Part 1: Determination of flexural strength".

[21] Weibull, W. 1951, "A statistical distribution function of wide applicability", *J. Appl. Mech.*, Vol. 18, pp. 293–297

[22] Kaule, F., Wang, W. & Schoenfelder, S. 2013, "Modeling and testing the mechanical strength of solar cells", *Solar Energy Mater. & Solar Cells* [in press].

[23] ASTM C-1239-07 (2007), "Standard practice for reporting uniaxial strength data and estimating Weibull distribution parameters for advanced ceramics".

[24] Yasutake, K. et al. 1986, "Crack healing and fracture strength of silicon crystals", *J. Mater. Sci.*, Vol. 21, pp. 2185–2192.

[25] Klute, C., Schoenfelder, S. & Bagdahn, J. 2011, "Crack

investigation in monocrystalline silicon before and after annealing", *Proc. 21st Worksh. Cryst. Si. Sol. Cells & Mod.*, Breckenridge, Colorado, USA.

[26] Schneider, A. et al. 2002, "Bow reducing factors for thin screenprinted mc-Si solar cells with Al BSF", *Proc. 29th IEEE PVSC*, New Orleans, Louisiana, USA.

About the Authors

Ringo Koepge received his Diploma degree in material science from Martin Luther University Halle-Wittenberg in 2010. Since 2010 he has been working as a research scientist with the Mechanics of Wafers and Cells team at the Fraunhofer Center for Silicon Photovoltaics CSP in Halle. His research in the field of strength and breakage issues of silicon photovoltaics wafers focuses on the characterization of silicon material and wafers.

Frank Wegert received his Diploma degree in mechanical engineering from Rostock University in 1990. He works for several international companies as an expert in machine design and process engineering. He joined Hanwha Q Cells in 2006 and is currently a senior staff expert, responsible for technical key projects in the development and optimization of machines in cell and module production as well as handling technologies.

Sven Thormann studied business engineering at Fachhochschule Schmalkalden, Germany, and received his Diploma degree in 2001. For his thesis Sven worked on a pad printing process for front-side metallization on EFG material. Since 2005 he has been working for Hanwha Q CELLS and is responsible for the mechanical reliability of wafers, cells and cell behaviour in modules.

Stephan Schoenfelder studied mechanical engineering at HTWK Leipzig, and received his Ph.D. in 2010 from Martin Luther University Halle-Wittenberg. He has been working at Fraunhofer IWM and Fraunhofer CSP in Halle since 2004, with a six-month stay at MIT in Cambridge, Massachusetts, in 2008. The research focus of his group is the manufacturing, strength and breakage of silicon wafers in photovoltaics.

Enquiries

Ringo Koepge
Group Silicon Wafers
Fraunhofer Center for Silicon Photovoltaics CSP
Otto-Eissfeldt-Str. 12
06120 Halle (Saale)
Germany

Tel: +49 345 5589-5311
Fax: +49 345 5589-5999
Email: ringo.koepge@csp.fraunhofer.de
Website: www.csp.fraunhofer.de

Thin Film

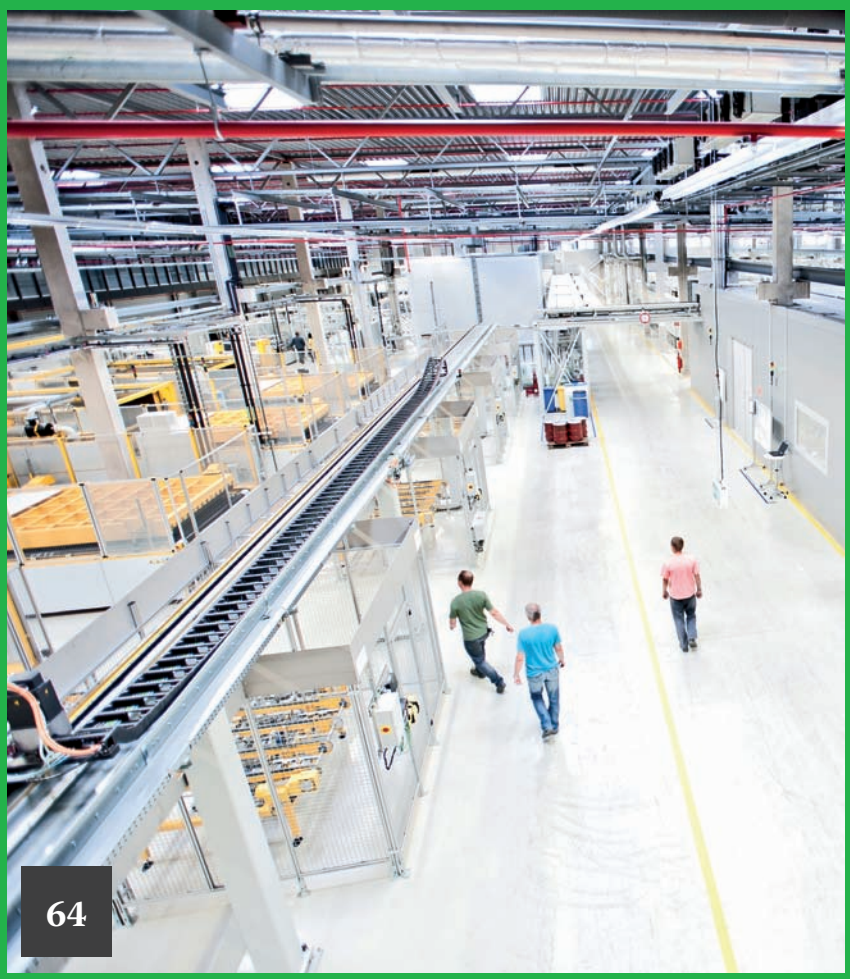

64

News

Hanergy's major CIGS plans unveiled with 5.25GW of turnkey capacity

Following the company's acquisition of CIGS firms Solibro, Miasolé and Global Solar, Hanergy has announced plans to add new turnkey CIGS manufacturing capacity totalling 5.25GW.

The latest CIGS capacity plans appear similar to Hanergy's previous a-Si framework supply contract using its in-house equipment subsidiary Apollo, formerly known as Apollo Solar Energy Technology Holdings to deliver the new turnkey line. Hanergy has yet to identify the proposed phasing of the 5.25GW of new CIGS capacity. Hanergy stated that establishing a strong market position in the CIGS turnkey line market was vital for the company.

The company will also expand turnkey a-Si manufacturing capacity by 4.75GW for a mix of both a-Si/uc-Si and a-Si/a-SiGe.

Source: Solibro/ Hanergy

Hanergy has unveiled plans to add new CIGS manufacturing capacity totalling 5.25GW.

R&D News

First Solar hits cost reduction milestone

In issuing third quarter 2013 financial results, thin-film market leader First Solar, reported its largest quarterly decline in its CdTe module cost per-watt since 2007.

As a result of its manufacturing cost reduction program, the company said it had successfully met significant milestones in re-establishing itself as the lowest-cost PV manufacturer in the industry, reducing module manufacturing cost by US$0.08 per watt or 12% quarter-on-quarter.

The company demonstrated that it had met its conversion efficiency roadmap targets this year. Taking the 14.1% module efficiency achieved on its best line at its Perrysburg facility, First Solar said that this pointed to a cost per watt of US$0.49. (plus pic First Solar machine, credit First Solar)

First Solar to build 3.28MW PV research plant for University of Queensland

First Solar is to build a 3.28MW PV plant for use as a research facility at the University of Queensland in Australia. The US thin-film company and the educational institution will make use of an AUD$40.7 million (US$39.2 million) grant from the Australian government.

Funding from the grant will also go to the University of New South Wales which will also collaborate on forthcoming projects.

The new solar park will use 34,000 First Solar CdTe thin-film modules, while First Solar will also provide engineering, procurement and construction (EPC) services. Project management will be overseen by the University of Queensland's Property and Facilities Division, which will also take over operation and management of the park upon its completion, scheduled for the end of 2014. The plant is being seen by the University of Queensland as a pilot project for two PV power plants in New South Wales, to be built by First Solar with Australian firm AGL Energy, totalling 155MW capacity. All three projects are also being supported by the Australian Renewable Energy Agency (ARENA).

Array Technologies completes world's largest thin-film tracking system

Array Technologies has supplied the 'Mount Signal' 265MW solar plant in Calexico, California with its Dura Track HZ solar tracking system.

Array Technologies was awarded the tracking supply contract in November 2012. The 265MW project is said to be the largest tracking system for thin-film installed in the world to date.

The project uses thin-film panels manufactured by First Solar, and is being constructed by Abengoa. Array Technologies completed the shipment several weeks early, but was challenged with the thin-film panels' frameless design, so used a unique patent-pending bowed tracker rack. Array Technologies said using the specifically designed bow-truss solution saved on labour and material requirements for a speedier installation.

Efficiencies

Solibro produces 18.7% efficiency CIGS cell in lab

Confirmed by the Fraunhofer Institute for Solar Energy Systems ISE, Hanergy subsidiary, Solibro has achieved a conversion efficiency of 18.7% in a lab produced copper-indium-gallium-selenium (CIGS) sub-module (5x5cm2), one of the highest reported for CIGS technology.

Solibro Research AB in Sweden fabricated the sub-module which had an aperture area of approximately 16cm2, using laboratory equipment. However, Hanergy said that fabrication of the sub-module used production processes and manufacturing type conditions, which are expected to be commercialised, though no timelines were given.

ZSW achieves record lab CIGS cell efficiency of 20.8%

The Centre for Solar Energy and Hydrogen Research Baden-Württemberg (ZSW) has achieved a record 20.8% conversion efficiency with a copper indium gallium diselenide (CIGS) thin-film PV cell.

This beats the official record for a multicrystalline PV cell, which stands at 20.4%. ZSW had held the previous CIGS record of 20.3% on glass. The results have been officially confirmed by the Fraunhofer Institute for Solar Energy Systems ISE. ZSW is now working to transfer the optimised CIGS process to modules. Market-standard CIGS modules currently attain efficiencies of 14 to 15%.

Thin-film consumer goods: Apple files for solar power management system patent

Technology manufacturing giant Apple has applied to patent a power management system in the US to utilise portable solar panels. The Apple system would use solar power for iPhones, Macbooks and iPod touch without needing to plug into a mains socket to recharge. The use of solar power would aid devices currently dependent on mains sockets for power and recharging. The system would accept direct current

(DC) from solar panels, and AC current using a system micro controller (SMC), to an AC-DC adapter, so devices can use both solar power and an adapter. It uses existing technologies including maximum power point tracking (MPPT) and would not use a converter circuit, allowing adapter and solar power use simultaneously to power devices or recharge batteries. Previously solar panels were considered too bulky for Apple products, but a portable solar panel accessory connecting to devices using a USB connector or other ports would be used with the power management to increase portability.

Ascent Solar Q3 financial results 'validate strategy'

Thin-film developer Ascent Solar (Ascent), which integrates thin-film panels into its own range of consumer products, reported in its Q3 2013 financial results that product revenue was up by US$102,000 over the previous quarter.

Ascent stated that it expects expansion of the Enerplex range and distribution network to drive further revenue increases in subsequent quarters. Ascent launched several new additions to the Enerplex range during the period, including Jumpr Mini, a 6mm thick 1350mAh solar powered booster accessory for smartphones and a line of Enerplex products which carry the official branding of American football team Denver Broncos.

IKEA to sell solar PV at all UK stores

Within the next 10 months, all 17 UK IKEA stores will stock, sell and install solar PV modules. The move forms a wider part of the Swedish furniture giant's partnership with Hanergy.

IKEA made the decision to stock solar in all its stores after a successful pilot project at its Lakeside store in East London sold around one solar PV array every day. Shoppers will be able to buy a system outright or opt for a solar finance package that would require no upfront payment. Hanergy will be offering a "full solar service" in-store, including consultation and design as well as installation, maintenance and ongoing energy monitoring.

Thin-film shakeout

Solexant rebrands as Siva Power and bets all on CIGS

Silicon Valley manufacturer, Solexant, has announced a relaunch as Siva Power and a transition to focusing exclusively on CIGS thin-film PV technology.

The transition will see the company moving to high-volume manufacturing with the building of its first production line, a 300MW facility that it claims outmuscles other thin-film production lines threefold.

The company said after investigating several solar technologies, it had concluded that CIGS thin-film offered the most promise of achieving sub-US$0.40 per watt solar costs. The company had initially been planning to build a 100MW cadmium telluride (CdTe) thin-film production line, but cancelled this after deciding to focus on what it saw as lower cost forms of production.

Honda to shut solar subsidiary in 2014

Japanese car maker Honda has announced it will close its thin-film manufacturing subsidiary Honda Soltec in spring 2014. In a statement Honda said the falling cost of silicon was one of many factors that meant it was unable to remain competitive.

The unit had developed its own copper, indium, gallium and selenium (CIGS) module and manufactured from a 30MW production hub. It will continue taking orders until February 2014 and will provide after sales support via a separate Honda affiliate once Soltec has been dissolved. Honda lists the firm's capital investment at ¥4 billion (US$40.5 million). Soltec was established in 2006.

Manz reaches record revenue, despite only €7.5 million from solar segment

Strong revenue growth from its Display segment helped major manufacturing equipment firm Manz report record revenue for the first nine-months of 2013.

The company reported record revenue of €213.0 million (US$285 million), an increase of 44%, compared with the prior year period. Sales in its Solar segment were only €7.5 million (US$10.05 million), compared to €14.9 million (US$20.0 million) in the previous year period.

Manz said that it expected record revenue for the full-year of between €260 million (US$348 million) and €270 million (US$362 million) and EBIT positive, despite continued investments in its Solar segment's R&D activities.

Repositioning and new markets

First Solar heading to Japan to build PV power plants and tap residential market

With an initial plan to invest around US$100 million, First Solar has said it will build PV power plants in the booming Japanese market, both directly and with Japanese companies in partnership.

Japan has not previously been a target market for First Solar with its CdTe thin-film modules.

The company noted that the Japanese government has set a target to install 28GW by 2020.

Market research firms are in agreement that the Japanese market in the next two years is expected to become one of the largest after China, spurring overall record global demand.

First Solar has also signed a distribution agreement through April 2015 to sell its yet to be produced high-performance TetraSun developed monocrystalline modules in Japan to the residential market through JX Nippon Oil & Energy Corporation.

Solar Frontier Italy deal seeks to capitalise on self-consumption trend

Japanese thin-film manufacturer Solar Frontier is to introduce its SolarSets range of standardised PV systems to the Italian residential market after agreeing a distribution deal with P.M. Service. P.M. Service will act as authorised distributor for the systems, which combine standardised sets of Solar Frontier modules, inverters and cabling.

With Italy's 'Conto Energia V' tariff programme being wound down, there is an increasing emphasis on PV self-consumption and P.M. Service said the SolarSets range was well suited to this environment. The SolarSet system works by optimising all the advantages of CIS thin-film technology – such as its performance under low light conditions and power generation in partial shading – using a new series of Solar Frontier inverter.

Hanergy takes first steps in US downstream market

Thin-film manufacturer Hanergy has made its first move into the US downstream market with the acquisition of a 19MW project in Pittsburg, California. According to a statement made to the Hong Kong stock exchange, the company has purchased the early-stage solar farm from Delaware-based LSP Generation Holdings. Hanergy panels will now be used for the installation. A 20-year power purchase agreement (PPA) was already in place and is expected to start operations in November 2014. The move will put Hanergy and First Solar in direct competition for downstream business in the latter's domestic market.

Improvements in CdTe module reliability and long-term degradation through advances in construction and device innovation

Nicholas Strevel, **Lou Trippel**, **Chad Kotarba** & **Imran Khan**, First Solar, Perrysburg, Ohio, USA

ABSTRACT

Recent advances in cadmium telluride (CdTe) research and development have improved the long-term power-output degradation and extended reliability test performance of First Solar's thin-film CdTe PV modules. This paper reviews the characterization results of the new First Solar cell structure with improved back-contact design that better manages the fundamental power-output degradation mechanism. First Solar's proprietary 'Black' series module construction significantly enhances the long-term durability and extended test performance of the modules. The accelerated lab-testing methods, field testing and associated analyses are discussed. These advances in the solar cell performance, coupled with upgraded module materials, further substantiate the long-term power-generating capability of First Solar's CdTe PV modules in harsh operating conditions.

Introduction

The rapid expansion of the worldwide PV industry over the last 10 years has been driven by significantly reduced PV module cost trajectories and has resulted in geographical expansion of successful PV markets. These wider geographical applications reinforce the need for PV modules to endure harsh operating conditions for 25+ years. New materials and technical innovations that reduce costs, while ensuring long-term performance and durability, are key to delivering reliable power output over time and competitive PV systems to project owners and investors.

Fundamentally, thin-film PV modules have two primary mechanisms of power loss in the course of time. First, the module construction and materials that encapsulate the semiconductor device can weaken or degrade through harsh environmental exposure, sometimes enough to allow corrosion of the properly functioning cells, which could result in loss of power. Second, the semiconductor devices themselves experience stress over the lifetime of operation and slowly become less efficient at converting sunlight into DC electricity. This effect, also known as *long-term degradation*, while common to all PV technologies, manifests itself through different mechanisms depending on the construction and characteristics of the semiconductor [1]. First Solar's Series 3 Black (S3 Black) module has been successfully developed to achieve robust long-term package durability via upgraded encapsulating materials. Building on the S3 Black platform, the newest First Solar Series 3 Black Plus (S3 Black Plus) module improves the long-term power output degradation through innovation in device technology.

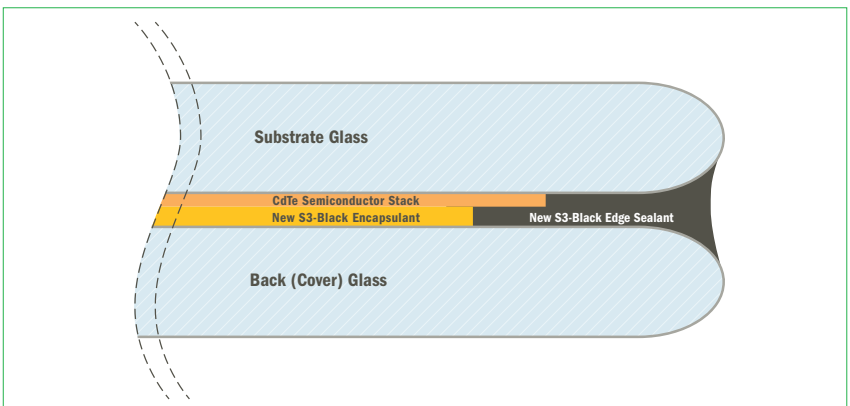

Figure 1. Cross section of First Solar's S3 Black and S3 Black Plus modules.

"First Solar's Series 3 Black (S3 Black) module has been successfully developed to achieve robust long-term package durability via upgraded encapsulating materials."

Advanced CdTe module packaging technology and performance – material selection

Driven by continuous improvement, the S3 Black module, launched in early 2013, features a durable packaging system that is the result of extensive subscale and product-level testing and development, incorporating innovative and highly capable materials. S3 Black features, between the glass laminates, an upgraded encapsulant that acts as the primary laminate adhesive, and an improved butyl-based edge sealant material that extends around the module perimeter, designed to block water ingress and provide electrical insulation. Fig. 1 shows the cross section of this construction.

Central to the S3 Black module design is a new, high-performance olefinic encapsulant. Compared with most conventional EVA-based thermosetting encapsulants, the S3 Black encapsulant has a water vapour transmission rate (WVTR) that is several times lower. While the edge sealant is designed to be the primary moisture barrier, having an

encapsulant with a low WVTR serves as a secondary barrier against environmental elements. The effect of encapsulant barrier properties on water ingress has been extensively covered in the literature [2]. In addition, the S3 Black encapsulant has a measured volume resistivity of $10^{15}\Omega$cm, which is two orders of magnitude higher than most conventional EVA-based thermosetting encapsulants. Beyond the moisture barrier and bulk electrical properties, the material selection process was dominated by the excellent adhesion characteristics of the S3 Black encapsulant. Extremely high bond strengths to glass were observed after harsh accelerated cycles, such as 2000 hours of 85°C/85% relative humidity (damp heat), 200 thermal cycles –40 to +85°C, and 85°C hot water immersion. When a relatively wide manufacturing processing window is factored in, the upgraded polyolefin S3 Black encapsulant becomes a strong candidate for PV module packaging material.

The module product name 'S3 Black' is a direct reference to its construction using an upgraded black edge sealant and its carbon-based colorant system. At a low loading level in the edge sealant formulation, carbon does not negatively affect bulk electrical properties, yet provides the benefits of absorbing UV light and acting as a radical scavenger. While selecting a packaging system with an inherent tolerance to extreme environmental conditions was a clear target of the S3 Black development programme, it was also desired to focus on edge sealants that meet component-level requirements for solid insulation, as defined by IEC in DSH 1051 [3]. An integral part of meeting requirements for solid insulation involves achieving a sufficient relative thermal index (RTI), tested per UL 746B [4]. After a test sequence that involved adhesion and dielectric strength measurements before and after long-term thermal exposure, the S3 Black edge sealant was established to have an RTI of 105°C. Such a rating is considered to be a strong indicator of the resilience of the S3 Black module design to hot, arid conditions. In addition, the S3 Black edge sealant was measured to have a volume resistivity of 10^{15} to $10^{16}\Omega$cm, which is more than two orders of magnitude higher than that of the edge sealant used with the parent S3 module design, and more than ten orders of magnitude higher than that in the technical guidance provided by UL 746C for electrically insulating materials [5]. Coupling the aforementioned technical factors with a higher loading of moisture-absorbing desiccant filler, the S3 Black edge sealant is viewed as an innovative material that provides excellent protection from environmental conditions throughout the rated service life.

Accelerated testing as a predictor of long-term field performance

PV modules are typically warranted for 25 years of field performance. With rapid innovation cycles in the industry, one cannot simply wait for 25 years of field exposure to validate long-term performance; rather, the PV industry has come to rely upon laboratory accelerated testing protocols to more rapidly assess the suitability and relative eventual performance of modules in the field. To test the reliability of solar modules, a number of internationally accepted accelerated stress-testing methods are used. These tests follow the general format of an initial test sample measurement, an accelerated environmental exposure, and then final power and safety measurements of the test sample. The three most common stressors for all durable goods, including PV modules, are damp heat (DH: 85°C, 85% relative humidity), thermal cycling (TC: –40 to +85°C), and humidity–freeze (HF: –40 to +85°C, 85% relative humidity) [6]. Additional stressors – such as UV exposure, electrical bias conditions, hail impact and mechanical loads – are also a part of these test protocols.

Damp-heat testing is conducted at 85°C and 85% relative humidity for a standard duration of six weeks (or 1000 hours). Thermal-cycling and humidity–freeze testing both follow a specific profile specified by the IEC standard

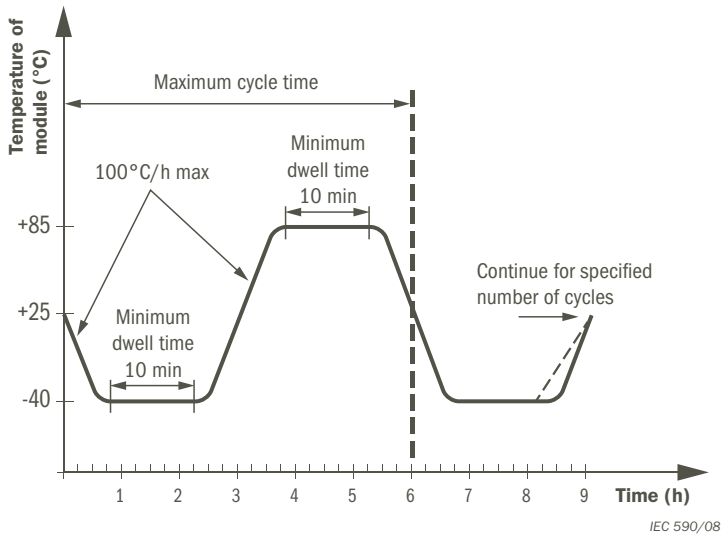

Figure 2. IEC 61646 thermal-cycling profile.

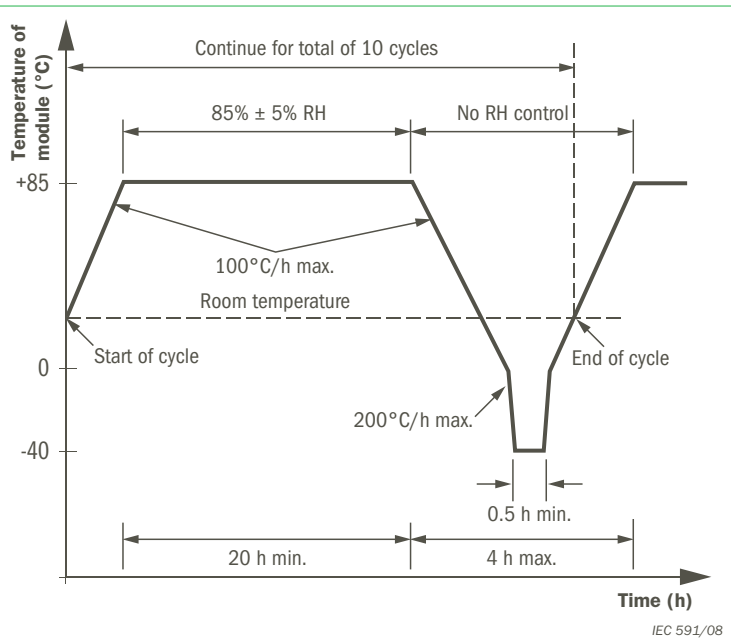

Figure 3. IEC 61646 humidity–freeze profile.

(IEC 61646): a standard TC test consists of 200 cycles, with the profile shown in Fig. 2; for HF testing, 10 cycles are used and a different profile followed, as shown in Fig. 3.

For over a decade the PV industry has relied on these standard IEC test protocols for basic evaluation of PV modules. IEC 61646 (thin-film) [6] and IEC 61215 (c-Si) [7] type approval standards, along with the IEC 61730 safety standard [8], have provided a framework of certification testing which assures a common minimum level of test performance and which has become de facto in the industry. Conventional IEC 61646/IEC 61215/IEC 61730 standards define a parallel sample test protocol whereby one group of sample modules are exposed to one stressor (i.e. 200 thermal cycles), while a different group of modules are exposed to an alternative stressor (i.e. 10 humidity–freeze cycles).

In recent years, industry stakeholders have recognized the need to further differentiate PV modules by developing extended test durations, sequential testing protocols and application-specific tests which give additional insight into the long-term performance, reliability and durability of PV modules.

> "Industry stakeholders have recognized the need to further differentiate PV modules by developing extended test durations, sequential testing protocols and application-specific tests."

Long-term parallel testing

Long-term parallel testing has been developed in recognition of the need to extend test durations to better differentiate PV modules in long-term field performance. One example is the RETC Thresher Test [9], which builds on the basic parallel test architecture of the conventional IEC tests and defines "a long-term reliability test programme that will not only help in differentiating products, but also in determining the degradation patterns of ... solar modules". In the Thresher Test the conventional IEC test environmental stress exposure durations are multiplied by a factor of two to four in order to identify those modules with truly differentiated long-term reliability and performance.

Long-term sequential testing

Recognizing that modules in the field are exposed to combinations of stresses over time, long-term sequential testing builds upon the extended durations of extended parallel testing by additionally requiring that the same modules be exposed to the extended environmental stresses in series rather than in parallel. One example of this sequential test protocol is the TÜV Long-Term Sequential Test (TÜV LST). Fig. 4 shows the difference in testing profile of these two extreme durability initiatives.

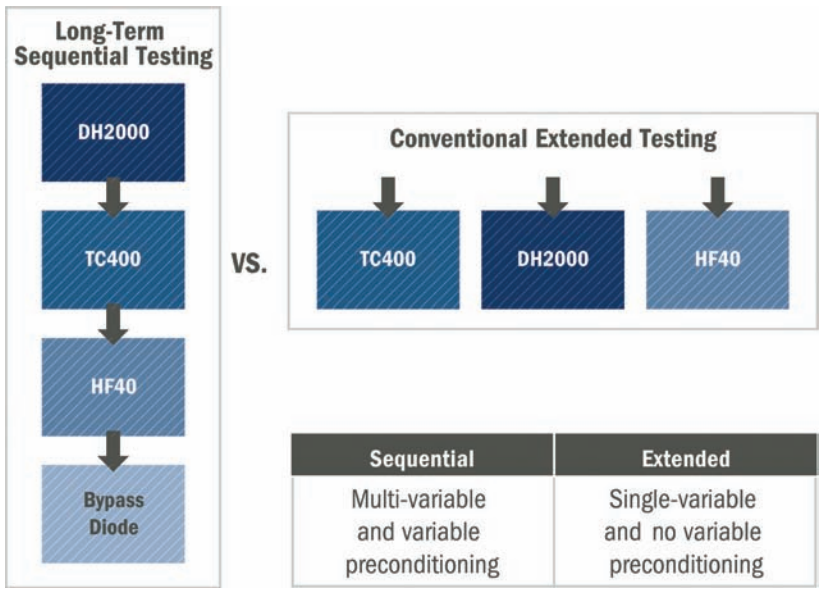

Figure 4. Long-term sequential vs. parallel extended test comparison [10].

Application-specific testing

While conventional IEC PV module type approval and safety tests include expected environmental stresses as well as phenomenological tests for wind loads, snow loads, hail impact, etc., there remain some specialized field applications or locations that might warrant additional specialized harsh environment tests. For PV module application in corrosive marine environments, the IEC 61701 Salt Mist Corrosion Test has been developed to ensure that performance and package integrity are maintained: "This testing sequence is more suitable to reflect the corrosion processes that happen in PV modules subjected to permanent or temporary corrosive atmospheres" [11]. Other harsh environment risks include exposure to wind-blown particulate as a result of desert sandstorms. IEC 60068-2-68 is applied to PV modules for evaluating robustness against particulate effects (such as sandblasting) which could reduce incident light capture in the module or otherwise damage its packaging [12]. Manufacturer-specific tests can also be used to supplement standards-based tests, especially when no international test convention is defined. The evaluation of PV modules on the basis of both of these standardized and non-standardized application-specific tests provides additional confidence in the appropriate and durable application of PV modules in their intended environments.

While the IEC tests are still the industry standard for bringing a product to market, going beyond these tests in terms of both duration and severity is critical to demonstrating the differentiation of those solar modules that are able to handle the harshest climates, demonstrate the lowest long-term degradation, and provide stakeholders with the lowest risks for their long-term investments.

Internal qualification and advanced testing

A combination of the selection of high-quality materials and the innovative construction of the S3 Black and S3 Black Plus modules has been subjected to the aforementioned extended reliability tests to demonstrate their robust performance in extreme conditions for durations far beyond those specified in standard IEC61646 and IEC61730 testing. For example, First Solar subjected the Series 3 Black modules to a test duration of more than six times that of the typical 1000-hour DH test. The results of a sample population of 25 modules are presented in Fig. 5.

It is important to note that because of device metastabilities the modules experience a fully recoverable dark storage state after prolonged exposure in dark environmental chambers. After a few cycles, a light soaking recovery

process is completed to eliminate the dark storage effects and bring Pmpp (power at the maximum power point) back to normal; this was conducted after 2352 hours and 4368 hours, and at test completion at 6384 hours. Fig. 5 shows that after this extreme testing, Pmpp of the module population is still within –4 to –10%, which clearly demonstrates the robustness of the S3 Black Plus module's encapsulation and packaging integrity in any of the harshest climates on earth. First Solar also tested the S3 Black modules with a duration five times that of the IEC TC200 test. The test data shown in Fig. 6 also shows no measurable power reduction after this extended duration.

External qualification

S3 Black modules, as the predecessor of the S3 Black Plus modules, were the first and only thin-film modules to date to pass two of the most difficult and strenuous independent tests of module durability, reliability and long-term degradation: the Thresher Test (long-term parallel) and the, even harsher, Long-Term Sequential Test (long-term sequential), both evaluated by TÜV Rheinland.

> "S3 Black modules were the first and only thin-film modules to date to pass two of the most difficult and strenuous independent tests."

First Solar modules were shown to exhibit power output degradation of less than 5% after completion of the Thresher Test, providing a high level of confidence in the long-term degradation rates of First Solar modules, and outperforming warranted degradation rates over time. First Solar's success in the Long-Term Sequential Test results for its modules places it on an exclusive list with only five other module manufacturers who have demonstrated this capability at the time of publication [13–17]. In addition, First Solar S3 Black and S3 Black Plus modules have passed the application-specific IEC 61701 Salt Mist Corrosion Test with the highest level of exposure. Moreover, both module types have successfully passed the IEC 60068-2-68 Desert Sand Resistance Test, demonstrating robustness against sandstorms and providing performance confidence in harsh operating environments.

First Solar's S3 Black Plus modules are built on the core S3 Black construction, maintaining the highest levels of extended reliability and performance achieved via extended parallel, sequential and application-specific testing. S3 Black Plus modules further contain an improved device structure, which will be discussed next.

CdTe device degradation and performance

Literature and degradation mechanism review/new back contact and device structure

Research in CdTe PV has been ongoing for over 40 years, but not until recently have such significant achievements been made in demonstrating its

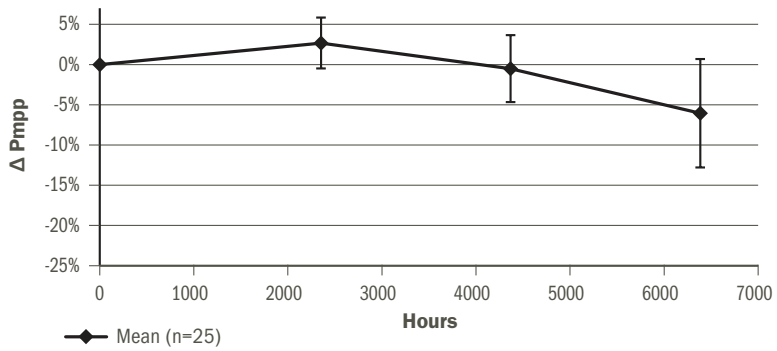

Figure 5. Results of extended damp-heat testing.

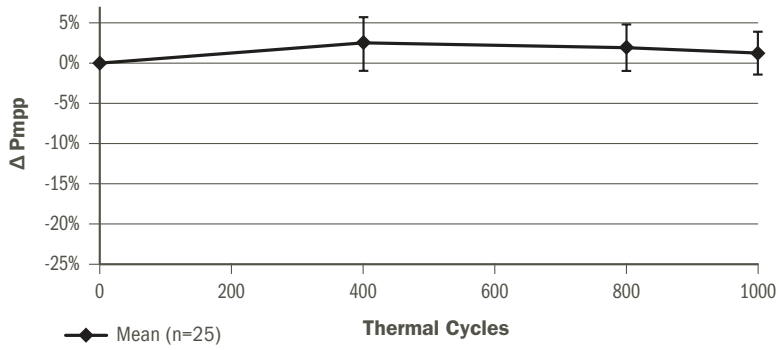

Figure 6. Results of extended thermal cycling.

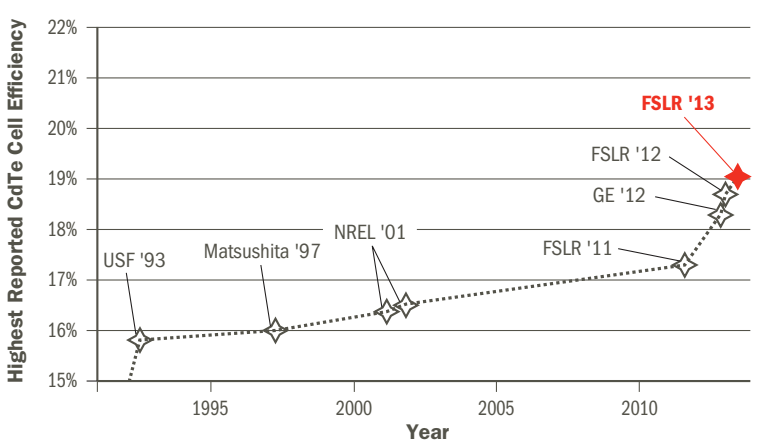

Figure 7. World-record CdTe cell efficiency (reproduced from Gloeckler et al. [18]).

efficiency potential [18]. Fig. 7 shows the recent trends in CdTe device world-record performance.

Not only is CdTe one of the lowest-cost technologies to manufacture [19], but it also has a band gap in the optimum range for single-junction semiconductors [20]. One factor for the increased laboratory efficiency has been advancements in the CdTe back contact. For a high-efficiency cell it is imperative to have an ideal semiconductor–metal interface and minimize the losses from the back contact. For p-type CdTe these losses or non-idealities can result from a combination of high-resistance layers and unfavourable valence energy-band alignment.

It is well established that using zinc telluride (ZnTe) as an interlayer improves the valence band offset to p-type CdTe and, with the optimized work function, enables a more ohmic and stable back contact [21,22]. First Solar's initial development of this improved ZnTe back contact was first demonstrated by an NREL-verified record 17.3% cell efficiency in 2012 (see Fig. 7). Following the established path of prior cell-to-module integration successes, First Solar has now migrated this cell-level advancement into a proprietary high-volume module-manufacturing process with an improved redesigned back contact incorporating the ZnTe layer into the full-scale module. The full-scale module production process demonstrates a nameplate efficiency improvement of approximately two to three power bin classes, or 5–8Wp. The current production device stack and the new product with the ZnTe interlayer are shown in Fig. 8.

The cell-level improvement is observed by the increase in open-circuit voltage (V_{oc}) and fill factor (*FF*). The improvement in the back-contact electrical behaviour is evident if the solar cell is subjected to a forward bias in the dark. Fig. 9 shows the *I-V* curve of the ZnTe-based back contact, which behaves like an ideal p-n diode with a sharp turn-on voltage that progressively increases with lower temperature.

The non-ZnTe device stack has a substantial amount of current 'roll-over' [23], and the electrical conduction suffers further at lower temperatures, where the carriers are less energetic and the impact of the interface barrier becomes more pronounced. The improvement in back-contact electrical behaviour results in a nearly linear V_{oc} vs. temperature profile, with even higher values of V_{oc} observed at lower temperatures, as shown in Fig. 10.

Hence there is a higher and linear relative increase in efficiency with lower operating temperatures, which naturally results in an increased magnitude of the efficiency temperature coefficient. For the S3 Black Plus product with a ZnTe-based back contact, the efficiency temperature coefficient will nominally be –0.29%/°C compared with the standard value of –0.25%/°C [24]. While this will slightly reduce specific annual energy yield, the increased initial efficiency will outweigh this effect, and the result will be that more total energy is produced per module. Note that the S3 Black Plus temperature

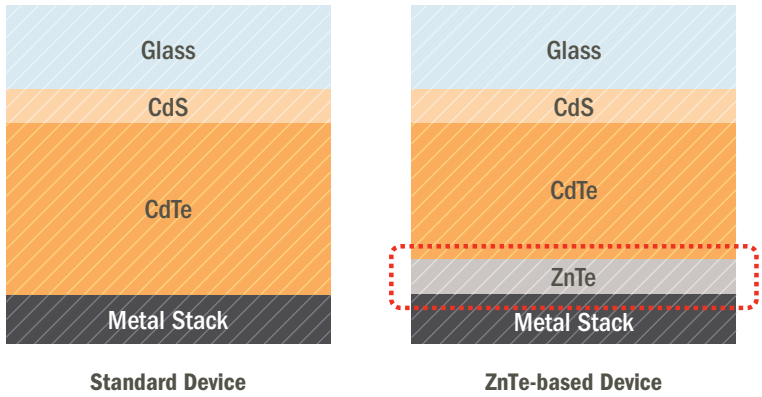

Figure 8. S3 Black (standard) and S3 Black Plus (ZnTe-based) device stack comparison.

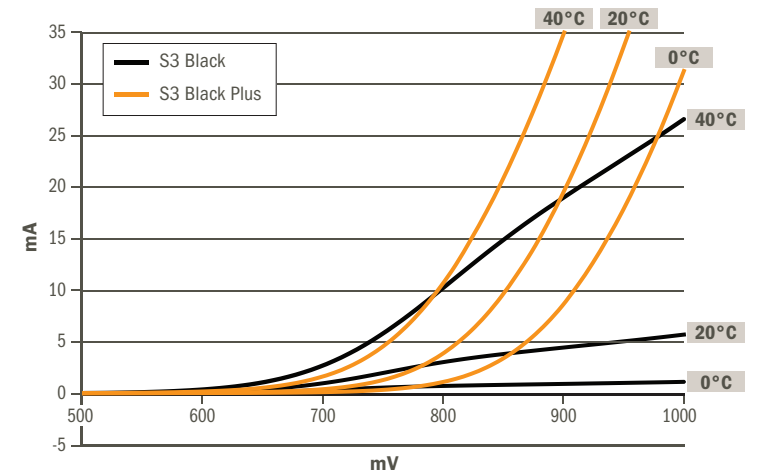

Figure 9. Comparison of the *I-V* curves of S3 Black (standard) and S3 Black Plus (ZnTe).

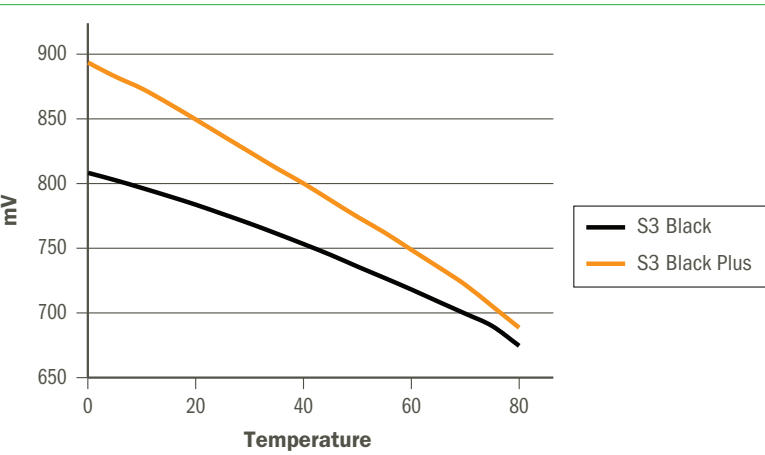

Figure 10. Comparison of back-contact V_{oc} behaviour vs. temperature.

coefficient remains demonstrably better than that of crystalline silicon solar modules, which preserves the high-temperature performance advantage that is characteristic of CdTe modules, resulting in higher specific annual energy yields [25].

Extended testing of the ZnTe back contact

First Solar has a rigorous qualification programme that encompasses accelerated stress testing, independent validation of key tests in reputable external laboratories, and validation through field testing. A detailed characterization of the module performance – including temperature coefficient, spectral response and initial stabilization – is a key input to the energy prediction model. In conjunction, the stress tests and characterization are performed on the standard non-ZnTe-based product for comparative purposes. The existing First Solar device platform already has a proven track record, with more than 18 years of field data [25,26], along with more than 8GW of field deployment history. Based on extensive prior history, an established benchmark correlating existing field performance with lab stress testing is available for evaluating the relative long-term performance improvement, and uniquely enables First Solar to substantiate its conclusions from the qualification process.

> "A detailed characterization of the module performance is a key input to the energy prediction model."

CdTe cell reliability has historically been linked to back-contact stability and the migration of Cu from the Cu-rich back contact, along the CdTe grain boundaries, to the main CdTe/CdS heterojunction [23,24]. During the operating life of the module in the field, higher levels of Cu accumulate at the CdTe/CdS interface and this contributes to progressively lower cell efficiency or power output. For its existing standard product, First Solar has developed processing techniques that substantially reduce the sensitivity of the CdTe/CdS heterojunction to the presence of Cu [24]. As will become evident in the subsequent discussion, the ZnTe-based back contact builds on this established platform and substantially improves the long-term cell reliability of the CdTe device.

The long-term power degradation of a cell can be assessed through accelerated tests in the lab by using elevated temperature and bias conditions [27,28]. In Fig. 11 the power loss with time is shown for the current standard product and compared with that for the ZnTe-based module.

The devices are stressed under accelerated conditions incorporating high-bias conditions, extreme temperatures and full-spectrum light of power density greater than 1000W/m^2. At the 300-day accelerated exposure point, the ZnTe device has a power loss of less than 10% compared with 17% for the standard device. The aforementioned First Solar benchmarks indicate that this 300-day accelerated exposure is representative of the relative long-term field performance of modules with the ZnTe back-contact and prior-generation products. This result shows a significant improvement in the long-term stability and device performance of the ZnTe-based contact. The improvement over plant lifetimes in long-term degradation rate afforded by the ZnTe-based back contact enables First Solar's long-term degradation guidance to be improved to –0.5% per annum for all climates.

It has been reported that the presence of a ZnTe layer in the back

contact retards Cu diffusion and maintains a Cu-rich back contact [29]. While these assessments are typically based on Cu migration due to thermal diffusion, the curtailment of the same underlying phenomenon is also responsible for the improvement in long-term cell stability. This aspect further manifests itself with much-improved robustness of performance against temperature under accelerated light soak testing. Fig. 12 shows a comparison of power loss after modules were exposed to three different temperature stress levels for equivalent test durations.

The results illustrate a reduced impact of temperature on cell power degradation for the ZnTe-based back-contact device. The maximum power point voltage (V_{mp}) degrades by only 6% and stabilizes more quickly, as shown in Fig. 13. This stability helps system-level design, where additional considerations for minimizing the drift in V_{mp} can be taken into account.

The new device stack is also subjected to special durability testing in which the module construction is intentionally compromised to expose the active semiconductor cell to harsh environmental conditions. This approach far exceeds the IEC standards but conforms to the internal qualification programme and to the stringent benchmarking exercise against the standard product. Combining the new back contact with the superior S3 Black construction leads to a field-durable S3 Black Plus module that has robust lifetime performance in the harshest of operating conditions, with a clear performance advantage in hot and humid climates.

Field testing and predictability

As part of First Solar's standard product launch and qualification process, extensive multi-climate (hot/arid, hot/humid, temperate) field testing is conducted to ensure reliable field performance and that energy predictability remains accurate and within expectations. Of particular interest, for a hot climate evaluation, six ~100kW pre-production systems were fielded in April 2013 at a commercially operating power plant in Arizona, USA, to assess their real-world initial performance and for comparison with the benchmark of First Solar's monitored fleet using a non-ZnTe back contact. All arrays were matched in their configurations. This test location is considered an ideal environment for evaluating the impact of high temperatures on outdoor performance, where module cell temperatures are routinely elevated to high-stress conditions and can reach up to 75°C. This data is illustrated in Fig. 14.

The orange dots in Fig. 14 highlight the six S3 Black Plus arrays among the fleet of over 415MW (AC) of commercially operating First Solar PV projects. In this test the S3 Black Plus arrays, incorporating the ZnTe back contact, demonstrated a 5–8% increase in total DC energy produced, confirming the respective nameplate power improvement over existing non-ZnTe products. All the systems are measured by their predicted energy ratio (PER), which is the lifetime ratio of actual energy produced and energy predicted. The PER substantiates First Solar's field performance record and validates First Solar's accuracy in predicting field performance. For product generations prior to S3 Black Plus, a degradation guidance of –0.5%/year in temperate climates and –0.7%/year in high-temperature climates is modelled into predictions.

As shown in Fig. 14, the performance of utility-scale systems monitored over their lifetimes is consistently tracking near 100% of the P50 prediction energy [30,31] inclusive of prior multi-year degradation rate guidance. When this field performance history of older product generations is linked to the aforementioned lab light soak testing (Fig. 13), and the relative improvement of S3 Black Plus in lab light soak testing is observed, the basis of the 0.2% per annum improvement in P50 degradation guidance of S3 Black is established, despite limited long-term field performance history. (P50 degradation guidance is the average expected annual system power loss.) While the field performance data for the new S3 Black Plus system is limited, the performance to date indicates that the operation of these systems is consistent with First Solar's energy prediction model; this supports the conclusion that the S3 Black Plus module performance can be predicted accurately and consistently.

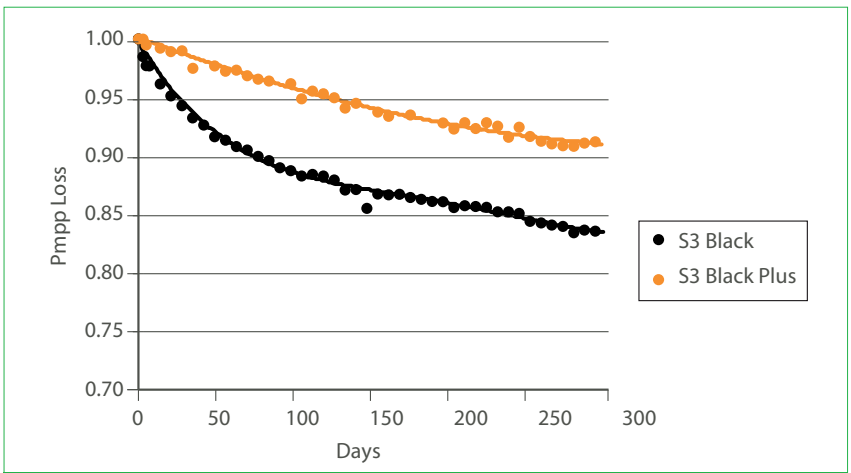

Figure 11. Power loss after accelerated light soak exposure.

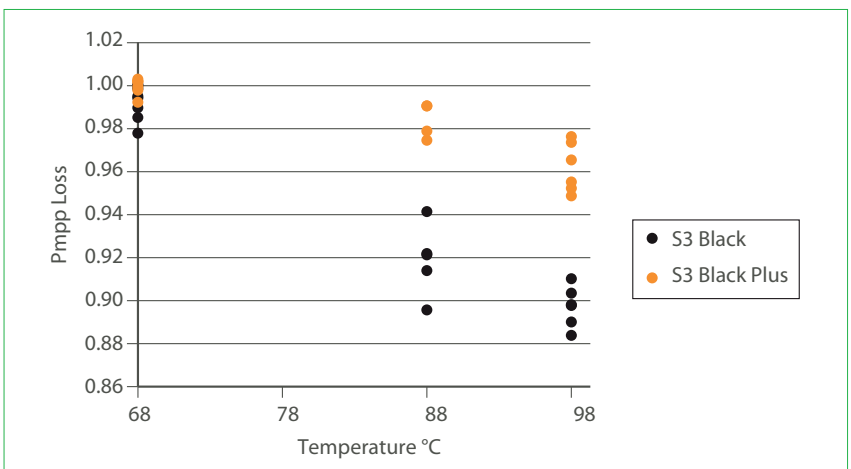

Figure 12. Comparative power loss vs. accelerated temperature stresses.

"First Solar's S3 Black modules provide numerous enhancements to long-term extended reliability test performance compared with previous First Solar products."

Conclusions

First Solar's S3 Black modules have been rigorously tested by leading external laboratories as part of a commercial launch, and provide numerous enhancements to long-term extended reliability test performance compared with previous First Solar products. Via the Long-Term Sequential Test, superior results have been demonstrated compared with most competitor modules in the PV marketplace, regardless of technology type. The new ZnTe back contact incorporated within the S3 Black Plus module platform improves initial module efficiency and increases robustness against thermal and bias-driven power degradation, resulting in a reduction in long-term power degradation rate guidance. By incorporating all of these characteristics, the S3 Black Plus module demonstrates increased energy production over the life of the power plant, as well as increased confidence in predictability, long-term performance and durability of power plants containing First Solar module technology.

References

[1] Jordan, D.C. & Kurtz, S.R. 2012, "Photovoltaic degradation rates – An analytical review", NREL.

[2] Kempe, M.D. 2005, "Control of moisture ingress into photovoltaic modules, NREL/CP-520-37390.

[3] IEC CTL Decision Sheet 1051, "Qualification of cemented joints as reinforced solid insulation", IEC 61730-1: 2004 (Edition 1) + A1: 2011.

[4] UL 746B: 2009 (Edition 3), "Polymeric materials – Long term property evaluations".

[5] UL 746C: 2004 (Edition 6), "Polymeric materials – Use in electrical equipment evaluations".

[6] IEC 61646: 2008 (Edition 2), "Thin-film terrestrial photovoltaic (PV) modules – Design qualification and type approval".

[7] IEC 61215: 1993 (Edition 1), "Crystalline silicon terrestrial photovoltaic (PV) modules – Design qualification and type approval".

[8] IEC 61730: 2004 (Edition 1),

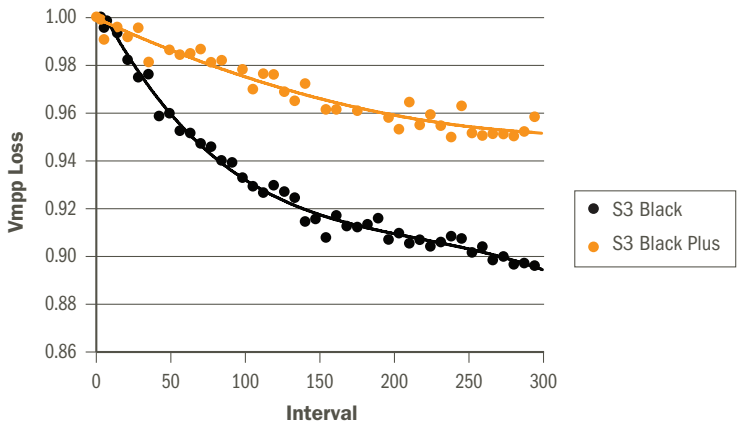

Figure 13. Voltage loss after accelerated MPP (maximum power point) light soak exposure.

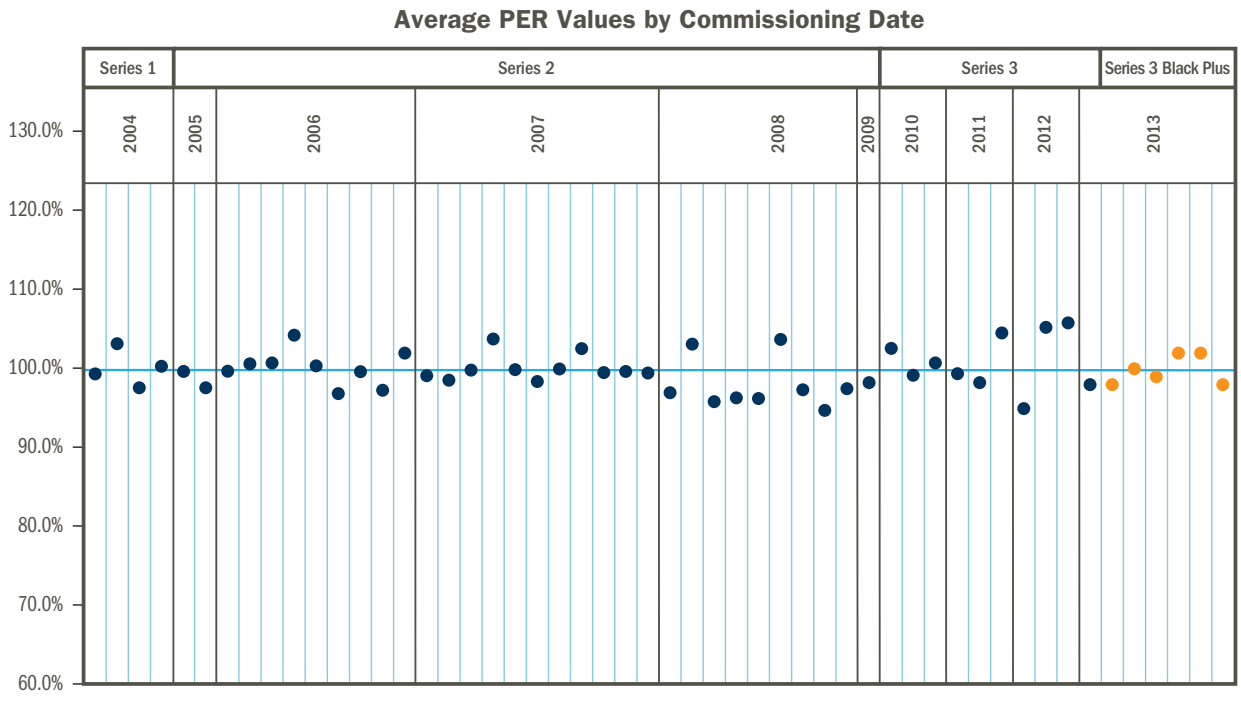

Figure 14. Performance predictability of ZnTe back-contact modules.

"Photovoltaic (PV) module safety qualification".
[9] RETC 2011, "The Thresher Test" [http://www1.eere.energy.gov/solar/pdfs/pvmrw2011_csi_thresher.pdf].
[10] Tamizh-Mani, M.G. 2012, "Long-term sequential testing (LST) of PV modules", TÜV Rheinland PTL [http://www1.eere.energy.gov/solar/pdfs/pvmrw12_wedsam_tuv_tamizhmani.pdf].
[11] IEC 61701: 1995 (Edition 1), "Salt mist corrosion testing of photovoltaic (PV) modules.
[12] IEC 60068-2-68: 1994 (Edition 1), "Environmental testing – Part 2-68: Tests – Test L: Dust and sand".
[13] SunPower 2013, "SunPower solar panels complete Atlas testing program", *Solar Industry*, June [http://www.solarindustrymag.com/e107_plugins/content/content.php?content.12880].
[14] Kyocera Corporation 2011, "Kyocera modules pass TÜV's Long-Term Sequential Test" [http://global.kyocera.com/reliability/file01.html].
[15] Hanwha SolarOne Co. 2012, "Hanwha SolarOne's SF260-36-1PxxxL module among the first in the industry to pass rigorous TÜV Rheinland Long-Term Sequential Test [http://investors.hanwha-solarone.com/releasedetail.cfm?ReleaseID=672965].
[16] pv magazine 2013, "Panasonic HIT solar panels meet TÜV long term sequential test challenge", April [http://www.pv-magazine.com/services/press-releases/details/beitrag/panasonic-hit-solar-panels-meet-tv-long-term-sequential-test-challenge_100010832].
[17] China Post News Staff 2012, "Inventec Energy passes TÜV's modules test", *The China Post*, November [http://www.chinapost.com.tw/taiwan/national/national-news/2012/11/30/362540/Inventec-Energy.htm].
[18] Gloeckler, M., Sankin, I. & Zhao, Z. 2013, "CdTe solar cells at the threshold to 20% efficiency", *IEEE J. Photovolt.*, Vol. 3, No. 4, pp. 1389–1393.
[19] First Solar 2013, Q3 Earning Presentation [http://investor.firstsolar.com/].
[20] Shockley, W. & Queisser, H.J. 1961, "Detailed balance limit of efficiency of p-n junction solar cells", *J. Appl. Phys.*, Vol. 32, No. 3, pp. 510–519.
[21] Gessert, T.A. et al. 1996, "Development of Cu doped ZnTe as a back contact interface layer for thin film CdS/CdTe solar cells", *J. Vac. Sci. Technol. A*, Vol. 14, No. 3.
[22] Rioux, D., Niles, D.W. & Hochst, H. 1993, "ZnTe: A potential interlayer to form low resistance back contacts in CdS/CdTe solar cells", *J. Appl. Phys.*, Vol. 73, pp. 8381–8385.
[23] Cahen, D., Hodes, G. & Gartsman, K. 2000, "Overcoming degradation mechanisms in CdTe solar cells", Second Annual Report, August, Weizmann Institute of Science, Rehovol, Israel.
[24] First Solar 2013, Series 3 Black Plus Datasheet, December.
[25] Strevel, N., Trippel, L. & Gloeckler, M. 2012, "Performance characterization and superior energy yield of First Solar PV power plants in high-temperature conditions", *Photovoltaics International*, 17th edn, pp. 148–154.
[26] NREL, SCI (Solar Cells Inc.) 2013, NREL Module Performance Report, First Solar Application Note PD-5-615, October.
[27] Albin, D.S. 2008, "Accelerated stress testing and diagnostic analysis of degradation in CdTe solar cells", *Proc. SPIE*, Vol. 7048, No. 1.
[28] Corwine, C.R. et al. 2004, "Copper inclusion and migration from the back contact in CdTe solar cells", Department of Physics, Colorado State University [www.physics.colostate.edu/groups/photovoltaic/PDFs/CuMigrAsPub.pdf].
[29] Narayanswamy, C., Gessert, T.A. & Asher, S.E. 1999, "Analysis of Cu diffusion in ZnTe-based contacts for thin-film CdS/CdTe solar cells", *AIP Conf. Proc.*, Vol. 462, No. 1.
[30] First Solar 2013, "Series 3 recommended parametric descriptions for PVSYST", First Solar Application Note PD-5-301-03 PRO MS.
[31] First Solar 2013, "System parameter specs for PVSYST simulations", First Solar Application Note PD-5-301-SS.

About the Authors

Nicholas Strevel is a technical sales manager at First Solar, specializing in PV module technology and performance. He has worked in the thin-film PV technology field for seven years, in module manufacturing, application engineering and business development. Prior to joining First Solar, he held positions in application engineering and process engineering at United Solar Ovonic, both in the USA and in Germany. Nicholas has a B.S.M.E. in mechanical engineering from Michigan State University, and also studied at the Rheinisch-Westfälische Technische Hochschule Aachen.

Lou Trippel is currently the PV module product line director at First Solar, where he leads global module product management and is responsible for First Solar's PV module product life cycle management. He has a bachelor's degree in electrical engineering from the University of Dayton, Ohio, and a master's degree in technology management from Stevens Institute of Technology, New Jersey. Since joining First Solar in 2007, Lou has held several positions on First Solar's module product management and power plant technical sales teams, where he has both performed and led application engineering, plant energy prediction, global technical sales and product management functions.

Chad Kotarba is an engineer at First Solar, specializing in next-generation material and process development. He has worked in the alternative energy industry for nine years, in engineering roles that have spanned both CdTe and a-Si thin-film PV modules, metal hydride/alkaline fuel cells, and microtubular solid oxide fuel cells. Chad has a B.S. in chemistry and an M.S. in alternative energy engineering from Wayne State University in Detroit.

Imran Khan received a Ph.D. in electrical engineering from Purdue University, West Lafayette, Indiana, and a bachelor's in electrical engineering from SUNY Stony Brook, New York. He is the integration manager of device technology at First Solar, where his responsibilities include efficiency improvement, process development and integration, product characterization and reliability physics. Prior to joining First Solar, he was at AMD/Spansion, where he led and carried out work on semiconductor device characterization, modelling and performance improvement.

Enquiries

N. Strevel
Manager – Technical Sales
First Solar, Inc.
28101 Cedar Park Blvd
Perrysburg, OH 43551
USA

Tel: +1 419 662 7015
Email: nstrevel@firstsolar.com

A methodology for testing, characterization and prediction of edge seal performance in PV modules

Kedar Hardikar, **Dan Vitkavage**, **Ajay Saproo** & **Todd Krajewski**, MiaSolé, Santa Clara, California, USA

ABSTRACT

A critical failure mechanism of PV modules is the degradation in performance as a result of exposure to temperature and humidity during a typical product lifetime of over 25 years. The time to failure of a PV module attributable to moisture ingress under given field conditions involves multiple factors, including encapsulant and edge seal moisture barrier performance as well as the degradation rate of particular solar cells when exposed to moisture. The aim of the work presented here is to establish a conservative estimate of field lifetime by examining the time to breakthrough of moisture across the edge seal. Establishing a lifetime model for the edge seal independent of the characteristics of the encapsulant and solar cells facilitates the design optimization of the cells and encapsulant. For the accelerated testing of edge seal materials in standard temperature- and humidity-controlled chambers, a novel test configuration is proposed that is amenable to varying dimensions of the edge seal and is decoupled from encapsulated components. A theoretical framework that accounts for the presence of desiccants is developed for analyzing the moisture ingress performance of the edge seal. Also developed is an approach to analyzing test data from accelerated testing which incorporates temperature dependence of the material properties of the edge seal. The proposed equations and functional forms have been validated by demonstrating fits to experimental test data. These functional forms and equations allow the prediction of edge seal performance in field conditions characterized by historical meteorological data. In the specific case of the edge seal used in certain MiaSolé glass–glass modules, this work has confirmed that the edge seal can prevent moisture ingress well beyond the intended service lifetime in the most aggressive climate conditions evaluated.

Introduction

According to the recently announced first ever US roadmap for CIGS technology [1], this technology is positioned to lead solar efforts in the USA. The degradation in performance of CIGS-based modules due to moisture ingress is a concern and has also been reported as a failure mechanism in c-Si modules [2]. Additionally, the degradation of encapsulated electronic components caused by moisture ingress is a problem in other products, for example those in the consumer electronics industry, where critical components such as electronic displays and IC metallization may be at risk of degraded performance as a result of moisture ingress and corrosion [3,4].

> "The degradation in performance of CIGS-based modules due to moisture ingress is a concern."

There have been several attempts in the past to develop techniques and models to predict the lifetime of PV modules with moisture ingress as a proposed mechanism leading to failures or degradation in performance [5–8]. It is standard practice in the consumer electronics industry to use the Hallberg-Peck relation [9–11] for analyzing the data from reliability testing of IC packages involving temperature and humidity. In all of these scenarios, predicting the time to failure of the product because of moisture ingress hinges upon the convolution of two factors – moisture barrier performance and degradation of the encapsulated components – when exposed to moisture. The third factor involved in these predictions is the development of schemes to model fluctuations in the ambient conditions that the product is subjected to during its lifetime, and relating these variations to the test conditions [5]. The results of a typical experimental scheme are often specific to a particular design or a set of encapsulated components. While such a holistic approach to predicting the reliability of components is necessary, a somewhat different approach – independently examining sealant lifetime – is required, in order to allow an independent optimization of other design elements and component selection.

Fig. 1 shows the typical structure of a glass–glass PV module. In the construction of a glass–glass module there are four main components pertinent to the discussion in this paper. PV cells are encapsulated in the main encapsulant. The structure is laminated between two pieces of glass. Along the periphery of the module between the two glass pieces is an edge seal. In PV modules the encapsulant chosen has additional constraints placed on it, such as transmission of light, and hence one may not be able to choose a material that in itself is an adequate moisture barrier. A common approach to overcome this constraint in PV modules is the use of an edge seal of appropriate width as shown in Fig. 1. The edge seal can have significantly better moisture barrier performance relative to the encapsulant without any constraint with regard to light transmission. Since the use of glass on two sides of the encapsulated cell effectively prevents moisture from directly reaching the encapsulated cell, the primary path for moisture ingress is through the edge seal and then through the main encapsulant via lateral diffusion. The width of the edge seal corresponds to a non-active area of the PV module: a judicious choice of material and width of the edge seal is therefore critical for maximizing the active area of the module while not compromising the moisture barrier performance of the product. One approach to designing and developing PV modules that

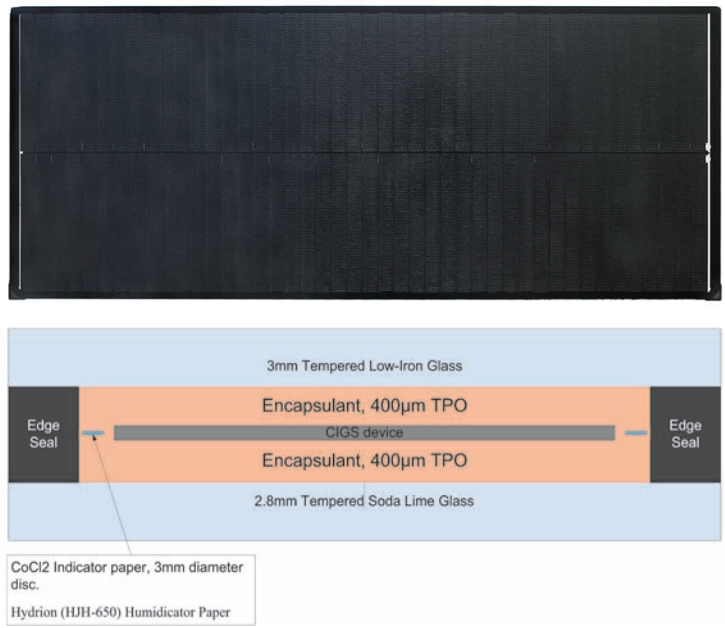

Figure 1. MiaSolé glass–glass module: (a) Planar view; (b) Cross section representation, with $CoCl_2$ indicator paper used for product level moisture ingress testing.

incorporate edge seals is to co-optimize the edge seal and the components for every design permutation. With the use of such an approach, however, the duration and cost of validation can be prohibitive. The proposed approach of decoupling edge seal validation from other design components allows shorter design cycles.

> "A judicious choice of material and width of the edge seal is critical for maximizing the active area of the module while not compromising the moisture barrier performance of the product."

Typically, the design and materials for an edge seal are arrived at by first selecting a material based on its properties, such as diffusivity, solubility and permeability at different temperature and humidity conditions, which are presumed to be predictive of field performance. This is followed by an assessment of the edge seal performance from product level tests that use manifestations of failure modes, such as corrosion, hydrolysis of plastics, or cell degradation. Such product degradation, which combines edge seal performance with the characteristics of other components, acts as the sensor for moisture ingress. This approach does not provide an independent means of validating the field performance of the edge seal, which is necessary for employing the design approach outlined above.

The measurement techniques that focus on the characterization of material properties often involve sample preparation that may not be representative of how the material is prepared in the end product. Standard moisture permeation testing techniques (i.e. MOCON) have been used to carry out basic comparisons of sealant properties [12]. However, this testing suffers from the need to use a defect-free self-supporting film or a carrier film. Both of these issues result in either longer test times (due to sample thickness) or convoluting factors from the support. Moreover, the material used in these tests may not be subjected to exactly the same manufacturing conditions that are seen during mass production.

Another factor to consider is the test time required to see the device degradation in a typical module assembly. For certain MiaSolé production module assemblies subjected to some of the highest widely accepted acceleration factors (85°C/85%RH), it requires well in excess of 8000hrs to see a discernible signal. In order to overcome this issue, the test structure dimensions should enable a shorter time to detect a signal in a manner that can be scaled to product-level dimensions, but the scaling methodology adopted would need to be validated. It is therefore desirable to have a framework of testing, analysis and modelling such that data, from tests carried out in standard environmental chambers and with the material in a form representative of end product use, are directly translatable to lifetime estimation.

In summary, the three main objectives of this paper are:

1. To develop a theoretical framework which facilitates the analysis of moisture ingress data obtained in environmental chamber testing in a manner that enables the prediction of edge seal lifetime in field conditions.

2. To provide a relatively inexpensive test configuration to assess moisture barrier performance of the edge seal material in its end product form and decoupled from other components.

3. To provide functional forms that translate these test results to field conditions characterized by meteorological data. The methodology presented in this paper maintains consistency between the analysis of test results and the analysis of weather conditions to which the product is subjected during its lifetime.

The organization of this paper is as follows. First, a theoretical framework under which the testing and analysis is performed will be developed. The objective of this section is to lay out the framework in order to conjecture certain functional forms for the time to failure of the edge seal material being tested and use them for predicting the field performance. Next, the test sample and experimental set-up are discussed in detail, followed by the experimental data. After an analysis of the experimental data, the discussion moves on to the validation of the use of the proposed functional forms. Finally, the results are used for predicting the field performance of a particular edge seal, employed in certain MiaSolé products, in selected locations around the globe.

Theoretical background

The diffusion of moisture through a barrier material is a process which involves adsorption of moisture on the exposed surface of the edge seal followed by diffusion of moisture through the edge seal. The primary driving force for any diffusion process

is the concentration gradient of the diffusing species (Fick's Law). Typically the maximum concentration of moisture at the exposed surface of the edge seal is a function of the solubility of the material. The propagation of moisture through the edge seal is a function of the diffusivity of the material. Expected variation of the diffusion time and length scales can be obtained by considering the 1D diffusion equation

$$\frac{\partial C}{\partial t} = D\frac{\partial^2 C}{\partial x^2} \quad (1)$$

where C = moisture concentration, D = diffusivity of the material, t = time and x = distance from the exposed edge.

By merely considering the dimensions of the quantities involved in Equation 1, it can be shown that the extent to which the moisture penetrates x^* in time t has a $\sqrt{t}$ dependence, i.e. $x^* \propto \sqrt{t}$. It also follows that the time t^* for moisture to penetrate a distance l has the dependence given by $t^* \propto l^2/D$. Formal analytical solutions to the diffusion equation for various boundary conditions can be found in Crank [13]. For an unbounded medium (1D) with concentration at the edge given by $C(0, t) = C_0$, the solution is given by

$$C(x,t) = C_0\left[1 - erf\left(\frac{x}{2\sqrt{Dt}}\right)\right] \quad (2)$$

where *erf* denotes the error function. This implies that when edge seal configurations of different widths x are tested to 'failure' (defined by moisture penetration), the expected variation of the time to failure (t_f) is

$$t_f = Ax^2; \quad A \propto \frac{1}{D} \quad (3)$$

In PV modules it is customary to use edge seal materials which have desiccants embedded in them. The role of the desiccant is to consume moisture migrating through the edge seal by a chemical reaction, thereby further delaying the time to initial moisture breakthrough. Assuming that the desiccant is uniformly loaded throughout the material, the amount of moisture consumed before the moisture penetrates through the entire width of the edge seal is proportional to the width of the edge seal. Hence, the additional delay because of the presence of desiccant is expected to be proportional to the width of the edge seal. Thus, in the presence of desiccant, the expected variation of the time to failure for an edge seal (as a function of width x) is

$$t_f = Ax^2 + Bx \quad (4)$$

where A and B are constants to be determined. Since the prediction of edge seal performance in the field is of particular interest, it is necessary to consider how constants A and B in Equation 4 might vary with changes in ambient conditions. The following discussion is intended to develop likely functional forms for the constants A and B; the functional forms that are conjectured here are later validated by experimental data.

First, it is observed that the 1D diffusion equation (Equation 1) in an unbounded medium with concentration C_0 at the free edge results in non-zero concentration in the *entire* domain, even at infinitesimal time increments, because of the parabolic nature of the partial differential equation. Hence, the definition of 'moisture penetration' is really dependent on the identification of a threshold value $C = C^*$ at which the penetration is considered a failure. In practice, C^* corresponds to the concentration required for the sensor to detect the moisture past the edge seal, with the underlying assumption that the sensor threshold is representative of the failure threshold. Using Equation 2, the time to failure (t_f) for a diffusion-dominated process (not taking into account desiccant) is expected to have a functional form consistent with

$$C^* = C_0\left[1 - erf\left(\frac{x}{2\sqrt{Dt_f}}\right)\right] \quad (5)$$

Rewriting Equation 5 to solve for time to failure yields

$$t_f = \frac{x^2}{4D\left[erf^{-1}\left(1 - \frac{C^*}{C_0}\right)\right]^2} \quad (6)$$

The quantity in parentheses denotes the inverse of the error function. Reconciling Equation 6 with Equation 3 suggests that in Equation 4 we should expect

$$A \propto \frac{1}{D\left[erf^{-1}\left(1 - \frac{C^*}{C_0}\right)\right]^2} \quad (7)$$

To identify a suitable functional form for analysis of experimental data it is first noted that the diffusivity D is expected to have an Arrhenius variation with temperature [4,13]

$$D = D_0 \exp\left(-\frac{\varepsilon_a}{kT}\right) \quad (8)$$

where D_0 is the reference value of diffusivity, ε_a is the activation energy and T is absolute temperature. Hence, the constant A is expected to have an exponential variation $A \propto \exp(\gamma/T)$, where γ is treated as a fit parameter.

Now let $\lambda = C^*/C_0$. Fig. 2 shows a plot of the function $f(\lambda)$ and suggests a corresponding linear approximation for $f(\lambda)$ given by

$$f(\lambda) = \frac{1}{\left[erf^{-1}(1-\lambda)\right]^2} \approx \alpha_1 + \beta_1\lambda \quad (9)$$

where $\lambda = C^*/C_0$. The linear approximation is representative of $f(\lambda)$, particularly at lower values of $\lambda = C^*/C_0$. For the detection of moisture ingress, one would indeed expect $\lambda = C^*/C_0$ to be sufficiently small. In any case, for a particular detection threshold an appropriate linearization that is representative of the function in the neighbourhood can be chosen. Combining Equations 7–9 it is proposed that constant A in Equation 4 for various conditions should have a functional form given by

$$A = \left(\alpha + \frac{\beta}{C_0}\right)\exp\left(\frac{\gamma}{T}\right) \quad (10)$$

where C_0 is the edge concentration. The edge concentration, in turn, depends on the absolute humidity for given ambient conditions and the solubility of the material. Since the constants β and γ are to be determined on the basis of experimental data, C_0 may be used as absolute humidity for given ambient or test conditions. Factors relating to the absolute humidity and edge concentration can be absorbed in β, and the exponential term determined by the fit. Note that, on the basis of this choice, the fit parameter γ may not represent the activation energy ε_a for diffusion alone. If necessary, this functional form can always be maintained by means of suitable changes to the fit parameter definitions if relative humidity is used to characterize edge concentration rather than absolute humidity. As will be shown later, the proposed functional form in Equation 10 demonstrates excellent agreement with the experimental data. In conventional techniques such as the use of the Hallberg-Peck relation [9], it is customary to use relative humidity for the analysis of moisture ingress instead of absolute humidity. Absolute humidity is related to temperature as

well as to relative humidity, and hence, as far as analysis of experimental data is concerned, the functional form in Equation 10 is justified as long as it is validated by an appropriate fit to experimental data. It is the authors' view that the distinguishing factor in using the functional form in Equation 10 is that it is based on an analytical solution to the diffusion equation and is an approximation to the solution derived on a rational basis.

Note that constant B in Equation 4 is dependent on the reaction rate for the reaction between the moisture and the desiccant. Compared with the time scale of moisture diffusion, the reaction is expected to be instantaneous. The constant B may therefore be assumed to depend only on C_0, and the proposed functional form for B is

$$B = \frac{q}{C_0} \qquad (11)$$

where q is a constant to be determined from experimental data. As in the case of Equation 10, the functional form in Equation 11 will need to be justified later using appropriate experimental data. In concluding this section it is noted that Equation 4 combined with Equations 10 and 11 provides the required functional forms for analyzing experimental data for moisture breakthrough time in the accelerated tests involving different temperature and humidity conditions. As expected, the proposed functional form suggests that, as absolute humidity C_0 decreases, the breakthrough time of the edge seal tends to infinity, and that, as temperature increases, the breakthrough time of the edge seal decreases. Both of these relationships are preserved while the quadratic dependence of breakthrough time on width of the edge seal is maintained.

Experimental set-up, results and analysis

In previous product-level testing for moisture ingress at MiaSolé, $CoCl_2$ impregnated paper (Micro Essentials Laboratory, Hydrion Humidicator Cat. No. HJH-650) was used as an indicator on various glass/glass module constructions (see Fig. 1(b)). Breakthrough was determined to be the point at which the paper turned from its blue anhydrous state to one of its hydrated-state colours. However, even with edge seal widths of approximately 3–4mm (dimensions at which reasonable precision can be maintained in a typical glass/glass structure), most experiments with desiccated edge seals tended to

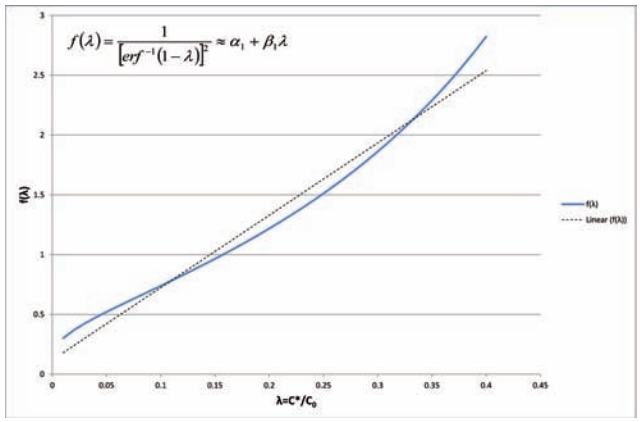

Figure 2. Approximation used in Equation 9.

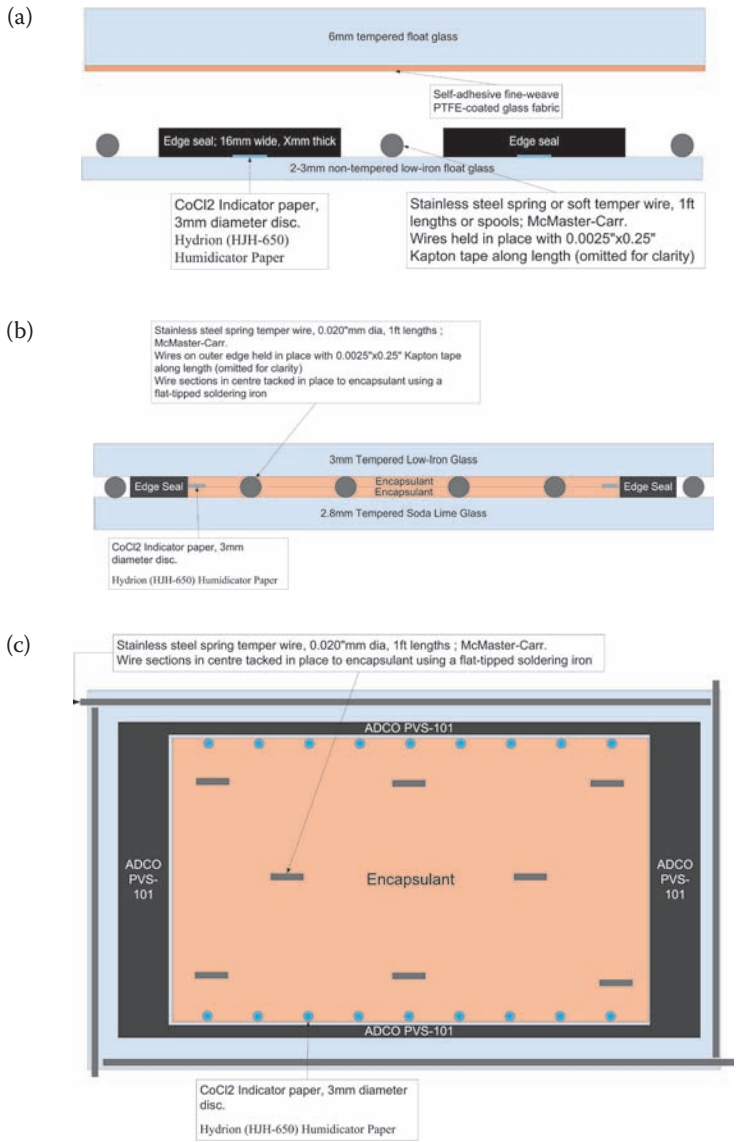

Figure 3. Sample construction for accelerated testing: (a) Type I samples; (b) Type II samples; (c) Planar view of Type II samples.

take in excess of 2000hrs at 85°C/85%RH to reach the breakthrough point. The 85°C/85%RH condition is one of the most aggressive conditions that can be controllably managed in available environmental chambers. In order to test a wider range of conditions to validate modelling parameters, it is necessary to extend the experimental conditions to lower acceleration factors. This, along with the time factor, renders the use of only glass–glass samples unfeasible.

"Most experiments with desiccated edge seals tended to take in excess of 2000hrs at 85°C/85%RH to reach the breakthrough point."

Two types of samples were therefore prepared for testing based on the experimental set-up described earlier:

1. Type I samples: plaques with a thin layer of edge seal material (~1mm) applied to the glass, and moisture indicator paper ($CoCl_2$ impregnated paper) against the glass. See Figs. 3(a) and 4(a).

2. Type II samples: glass–glass mini-modules with narrow edge seal (~3mm), encapsulant and moisture indicator paper ($CoCl_2$ impregnated paper). See Figs. 3(b), 3(c) and 4(b).

The first type of sample – Type I – facilitates sub-1mm path lengths, which result in testing times reduced by an order of magnitude. In order to address potential convolution from interfacial diffusion along the edge seal and glass interface in the glass–glass edge seal structure, a second type of sample – Type II – was constructed, and data from overlapping path lengths were shown to be equivalent. Samples of Type I provide quick turnaround in terms of moisture penetration results for smaller dimensions, while samples of Type II are consistent with a typical module construction.

Type I samples

Fig. 3(a) shows the Type I sample construction. The sample consists of using indicator paper on the glass with the edge seal material directly above it. The width of the edge seal material (see cross section in Fig. 3(a)) is significantly greater than its thickness above the indicator paper, thereby ensuring that the primary path (shortest) of moisture diffusion to the indicator paper is through the thickness of the edge seal material above it. The sample is constructed using 3mm discs of moisture paper, and dispensing edge seal material onto it, with the whole structure supported on glass. Compression of the edge seal during lamination was achieved through the use of a tempered glass plate (6mm soda lime glass, 305mm × 205mm) to which a thin self-adhesive PTFE fibreglass fabric had been attached as a release layer. Lamination was carried out in a standard laboratory-scale flatbed vacuum laminator. The process set-points were as follows: platen temperature = 160°C, vacuum time = 6min (pressure at less than 100Pa after 1min), transition to full atmospheric press = 1min, and press time = 8min. Precise control of the edge seal thickness was achieved through the use of precision-formed stainless steel wire (McMaster-Carr) as spacers set between the test sections. The spacers were held in place with high-temperature ¼" × 0.0025" Kapton tape (McMaster-Carr 7648A71 and 7648A711). The placement of these spacers is illustrated in Fig. 3(a) and also in Fig. 4(a). The use of 2mm-thick (305mm × 205mm) non-tempered glass as the sample support allowed simple cross-sectioning, confirming the thickness of the edge seal over the indicator paper. For these samples, one platen had several moisture indicator discs (36 per platen). There were two such platens tested per chosen condition.

Type II samples

Figs. 3(b) and (c) show the glass–glass sample construction (Type II) for the accelerated testing of edge seal material; this sample structure more closely represents that of a typical module. However, because of variations in glass thickness and the encroachment of encapsulant into the edge seal, the path length variability can be higher than for the thin layer samples. In order to minimize the path length variation, a method was developed to control the compression of the edge seal/encapsulant structure. This consisted of wire spacers placed at the edges of the glass samples as well as small (5–10mm long) pieces of wire placed in the encapsulant to act as hard stops for the compression of the glass during lamination. The thickness of the spacers/edge seal was chosen such that the edge seal was allowed to compress a minimum of 20% of its thickness to ensure proper wet-out of the glass. The initial width of the edge seal in the test area was determined through experimentation to produce the desired final path length after lamination for the various samples. The path lengths for actual tested samples were confirmed by cross-sectioning right next to the indicator paper disc locations.

In both cases (Type I and Type II samples), breakthrough time is characterized by the detection of the onset of colour change of the moisture indicator paper described earlier. Fig. 4 shows representative images of two types of sample.

It follows from Equations 4, 10 and 11 that the goals of the experimental design are to:

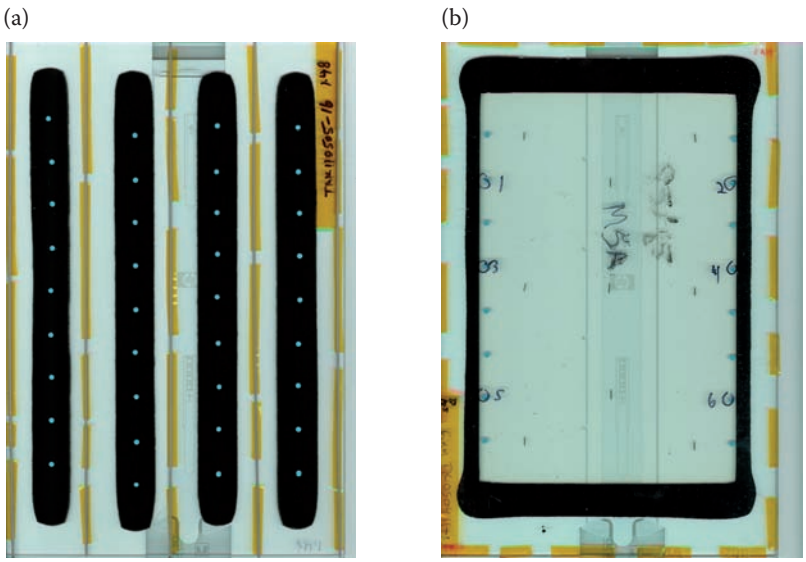

Figure 4. Laminated sample with thickness/width of the edge seal material controlled by SST wires used as spacers: (a) representative Type I sample; (b) representative Type II sample.

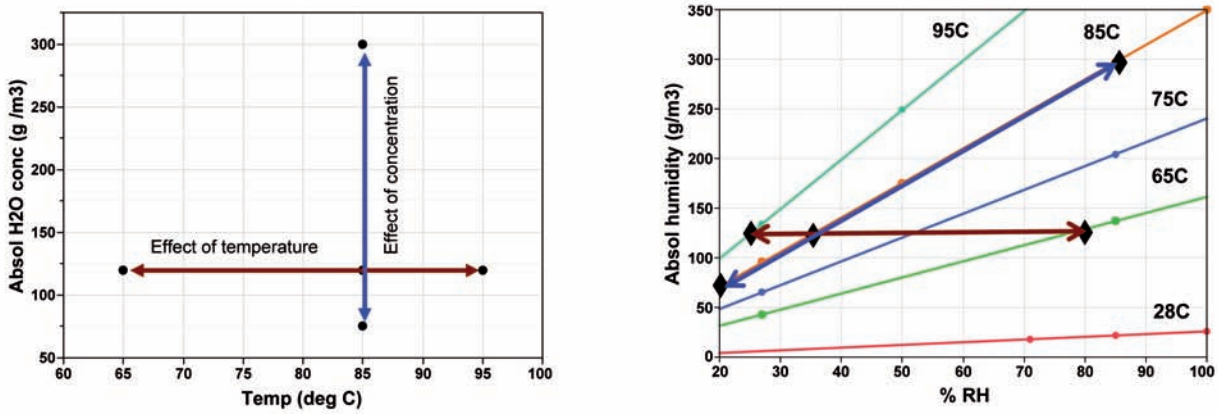

Figure 5. Test conditions chosen in accelerated testing in terms of temperature and concentration and equivalent representation in terms of temperature and relative humidity.

1. Validate the form of Equation 4, which describes a quadratic dependence of breakthrough time on edge seal width.

2. Validate the form of Equations 10 and 11 and demonstrate that the factor A exhibits Arrhenius dependence on temperature and that factors A and B exhibit hyperbolic dependence on moisture concentration.

3. Determine the parameters α, β, γ and q.

These goals can be accomplished by choosing experimental conditions such that the effects of concentration and temperature, associated with functional forms described in Equations 10 and 11, are evaluated independently of each other. An orthogonal experimental design was employed, wherein three temperatures are used at a given concentration and three concentrations are used at a given temperature, with a common temperature and concentration. The next question relates to the choice of the concentration and temperature levels. The considerations and constraints include:

- The degree of acceleration should allow a practical test duration.
- Over the range of chosen conditions, the materials should be expected to behave in a similar fashion to that for conditions encountered in field deployment.
- Environmental chambers should be able to maintain the set conditions, which precludes extreme temperature and relative humidity conditions.
- It should be possible to fabricate and measure edge seal path lengths dictated by the experimental conditions/durations.

At the outset, data for similar materials from Kempe et al. [6] were used to estimate breakthrough times for different conditions. When all the considerations and constraints were taken into account, the test conditions shown in Fig. 5 were arrived at. Finally, the temperature and moisture conditions were then translated into temperature and relative humidity conditions to accommodate the conventional way of setting up environmental chambers.

The change in colour of the indicator paper was monitored by scanning the sample on a flatbed system and by visual inspection. A colour change relative to the baseline was taken as an indication of moisture breakthrough. The colour change was monitored by inspections every 24hrs for the first 360hrs of exposure. One of the limitations of the approach presented here for monitoring is that opening and closing the chamber for inspection introduces delays owing to the time taken by the chamber to reach equilibrium after inspection. Because of this, the resolution of time to failure is limited to ±12hrs, which is a significant limitation for samples of small thickness. The frequency and time of inspection was adjusted based on estimated breakthrough times as more data became available, but this never exceeded 72hrs, and, in some instances of small-thickness samples, the measurements were repeated. Whenever there was an uncertainty in breakthrough time because of colour change between two inspections, the mid-point of the two times was chosen as the time to failure. In some cases the colour change approximately coincided with the inspection times and was recorded accordingly. In short, based on the inspection schedule that was practical, the best estimate of time for change of colour was chosen as the breakthrough time. Typically, all of the indicator paper discs changed colour within the sample in a single 24hr inspection interval. This limited our ability to understand the statistical variation within the samples. However, the colour change was found to be consistent across the entire platen in all of the observations, which therefore established the consistency of the breakthrough time for the group of data points.

> "The proposed functional forms show a very good fit to the experimental data."

Figs. 6(a) and 7(a) show the results obtained from accelerated tests conducted in this manner. Each data point on these plots represents the average thickness over a number of discs for that condition and the breakthrough times as observed by the onset of colour change. As can be seen, the proposed functional forms show a very good fit to the experimental data. The corresponding constants (fit parameters) have also been extracted from these fits and are shown in Figs. 6(b), 7(b) and 7(c).

Prediction of field performance

This section addresses the question of incorporating varying ambient conditions in order to predict field performance of edge seal material using results from accelerated testing. The variation of ambient conditions (T, RH) essentially results in the variation of edge concentration, C_0, as a function of time for a given edge seal configuration, and the variation of

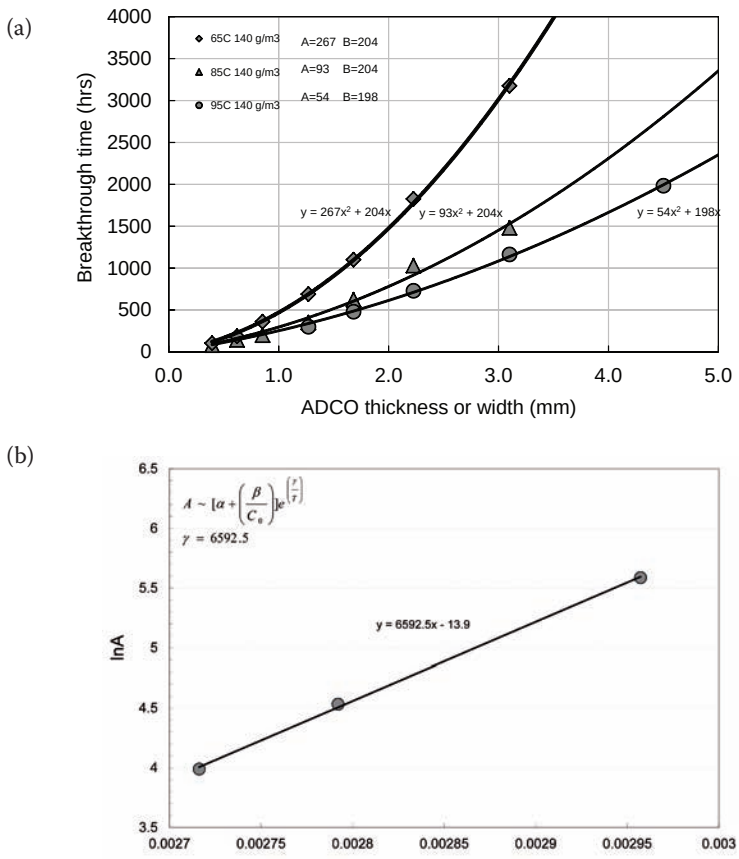

Figure 6. Experimental results of varying temperature at constant absolute humidity: (a) demonstration of quadratic variation of breakthrough time with width; (b) obtaining the Arrhenius variation for constant A.

diffusion coefficient, D, as a function of temperature (which in turn changes as a function of time). It is instructive to consider first the effect of temporal variation in diffusion coefficient. In this case Equation 1 can be written as

$$\frac{\partial C}{\partial t} = D(t)\frac{\partial^2 C}{\partial x^2} \qquad (12)$$

The solution to this diffusion equation for the 1D case may be obtained by introducing a new transformation variable

$$\tau = \int_0^t D(\xi)d\xi \quad \Rightarrow \frac{\partial C}{\partial \tau} = \frac{\partial^2 C}{\partial x^2} \qquad (13)$$

and is given by

$$C(x,t) = C_0\left[1 - erf\left(\frac{x}{2\sqrt{D_{\text{eff}}t}}\right)\right] \qquad (14)$$

where

$$D_{\text{eff}} = \frac{1}{t}\int_0^t D(\xi)d\xi \qquad (15)$$

Note that for a time sufficiently long, a practical approximation to this result for the case in question may be obtained by carrying out the integral in Equation 15 over a representative period of variation, such as a typical meteorological year (TMY). The solution given by Equation 14 holds for the special case of edge concentration remaining constant over the period of interest.

The effect of time-varying the edge concentration can be examined separately. Assume that the period of variation of edge concentration is small (daily) compared with the diffusion time (expected breakthrough time of several years). To examine how far into the edge seal the time variations of the edge concentration will have a significant effect, the problem defined by the following equation can be considered

$$\frac{\partial C}{\partial t} = D\frac{\partial^2 C}{\partial x^2} \qquad (16)$$

with the conditions

$$C(0,t) = C_0 \sin \omega t$$
$$C(x \to \infty, t) = 0 \qquad (17)$$

It can be shown that the solution to the problem represented by Equations 16 and 17 is given by

$$C(x,t) = C_0 \exp\left[-\left(\sqrt{\frac{\omega}{2D}}\right)x\right]\sin\left(\omega t - \left(\sqrt{\frac{\omega}{2D}}\right)x\right) \qquad (18)$$

It is seen that, because of the exponential pre-factor, the oscillations of edge concentration with time are damped out within a short distance into the edge seal. For $\omega = (2\pi/24)\text{hr}^{-1}$ and a representative diffusivity value of $0.2\text{mm}^2/\text{hr}$, the associated length scale is given by $l \approx \sqrt{(2D/\omega)} = 1.2\text{mm}$ for decay by $\exp^{-1}$, i.e. a reduction to 36% of the outside amplitude. Typical edge seal widths in PV modules are an order of magnitude larger (~10mm) and hence, for practical purposes, an average concentration at the edge may be considered for this analysis. Note that seasonal variations (period ~3 months) may manifest themselves at a fraction of external amplitudes at the inner edge of the edge seal. However, in the case of PV modules, it is common to use edge seals loaded with desiccants as pointed out earlier. Hence, the magnitude of variations at the inner edge of the edge seal, even for seasonal variations, is not expected to be significant until the desiccant in the edge seal is consumed. On the basis of these considerations, an average concentration over a TMY was used for the analysis.

> "Oscillations of edge concentration with time are damped out within a short distance into the edge seal."

From the discussion above and the results in Equations 14, 15 and 18, the following methodology is proposed for predicting field performance of edge seal materials tested:

1. Obtain the breakthrough time in various tests in standard temperature- and humidity-controlled chambers.
2. Determine the fit parameters A, B and γ given by Equations 10 and 11, as shown in previous sections. This involves obtaining the fit parameters α, β and q in Equations 10 and 11.
3. Establish the average absolute humidity for a given location using TMY data.
4. Work out an equivalent temperature for a location using TMY data from

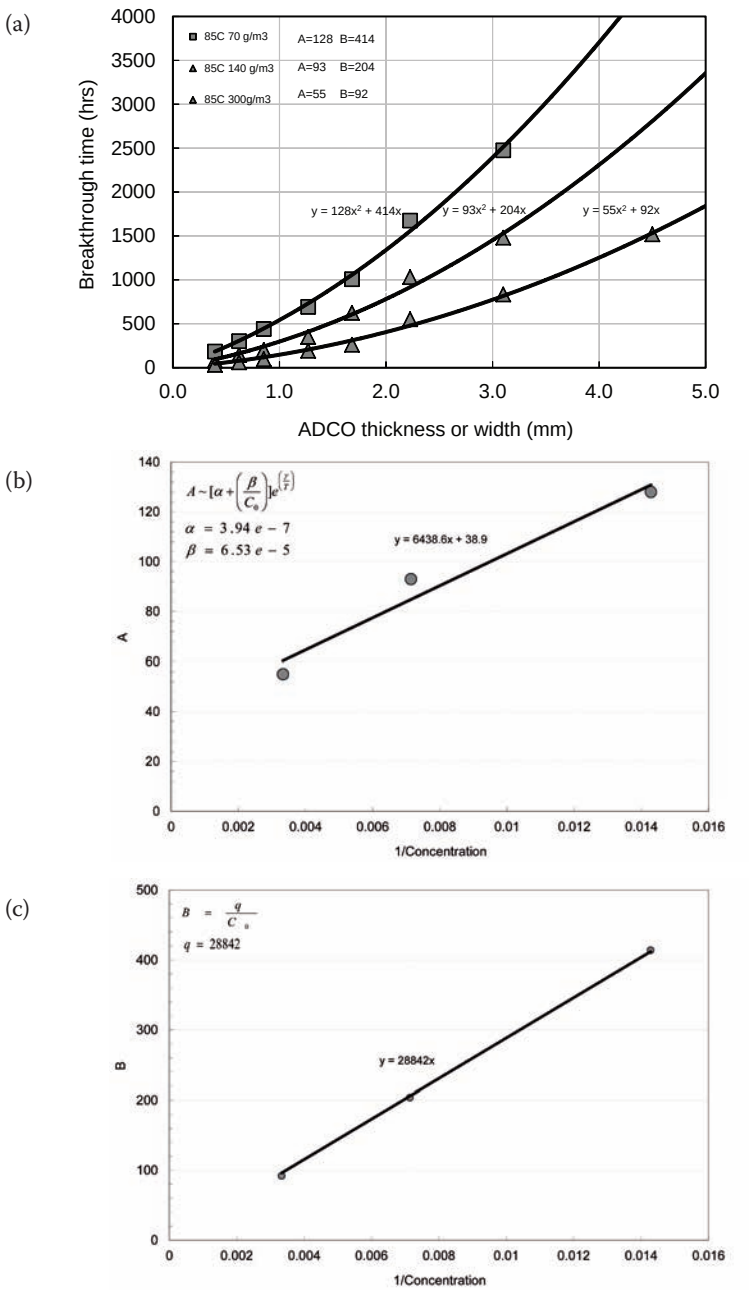

Figure 7. Experimental results of varying absolute humidity at constant temperature: (a) demonstration of the proposed quadratic variation of breakthrough time with width; (b) obtaining the fit parameters α and β; (c) obtaining the fit parameter q.

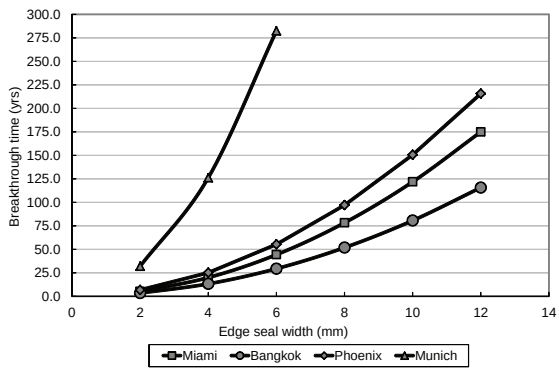

Figure 8. Predicted edge seal moisture breakthrough time for a particular edge seal used in certain MiaSolé glass–glass modules at selected locations.

$$\exp\left(-\frac{\gamma}{T_{eq}}\right)=\frac{1}{t_{1yr}}\int_0^{t_{1yr}}\exp\left(-\frac{\gamma}{T(t)}\right)dt \quad (19)$$

where the integral is performed over a typical year. An option to improve upon this estimate of T_{eq} is to use models validated by correlation to field data and to use T(t) as the module temperature for given ambient conditions in the TMY data, rather than using the ambient temperature directly.

5. Calculate A and B for field conditions.

6. Substitute these values for A and B in Equation 4 to predict the field breakthrough time of the edge seal material at a given location.

Using the above approach, edge seal breakthrough time has been predicted for a particular case of edge seal used in certain MiaSolé glass–glass modules. These predictions are given in Fig. 8: it is seen that the predicted edge seal lifetime with edge seal width ~10mm is far beyond the intended service lifetime, even for hot and humid locations.

> "In a particular case of edge seal, it was established that moisture ingress can be prevented well beyond the intended service lifetime."

Conclusion

The purpose of this work has been to provide a theoretical framework, an experimental technique for accelerated testing, and a method consistent with the theory for assessing edge seal field performance in a way that is decoupled from other components in a PV module. A theoretical framework was developed using an analytical solution to the 1D diffusion equation and observations of the mathematical characteristics of associated functional forms. This enabled functional forms to be proposed for the variation of breakthrough time (moisture penetration) with given edge seal width under different ambient or chamber conditions. A relatively inexpensive test technique was developed such that the tests can be conducted in standard environmental chambers used for product level testing. Proposed functional forms were validated by experimental data from accelerated testing. A methodology based on the developed theoretical

framework was provided for predicting field performance of the edge seal from the results of accelerated testing. In a particular case of edge seal used in certain MiaSolé glass–glass modules, it was established that moisture ingress can be prevented well beyond the intended service lifetime, even for the most aggressive climate conditions evaluated.

References

[1] U.S. Photovoltaic Manufacturing Consortium (PVMC) 2013, "U.S. CIGS photovoltaic roadmap", July.

[2] Pern, J. 2008, "Module encapsulation materials, processing and testing", APP Int. PV Reliab. Worksh., Shanghai, China.

[3] Livingston, H. "SSB-1: Guidelines for using plastic encapsulated microcircuits and semiconductors in military, aerospace and other rugged applications", Report, Solid State Dev. Comm. Gov. Electron. Inf. Tech. Assoc. (GEIA).

[4] Shirley, C.G. 1994, "THB reliability models and life prediction for intermittently-powered non-hermetic components", *Proc. 32nd Ann. Int. Reliab. Phys. Symp.*, San Jose, California, USA, pp. 72–77.

[5] Coyle, D.J. 2013, "Life prediction for CIGS solar modules part 1: Modeling moisture ingress and degradation", *Prog. Photovolt.: Res. Appl.*, Vol. 21, pp. 156–172.

[6] Kempe, M.D. et al. 2010, "Evaluation and modeling of edge-seal materials for photovoltaic applications", *Proc. 35th IEEE PVSC*, Honolulu, Hawaii, USA.

[7] Otth, D.H. & Ross R.G. 1983, "Assessing photovoltaic module degradation and lifetime from long term environmental tests", *Proc. 29th Inst. Env. Sci. Ann. Meet.*, pp. 121–126.

[8] Osterwald, C.R. & McMahon, T.J. 2008, "History of accelerated and qualification testing of terrestrial photovoltaic modules: A literature review", *Prog. Photovolt.: Res. Appl.*, Vol. 17, No. 1, pp. 11–33.

[9] Hallberg, O. & Peck, D.S. 1991, "Recent humidity accelerations, a base for testing conditions", *Qual. Reliab. Eng.*, Vol. 7, pp. 169–180.

[10] Peck, D.S. 1986, "Comprehensive model for humidity testing correlation", *Proc. IRPS*, pp. 44–50.

[11] Peck, D.S. 1970, "The design and evaluation of reliable plastic encapsulated semiconductor devices", *Proc. IRPS*, pp. 81–93.

[12] Rasal, R.M. & Snowwhite, P.E. 2010, "Solar edge sealants with a better balance of properties", Poster Session, PV Mod. Reliab. Worksh., Denver, Colorado, USA.

[13] Crank, J. 1975, *The Mathematics of Diffusion*, 2nd edn, Oxford: Oxford University Press.

About the Authors

Kedar Hardikar is a staff scientist at MiaSolé and holds a Ph.D. from the Division of Engineering, Brown University. His roles at MiaSolé include assisting product development, improving reliability of the product, and leading selected research and development projects using analysis and computational models. An author of several technical publications, Kedar held several key positions over a period of more than 10 years in the semiconductor capital equipment industry and in the consumer electronics industry before joining MiaSolé.

Dan Vitkavage holds a Ph.D. in chemistry from the University of North Carolina at Chapel Hill. He has authored numerous technical publications and presentations and is the holder of 18 US patents. Dan has held a range of technical and management positions within the semiconductor industry, both in the area of IC fabrication and in PV. He is currently a senior director of technology for Lam Research Corporation.

Ajay Saproo is the director of reliability and process integration at MiaSolé. He is responsible for ensuring product performance and reliability, including the development of tests and solutions relating to reliability problems, technology qualification, product certification, lifetime models and field validation. Ajay holds an M.S. in electrical engineering from the University of Cincinnati.

Todd Krajewski is the process development manager for flexible modules at MiaSolé. He holds a bachelor's degree in chemistry and is a co-inventor on 10 issued patents and numerous patent applications. Todd's focus has been on polymer synthesis, ultra-barrier films and material integration in the semiconductor, OLED and solar fields.

Enquiries

Kedar Hardikar
MiaSolé
2590 Walsh Ave
Santa Clara, CA 95051
USA

Tel: +1 408 919 5702
Email: khardikar@miasole.com

PV Modules

News

Court approves Shunfeng's US$500 million Suntech deal

A Wuxi court has approved Shunfeng Photovoltiac International's purchase of Suntech Power's manufacturing arm. Suntech Wuxi's factories will increase output with all outstanding wages and taxes to be paid in full. Ongoing contractual obligations will be fulfilled. Shunfeng has already intimated that it would resume production lines that have previously been closed. An additional 1GW of module production could resume and a 1.6GW cell production line, closed since August 2012, could be brought up to a level of 1.2GW after the acquisition is settled. The acquisition of Suntech Wuxi by Shunfeng is designed to enable the company to expand into solar cell and module production so that it can move downstream and build PV power plants primarily in the China market.

Shunfeng's acquisition of Wuxi Suntech has been approved.

Innovations

Motech displaying 20.5% monocrystalline 'Sirius' cell

Motech Industries will make its new 'Sirius' cell which comes with a 20.5% conversion efficiency, available in the first quarter of 2014. The Sirius 60-cell solar module is said to provide improved temperature coefficient and low light behaviour and offers power classes up to 280W. A 72-cell solar module with power classes up to 335W is also planned with modules available upon request.

Dr. Allen Wu, VP sales and marketing at Motech, Taiwan said: "This is a truly meaningful development since the Sirius Monocrystalline cell's higher capability leads to premium module power output and efficiency, which makes it a natural choice for our customers. Motech continues to effectively improve the conversion efficiency through the innovation of its R&D and manufacturing team in process optimisation and material enhancement."

Panasonic displays special order double bifacial HIT module

Panasonic Eco Solutions North America displayed its new 'HIT Double' bifacial solar panel 'VBHN225DA02' at Solar Power International 2013 in October. The HIT Double was exhibited as a reference model and special order-based product, designed to allow power generation from both sides of the solar cell. Panasonic HIT Double has a double-sided glass structure with laminated HIT solar cells inside.

This structure allows the solar panel to capture sunlight and generate power from both sides of the solar panel, which is claimed by the company to potentially generate up to 30% more electricity than the standard single-sided HIT module under the same conditions. The company first introduced the double bifacial HIT solar panel in 2012 for the US and European markets, later followed that year with availability in Japan.

LG Electronics continues global roll-out of 'MonoX NeON' module

Mometnum continues to build for LG Electronics' most important solar module product roll-out since the company's involvement in the PV industry began.

The LG 'MonoX NeON' module was displayed at Solar Power International, featuring a suite of mainstream N-Type cell manufacturing technology tweaks that include selective emitters, fine line electrodes, surface passivation and lightweight construction, all in a compact 60-cell panel design.

The result is a module series that delivers high-efficiency output of up to 300 watts with 18.3% module efficiency. Very much with the US market in mind, LG is previewing a new AC solar module with an integrated LG-developed and LG-manufactured microinverter, both planned for introduction in 2014.

Accreditations

CNPV readies for Japanese push with JET certification

Solar manufacturer CNPV has attained certification from Japan Electrical Safety & Environmental Technology Laboratories (JET) for its range of modules, clearing the way for them to enter the Japanese market. The company's Optimal Premium Series were required to pass the JET tests, which cover design, construction, reliability and performance.

"The JET certification process is highly stringent," said Bypina Veerraju Chaudary, COO and CTO, CNPV. "PV module components must meet not only IEC61215 and IEC61730 standards, but also UL1730, UL746C and UL94 standards. The testing and review processes took numerous months.

Panasonic displays special order double bifacial HIT module.

SunPower's E20/327 solar modules pass PV Evolution Labs PID test

SunPower has said that its E20/327 solar modules have passed potential induced degradation (PID) testing at PV Evolution Labs.

The company said that its modules achieved less than a 0.2% power loss during the PID tests. PV Evolution Labs PID test includes a 600 hour damp heat conditioning, as defined in international testing standards, and maximum rated voltage stress.

SunPower noted that during the testing period, visual inspections, flash testing and high-resolution electroluminescence images are taken to accurately evaluate and monitor the panel's durability. After 100 hours of testing, a panel must demonstrate less than five percent power loss and less than 10 percent after 600 hours to pass the test.

However, the company claimed, without providing further details that only 50% of all modules tested successfully passed the program's criteria. SunPower also claimed that of the 50% of modules that failed PID testing, power losses ranged from 18% - 87%. The company did not provide further details to support the claims.

CSUN gains TUV Rheinland certification for Turkish factory

China Sunergy has gained TUV Rheinland certification for its factory in Turkey. The Chinese manufacturer will produce both cells and modules in Turkey.

As a result it will be able to ship products free of trade restrictions created by the dispute between Beijing and Brussels and any future duties that could be levied against Chinese firms.

Modules assembled with Chinese-produced cells would still be part of the price undertaking agreed between China and the EU in July. The company has already acquired the necessary carbon footprint certificates to enable its customers to take part in the French tender process for projects above 250kW. The modules passed TUV Rheinland's tests to attain IEC61215 and IEC61730 certification. The factory is now running at full capacity.

Q CELLS' 'Q.PRO-G3' modules pass cyclone test

Tested at the James Cook University's Cyclone Testing Station (CTS) in Townsville, Australia, Hanwha Q CELLS' 'Q.PRO-G3' modules have passed tests that include withstanding wind speeds of up to 240 km/h. The Q.PRO-G3' modules differ from conventional modules by employing a thinner (35mm) frame design and features a high-tech aluminium alloy that allows for wind loads of up to 5,400 Pa while reducing module weight to 19 kg. CTS undertook static and dynamic testing. In the first test, increasing pressure was applied onto the backside of the modules' back until it collapsed. The second test simulated the effects of dynamic loads by alternately pushing and releasing pressure onto the back of the module. During the test, a maximum pressure of 7kPa was applied in a total of 10,360 cycles to simulate a cyclone.

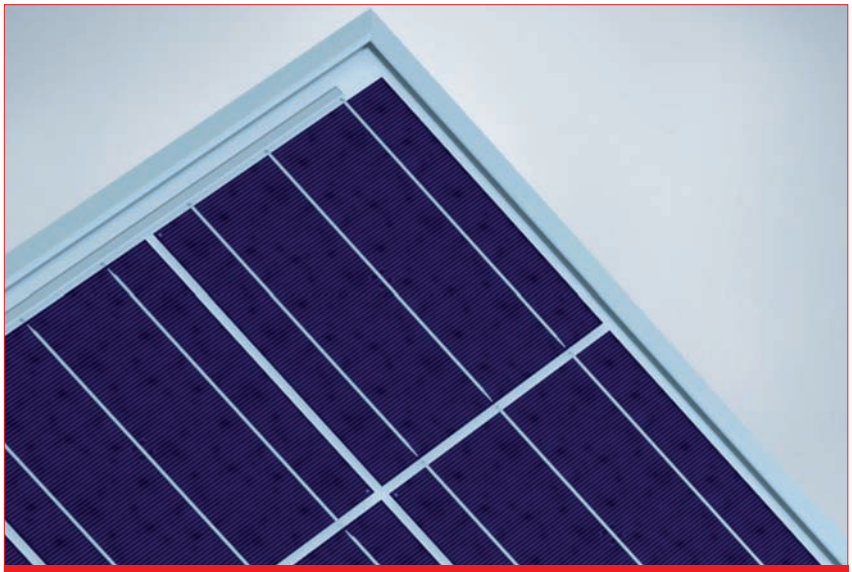

Q CELLS' 'Q.PRO-G3' modules have passed cyclone testing.

New UK certification boosts JinkoSolar's EU market credentials

Chinese module manufacturer JinkoSolar has had its polycrystalline products certified by the independent UK-based engineering consultancy OST Energy. The new status will boost the bankability of the company's modules in the EU market and Britain in particular.

The modules exceeded standard industry efficiency ratings according to JinkoSolar. OST Energy has certified that Jinko's production facilities are in line with the lender requirements set out by the Wold Bank. The facilities were also approved for their environmental, health and safety standards.

Fraunhofer and Wavelabs sign agreement to produce LED PV module tester

German research and development institute Fraunhofer Centre for Silicon Photovoltaics (Franuhofer CSP) has announced that it will develop an LED-based solar simulator with Wavelabs Solar Metrology Systems after the two companies signed a cooperation agreement. The simulator, Sinus-2100, will be used to test PV modules, with Fraunhofer claiming that the new product will demonstrate an "almost flawless" efficiency measurement. Sinus-2100 uses LEDs of 21 different colours and allows module makers to choose the exposure time of the test, which Fraunhofer argues is beneficial to makers of high efficiency modules that need a longer exposure time. The new product will be based on technology used in the Sinus-220 tester already being produced at Wavelabs Solar Metrology Systems. The two companies expect the Sinus-2100 to go into production at the beginning of 2015.

Jinko Solar gains Japan certification

Jinko Solar has become the latest module manufacturer to have its modules certified by the Japan Electrical Safety & Environmental Technology Laboratories (JET). The JET certificates will enable the company to take advantage of the burgeoning market in Japan. Yingli Green, CNPV and ReneSola have all announced approval from JET for their PV modules in 2013. The introduction of a feed-in tariff (FiT) has triggered a surge in applications for projects in Japan.

Solar-Fabrik qualifies for higher French FiT rate with VDE certificate

European module manufacturer, Solar-Fabrik has obtained new certification from VDE, giving its customers access to increased feed-in-tariff (FiT) rates in France. The "made in Europe" certificate has been awarded to Solar-Fabrik's Premium incell modules (size L and XM). The certificate was awarded on account of Solar Fabrik using European cells in its German-manufactured modules. VDE is one of the largest technical and scientific associations in Europe, providing product testing, registration and certification. The French Ministry of the Environment grants PV installations a 10% FiT increase for using premium modules with European cells, whereas cells from outside Europe only receive a 5% increase.

Kyocera has raised its solar panel sales target by 20% to 1.2GW.

Kyocera raises solar panel sales target 20% to 1.2GW

Kyocera has increased the annual sales target for its solar module business from 1GW to 1.2GW. In the company's first half results for the 2014 fiscal year, it recorded a 15% sales increase from US$6.2 billion to US$7.1 billion. Kyocera, which works in a number of electronic and industrial markets, said its solar business had performed especially well citing the expansion of the Japanese solar sector as a key contributor. "In the first half, consolidated sales increased significantly in our solar energy, telecommunications equipment and information equipment businesses. Combined with the effects of the yen's depreciation against the dollar and euro, we achieved a 15% revenue increase year-on-year and recorded our highest half-year sales to date," said Goro Yamaguchi, president, Kyocera Corporation said in a statement.

Hanwha SolarOne shifting strategy to higher value markets

Hanwha SolarOne is shifting its position in the PV industry in an attempt to improve business opportunities and financial condition in light of its slow recovery, compared to tier one Chinese rivals. The company will focus on improving competitiveness and profitability position by focusing on what it described as "high-end market[s]".

High-end markets can be interpreted to be those with higher ASPs as well as focusing on sectors such as residential rooftops and the downstream project sector, which have the ability to provide higher margins. According to Hanwha SolarOne, it will focus on the EU residential market, notably the UK as well as the Japanese market and what it described a "high-priced segments in the North America market".

REC splits up company, makes IPO

At the beginning of October, Renewable Energy Company ASA (REC) held a public share offering for its new division, REC Solar. After REC divided its manufacturing and sales operations to create REC Silicon and REC Solar, REC Solar was placed on the Oslo stock exchange for initial public offering (IPO). Remaining shares were allocated to pre-existing shareholders under a previous agreement to purchase any of the remaining shares by the public offering deadline. Out of REC Solar's share capital of NOK40 million (US$6.755 million), the shares were divided into 40 million, at NOK1.00 each (US$0.17). REC Solar was listed on the Oslo Stock Exchange on 25 October. REC no longer owns any of the shares after completion of the IPO, with REC Solar debt free. All REC operations in silicon are to continue in Moses Lake and Butte, US. REC Solar's senior vice president for sales and marketing, Luc Graré said the division of REC group into two separate entities allowed the company to "invest heavily in research and development again".

Kyocera has raised its solar panel sales target by 20% to 1.2GW.

Product Reviews

Bürkle

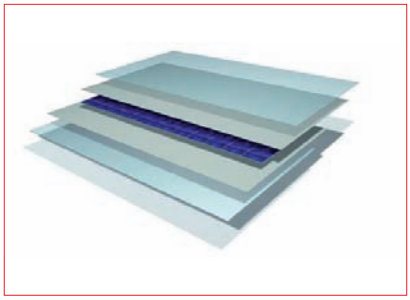

Bürkle unites three process steps for glass-glass module lamination

Product Outline: Bürkle's single opening e.a.sy-Lam VFF lamination line is designed for a wide range of products, combined with high throughput and flexibility that unites three process steps in one line. Cycle times of less than 12 minutes with glass thicknesses of 2 x 3.2 mm are achievable.

Problem: Glass-glass modules offer excellent opportunities for added value as well as significant development prospects, and wide usage options due to their range of variants. They are superior to modules with backsheets due to their structure, in particular with respect to stable value but have higher production costs.

Solution: The Bürkle e.a.sy-Lam VFF processes various encapsulation foils and glass thicknesses. It can also laminate glasses with a thickness of only 1mm. The lamination process is combined and is made in two stages: first, in a vacuum lamination step using a membrane (pre-lamination, evacuation and sealing of a module) and subsequently in a heated flat press for final lamination. These two lamination steps, which are consecutively arranged, are followed by an optional cooling step. Bürkle claims its lamination process provides homogenous cross-linking, minimised material stress and significantly reduced warping potential of the module. An additional advantage is that no over-pressing or pinching occurs at the module edges.

Applications: Both glass-glass and glass-foil modules can be laminated.

Platform: The e.a.sy-Lam VFF is available in two versions with different capacities. While the e.a.sy-Lam VFF 2135 has a useful area of 2.100x3.500mm, the e.a.sy-Lam VFF 2141 has an useful working surface of 2.100x4.100mm. Glass-glass modules with the standard formats of approximately 1.000x1.700mm and approximately 1.000x 2.000mm as well as special module formats.

Availability: Currently available.

Festo

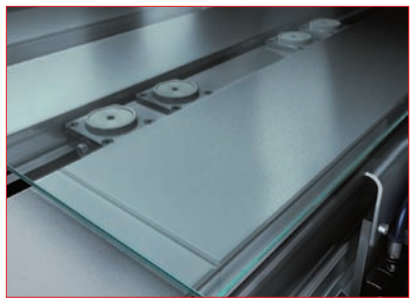

Festo's ATBT air cushion plates provide fast and reliable glass substrate transportation

Product Outline: Festo has launched its new ATBT air cushion plates, which are claimed to provide for a fast and gentle transportation of PV module glass substrates, amongst other specialist applications. They make contactless handling of substrates easy, regardless of their size and weight.

Problem: Improving cycle-times while reducing damage and scrapped substrates reduces overall COO. Providing limited flex and shock to substrates while transporting or in buffer zone areas can also improve productivity and throughput to PV module assembly.

Solution: The ATBT air cushion plates generate a thin air cushion on the fine surface, which enables the glass panels and delicate films used in the solar and electronics industries to glide evenly. The air cushion plate uses an air-permeable material. This ensures a constant air flow with low compressed air consumption and allows thin-film modules, coated on both sides, to travel through the manufacturing process on an air cushion without contact. Electric drives control the modules during the process, while suction cups made of special material don't leave any residue behind on the thin-film cells. A diagnostic module measures the exact distance between the glass and the air cushion plate and uses this to control the air consumption in an energy-efficient manner.

Applications: PV glass substrate handing, notably for loading and unloading, intermediate buffers, lifting and centering.

Platform: For the easiest selection of ATBT air cushion plates, Festo has created an engineering software tool. It allows the design engineer to enter the design parameters and therefore select the correct air cushion plate for their application.

Availability: Currently available.

MBJ Solutions

MBJ Solutions combines high-speed with high-resolution electroluminescence inspection

Product Outline: MBJ Solutions has expanded its product portfolio for electroluminescence inspection equipment with the new SolarModule EL-flasher HR and SolarModule EL-quickline, providing high-resolution fast cycle times.

Problem: Electroluminescence technology allows the visualization and detection of defects otherwise not visible to the human eye. Defects include micro-cracks, electrically not active areas or grid failures. Micro-cracks can progress over time and lead to a significant loss in module power.

Solution: With the SolarModule EL-flasher HR, MBJ is offering for the first time a high-resolution EL inspection system for integration into existing sun simulators. The system has already been successfully integrated into sun simulators from Berger and Pasan. It is particularly suitable for the use in PV labs due to the handling effort of the module is decreased to a minimum due to the combined measurement of IV-curve and EL in one unit. The EL system combines the speed of the quickline series with the high resolution of the EL-inline family, according to the company. The system can capture EL-images of a 6x12 solar panel with a resolution of 180µm per pixel within 6 seconds, including fully automatic defect detection that provides a cycle time of 20 seconds and allows the integration of additional testing procedures.

Applications: C-Si PV module electroluminescence inspection for labs and production facilities.

Platform: MBJ can offer various new options. Beside known options like barcode reader, automatic 2D cell measurement and software for the repair area now new options for testing the bypass diodes, a hipot test and the detection of hotspots can be integrated into the EL inspection systems.

Availability: Currently available.

The role of encapsulants in standard and novel crystalline silicon module concepts

Verena Steckenreiter, **Arnaud Morlier**, **Marc Köntges**, **Sarah Kajari-Schröder** & **Rolf Brendel**, ISFH, Emmerthal, Germany

ABSTRACT

Encapsulants play a crucial role in ensuring the long-term stability of the power output of PV modules. For many years the most popular encapsulation material for crystalline silicon modules has been ethylene vinyl acetate (EVA), which leads the market because of its cost-effectiveness. Innovations in crystalline silicon cell and module technology, however, have changed the requirements that the encapsulants have to meet. A wide range of other encapsulation materials is also available; such alternatives offer improved outdoor stability and gains in module performance. Furthermore, innovative module concepts that have new sets of requirements are under development. One attractive module concept in particular envisages the attachment of pieces of crystalline Si to the large module glass at an early stage, followed by the processing of the Si cell and the series interconnection at the module level using known processes from thin-film photovoltaics. This so-called thin-film/wafer hybrid silicon (HySi) approach relies heavily on module-level processing of Si solar cells, and is a new field of research. This paper discusses the applicability of silicone encapsulants for module-level processing and compares their requirements with those of conventional EVA.

Introduction

For a PV module to be a cost-efficient source of electricity, its lifetime needs to be as long as possible. Today's module manufacturers grant warranties of up to 30 years. During this time, the solar cells must be shielded from environmental stresses, such as wind and snow loads, humidity, temperature and UV radiation.

The encapsulant plays a crucial role in shielding solar cells from the elements: it is used to fix the cells behind a rigid transparent cover sheet to ensure protection against the outdoor environment, as shown in Fig. 1. The key features of the encapsulation material are:

- Suitable transparency in the solar-cell-relevant spectrum [1]
- Durability against UV light, temperature and humidity [2]
- Adequate mechanical adhesion to the glass, solar cell and metal components
- Low elastic modulus to buffer the solar cells mechanically from the glass [3]
- Electrochemically neutral material to avoid corrosion [3]
- Acceptable handling, processability and process-speed [4]

The stability of the encapsulation material itself is, moreover, of the utmost importance for the long-term stability of PV modules. In the wear-out phase the quality of the encapsulant determines the browning and delaminating speed and hence the service lifetime of the PV module. The delaminating phase is typically the beginning of the end of the service life [5]. Even if the delamination itself does not lead to a significant power loss of the PV module, the peeling process allows water to initiate electrochemical corrosion of the metal parts of the solar cells and interconnection ribbons.

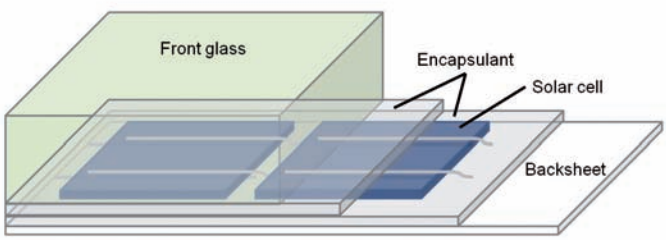

Figure 1. Lay-up schematic of a standard module.

> "The stability of the encapsulation material itself is of the utmost importance for the long-term stability of PV modules."

The first commercial modules used silicone rubber and polyvinyl butyral (PVB) as the encapsulant [6]. Since the early 1990s the most common encapsulation material used in PV modules has been ethylene vinyl acetate (EVA) [6]. Lots of materials have now been developed and are competing with EVA in the PV market, for example thermoplastic polyurethane (TPU), polyvinyl butyral (PVB), polyolefin (PO), ionomer, thermoplastic silicone (TPS) or silicone [7]. All these materials have specific advantages over EVA, but their higher prices have prevented their extensive use in the cost-driven PV market.

Silicon solar cells and PV modules, however, are continuously changing and improving significantly; this leads in some instances to changing encapsulant requirements and may increase the attractiveness of new encapsulants. Additionally, radically novel module concepts could emerge that have a different set of requirements for the encapsulant.

This paper summarizes the properties of the state-of-the-art encapsulant EVA, reviews the changing requirements for encapsulants of standard PV modules, discusses an innovative concept that requires module-level processing of solar cells, and investigates the challenges for the encapsulant in those concepts.

Properties of the standard encapsulant EVA

EVA is obtained by the copolymerization of ethylene and vinyl acetate in various ratios according to the field of application. The bulky vinyl acetate group hinders the crystallization of the material and acts as a plasticizer. Controlling the ratio of vinyl acetate in the copolymer allows the synthesis of materials with tuneable mechanical, chemical and electrical properties [8]: for solar-grade EVA, the typical vinyl acetate weight ratio is about 33% [9]. The use of EVA in PV modules requires a cross-linking step in the material processing, i.e. the irreversible formation of intermolecular covalent bonds between the chains, after which the polymer cannot be made molten but only softened by heating. EVA has a low melting point (60–80°C), and is therefore easily processable before it cross-links. This cross-linking is achieved during the lamination of the modules at temperatures between 140 and 160°C, and requires maintaining the module at these temperatures for 10 to 15 minutes, since the cross-linking reaction is not instantaneous. This step is still one of the most time-consuming steps in module production. EVA compounds destined for the solar industry contain initiators, such as peroxides or other radical-forming species, to allow cross-linking of the material. These initiators – as well as other additives, such as adhesion promoters, antioxidants and UV absorbers – are integrated in the polymer matrix during the extrusion of material into foils. The radical-forming initiators are activated by heat during lamination but are also degraded by UV light, or they simply evaporate when the EVA is not properly stored in an opaque sealed foil, resulting in a short shelf life. This has implications on module manufacturers' supply chains.

EVA degrades and discolours under exposure to UV light and is therefore usually protected by a UV stabilizer: this additive absorbs wavelengths under 350nm to protect EVA from harmful radiation, thus also limiting the photon flux reaching the solar cell. Nevertheless, UV absorbers are not sufficient for preventing the degradation of the material. Laboratory exposure of EVA laminates to UV destroys the UV absorber [2,10]: over time this leads not only to an increasing transparency of the material in the wavelength range 300–350nm, but also to a progressive decrease in transparency in the wavelength range 350–650nm, causing a noticeable yellowing of the material [9,11,12]. This yellowing is presumed to be due to the formation of π-conjugated products, which may occur on the polymer backbone itself [9] or on the by-products of degraded additives [12]. Silicone encapsulants [13] do not show absorption in this range, and their UV stability does not require the addition of a UV absorber, thus allowing an optimal transparency in this range. Furthermore, when exposed to UV light, thermoplastic and thermosetting silicone encapsulation materials display a lower decrease in discoloration and transparency than EVA over time [14].

Degradation of the embedding material under UV exposure, or through heat and moisture hydrolysis, leads to the release of acetic acid. The formation of such a product may have a direct impact on module performance stability, since acetic acid may contribute to the corrosion of the contacts and the metallization of the solar cells [15,16].

During the cross-linking process, the radical initiators are consumed, as are the stabilizing agents. Nevertheless, a short lamination time may lead to a large amount of reactive initiators remaining in the module. An ageing study carried out at ISFH on modules encapsulated with EVA with different degrees of cross-linking has shown that the residual peroxides and other cross-linking initiators reduce the weathering stability of EVA [2]. Under UV exposure or under damp-heat conditions, the EVA material containing residual cross-linking initiators has been shown to yellow faster and exhibit a greater amount of fluorescent degradation products than the fully cross-linked EVA, in which these initiators are depleted. Silicones demonstrate a higher stability against UV light and heat load than hydrocarbon polymers, as the intrinsic stability of the covalent bonds in silicone is much higher than that of the covalent bonds in polymers such as EVA or PVB [17].

> "Silicones demonstrate a higher stability against UV light and heat load than hydrocarbon polymers."

Two factors need to be taken into consideration in determining the ideal degree of cross-linking. On the one hand, a low degree of cross-linking leads to a low viscosity of the material, causing an outflow of the material from the module and eventually delamination. On the other hand, achieving a high degree of cross-linking with certain fast-curing materials containing large amounts of cross-linking initiators provokes the formation of bubbles in the laminate [2]. This negative effect of the residual chemically active additives on the stability of the encapsulant is a further argument in favour of thermoplastic materials for standard PV applications, as these will allow higher process flexibility for a manufacturer, without the need to take into consideration the consumption of the remaining cross-linking initiators.

Besides this susceptibility to degradation caused by the additives, pure carbonated polymers display an intrinsic sensitivity to high temperatures. EVA spontaneously degrades in a few minutes at temperatures of about 250°C [18], and a four-hour exposure of additive-free EVA to temperatures of about 180°C leads to a dramatic discoloration of the material.

Change in requirements for encapsulants because of improvements to standard PV modules

Several developments have led to enhanced requirements for encapsulants:

- Improvements to solar cells
- Newly identified degradation mechanisms
- Constraints due to cost-reduction measures

Improvements to solar cells

Today's solar cells have an improved UV response [19]. The UV blocker in an EVA-based encapsulant, however, typically absorbs the UV spectrum up to a wavelength of 360nm (10% transmittance) [20], which means that about 0.25% of the cell current is lost in the EVA [19]. Improving the UV transparency of EVA is therefore important [20]: one possibility is to change the UV blocker in the EVA. If the number of high-energy UV photons in the EVA is increased, however, there is a higher risk of browning and delamination of the encapsulant, because of the UV-driven decomposition of the EVA molecular

NovoPolymers

Your Innovative Encapsulant Partner

Reflectivity | Light Enhancement | Barrier

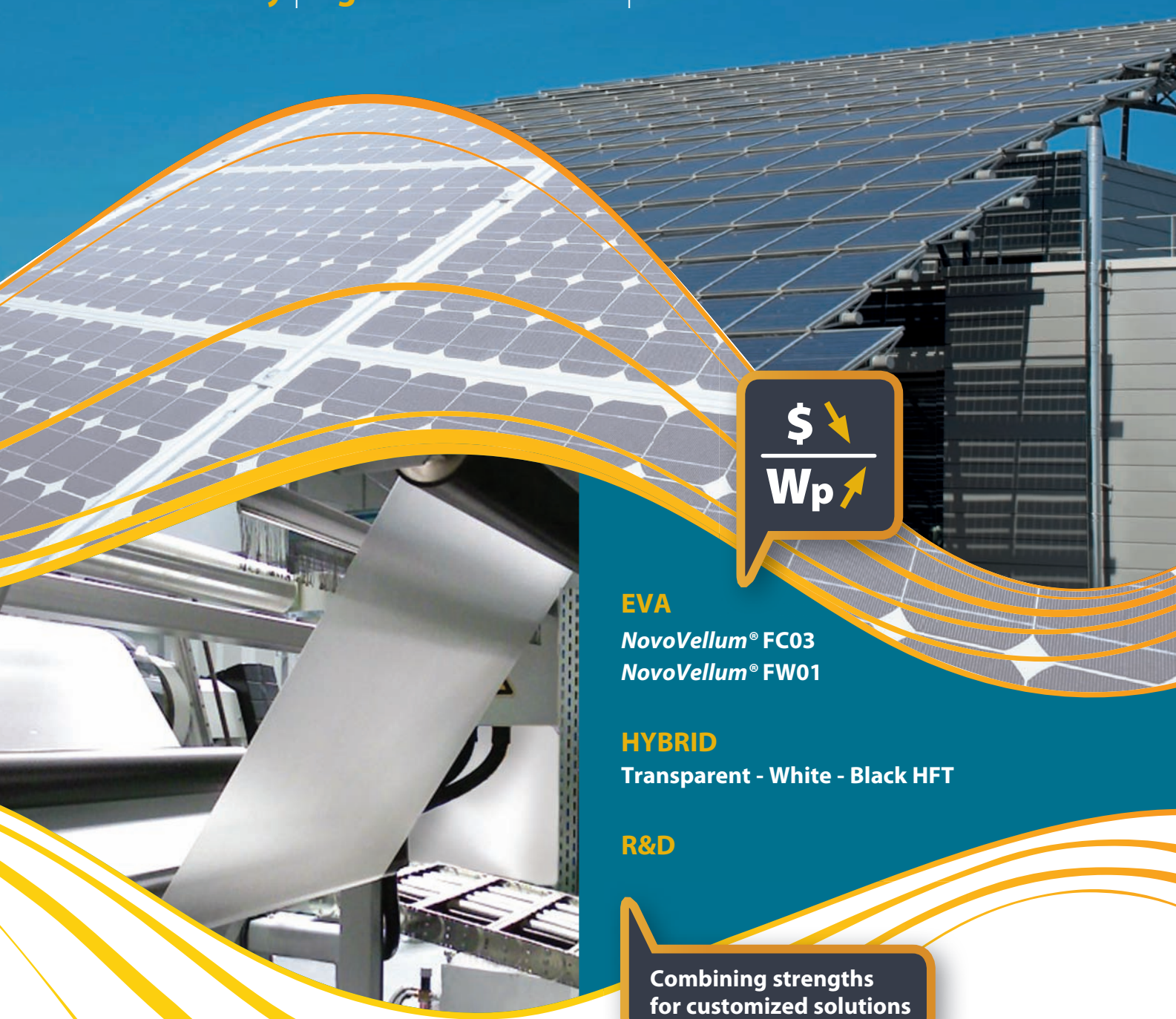

$ ↘ / Wp ↗

EVA

***NovoVellum*® FC03**

***NovoVellum*® FW01**

HYBRID

Transparent - White - Black HFT

R&D

Combining strengths for customized solutions

NovoPolymers

NovoPolymers NV | Rijksweg 8A, B-2870 Puurs | Belgium | T. +32 (0)3 820 14 59 | **www.novopolymers.com**

backbone. Other materials, such as silicone, are stable with respect to UV radiation and therefore do not require UV blockers, which allows the full advantage of the improved UV response of new cells to be realized. However, since these materials are still more expensive than EVA, the benefits of any cell-to-module power gained may be negated by the additional cost of the UV transparent encapsulant.

Newly identified degradation mechanisms

Besides solar-cell-related aspects, newly identified degradation mechanisms of modules demand improved characteristics from the encapsulants. Module manufacturers therefore currently face the challenge of producing solar modules free from potential-induced degradation (PID) [21]. There are many ways to achieve that goal [22,23], one option being to optimize the encapsulant. It is not yet clear what exactly causes the PID sensitivity of the encapsulation material. However, the UV-blocker concentration [24] and the specific bulk resistivity of the encapsulant [25] seem to influence the PID sensitivity of a PV module. A PID-optimized encapsulation material makes the module manufacturer less dependent on the cell manufacturer.

Constraints due to cost-reduction measures

The silicon wafer accounts for 30% of the module cost, so manufacturers try to reduce the thickness of the wafer material to decrease costs [26]. Thinner solar cells raise the requirements for the soldering process and for the mechanical decoupling of the solar cell from the module glass by the encapsulant. EVA materials have a glass transition (i.e. the transition between the brittle, vitreous state and the rubber-like state) above –20°C, and therefore within the temperature range of PV module applications [3]. A lamination material with a low modulus of elasticity and without a glass transition in the range of application may be necessary. From a mechanical point of view, silicone-based materials may therefore be a suitable alternative.

Emerging module concepts – towards module-level processing

As well as the continuous improvements in standard PV modules, the PV research community is currently exploring novel module concepts that offer additional cost-reduction potential. Thin-film/wafer hybrid silicon (HySi) technology [27,28] is a module concept that aims to combine the high efficiency potential of crystalline Si (c-Si) layers with the low cost per area of Si thin-film photovoltaics. This approach is considered to be an innovative option for cost reduction [29].

An integrated series connection for solar cells created from the porous silicon (PSI) layer transfer process [31,32] was demonstrated by Brendel and Auer [30] in 2001. A proof-of-concept mini-module achieved a power conversion efficiency of 10.6%.

Various concepts involving HySi technology are currently under investigation. The integrated-interconnect module (i^2-module) is being developed by imec [33]: the intention is to glue front-side-processed back-contact solar cells to a glass superstrate. This concept can potentially be used for very thin Si foils. A proof-of-concept device with a rear-side processing on a permanently bonded carrier has been demonstrated by imec; this solar cell device yielded a power conversion efficiency of 10.3%.

Another HySi concept is the crystalline silicon interconnected strips (XIS) module from ECN [34]: here, thin cell strips of thickness 3mm are processed into back-contact heterojunction solar cells. ECN currently glues front-side processed wafers to a superstrate; the bonded wafers are then separated into thin strips, which subsequently receive the a-Si:H junction and back-surface field (BSF) formation, metallization and interconnection. The attachment facilitates the handling of many small strips. A proof-of-principle device of 14 series-connected strip cells has demonstrated a V_{oc} of 8.5V [35], but no power conversion efficiency has yet been announced.

A HySi approach in which the rear side of two-side contacted solar cells is processed before bonding to a permanent module substrate has been proposed by ISFH [28]: the silicon wafers are passivated on the rear side and then bonded to an aluminium-coated glass. For this approach, laser pulses fire the aluminium locally through the passivation layer on the rear side of the solar cell to form contacts and provide the mechanical bonds. All subsequent process steps take place at the module level. The

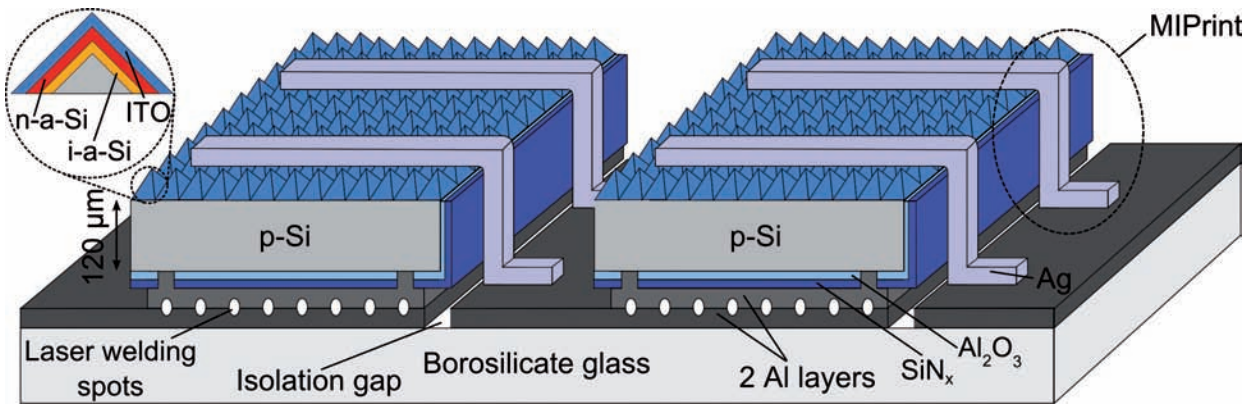

Figure 2. The module interconnection printing (MIPrint) technique for cell interconnection [38]. After the solar cell stripes are bonded to a substrate by laser welding, the screen-printing step is performed at the module level.

bonded wafers are textured and undergo a wet-chemical cleaning; they then receive an i-a-Si:H passivation and an n+ a-Si:H heterojunction. Next, an indium tin oxide is sputtered, and the silver screen printing is carried out. A single solar cell fabricated in this way demonstrates a power conversion efficiency of 19.1% [36,37].

ISFH has also demonstrated the so-called module interconnection printing (MIPrint) method [38]: the module interconnection of a-Si:H heterojunction solar cells of a MIPrint module, shown in Fig. 2, combines cell metallization and interconnection. Fig. 3 illustrates the interconnection of cells using a screen-printed metallization paste. The silver-containing paste is printed over the edge of the solar cells so that the front side of one solar cell connects to the underlying aluminium rear-side contact of the neighbouring solar cell. The designated area conversion efficiency of such a module is 17.0%, and lifetime testing is currently under way.

Many more HySi approaches in addition to those discussed here are conceivable. All HySi technologies apply at least one cell-processing step at the module level, with all the silicon wafers or stripes being attached to the module glass. The more attractive HySi approaches employ the majority of cell-processing steps at the module level. Module-level processing (MLP) imposes additional requirements on the encapsulant, since the encapsulant has to also withstand the processing environment and subsequently outdoor exposure, as well as allowing high cell efficiencies.

Typical MLP steps include, for example, wet-chemical cleaning, texturization, deposition of the passivation and the emitter, and metallization. This means the encapsulant must demonstrate sufficient resistance to the chemicals used during solar cell processing (alkaline texturization, laser-damage etch, wet-chemical cleaning); moreover, it has to be stable during processes that take place at elevated temperatures and low pressures. Potentially suitable encapsulation materials like silicones restrict the process temperature to a range of 200 to 260°C, thus allowing low-temperature processes such as passivation and junction formation by a-Si:H deposition. Apart from these process-related requirements, such encapsulants have to feature the same properties for sufficient long-term stability as those offered by the materials used for standard encapsulation. When used for sunny-side encapsulation, as suggested for some HySi approaches, transparency in the solar-cell-relevant spectrum is also essential.

Encapsulants for module-level processing

Standard encapsulant sheets, such as EVA, are not compatible with module-level processing owing to their thermal instability. Furthermore, thermoplastic materials are not suitable for this specific application because of their remelting characteristics at temperatures below those used in cell processing. Materials such as liquid thermosetting silicones offer possibilities beyond the standard encapsulation of wafer-based solar cells.

Addition-curing two-part silicones demonstrate sufficient stability during UV exposure and humidity–freeze cycling, as well as during chemical and thermal treatment [39]. Consequently, addition-curing two-part silicones are promising candidates for use in module-level processing. The cross-linking of this type of silicone occurs by catalysis through a Pt metal complex and is accelerated by heat [40]. As a result of the additional cross-linking after the mixing of the two components, no by-products are released.

"Addition-curing two-part silicones are promising candidates for use in module-level processing."

The most crucial process step of MLP in the presence of silicones is the passivation and junction formation by a-Si:H deposition. The impact of silicones on the passivation layer has been reported in the literature [33]. The annealing of silicone-bonded samples at temperatures in the range 235 to 300°C – analogous to an a-Si:H deposition and beyond – yields a sufficient thermal stability [39]. However, silicones may be affected by a combination of the effects of temperature, vacuum and plasma during the plasma-enhanced chemical vapour deposition (PECVD) of passivation layers.

To verify the quality of the passivation, two lifetime measurement methods are performed on Si samples that are glued to glass with silicones.

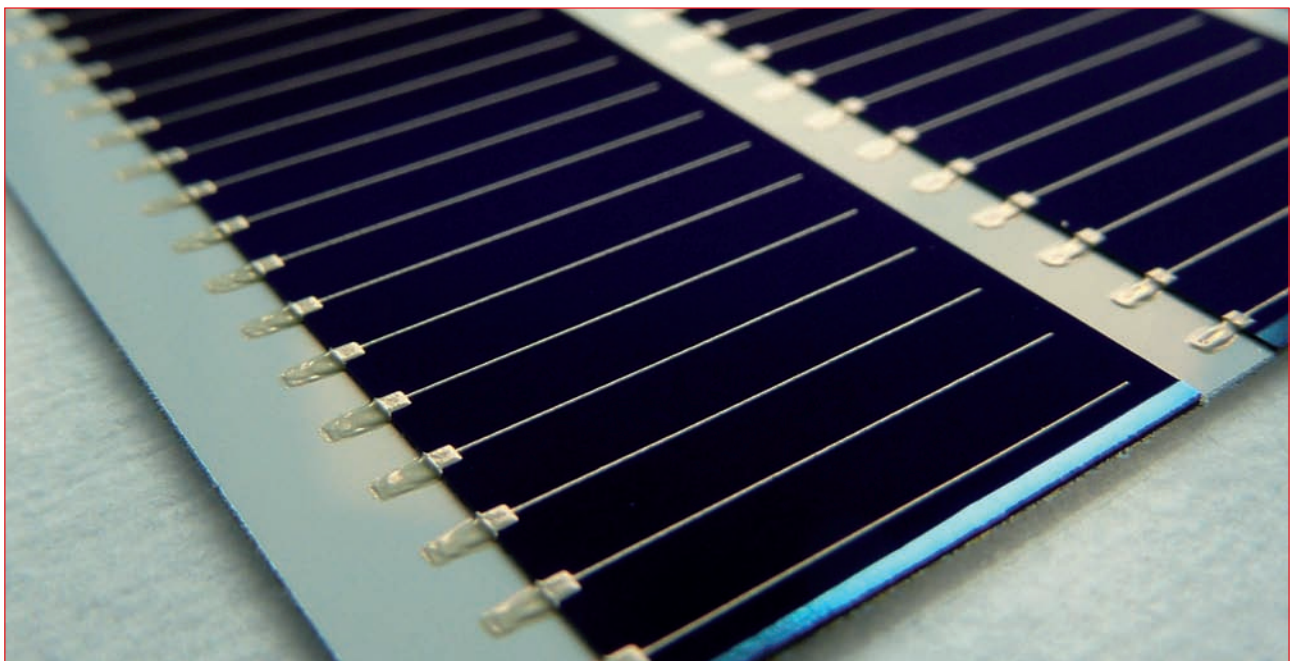

Figure 3. The screen-printed interconnection of cells in the MIPrint module prior to lamination [38].

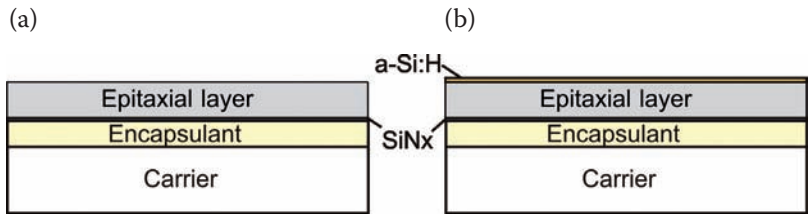

Figure 4. Cross section of a one-side passivated epitaxial layer glued to a carrier: (a) prior to the a-Si:H deposition; (b) after deposition.

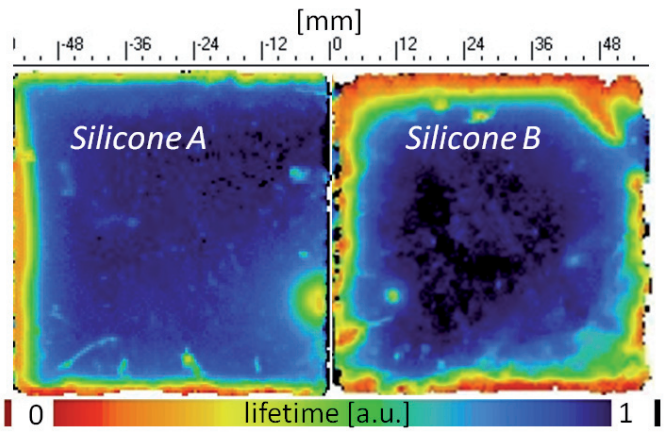

Figure 5. Thin Si layers that have been front-side passivated by SiN_x when still attached to the substrate wafer. After bonding with two-part silicones and detachment, these layers were rear-side passivated by a-Si:H.

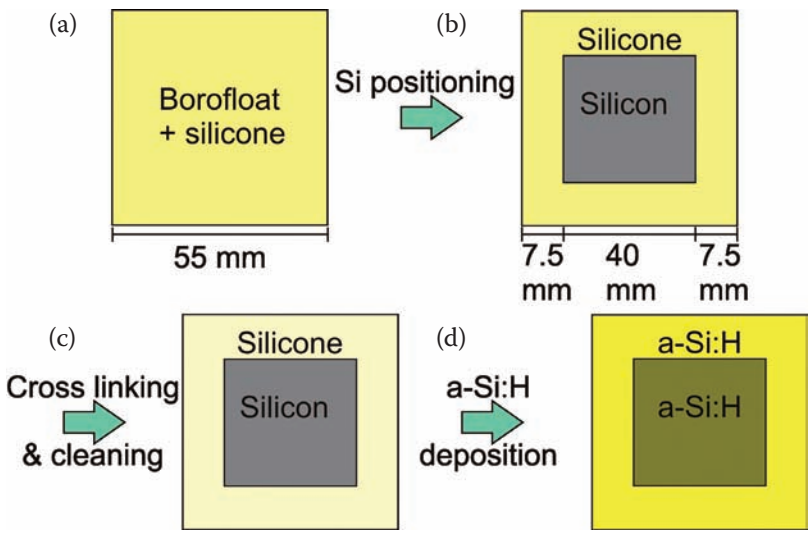

Figure 6. Process flow of the passivation process in the presence of uncovered silicone – schematical top view: (a) depositing of silicone to completely cover a Borofloat glass; (b) gluing of a one-side-passivated FZ Si sample onto the silicone, passivated side downwards; (c) cross-linking of the silicone accelerated by heat, and wet-chemical cleaning of the sample stack; (d) a-Si:H deposition.

For the first method, spatially resolved lifetime mappings are carried out using the microwave-detected photoconductivity decay (MWPCD) technique (WT-2000 by Semilab) [41,42]. The lifetime mappings show the quality of the passivation layer to a spatial resolution of 500µm. Local influences in the vicinity of the glue can be detected in a degradation of the lifetime close to the silicone.

For the second method, lifetime measurements using the quasi-steady-state photoconductance (QSSPC) method are performed [43]. In contrast to the MWPCD technique, this method does not provide a spatially resolved mapping, but allows the lifetime to be determined as a function of minority-carrier density. The surface recombination velocity (SRV) of the a-Si:H layers deposited in the presence of two-part silicones is calculated from the QSSPC measurements. The SRV quantifies the passivation quality and thus the potential outgassing effect of these silicones (which were not specifically developed for such processes).

To demonstrate the applicability of the gluing procedure to ultrathin silicon wafers, 30µm-thick silicon layers from a layer transfer with porous Si were used. One side was passivated with a silicon nitride layer; this side was then glued to a Borofloat glass using silicone. Fig. 4 shows the sample stack. After surface conditioning and cleaning, the thin Si layers received, on the rear side, an a-Si:H layer at 250°C for passivation.

Fig. 5 shows the MWPCD mapping of two epitaxial layers glued to Borofloat glasses using two different two-part silicones. The passivation quality is reduced, mainly near the edges of the samples, where the distance to the encapsulation material is small. The detrimental influence is significantly lower in the sample using silicone A (left) than in the sample using silicone B (right). With silicone A the effective lifetime is more homogeneous, and there is a decrease in effective lifetime at two of the four edges. The affected area is, however, limited to the region within 3mm of the edge.

To determine the SRV the experiments were carried out with floatzone (FZ) Si wafers. The influence of uncovered silicones on the passivation quality was investigated. Fig. 6 shows the process flow for the passivation process in the presence of uncovered silicone. First, silicone is deposited on Borofloat glass of dimensions 55mm × 55mm (Fig. 6(a)). Next, a one-side SiN_x-passivated FZ Si sample of dimensions 40mm × 40mm is glued to the centre of the Borofloat

glass (Fig. 6(b)). Cross-linking then occurs and the stack is wet-chemically cleaned (Fig. 6(c)). Finally, the FZ Si and the surrounding silicone receive an a-Si:H layer (Fig. 6(d)).

It was determined that the SRV is reduced by one to two orders of magnitude if uncovered silicones are present during the a-Si:H passivation. This indicates that the reduction of the passivation quality is caused by volatile components that leak from the exposed silicones when subjected to the effects of heat, vacuum and plasma. These components may contaminate the Si surface or interact with the precursors of the a-Si:H deposition process.

An additional pre-outgassing (i.e. the heating of the glued FZ Si wafer for two minutes at the process temperature and pressure of the subsequent a-Si:H deposition) was found to reduce the detrimental effects on the passivation layer. The best passivation was determined for silicone A with S_{rear} = (2.5±1.5)cm/s measured by the QSSPC method at the minority-carrier density $\Delta n = 10^{15}cm^{-3}$. Hence, this silicone allows an SRV of the a-Si:H layer as low as that for non-glued samples. Addition-curing two-part silicones are therefore promising candidates for module-level processing.

"An additional pre-outgassing was found to reduce the detrimental effects on the passivation layer."

Conclusion

The commonly used encapsulant EVA is a well-established low-cost material for standard applications in the field of c-Si PV. Thermoplastic materials, however, offer advantages such as a faster processing time and a higher stability and transparency. The balance between the cost structure of the new materials and the higher power output or the superior resistance to PID offered by their use will determine their success.

Recent novel hybrid silicon PV module concepts seek to combine the advantages of thin-film technologies with those of wafer technologies; however, additional requirements that are fundamentally different from those used for standard PV modules are imposed on encapsulants. One such requirement is that the encapsulant must be compatible with module-level processing. In particular, the a-Si:H deposition that is necessary for passivation or hetero-emitter formation is very sensitive to the presence of unsuitable encapsulants. It was shown that suitable silicone-based encapsulants enable the use of such module-level processes. Future work on even slimmer module-level processing sequences will show if cost-competitiveness with EVA and conventional module concepts can be achieved. There are, however, no technological obstacles to realizing the potential of the novel module concepts.

Acknowledgements

The authors thank H. Fischer for her valuable help with sample preparation, as well as R. Winter and A. Knorr for their help with processing. We are grateful for the financial support from REC ASA.

References

[1] McIntosh, K.R. et al. 2009, "An optical comparison of silicone and EVA encapsulants for conventional silicon PV modules: A ray-tracing study", *Proc. 34th IEEE PVSC*, Philadelphia, Pennsylvania, USA, pp. 544–549.

[2] Morlier, A. et al. 2013, "Influence of the curing state of ethylene-vinyl acetate on photovoltaic modules aging", *Proc. 28th EU PVSEC*, Paris, France.

[3] Kempe, M.D. et al. 2007, "Acetic acid production and glass transition concerns with ethylene-vinyl acetate used in photovoltaic devices", *Solar Energy Mater. & Solar Cells*, Vol. 91, No. 4, pp. 315–329.

[4] Kajari-Schröder, S. et al. 2010, "Modelling the curing dynamics of ethylene-vinyl acetate", *Proc. 25th EU PVSEC*, Valencia, Spain, pp. 4039–4043.

[5] Schulze, K. et al. 2012, "Untersuchung von Alterungseffekten bei monokristallinen PV-Modulen mit mehr als 15 Betriebsjahren durch Elektrolumineszenz- und Leistungsmessung", *Proc. 28. OTTI Symp. Photovolt. Solarenergie*, Staffelstein, Germany, pp. 194–195.

[6] Green, M.A. 2005, "Silicon photovoltaic modules: A brief history of the first 50 years", *Prog. Photovolt.: Res. Appl.*, Vol. 13, No. 5, pp. 447–455.

[7] Dow Corning Corporation 1978, "Develop silicone encapsulation systems for terrestrial silicon solar arrays", Doe/JPL954995-2.

[8] Henderson, A.H. 1993, "Ethylene-vinyl acetate (EVA) copolymers: A general review", *IEEE Electr. Insul. Mag.*, Vol. 1, No. 9, pp. 30–38.

[9] Czanderna, A.W. et al. 1996, "Encapsulation of PV modules using ethylene vinyl acetate copolymer as a pottant: A critical review", *Solar Energy Mater. & Solar Cells*, Vol. 43, No. 2, pp. 101–181.

[10] Kojima, T. et al. 2005, "Ultraviolet-ray irradiation and degradation evaluation of the sealing agent EVA film for solar cells under high temperature and humidity", *Solar Energy Mater. & Solar Cells*, Vol. 85, No. 1, pp. 63–72.

[11] Pern, F.J. 1996, "Factors that affect the EVA encapsulant discoloration rate upon accelerated exposure", *Solar Energy Mater. & Solar Cells*, Vol. 41/42, pp. 587–615.

[12] McIntosh, K.R. et al. 2011, "The effect of damp-heat and UV aging tests on the optical properties of silicone and EVA encapsulants", *Prog. Photovolt.: Res. Appl.*, Vol. 19, No. 3, pp. 294–300.

[13] Powell, N. et al. 2010, "Improved spectral response of silicone encapsulated photovoltaic modules", *Proc. 35th IEEE PVSC*, Honolulu, Hawaii, USA, pp. 2791–2794.

[14] Kempe, M.D. et al. 2009, "Accelerated stress testing of hydrocarbon-based encapsulants for medium-concentration CPV applications", *Proc. 34th IEEE PVSC*, Philadelphia, Pennsylvania, USA, pp. 1826–1831.

[15] Weber, U. et al. 2012, "Acetic acid production, migration and corrosion effects in ethylene-vinyl-acetate- (EVA-) based PV modules", *Proc. 27th EU PVSEC*, Frankfurt, Germany, pp. 2992–2995.

[16] Peike, C. et al. 2013, "Origin of damp-heat induced cell degradation", *Solar Energy Mater. & Solar Cells*, Vol. 116, pp. 49–54.

[17] Miller, D.C. et al. 2013, "Durability of polymeric encapsulation materials for concentrating photovoltaic systems", *Prog. Photovolt.: Res. Appl.*, Vol. 21, No. 4, pp. 631–651.

[18] Allen, N.S. et al. 2001, "Aspects of the thermal oxidation, yellowing and stabilization of ethylene vinyl acetate copolymer", *Polym. Degrad. Stabil.*, Vol. 71, pp. 1–14.

[19] Hahn, G. 2012, "Status of selective emitter technology", Proc. 25th EU PVSEC, Valencia, Spain, pp. 1091–1096.

[20] Schmid, C. et al. 2012, "Impact of high light transmission EVA-based encapsulant on the performance of PV modules", *Proc. 27th EU PVSEC*, Frankfurt, Germany, pp. 3494–3498.

[21] Naumann, V. et al. 2012, "Micro structural root cause analysis of potential induced degradation in

c-Si solar cells", *Energy Procedia*, Vol. 27, pp. 1–6.
[22] Koch, S. et al. 2012, "Potential induced degradation effects on crystalline silicon cells with various antireflective coatings", *Proc. 27th EU PVSEC*, Frankfurt, Germany, pp. 1985–1990.
[23] Mehlich, H. et al. 2012, "A new method for high resistance against potential induced degradation", *Proc. 27th EU PVSEC*, Frankfurt, Germany, pp. 3411–3413.
[24] Koch, S. et al. 2012, "Encapsulation influence on the potential induced degradation of crystalline silicon cells with selective emitter structures", *Proc. 27th EU PVSEC*, Frankfurt, Germany, pp. 1991–1995.
[25] Lechner, P. et al. 2012, "Estimation of time to PID-failure by characterisation of module leakage currents", *Proc. 27th EU PVSEC*, Frankfurt, Germany, pp. 3152–3156.
[26] SEMI PV Group 2013, "International technology roadmap for photovoltaic (ITRPV): Results 2012" [http://www.itrpv.net/Reports/Downloads/2013/].
[27] Cárabe, J. & Gandia, J.J. 2004, "Thin-film-silicon solar cells", *Opto-Electron. Rev.*, Vol. 12, No. 1, pp. 1–6.
[28] Brendel, R. et al. 2011, "High-efficiency cells from layer transfer: A first step toward thin-film/wafer hybrid silicon technologies", *IEEE J. Photovolt.*, Vol. 1, No. 1, pp. 9–15.
[29] Powell, D.M. et al. 2012, "Crystalline silicon photovoltaics: A cost analysis framework for determining technology pathways to reach baseload electricity costs", *Energy Environ. Sci.*, Vol. 5, No. 3, pp. 5874–5883.
[30] Brendel, R. & Auer, R. 2001, "Photovoltaic mini-modules from layer transfer by the porous silicon process", *Prog. Photovolt.: Res. Appl.*, Vol. 9, No. 6, pp. 439–443.
[31] Brendel, R. 1997, "A novel process for ultrathin monocrystalline silicon solar cells on glass", *Proc. 14th EU PVSEC*, Barcelona, Spain, pp. 1354–1357.
[32] Tayanaka, H. et al. 1998, "Thin-film crystalline silicon solar cells obtained by separation of a porous silicon sacrificial layer", *Proc. 2nd World Conf. PV Solar Energy Conv.*, Vienna, Austria, pp. 1272–1277.
[33] Govaerts, J. et al. 2013, "Development of a-Si:H/c-Si heterojunctions for the i²-module concept: Low-temperature passivation and emitter formation on wafers bonded to glass", *Solar Energy Mater. & Solar Cells*, Vol. 113, pp. 52–60.
[34] van Roosmalen, J. et al. 2012, "Crystalline silicon interconnected strips (XIS): Introduction to a new, integrated device and module concept", *Energy Procedia*, Vol. 27, pp. 604–609.
[35] Mewe, A. et al. 2013, "XIS: A low-current, high-voltage back-junction back-contact photovoltaic device", *Proc. 39th IEEE PVSC*, Tampa, Florida, USA.
[36] Brendel, R. et al. 2013, "Recent progress and options for future crystalline silicon solar cells", *Proc. 28th EU PVSEC*, Paris, France.
[37] Petermann, J.H. et al. 2013 [in preparation].
[38] Petermann, J. H. et al. 2013, "Module interconnection of both sides-contacted silicon solar cells by screen-printing", *Proc. 39th IEEE PVSC*, Tampa, Florida, USA.
[39] Steckenreiter, V. et al. 2013, "Qualification of encapsulation materials for module-level-processing", *Solar Energy Mater. & Solar Cells* [in press], DOI: 10.1016/j.solmat.2013.06.012.
[40] Kempe, M.D. 2010, "Evaluation of encapsulant materials for PV applications", *Photovoltaics International*, 9th edn, pp. 170–176.
[41] Kunst, M. & Beck, G. 1986, "The study of charge carrier kinetics in semiconductors by microwave conductivity measurements", *J. Appl. Phys.*, Vol. 60, No. 10, pp. 3558–3556.
[42] Kunst, M. & Beck, G. 1988, "The study of charge carrier kinetics in semiconductors by microwave conductivity measurements. II.", *J. Appl. Phys.*, Vol. 63, No. 4, pp. 1093–1098.
[43] Sinton, R.A. & Cuevas, A. 1996, "Contactless determination of current–voltage characteristics and minority-carrier lifetimes in semiconductors by quasi-steady-state photoconductance data", *Appl. Phys. Lett.*, Vol. 69, No. 17, pp. 2510–2512.

About the Authors

Verena Steckenreiter received her diploma degree in environmental protection from the University of Applied Sciences Bingen, Germany, in 2007. In 2008 she joined the Si thin-film technology group at the Institute for Solar Energy Research Hamelin (ISFH), where she has headed projects on alternative module-interconnection concepts since 2011. Her current areas of focus are module-level processing and kerf-less technologies.

Arnaud Morlier studied chemistry and received his Ph.D. in materials science from the Joseph Fourier University of Grenoble in France, specializing in thin-film polymer solar cell encapsulation. Since 2011 he has been working in the module and interconnection technology group at ISFH, focusing on material degradation in modules.

Marc Köntges received his Ph.D. in physics from the University of Oldenburg, Germany, in 2002 for his research in thin-film solar cells. From 2002 to 2005 he led the thin-film technology group at ISFH, and then became the head of the module and interconnection technology group. He is currently working on the development of characterization and production methods for PV modules.

Sarah Kajari-Schröder received her diploma degree in physics in 2004 and her Ph.D. in 2009 from the University of Ulm. She then joined the PV module group at ISFH, where the direction of her research was crack formation in solar cells, and the mechanical stability and reliability of PV modules. Since 2011 she has headed the silicon thin-film group at ISFH, focusing on the fabrication, handling and interconnection of ultrathin crystalline silicon wafers, cells and modules.

Rolf Brendel received his physics degree in 1987 from the University of Heidelberg and his Ph.D. in material science from the University of Erlangen. He worked on Si solar cells at the Max Planck Institute for Solid State Research and at the Bavarian Centre for Applied Energy Research. In 2004 he became a full professor of physics at the Leibniz University of Hanover and the director of the Institute for Solar Energy Research Hamelin (ISFH).

Enquiries

Verena Steckenreiter
ISFH
Am Ohrberg 1
D-31860 Emmerthal
Germany

Tel: +49 (0) 5151 999 325
Email: v.steckenreiter@isfh.de
Website: www.isfh.de

Don't let your advertising dollars go down the drain...

Be wise, advertise with the best.

Choose from a range of digital or print advertising solutions and gain brand association and relevant ROI from the world's most read solar news and information resources in English and Chinese language.

SOLAR MEDIA

Brands of Solar Media:

Photovoltaics International | PVTECH | PVTECH | PVTECH PRO | Solar Business Focus | DESIGN-BUILD SOLAR

For advertising opportunities please contact: Solar Media Ltd, info@solarmedia.co.uk,
Tel +44 (0) 207 871 0122, www.solarmedia.co.uk

Assessment of the cross-linking degree of EVA PV encapsulants

Manuel Hidalgo & **Dominique Thil**, Arkema, Sollia Laboratory at INES-LMPV, Le Bourget du Lac, & **Chistophe Dugué**, Photowatt, Bourgoin-Jallieu, France

ABSTRACT
This paper presents a comparison of different characterization methods used for determining the relative degree of cross-linking of samples of PV-type EVA films, obtained under three different process conditions in a vacuum PV laminator. The methods investigated are gel content measurements, rheological measurements and differential scanning calorimetry (DSC). For the latter, two distinct procedures are employed – the residual enthalpy method and the melt/freeze method.

Introduction

Hidalgo et al. [1] introduced a new characterization method for assessing the cross-linking degree of EVA encapsulant films used in the PV industry. That work presented the basis of the so-called Sollia method, which employs differential scanning calorimetry (DSC) and, in particular, the crystallization transition of EVA during a DSC melting and freezing type of experiment. In the last two years a great deal of work has been done on optimizing the test conditions (the test duration is now only 20 minutes per sample) and gathering experimental data for a significant number of industrial EVA encapsulant films. As a result, the Sollia method has now joined with another DSC method, proposed by Xia et al. [2] and based upon a completely different thermal transition (heat release during cross-linking), in an IEC international standard proposal for the characterization of the cross-linking degree of EVA encapsulant films [3]. The two DSC methods, referred to now as the melt/freeze (M/F) method (based upon the work of Hidalgo et al.) and the residual enthalpy (RE) method (based upon the work of Xia et al.), are complementary and offer the possibility of double-checking the cross-linking degree of a given sample.

> "The two DSC methods are complementary and offer the possibility of double-checking the cross-linking degree of a given sample."

This study uses both of these DSC methods, as described in the standard proposal, to determine the relative degree of cross-linking of a commonly used PV encapsulant film, under three different process conditions that might be used for the industrial lamination of PV modules. In order to check the consistency of the information thus obtained, the same samples were characterized using two different reference methods: 1) the well-known gel content method, widely used for the assessment of the cross-linking degree of EVA polymers; and 2) rheological measurements, carried out in the way initially described in Hidalgo et al. [1].

Experimental conditions: materials and methods

The PV encapsulant film was one that had been stored for several months, and the purpose of using three different process conditions was to allow the set point of the vacuum laminator's temperature to be varied, as would be done in an industrial facility when attempting to optimize this temperature parameter for a given EVA film.

The EVA film was provided by STR (reference Photocap 15420P/UF) and was received in September 2012, with a 6-month lifetime guarantee. The lamination of samples for cross-linking degree characterization was carried out in June 2013, meaning that the film was already regarded as 'old', although the storage conditions (cool chamber at 10°C, aluminized sealed packaging) were such that the use of this film for comparative purposes (testing of three different lamination temperatures) was considered acceptable.

The lamination of the EVA encapsulant films was carried out by stacking, downside up, a 15cm × 15cm, 3.2mm-thick glass plate, a thin Teflon non-adherent sheet to prevent the EVA/glass adhesion, two EVA sheets to be cross-linked, and one more Teflon non-adherent sheet. In this stack the two EVA sheets to be cross-linked were placed in the position that they would normally occupy in the lamination stack of a typical glass/EVA/cells/EVA/backsheet PV module. The stacks were laminated at three different set-point temperatures of 145, 150 and 160°C in an industrial-type 3S laminator (model S1815E), following a standard lamination procedure including degassing and cross-linking stages. The degassing step was set for a duration of 4 minutes, and the actual lamination time for a duration of 8 minutes, under approximately 900mbar of differential pressure.

The DSC measurements were carried out on the same samples at two different places (different operators, different equipment). The calorimeter used at the first location was a TA INSTRUMENTS DSC model Q 10, equipped with an RCS 90 cooling device, and at the other, a Netzsch DSC model 200F3. The samples weighed between 5 and 9mg, and the measurements were conducted under a continuous nitrogen flow of 50ml/min. No sample conditioning was applied before the DSC measurements. To generate the necessary data for the analysis with both the RE and the M/F methods, the DSC programme used was as follows:

1. Heat to 100°C at 10°C/min, which melts the sample and erases thermal history.
2. Cool to –20°C at 10°C/min, which 'freezes' the sample, making it crystallize. The crystallization peak is then analyzed according to the M/F method.
3. Heat to 225°C at 10°C/min, which makes the residual peroxide of the sample react. The enthalpy peak between 100 and 200°C, or between its two onset temperatures, is then analyzed according to the RE method.

4. Cool to –20°C at 10°C/min, which is only necessary if no highly cross-linked sample (near 100% gel content) is available. This cooling step will generate a second crystallization peak after all the residual peroxide of the sample has reacted. The second peak corresponds to a highly cross-linked sample which has continued to cross-link in the calorimeter during step 3.

5. Return to room temperature, which allows the sample to be unloaded from the calorimeter.

The rheological measurements were carried out using an Anton Paar Physica MCR 302 rheometer in a parallel-plates configuration and in the shear oscillatory mode. As described in Hidalgo et al. [1], carrying out a frequency sweep at 100°C has been found to be a good compromise for EVA encapsulants, whether uncross-linked or cross-linked. The elastic, G', and viscous, G'', components of the complex shear modulus were therefore measured at 100°C for a frequency sweep between 0.1 and 100Hz. The method described by Hidalgo et al., which consists of using a value of tan $\delta = G''/G'$ at 1Hz to characterize the degree of cross-linking, was applied herein.

The gel content measurements were carried out through solvent extraction in toluene at a soaking temperature of 60°C for at least 18 hours. Samples of size 1g were weighed and immersed in 100ml beakers with toluene and 0.1g of butylated hydroxytoluene (BHT) as an antioxidant. The beakers were covered with aluminium foils and kept in the oven at 60±5°C for at least 18 hours. The samples were subsequently paper filtered, and the residual material was dried at 105±5°C for four hours. Once cooled down to room temperature, the dried samples were weighed again, and the gel content was calculated using Equation 1.

Results and discussion

DSC analysis

Fig. 1 shows a typical DSC plot obtained using the five-step programme mentioned above. After steps 1 and 2, a crystallization peak corresponding to the actual state of the sample is obtained; from this peak, the three parameters of the M/F method (see below) may be determined. After step 3, the exothermic peak corresponding to the decomposition of residual peroxide, and further cross-linking of the sample in the calorimeter, is obtained; the surface under the curve (enthalpy) is used in applying the RE method. After step 4, a new crystallization peak for the sample which has been cross-linked further in the calorimeter is obtained. In the case where no highly cross-linked samples are available, the peaks obtained after step 4 may be used to determine the M/F parameters of highly cross-linked samples, as will be explained below.

Melt/freeze method

Fig. 2 shows the crystallization peaks corresponding to the three set-point temperatures for which every parameter of the M/F method has been calculated or graphically determined. The three M/F parameters are: 1) the maximum crystallization temperature, or peak

$$\%\ \text{gel content} = \frac{\text{Residual EVA weight after 18 hours soaking at 60°C, and subsequent drying}}{\text{Initial EVA sample weight}} \times 100$$

Equation 1.

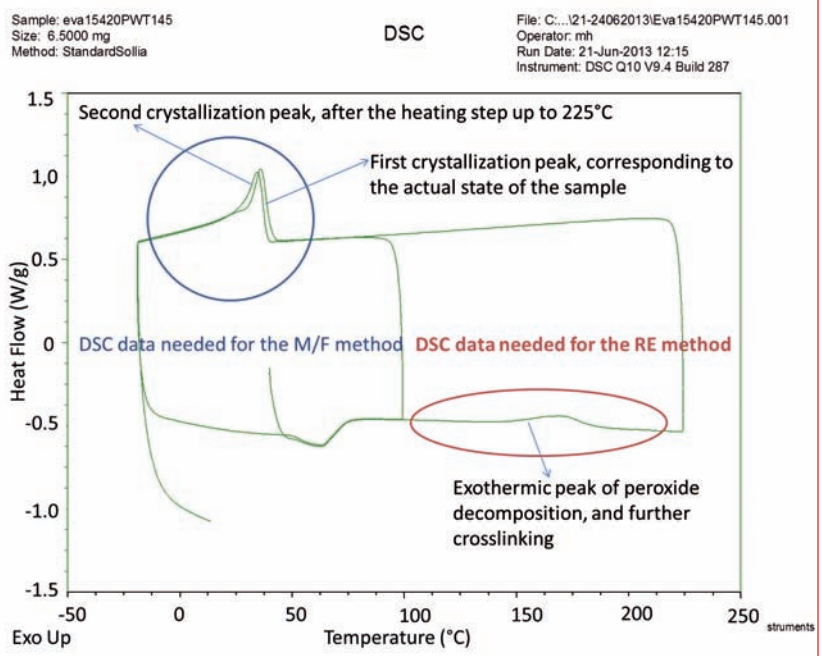

Figure 1. Specific heat flow as a function of temperature (plot produced by the five-step DSC programme).

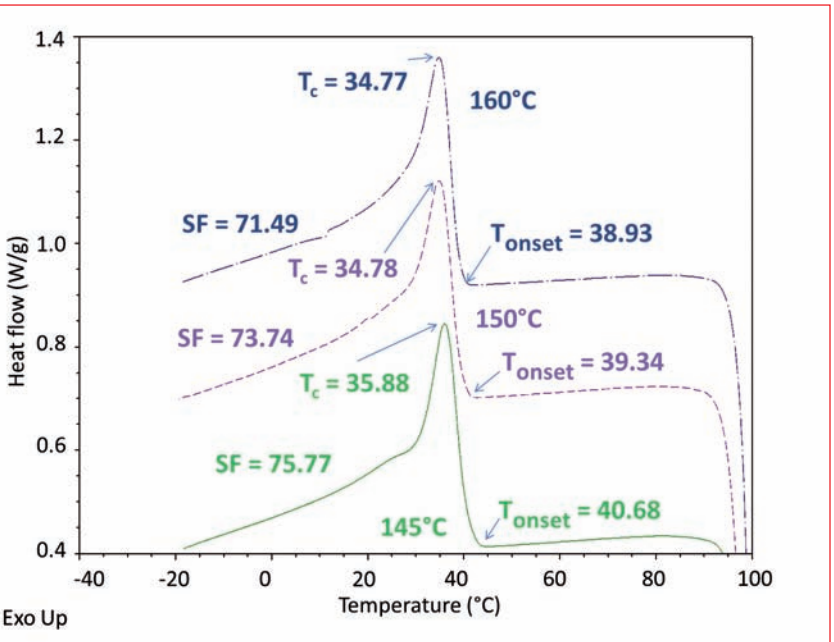

Figure 2. Crystallization peaks for each of the three samples laminated at set-point temperatures of 145, 150 and 160°C. (An offset has been applied to the heat flow curves in order to display the three peaks on the same graph.)

temperature (T_c); 2) the temperature of the onset of crystallization during cooling (T_{onset}); and 3) the shape factor (SF), which takes into account the concavity of the lower temperature part of the crystallization peak, i.e. between T_c and T_c – 20°C. It has been previously determined that the values of these three parameters decrease with the cross-linking level of EVA (see Hidalgo et al. [1] and Miller et al. [3] for details), and thus they constitute three different indicators of the conversion of the cross-linking reaction. The M/F method uses the values of these parameters for a given sample and compares them with those of an uncross-linked sample (giving the 0 bound of a percentage scale), as well as with those of a very highly cross-linked sample (giving the 100 bound of the percentage scale). When no highly cross-linked sample is available, the parameters from peaks obtained in step 4 of the above-mentioned DSC programme can be used. In this case, if several samples have been analyzed, different sets of parameters for step 4 peaks will be available, and the lowest values of these should be used to set the 100% bound of the scale.

Although a simple comparison of the raw values of the three M/F parameters for different samples already allows those that are more cross-linked than others to be distinguished, the M/F method features a more quantitative approach through the calculation of percentage cross-link (%XL) estimates for each parameter (T_c, T_{onset} and SF) by applying the formulas in Equations 2–4:

$$\%XL_{T_c} = \frac{T_c^{uXL} - T_c^{sample}}{T_c^{uXL} - T_c^{min}} \times 100 \quad (2)$$

$$\%XL_{T_{onset}} = \frac{T_{onset}^{uXL} - T_{onset}^{sample}}{T_{onset}^{uXL} - T_{onset}^{min}} \times 100 \quad (3)$$

$$\%XL_{SF} = \frac{SF^{uXL} - SF^{sample}}{SF^{uXL} - SF^{min}} \times 100 \quad (4)$$

where the superscripts 'uXL', 'sample' and 'min' correspond to the values obtained from the crystallization peaks of the uncross-linked sample, the actual sample under investigation and a highly cross-linked sample respectively.

In order to characterize, according to the M/F method, a given sample using a single estimate of its cross-linking degree, an arithmetic average of the three estimates given by Equations 2–4 has been empirically determined to be a good global estimate for a wide variety of commercial EVA encapsulants, and one which correlates well with the results obtained using other methods. Thus, the degree of cross-linking as determined by the M/F method may be obtained using Equation 5.

Residual enthalpy method

Fig. 3 shows the residual enthalpy peaks for the samples at the three set-point temperatures. The RE method, initially described in Xia et al. [2], uses the area under the enthalpy peak which appears in the temperature range 100–225°C. All DSC calorimeters are supplied with the appropriate software for determining the integral of heat flow vs. temperature curves, which results in the desired areas under the residual enthalpy peaks.

In Miller et al. [3] it is recommended, whenever possible, to integrate enthalpy peak curves in the temperature range of 100–200°C. At Arkema and Photowatt, recent findings indicate that for some commercial EVA encapsulant films, the upper integration limit must be slightly shifted to temperatures higher than 200°C. This is the reason why the authors consider it to be more generally applicable to integrate the residual

$$\%XL_{average}^{M/F} = \frac{(\%XL_{T_c} + \%XL_{T_{onset}} + \%XL_{SF})}{3}$$

Equation 5.

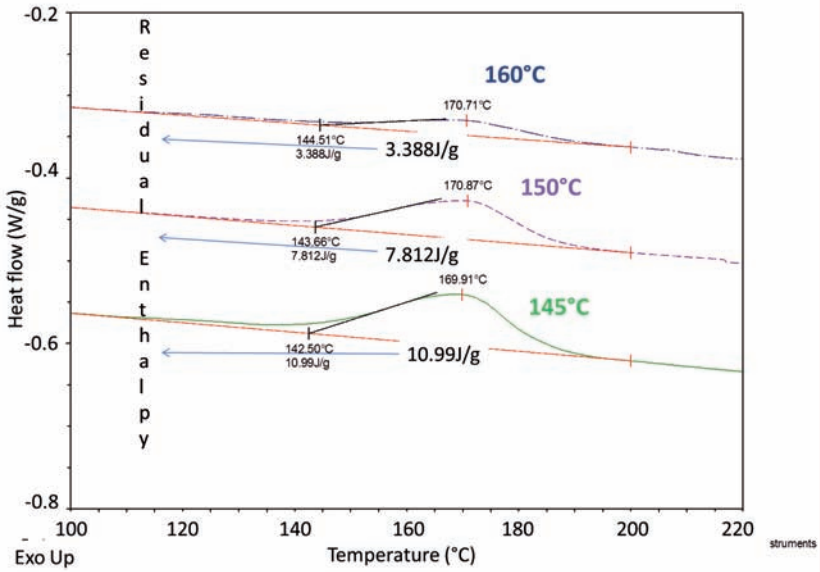

Figure 3. Residual enthalpy peaks for each of the three samples laminated at set-point temperatures of 145, 150 and 160°C. (An offset has been applied to the heat flow curves in order to display the three peaks on the same graph.)

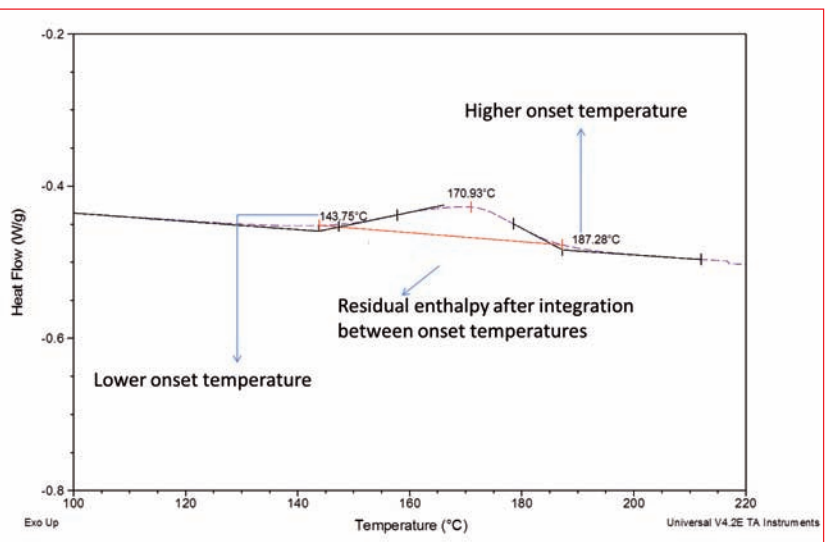

Figure 4. Determination of the integration limits for a residual enthalpy peak, from the peak's lower and higher onset temperatures.

enthalpy peak between its onset temperatures (lower and upper onsets), which can also be easily determined by commercial DSC software packages. Fig. 4 shows an example of integration between onset temperatures, instead of between the fixed 100–200°C limits as in Fig. 3. Whether the fixed 100–200°C limits, the onset temperatures limits, or any other temperature limits are used for integrating the enthalpy peaks, the important thing is that the same set of limits are used when comparing different samples.

"At Arkema and Photowatt, recent findings indicate that for some commercial EVA encapsulant films, the upper integration limit must be slightly shifted to temperatures higher than 200°C."

As in the case of the M/F method, the RE method provides a quantitative estimate of the degree of cross-linking by comparing the residual enthalpy of the sample under study with that for a sample of the same EVA in its uncross-linked (as-received) state. The degree of cross-linking as determined by the RE method may be obtained using Equation 6:

$$\%XL^{RE} = \frac{H_1 - H_2}{H_1 - 0} \times 100 \qquad (6)$$

where H_1 corresponds to the residual enthalpy of an uncross-linked sample and H_2 corresponds to the residual enthalpy for the actual sample under analysis.

As with the M/F method, the residual enthalpy is a distinctive parameter of the DSC plot of a sample (obtained through programme step 3 of the above-mentioned procedure), which decreases with the increasing degree of cross-linking of EVA. The form of Equations 2–4 is very much like that of Equation 6, which includes the assumption that for the upper bound (100%) of the %XL estimate from the RE method, the residual enthalpy is zero.

Rheological measurements

Rheology of molten or soft solid samples may be carried out in the shear mode with most conventional rotational rheometers. Among the many types of experiments that can be useful in determining the mechanical state of samples, and thus their cross-linking level, it was decided to carry out dynamic (oscillatory) experiments in the form of frequency sweeps at a constant temperature. The fixed temperature was selected so that the samples were beyond the end of the fusion of the crystalline part of EVA, while still at a sufficiently low temperature to avoid, or at least reduce to a minimum, the cross-linking of samples during the experiment.

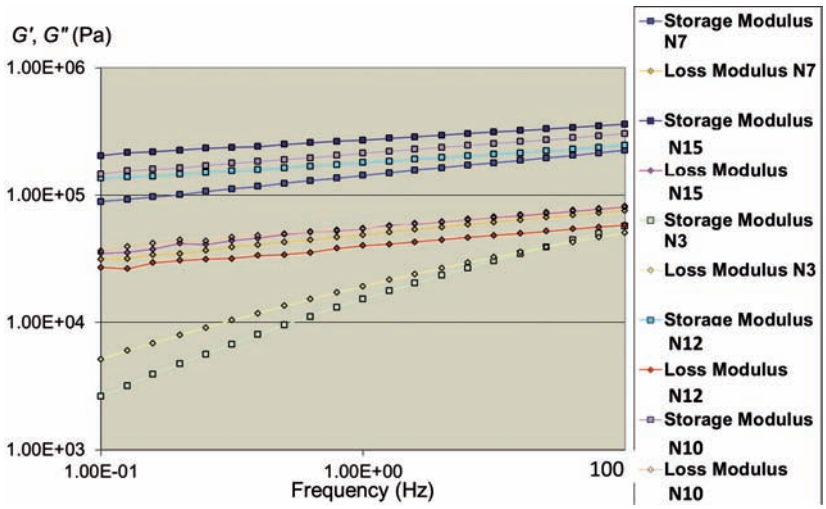

Figure 5. Elastic shear modulus (G') and viscous shear modulus (G'') as a function of frequency for samples in a previous study. The numbers 3, 7, 10, 12 and 15 represent the times taken for lamination using the same method as described in this study, for a hot-plate set temperature of 145°C in the PV laminator.

As reported in Hidalgo et al. [1], DSC experiments helped to establish that fixing the temperature at 100°C offered a good compromise. Dynamic experiments in isothermal conditions provide the values of the elastic and viscous (G' and G'') components of the complex shear modulus at different frequencies, as demonstrated in Fig. 5 for samples from previous work in which the set-point temperature for lamination was kept constant, and the lamination time was varied from 3 to 15 minutes. The value of G', when accurately known, can be directly related to a cross-linking density [4,5]. The accurate measurement of G', however, may be a delicate task. The approach taken here (and in Hidalgo et al. [1]) was to determine the ratio G''/G' of the viscous and elastic components of the complex shear modulus, alternatively known as tan δ. This method has been found to compensate for some of the errors introduced, for example through the geometry of the sample, which may lead to inaccurate values of G' [1]. Values of tan δ, at a given frequency, may thus be compared with one another, to obtain the relative degree of cross-linking of EVA samples. The values at 1Hz, for example, have been found to lead to systematic trends in EVA samples laminated for different times [1,6]. In the work reported in this paper, all samples are assumed to be, at least, fairly cross-linked, and the relative value of tan δ is expected to reflect the differences (however slight) in cross-linking degrees.

Solvent extraction (gel content method)

The solubility of EVA samples in good solvents depends strongly on their degree of cross-linking. For many years, solvent extraction methods have been used as quality control techniques by industrial polymer suppliers when there has been a need to determine the degree of cross-linking of EVA and other rubbery materials. Although various solvent extraction methods and operating conditions are used by EVA resin suppliers, as well as EVA PV film suppliers and PV module manufacturers, the gel content (or insoluble part) on a 0–100% scale is considered to be a useful specification in that it allows the comparison of samples having different degrees of cross-linking. In this study, the above-mentioned operating conditions (see 'Experimental conditions: materials and methods') were used to determine the gel content of the samples at three different set points for the lamination temperature.

"The solubility of EVA samples in good solvents depends strongly on their degree of cross-linking."

Cross-linking degrees from the different methods

Table 1 presents all the results for the different methods employed in this study. The gel content method, used as a reference by the PV industry and

Temperature set point (lamination)	%XL gel content method (toluene)	%XL M/F method (Netzsch)	%XL M/F method (TA Instruments)	%XL RE method (Netzsch)	%XL RE method (TA Instruments)	Rheology: tan δ @ 1Hz and 100°C
145°C	77	60	67	51	45	0.207
150°C	83	74	70	57	54	0.192
160°C	87	76	75	85	84	0.168

Table 1. Numerical values obtained for each of the three samples laminated at set-point temperatures of 145, 150 and 160°C, by using each of the four different methods discussed.

other polymer-related industries, yields a % gel content (insoluble fraction after solvent extraction), which is a direct weight percentage, and which is often considered to be an 'absolute' measurement of the cross-linking degree of a sample. It is important to note that this is not a measurement of the cross-linking density as defined in Flory [4], but it is believed to be related to it.

For both the M/F and RE DSC methods, Equations 2–6 allow the results to be expressed in a percentage scale. The percentage scale for these two DSC methods, however, is not comparable, in terms of absolute values, to the percentage scale of the gel content method: the %XL estimates yield relative values, therefore only allowing the comparison of samples from the same roll or grade of EVA film, with respect, for example, to different lamination conditions (time, temperature, pressure). In order to translate %XL values from the DSC methods into their equivalent % gel content values, a correlation analysis must be performed, preferably with a significant number of samples having different cross-linking degrees. It can be seen from Table 1 that all the methods reveal a consistent trend: the %XL estimates increase with set-point (lamination) temperatures, and the tan δ values decrease (more elastic, less viscous) as a function of these temperatures.

One of the trickiest questions when determining cross-linking degrees using any method is whether or not a given sample corresponds to a sufficiently cross-linked film. This question is of major importance and will be answered in terms of pass/fail criteria, as discussed in the next section.

Pass/fail criteria

A three-colour code has been adopted to account for empiric pass/fail criteria for each method. This code is indicated in Table 1 and has the following meaning:

- **Red:** insufficient cross-linking degree or level. It is risky to regard this level as satisfactory.
- **Orange:** the cross-linking degree may be sufficient. This level might be safe enough, but the method requires special attention, such as the user's skill and field experience, to determine if it can be used for production.
- **Green:** the cross-linking degree is good. This level is considered to be highly reliable.

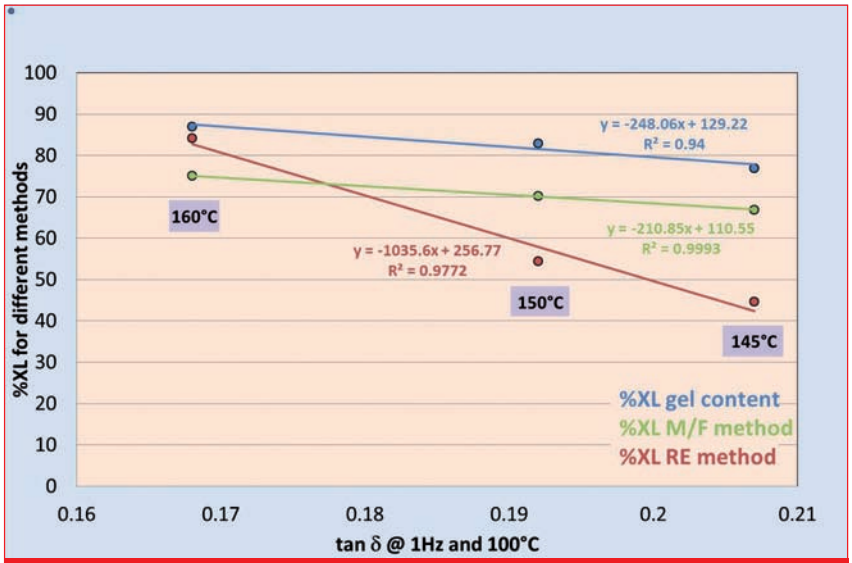

Figure 6. Correlation between %XL estimates from the gel content method and the two DSC methods (M/F and RE) with respect to the rheological parameter tan δ at 100°C and 1Hz.

The way these pass/fail criteria have been used in this study will now be described for each of the different methods.

For the *gel content method*, the current widely accepted pass/fail criterion states that suitable cross-linking is obtained if samples yield a gel content of higher than 75–80% [7] (the gel content minimum was only 65% in the early years of the use of EVA as a PV encapsulant in the 1980s [8]). For this study a gel content of below 75% is therefore regarded as insufficient (red), while a gel content of 80% or above is regarded as good (green); a value in between (75–79%) is considered to be probably sufficient (orange).

For the *melt/freeze method*, the pass/fail criteria depend on the EVA (supplier, grade) that is used. Thorough experimentation with the commercial STR Photocap 15420 P/UF used here has allowed us to consider values lower than 65% as insufficient (red), higher than 74% as good (green), and in between (65–74%) as probably acceptable, but with a careful follow-up necessary. These pass/fail criteria include close links with PV tests, such as damp-heat cycling.

For the *residual enthalpy method*, to the authors' knowledge there are no well-established pass/fail criteria, so those criteria described above for the gel content method were used.

Finally, for *rheological measurements*, carried out in the way explained in Hidalgo et al. [1] and Hidalgo and Medlege [6], and also used in this study, it was recently found that with at least four different grades of commercial EVA PV films, values above 0.25 may reflect insufficient cross-linking (red), values below 0.2 may be regarded as good (green), and values in between (0.25–0.2) could be sufficient (orange), but a certain amount of follow-up may be necessary.

Fig. 6 shows the correlation that exists between all %XL estimates (gel content, M/F and RE) and the rheological measurements. For DSC, the values from Table 1 corresponding to the measurements with the TA Instruments calorimeter have been used. As can be seen, there is a

good agreement with rheological measurements, with the M/F data yielding the best correlation.

Final comments and conclusions

The aim of this study was to show how different characterization techniques for determining relative cross-linking degrees of EVA encapsulant samples can be used in a specific example related to the optimization of a lamination process parameter (in this case the set point for the temperature of the heated plate of a vacuum laminator).

Besides the well-known gel content method and rheological measurements, which are used as references, two different DSC methods, currently being considered for the development of an international standard, were applied. These methods are easy to use, since only very small amounts (a few milligrams of unconditioned material with no particular geometrical form) of EVA film are required, and no particular sample preparation is necessary. The two DSC methods may be used either independently (two different short DSC programmes allow the gathering of the required data) or in a combined manner, with a single DSC programme generating the required data for both of them. The use of the two methods in combination results in a more reliable procedure for double-checking the outcome, since each has its advantages and drawbacks. The M/F method, for example, is considered to be more universally applicable (it can be used for 'old' as well as return-from-the-field samples, very low or very high cross-linking degrees, etc.), as it is based on a thermal transition of EVA; the RE method, on the other hand, is considered to be easier to use, as it is based on the analysis of a single parameter which can be readily obtained using standard DSC software.

> "The authors believe that it will be possible to realize a time-saving and reliability potential with the use of these new characterization methods."

The use of all these methods, including the gel content one, cannot be dissociated from the pass/fail criteria. The latter may be implemented in the follow-up process for one or more parameters, such as those obtained using the DSC methods (T_c, T_{onset}, *SF*, residual enthalpy), the rheological measurements (tan δ), or the solvent extraction data (% gel content). These pass/fail criteria may feature a more universal nature in the case of reference methods such as the gel content test or rheology, and may be more dependent on the type of EVA (formulation, base resin) in the case of the DSC methods. In this study, pass/fail criteria have been presented for one, widely used, grade of EVA encapsulant film. These criteria have been established to the best of the authors' knowledge for all the methods, based on their experience in working with commercial EVA films. These criteria may vary with different EVAs, especially in the case of the DSC methods, and should only be regarded as a guideline. It is expected that by applying the DSC methods, users will eventually become familiar with, and recognize the behaviour of, the EVA films that they employ, in such a way that they will ultimately be able to directly associate DSC plots with samples showing a sufficient or insufficient cross-linking degree, without even needing to calculate %XL estimates or refer to gel content characterizations. The authors believe that such a skill level can be acquired in a short time, and that it will be possible to realize a time-saving and reliability potential with the use of these new characterization methods.

Acknowledgments

The authors would like to thank the teams from the PV Module Laboratory (LMPV) at CEA-INES for the use of the PV laminator for the preparation of the samples, and a recently acquired rheometer for the rheological measurements, as well as the teams from Arkema-CRRA, for the use of the TA Instruments DSC calorimeter.

References

[1] Hidalgo, M. et al. 2011, "A new DSC method for the quality control of PV modules: Simple and quick determination of the degree of crosslinking of EVA encapsulants, and other properties", *Photovoltaics International*, 14th edn, pp. 130–140.

[2] Xia, Z., Cunningham, D.W. & Wohlgemuth, J.H. 2009, "A new method for measuring cross-link density in ethylene vinyl acetate-based encapsulant", *Photovoltaics International*, 5th edn, pp. 150–159.

[3] Miller, D.C. et al. 2013, "Examination of a standardized test for evaluating the degree of cure of EVA encapsulation", *Proc. Asian PVSEC* [in press].

[4] Flory, P.J. 1953, *Principles of Polymer Chemistry*. Ithaca, NY: Cornell University Press.

[5] Flory, P.J. & Erman, B. 1982, "Theory of elasticity of polymer networks. 3", *Macromolecules*, Vol. 15, pp. 800–806.

[6] Hidalgo, M. & Medlege, F. 2011, "Procédé de caractérisation d'un copolymère d'éthylène et d'acétate de vinyle", French Patent No. 1154579.

[7] Czanderna, A.W. & Pern, F.J. 1996, "Encapsulation of PV modules using ethylene vinyl acetate copolymer as a pottant: A critical review", *Solar Energy Mater. & Solar Cells*, Vol. 43, pp. 101–181.B.

[8] Cuddihy, E.F. et al. 1983, "Applications of ethylene vinyl acetate as an encapsulation material for terrestrial photovoltaic modules", JPL Publication 83-35, Pasadena, California, USA.

About the Authors

Manuel Hidalgo received his Ph.D. in macromolecular materials from Lyon I University. He is a senior research scientist at Arkema, and currently co-project leader at Sollia, a joint laboratory with the French Institute for Solar Energy (INES). He holds more than 50 patents and has published almost 30 papers in the polymer field.

Dominique Thil has been involved in R&D since 1990, mainly in the chemical process industry, and has two years' experience in the manufacturing of PV modules, including soldering and lamination. He currently works at the Sollia joint laboratory within INES.

Christophe Dugué is a process engineer with 22 years' experience in the field of PV energy at EDF ENR PWT (Photowatt). He is currently a co-project leader for the installation of a new production line of PV modules.

Enquiries

Dr. Manuel Hidalgo
Arkema
Sollia Laboratory at INES-LMPV
Savoie Technolac
50, avenue du Lac Léman – BP332
73377 Le Bourget du Lac Cedex
France

Tel: +33 (0) 4 79 60 14 53
+33 (0) 6 78 03 98 06
Email: Manuel.HIDALGO@cea.fr
manuel.hidalgo@arkema.com

Power Generation

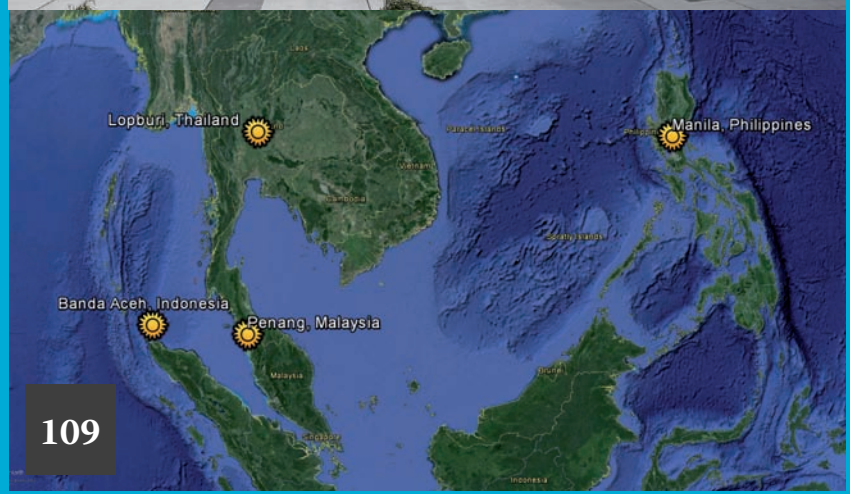

News

Obama sets 20% renewables target for US government by 2020

President Obama has set all US government agencies a 20% renewable energy generation target by 2020. Federal electricity use is expected to draw 7% from renewable sources for the fiscal year of 2013. The US government is the largest energy consumer in the country. The targets, which only apply to electricity consumption, will be phased in gradually. Agencies must draw not less than 10% of their electricity from renewables by 2015, 15% in 2016 and 2017, 17.5% in 2018 and 2019 and not less than 20% by 2020. Departments are urged do so by funding and installing their own generation through on- or off-site renewables. They can also purchasing power from third-party owned clean energy plants built at their request, by purchasing renewable power from the grid or by paying for renewable energy certificates. All power must be from renewable sources less than 10 years old. The target was mentioned in previous climate action speeches by the president but is now set in motion following a Presidential Memo.

Obama has set a 20% renewables goal for US government by 2020.

New markets

Solar joint venture in Turkey

Module and cell manufacturer Talesun has partnered with local energy firm Anadolu Enerji to develop and build solar farms in Turkey. The joint venture will also look at opportunities to leverage its base in Ankara for projects in neighbouring countries as well. The companies will arrange pre- and interim-finance through to construction before handing off projects to investors. Turkey currently has a very low base of installed solar projects with just 3MW connected at the start of 2013. Increased feed-in tariffs and streamlined application processes for projects up to 1MW have cleared the path for the country to make serious progress towards its 3GW solar target for 2023.

Talesun and Anadolu Energie have formed a solar joint venture in Turkey.

Qatar to use water reservoir rooftops for solar

Qatar will use the roofs of water reservoirs for solar energy generation Ahmed Nasser al-Nasser, technical affairs director of Kahramaa, Qatar's general electricity and Water Corporation, told the Solar Qatar Summit in November. Kahramaa is looking to utilize PV solar and other types of solar energy such as thermal and CSP. The rooftop initiative follows the Qatar government announcing an installation target of 200MW of PV in October. The Ministry of Energy and Industry has said the target is beginning its first phases with a pilot project of 5-10MW for water desalination in Duhail. The developments in solar energy in Qatar are part of the Qatar National Food Security Programme, established in 2008 for Qatar to be self-sufficient in food production, requiring sustainable domestic energy to support desalination. The solar announcements are also in line with Qatar's 'Green Qatar 2022' plan for hosting the FIFA world cup in 2022, and part of the Qatar National Vision 2030, also set up in 2008. Also this month Qatar Solar Technologies (QSTec) partnered with Qatar Electricity and Water Corporation (QWEC) to research solar energy possibilities in Qatar, signing an MoU as part of the Qatar National Vision 2030.

Brazilian state to host solar energy-only tender auction

The Brazilian state of Pernambuco was due to host Brazil's first solar-only energy tender auction on 20 December 2013 after *Photovoltaics International* went to press. According to the Brazilian state of Pernambuco's news blog, the state moved the intended auction forward two months from the previous date of 18 February 2014. The auction is part of the state government's sustainable PE programme (PE Sustentável).

The auction has been organised to promote awareness of solar energy and boost the solar market. The auction is to be coordinated by the executive secretary of energy for the department of water resources and energy, Eduardo Azevedo, who will consolidate demands and determine the amount of energy lots traded, organising buying and selling of energy.

Solar project national debuts

Uzbekistan gains development bank loan for first solar power plant

The Asian Development Bank (ADB) will help Uzbekistan to build a 100MW solar project, the country's first utility-scale solar power plant. ADB will lend US$110 million from its Asian development fund to the 'Samarkand Solar Power Project' in Samarkand. A further US$200 million of funding is to come from Uzbekistan's Fund for Reconstruction and Development, and Uzbekenergo, the governing body for supplying electricity in Uzbekistan. Uzbekenergo, which is responsible for half of central Asia's energy generation capacity, will manage the solar project.

The Samarkand project will take five years to develop and construct, with a completion date of 2019. The project is will be used to promote large-scale solar power in the country and tackle recent power shortages. It will also diversify Uzbekistan's energy mix which is currently heavily reliant on fossil fuels. The International Solar Energy Institute (ISEI), a training centre for solar technicians in East Africa, will be responsible for capacity building. Uzbekistan is aiming to be the region's solar energy hub and leader in solar technology. The ISEI is to help Uzbekistan in reaching this ambition.

Technology developments

TI offers first reconfigurable DC arc detect reference solution

Texas Instruments has introduced its answer to safeguarding high-power DC systems against potentially catastrophic arc faults. The industry's first fully programmable DC arc detect reference solution, the RD-195 makes it faster and easier to safeguard against damage. Electrical arc faults, predominantly due to faulty junction box components and/or design, have been known to cause PV module system fires. Now designers can program the RD-195 to optimise the balance between arc detection accuracy and false detection prevention to meet their system needs.

Brazil's Pernambuco state was due to host solar energy only tender auction.

IBM offers advanced power and weather modeling to tackle intermittence issues

IBM has introduced an advanced power and weather modeling technology that will help utilities increase the reliability of renewable energy resources. The solution combines weather prediction and analytics to accurately forecast the availability solar PV energy. The Hybrid Renewable Energy Forecasting" (HyRef) technology uses weather modeling capabilities, advanced cloud imaging technology and sky-facing cameras to track cloud movements, while sensors on the turbines monitor wind speed, temperature and direction.

Power generation policy

Japan PV demand to remain high despite FiT cuts

Trendforce research division EnergyTrend has issued a report claiming that PV demand is expected to remain strong in Japan for 2014 and 2015 in spite of rumoured feed-in tariff cuts. The company has reported "rumours" that the Japanese Ministry of Economy, Trade and Industry is considering cutting the feed-in tariff subsidy for PV downward to ¥34/kWh (US$0.33/kWh) in 2014 and to ¥30/kWh (US$0.29/kWh) in 2015. The company did not cite a source for the rumours, although it has been understood from the beginning of the feed-in tariff's implementation in July 2012 that a further managed degression is possible next year.

Berlin Energy generation attended by 16,000

An estimated 16,000 protestors attended a demonstration in Berlin on Saturday, aimed at 'saving' Germany's Energiewende

Berlin's energy protest was attended by 16,000.

renewable energy policy from possible attack by the incoming coalition government.

Demonstrators marched under the united slogan "Save Energy Revolution: The sun and wind instead of fracking, coal and nuclear" as they attempted to get across a message of increasing renewable energy capacity and energy efficiency to lawmakers. The event included a symbolic protest on the lawn of the Reichstag.

While some commentators were pleased that the coalition deal struck between Angela Merkel's union of Christian conservative parties and the centre-left Social Democratic Party (SPD) included 'bandwidth' targets for renewable energy generation, others felt the coalition deal would slow down the introduction of renewable energy capacity.

Survey reveals Australia loves solar but clean energy support reaches crossroads

The representative association for trading renewable energy certificates (RECs) Agents Association Household Solar in Australia has released the very positive results of a solar survey at the same time as a bill to abolish the Clean Energy Finance Corporation (CEFC) enters the

senate. The survey found that two million homes have solar but the love affair is at risk as government support wanes. On 13 November the CEFC Bill 2013 was introduced into parliament by the newly elected coalition government. If the abolition of the CEFC for financing renewable energy and energy efficiency schemes is passed, all of CEFC's funds will be transferred to the treasury.

Europe solar support reforms

Netherlands scraps distribution charge for solar installs

The Netherlands has removed a distribution fee for solar owners looking to put excess power back onto the grid. The national transmission operator, Netbeheer Nederland, said a connection fee for grid access would remain in place but from 1 January 2014, the distribution fee would not apply to solar installations. Netbeheer Nederland stressed that solar installations must have their own distinct connection and be registered separately.

German coalition sets self-consumption charge

The coalition deal struck between Angela Merkel's union of conservative parties and the centre-left SPD includes a surcharge on self-consumed electricity. While feed-in tariff (FiT) provisions will remain the same for PV generated electricity, the agreement, which still requires the approval of around 470,000 SPD members via a referendum in December, will mean that fees will have to be paid by off-grid consumers of self-generated electricity.

Spanish solar reforms could break EU laws

The proposed retroactive changes to solar support in Spain could be in breach of two EU directives, according to industry bodies. Spain is currently pushing through legislation that charges consumers who use solar power generated by their own panels.

The tariff has been set higher than the cost of standard electricity from the grid. The country is looking to claw back an estimated energy budget deficit of €26 billion (US$34 billion). But the proposed retroactive changes to solar support in Spain could be in breach of two EU directives, according to industry bodies.

EU PV Parity Project calls for more support of PV self consumption

A European Commission-financed project aimed at increasing PV penetration has concluded with a call for a new regulatory structure to support self-consumption of solar power in the EU. The final report of the PV Parity Project said PV policy needed to be readjusted to account for the growing use of solar power to save energy not just to generate investor returns. The PV Parity project, which winds up this month, has since 2011 been exploring PV competitiveness in 11 European countries and ways of supporting greater PV penetration.

EPIA: Time for utilities to embrace solar

Utility companies should embrace solar energy rather than trying to block it, the European Photovoltaic Industry Association (EPIA) has said.

The trade group has also called for governments to overturn damaging retroactive changes to support mechanisms for PV or risk their own credibility and their countries attractiveness to investors. A number EU of countries, including France, Spain, Greece, Belgium and Italy have adjusted support schemes or introduced new charges for solar energy installations.

In the US and now in Europe, some utility firms have campaigned for cuts to subsidies and the imposition of grid usage charges.

Product Reviews

AEG Power Solutions

AEG Power Solutions offers compact outdoor central inverters for harsh conditions

Product Outline: AEG Power Solutions (AEG PS) has introduced two new additons to its broad inverter line for the Americas market. The Protect PV.500 OD UL and Protect PV.630 OD UL are compact, high-efficiency central solar inverters. They are both UL-certified, and are designed for American utility-scale applications on ground installations in harsh environments. Also new, the TKS-P is a complete turnkey system based around the inverters, designed for utility-scale PV megawatt power plants.

Problem: With the majority of utility-scale PV power plants located in harsh environments around the globe, high uptime and reliable performance of central inverters are essential for long-term project performance.

Solution: A key feature of the broad Protect PV inverter line is a power stack with advanced measuring and control technology enabling DC input voltages of up to 1000VDC and peak efficiencies of 98.4%. The inverters support a wide operating temperature range of -4˚F to +122˚F, while their light weight (3.638 lbs) and small dimensions (87 x 89 x 36 in) make them easier to transport, install, and service. The turnkey solution TKS-P includes additional components such as transformers and medium-voltage switchgear, and is delivered to the installation site fully equipped and tested.

Applications: PV power plants in harsh environments.

Platform: The proprietary cooling system provides optimal air circulation within the inverter. The enclosure of double-walled aluminium with a stainless steel plinth can easily be mounted on concrete foundations.

Availability: Currently available.

DEGER

D100 tracking system from DEGER optimized for greater yield and lower-cost installation

Product Outline: DEGER has introduced a new generation of tracking systems that have numerous technical enhancements with a price level that is more than 20% lower than previously possible The first product in this new generation is the 'DEGERtracker D100' designed for greater yield and lower-cost installation.

Problem: Maximizing yield of a PV power plant while providing competitive levelized cost of electricity (LCOE) is becoming increasingly important in the lower subsidized and non-subsidized markets.

Solution: The DEGERtracker D100 is said to be faster and easier to assemble, providing for greater yield and lower costs than predecessor models. DEGER also simplified electrical installation with sensor technology and connecting cables preassembled, and cable routing and strain relief already prepared. Thus wiring inside of the systems becomes superfluous, and possible sources of error during installation are largely eliminated. This reduces both costs and installation times. The new, easily comprehended assembly instructions provide the installer with additional support. Field tests conducted by the Materials Testing Institute (MPA) at the University of Stuttgart verify the high performance of the new systems. With their additional safety margins they withstand loads that exceed the standard limits specified by the manufacturer by up to fifty percent.

Applications: Ground-mount, large-scale PV power plants.

Platform: The DEGERtracker D100 covers up to 70.6 square meters of module space and operates with all conventional modules. The rated output is between 8,000 and 12,000 watts peak (Wp), depending on the module type. One-piece support frames are also available as well as a detachable support frame that lowers freight charges.

Availability: Currently available.

Kipp & Zonen

Revised radiometer ventilation unit from Kipp & Zonen improves reliability and accuracy of weather measurements

Product Outline: Kipp & Zonen has introduced the CVF4, a new ventilation unit for its pyranometer and pyrgeometer range, used in commercial and utility-scale PV power plants to accurately monitor weather conditions.

Problem: Ventilation of radiometers is said to improve the reliability and accuracy of the measurement by reducing dust on the dome of the radiometer and removing the threat of dew, rain droplets and melting frost and snow, which would otherwise affect the measurement.

Solution: The CVF4 ventilation unit was developed using the latest flow simulation software and micro flow and temperature measurement devices to maximize the performance of radiometers. At the top of the pyranometer dome the flow is very high and it swirls to improve the air distribution over the dome. The position of the heaters and the new cover material ensures that only half the heating power is needed to melt frost and snow compared to older ventilation unit designs.

Applications: CVF 4 is designed to be used with Kipp & Zonen CMP 6, 11, 21, 22 and SMP11 pyranometers, the CGR 4 pyrgeometer and the CUV 5 total UV radiometer.

Platform: The cover of the ventilation unit can be removed without tools to check the radiometer desiccant. The improved access to the ventilation fan fitter and the radiometer, is said to make maintenance easier.

Availability: Currently available.

In-field performance of a polycrystalline versus a thin-film solar PV plant in Southeast Asia

Setta Verojporn & **Philip Napier-Moore**, Mott MacDonald, Bangkok, Thailand

ABSTRACT

This paper considers the relative technical and economic performance, for selected sites in Southeast Asia, of PV plants using crystalline and thin-film PV module technology. Technical performance estimates are based on a forensic analysis of in-field data for two grid-connected PV installations in Thailand using polycrystalline and thin-film PV modules. These two case studies help to validate the performance simulation approach for the other considered countries with similar environmental conditions. The case studies show that Mott MacDonald's yield analysis approach demonstrates acceptable accuracy for energy yield assessment in a grid-connected PV plant, at least under the observed environmental conditions, which are most relevant to Southeast Asia plants with polycrystalline and thin-film PV modules installed. The findings presented in this paper are relevant to project developers and investors who have an interest in selecting solar PV technologies for Southeast Asian regional conditions.

Introduction

With over 102GW of cumulative global solar energy installed capacity at the end of 2012, crystalline silicon (c-Si) technology currently holds (and has so far always held) the world's largest market share of installed capacity of all PV module technologies [1]. The global market share of c-Si technology production is anticipated to maintain its position of at least 80% until 2017; this is primarily driven by continued rapid growth in installed solar PV plant capacity in Asia, particularly China and Japan, together with the competitively low production costs of c-Si technologies. Thin-film technologies have come off second best with around 14% market share of global production capacity in 2012, and are expected to grow at a lower rate than polycrystalline technologies until 2017 [1].

Significant drops in c-Si module prices (with a wide range of PV module quality, however) in the past few years [2], and c-Si technology's generally higher efficiency under standard test conditions (STC) compared with thin-film technologies, are undoubtedly two of the key influences contributing to polycrystalline PV modules' current domination of the market. Nonetheless, thin-film PV modules are commonly known as the 'better-performing' (i.e. higher specific yield) PV module technology under high-temperature and low-irradiance conditions, which are the two main factors determining any PV module's in-field performance and therefore the performance of the PV plant in question. One in-field operating data analysis in particular has shown that some thin-film technologies perform significantly better than c-Si modules in hot and humid climatic conditions [3]. Given that the PV module is the most significant single driver of plant performance, developers must carefully select a PV module technology to suit the designated climatic conditions of a PV plant while optimizing land area, in order to maximize project profit. With the above in mind, to optimize the PV project performance and profit, a number of other factors also need to be considered, including other key equipment, plant design, capital expenditure by technology, and climatic conditions.

> "Developers must carefully select a PV module technology to suit the designated climatic conditions of a PV plant while optimizing land area, in order to maximize project profit."

A great deal of constructive comparison of these two technologies is publicly available based on laboratory testing, an understanding of PV module fabrication, and the market price. That said, a fair comparison of plant performance for these two technologies cannot easily be given: a number of PV module performance features and plant design issues that significantly affect the overall performance of the PV plant are not adequately characterized by the PV module data sheet and standard laboratory tests.

Building on available generic comparisons of these two technologies, this paper initially provides case studies using high-resolution in-field data from two existing plants in Thailand (using polycrystalline and tandem-junction thin-film PV modules respectively) to validate the performance-modelling approach adopted. This validated approach will finally be further applied to gain more insight into how these two technologies perform at other regional site locations with similar climatic conditions.

This paper shares experiences and makes recommendations based on the different criteria that can be used to make a decision between using polycrystalline or thin-film PV modules.

Validation of PV plant performance modelling from in-field data

Before the relative performance of crystalline and thin-film plants is modelled, this section presents a validation, using in-field operating data from two case-study plants in Thailand, of the performance simulation method employed.

In-field operating data are mainly useful for understanding the performance characteristics of a PV module in an outdoor environment rather than its durability, because of the short-term nature of such available data from most PV module suppliers. Ideally, in-field data would exist from outdoor installations at independent test facilities, with more extensive performance monitoring and diagnostic capability than is customary at power plants. Such independent test

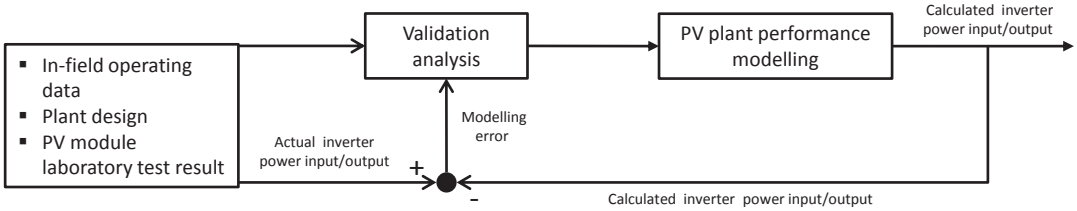

Figure 1. Methodology flow chart for PV plant performance-modelling validation.

Parameter	Unit	Resolution	Measuring device
Global horizontal irradiance	W/m^2	1 minute	Horizontal pyranometer
Global inclined irradiance	W/m^2	1 minute	Inclined pyranometer
Inverter input*	kW	1 minute	Inverter data logging device
Inverter output	kW	1 minute	Inverter data logging device
Ambient temperature	°C	1 minute	Ambient temperature sensor
Module temperature	°C	1 minute	Module temperature sensor

*Not available for Plant PC because of inadequate uncertainty level of the measurement device at the inverter

Table 1. Measured operating data for Plant PC and Plant TF.

facilities would usually have PV modules from a number of manufacturers, with these modules installed alongside each other for consistent comparison.

In cases where plant performance data are provided, in the authors' experience these have rarely been gathered and reported in accordance with recognized standards, so cannot always be taken as reliable and comparable without proper data quality checks. Another limitation of in-field data is that performance (and durability) evidence for one location with a given set of environmental conditions does not necessarily equate to similar performance at other locations.

This part of the paper focuses on a case study of seven days' available high-resolution in-field data, to gain more insight into the differences in PV module performance between polycrystalline and thin-film technologies, and to validate the adopted performance-modelling approach by the use of a combination of laboratory test data, plant design documentation and high-resolution in-field data from two existing plants (using polycrystalline and tandem-junction thin-film PV modules respectively).

The state-of-the-art software PVsyst (version 5.65) is widely considered an industry standard for solar PV plant performance simulation, and was used by Mott MacDonald in combination with other in-house models for this validation exercise. Since this analysis focuses on the difference in performance between two module technologies, the PV plant performance has been validated up to inverter level so that other unrelated losses (e.g. AC cable losses and transformer losses) can be disregarded. The simplified methodology flow chart of this analysis is illustrated in Fig. 1.

Overview of two utility-scale plants and their in-field data

The two projects in this analysis have been named 'Plant PC' and 'Plant TF' (for the purposes of confidentiality): they are in Thailand and use polycrystalline and thin-film PV modules respectively. The locations of the two solar PV plants analyzed are in northeastern and central Thailand, at latitudes between 14 and 15° N. A performance validation exercise for Plant PC specifically has been presented in a previous paper [4], which gives further details about the analytical approach adopted.

Table 1 shows the parameters that were used in this analysis over seven days. Mott MacDonald notes that not all of the provided parameters were used in this analysis, because of error, inconsistencies with other parameters, high uncertainties or inappropriate measurement principles, and are therefore not listed in Table 1. This operating data was quality-checked to help ensure that only reliable data were used for further analysis.

PV plant performance modelling up to inverter level

Losses were calculated on a one-minute basis using Mott MacDonald's in-house modelling, to give a more accurate prediction for the parameters dependent on actual irradiation and ambient temperature than would be possible using hourly time steps in PVsyst. In order to investigate the consistency of this approach, the in-house modelling used in this analysis is a higher-resolution reproduction of PVsyst modelling.

This analysis validates the PV plant performance modelling up to inverter input and inverter output levels for Plant PC and Plant TF respectively, given data availability. In this study the STC efficiency of the polycrystalline module used is 54% higher than that of the thin-film modules. A description of the approach and data used to estimate associated losses is given in Table 2.

Overall results

Based on the above validation approach, total calculated energy at the inverter level was compared with actual energy measured: the results are shown in Table 3. Total calculated energy delivered at the inverter input and output levels, after data screening, is 99.40% and 100.86% of total actual inverter energy measured at Plant PC and Plant TF respectively. These differences are within the margin of error of the metering equipment (±3% for AC inverter power measurements, ±2% daily for irradiance).

Taken together with the high correlation coefficient between calculated and actual inverter power input and output on a one-minute basis, the results of this analysis demonstrate good agreement between Mott MacDonald's in-house modelling and

Type of loss	Source	Approach
Spectral	PVsyst	Based on the sun angle profile computed in PVsyst, Mott MacDonald has calculated irradiance-weighted average air mass (AM) per kWh for the period observed close to the STC condition of AM1.5. Spectral losses have therefore been neglected in this analysis.
Shading	PVsyst	Hourly shading loss profile from PVsyst was applied in this 1-minute analysis over 7 days using a linear interpolation approach.
Angular	PVsyst and module supplier	Hourly angular loss profile of PV module observed from PVsyst was applied in this 1-minute analysis over the period observed using a linear interpolation approach.
Low-irradiance performance	Module supplier	The low-irradiance test data provided for the module supplier was used to calculate low-irradiance loss on a 1-minute basis. Expected degradation has also been taken into account in the PV module's efficiency in all irradiance conditions.
Temperature losses	PVsyst	Actual module temperatures are used together with the rated 'temperature coefficient of P_{max}' for the PV module. While this calculation of temperature loss is a simpler linear approach than that with PVsyst, there are, in this case, negligible differences in the result of this calculation step. PVsyst does not allow module temperatures to be directly input, but instead calculates cell temperature from ambient temperature and irradiance, which can result in errors. Given that operating data are available, Mott MacDonald's in-house simulation uses actual module temperature data and provides results that are more consistent with actual performance data than if the PVsyst approach were used.
Power tolerance	Module supplier	PV module flash test results for both plants have shown a positive average tolerance (gain).
Mismatch	Module supplier	Flash test results of the delivered PV modules used in the plant and string configuration data, together with Mott MacDonald's in-house analysis, were used to calculate average mismatch losses.
Ohmic, DC	Plant design	DC loss or I^2R loss has been calculated based on the given cable size and lengths from the modules to the inverters.
MPPT performance	Weather	Because of the clear-sky operating data received and the inverter characteristics, the MPPT (maximum power point tracking) performance loss has been considered negligible over this period, since the maximum power point of each array remains relatively stable.
AC/DC conversion performance*	Inverter supplier and PVsyst	AC/DC performance loss has been calculated from the inverter performance curve in the PVsyst library, corroborated against the supplier data sheet.
Dust	Module-cleaning schedule	In accordance with the module-cleaning schedule, the modules at both plants were cleaned immediately before the observation period. For Plant PC, dust/soiling loss was assumed to be negligible in this analysis. For Plant TF, the observation period was affected by significant soiling due to on-going construction at a nearby site. A nominal average soiling loss of 1.28% was determined from an additional analysis and was derived from calculated module power output at the STC condition.
Availability	Operating data	On the basis of the operating data, availability has been estimated at 100% over the observation period.

*Only used for Plant PC to validate the plant performance at inverter output level

Table 2. Treatment of losses at Plant PC and Plant TF in plant performance modelling.

actual plant performance for the specific losses considered under the observed environmental conditions for both plants.

"The results of this analysis demonstrate good agreement between Mott MacDonald's in-house modelling and actual plant performance for the specific losses considered."

Performance comparison of polycrystalline and thin-film technologies

On the basis of the validated PV plant performance modelling discussed above, this section compares the performance of polycrystalline and thin-film technologies at other regional site locations with similar climatic conditions. Since the two specific PV modules (polycrystalline and thin-film) from the validation analysis have been proved to show good agreement with actual outcomes, these two modules were also chosen for this comparison exercise.

Thailand, Malaysia, Indonesia and the Philippines were selected for this comparison exercise because of their potential PV market sector growth [5]. Each location in these countries was nominated by an area with a known high global horizontal irradiation (GHI) resource for the respective country, with reference to public domain data.

The four tropical locations chosen for the comparison are indicated in Fig. 2, with their respective annual GHIs and ambient temperatures shown in Table 4.

	Calculated energy compared with actual energy		Correlation coefficient
	measured at inverter input	measured at inverter output	
Plant PC	-	99.40%	99.49%
Plant TF	100.86%	-	99.93%

Table 3. Comparison of calculated and actual energy at inverter level for Plant PC and Plant TF.

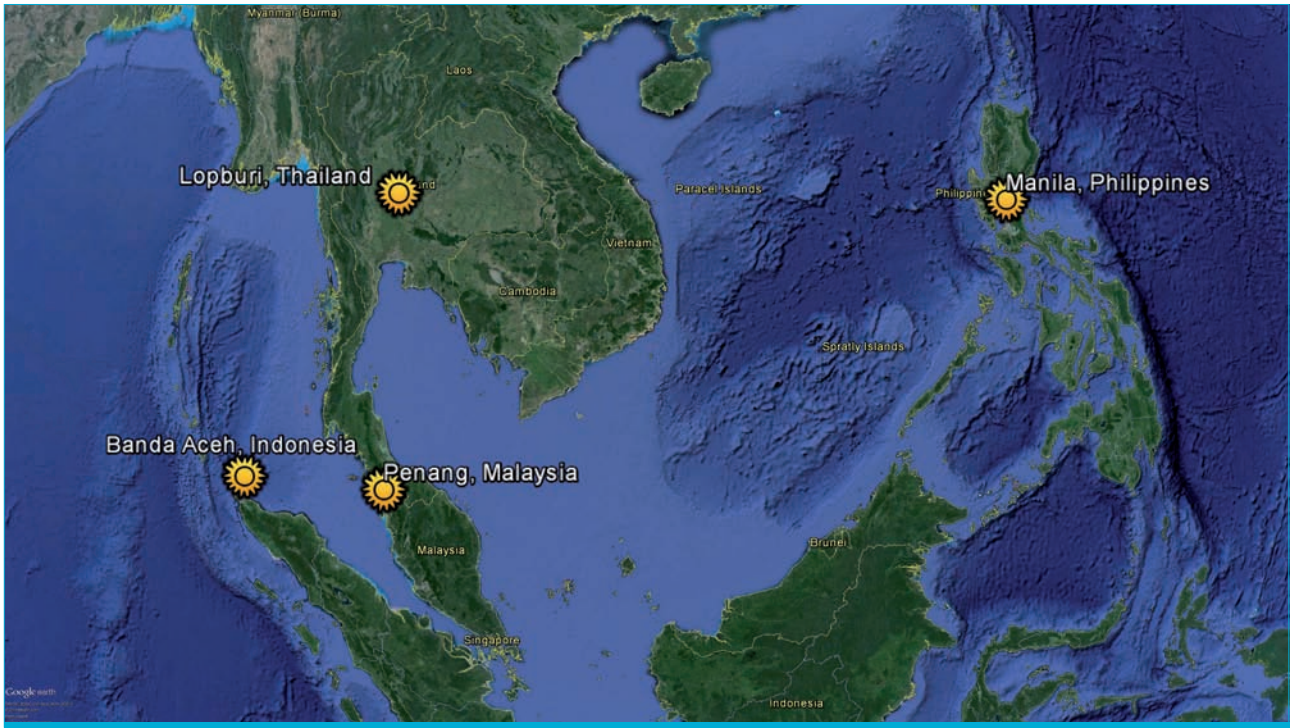

Source: Google Earth 2013

Figure 2. Selected locations for the comparison exercise.

	Lopburi, Thailand	Penang, Malaysia	Banda Aceh, Indonesia	Manila, Philippines
Annual GHI [kWh/m^2] (source)	1838 (SERL/DEDE satellite*)	1794 (Meteonorm v7)	1701 (Meteonorm v7)	1779 (Meteonorm v7)
Annual average ambient temperature [°C] (source)	28.36 (TMD**)	27.88 (Meteonorm v7)	27.65 (Meteonorm v7)	27.85 (Meteonorm v7)
PV module tilt angle [degrees]	15	5	5	14
Uplift	2.7%	0.3%	0.3%	1.4%
Global inclined irradiation [kWh/m^2]	1888	1799	1706	1804

* Solar Energy Research Laboratory satellite-based data, Silapakorn University, together with Department of Alternative Energy Development and Efficiency, Ministry of Energy, Thailand
** Thailand Meteorological Department

Table 4. Locations chosen for the comparison exercise.

For this comparison exercise, a fixed module tilt angle is proposed for each location to maximize the irradiation received by the fixed solar modules in each location. The fixed module tilt angles and annual irradiances in the inclined plane obtained from PVsyst are also shown in Table 4.

Simplifying PV performance modelling assumptions

In order to conduct a representative comparison of performance between the two technologies, a number of assumptions have been made for the inputs to the PV plant performance modelling for all cases, specifically:

- Similar PV module installation capacity.
- Similar AC:DC ratio of 1:1.22.
- Fixed ground-mounting structure.
- Similar shading losses (entailing a greater land area for the thin-film plant).
- In certain sections of DC cable installation, DC cable length for the thin-film plant is assumed to be twice that of the polycrystalline module PV plant because of the larger area required for thin-film module installation.
- Similar central inverter model, AC cable size and transformer model.
- Spectral losses are estimated on the basis of the sun angle computed in

PVsyst regardless of actual atmosphere and air pollution conditions.

- No soiling losses, plant outages or grid outages.
- Land is not limited.
- Durability of the plant to perform for a project lifetime of 25 years.

Based on the above assumptions, a typical conceptual plant design for each of the polycrystalline and thin-film plants was developed in order to estimate actual average expected performance in each location. For example, the string configuration was designed to be compatible with a selected central inverter for each PV module technology. The number of modules per string for polycrystalline plants is therefore not the same as for thin-film plants because of the different electrical characteristics of these two PV module technologies.

The power tolerance and mismatch losses in this exercise are based on the actual flash test results of the PV modules used at the two plants considered in the validation analysis together with their respective string configuration designs.

Degradation estimates of 1.00% and 1.55% in the first year of operation, which are derived from the PV module laboratory test results and in-field operational data, were applied for the polycrystalline and thin-film plants respectively. For subsequent years, a degradation rate of 0.50% was assumed and applied for both PV module technologies. The system degradation (inverter, transformer, cable, switchgear, etc.) was, however, assumed to be negligible over 25 years.

The validated PV plant performance modelling (combination of PVsyst and Mott MacDonald in-house modelling) has taken into account the above-mentioned concept design and assumptions together with two selected specific PV modules' specification and laboratory test data. The results of this comparison exercise are explained further in the next section.

Comparison results

PV performance modelling was carried out for each location (eight PV plants in total). Since the purpose of this analysis is to compare the PV plant performance of two PV module technologies, the normalized modelling results with key PV module losses of the thin-film plants (relative to the polycrystalline plant at each location) are given in Fig. 3.

Fig. 3 shows that over 25 years the thin-film plant can produce around 0.8–1.4% higher energy output than the polycrystalline plant in the selected four locations. This is mainly because of two key module performance factors: temperature losses and low irradiance losses. On the basis of the modelling results, the thin-film PV module's temperature and low irradiance losses are respectively around 50% and 40% lower than those of the polycrystalline PV module, for the two specific PV module models considered here. In general, for the two specific modules in this analysis, the thin-film plant will yield slightly higher performance and energy output than the polycrystalline plant over 25 years.

> "The thin-film PV module's temperature and low irradiance losses are respectively around 50% and 40% lower than those of the polycrystalline PV module."

In order to make a meaningful economic comparison, the levelized cost of energy (LCOE) was also calculated. The LCOE is a calculation of the cost of generating electricity at the point of connection to a load or electricity grid. It includes the initial capital and discount rate, as well as the costs of continuous operation and maintenance. Financial parameters based on the authors' experience of utility-scale solar PV plants in Thailand and the Southeast Asia region were assumed for the purpose of the LCOE calculation, as shown in Table 5.

An equivalent-capacity plant using thin-film PV modules normally requires a larger installed area than one using polycrystalline PV modules: the material and labour cost of thin-film plants for PV module installation, mounting structure, foundation, cabling and land preparation work is therefore higher. On the basis of the breakdown price of EPC work for a large sample of solar PV plants in Thailand, an 18% difference in the EPC price (excluding

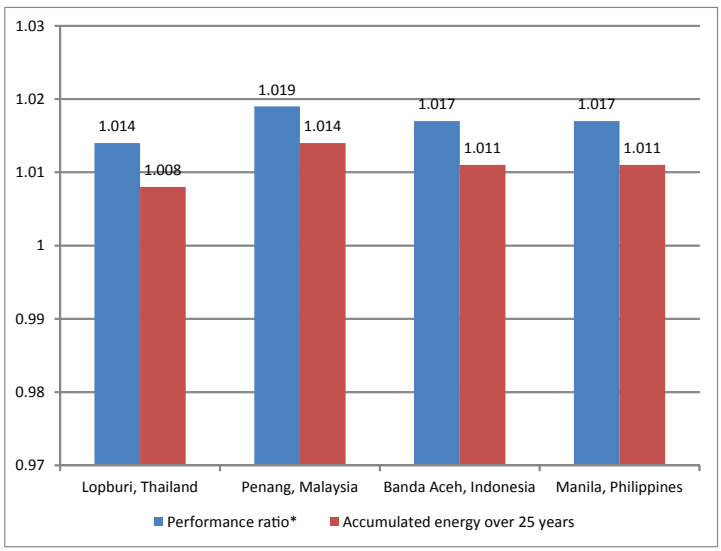

*Before degradation rate is taken into account

Figure 3. Normalized modelling results for thin-film plants (relative to the polycrystalline plants at each location).

Financial parameters	Polycrystalline plant	Thin-film plant
PV module price [US$/Wp]	0.60	0.42
EPC price excluding PV modules [US$/Wp]	1.00	1.18
Total EPC price [US$/Wp]	1.60	1.60
CAPEX* [US$/Wp]	2.00	2.00
OPEX [US$/Wp]	54.0	55.5
OPEX escalation rate	4%	4%
Discount rate	10%	10%

*Total EPC price is assumed to be 80% of CAPEX

Table 5. Financial parameter assumptions.

	Lopburi, Thailand	Penang, Malaysia	Banda Aceh, Indonesia	Manila, Philippines
Normalized LCOE	1.001	0.996	0.998	0.998

Table 6. Normalized LCOE for thin-film plants (relative to polycrystalline plants at each location).

PV modules) as a result of this additional work was estimated.

As shown in Table 5, the per unit CAPEX of the thin-film plant is assumed to be equal to that of the polycrystalline plant, because the lower module price is offset by the higher EPC price excluding PV modules. This results from the differences in PV module price and construction work for these two PV module technologies, on the basis of price benchmarks in Thailand and the Southeast Asia region; however, the analysis results will be highly sensitive to actual tender prices, as well as to land prices, which can be expected to vary over time and on a project-by-project basis. Given that land purchase or rental costs vary significantly within and between countries, it is not possible to take into account the relative impact of this in a meaningful way in this comparative analysis. For the study discussed in this paper, a simplifying assumption was therefore made that the solar project company owns adequate land for installing either of the PV module technologies without a land cost impact.

Based on the above assumptions, together with annual energy output results from PV performance modelling as given in Fig. 3, the normalized LCOE results for the thin-film plants (relative to the polycrystalline plant at each location) are given for a 25-year project lifetime in Table 6. The results in Table 6 show that the LCOE in US$/kWh of the thin-film plant differs by less than 1% from that of the polycrystalline plant, with a marginally higher cost for electricity generated by the thin-film plant at Lopburi, Thailand, but lower for other locations. The marginal difference in LCOE shown by this analysis is due to the assumed equivalent CAPEX of both plants, and to the higher OPEX of a thin-film plant (with a greater area to maintain) being offset by higher energy production over the project lifetime.

As mentioned earlier, this comparison exercise focused on two specific PV modules for which the performance had been validated and confirmed to be in line with actual in-field performance through the modelling employed. While the conclusions apply for one specific tandem-junction PV module, a number of other thin-film module technologies (a-Si-based single- or multiple-junction and cadmium telluride PV modules) have a similar performance profile and would lead to similar conclusions. The outcome of an approximately equivalent LCOE is nonetheless sensitive to the specification of the PV modules, along with the other given technical and financial assumptions.

Conclusion

For the two specific models of PV module considered, the results of the study discussed in this paper showed an approximately 1% higher plant yield for thin-film modules than for crystalline modules, under the prevailing climatic conditions of high temperature and diffuse irradiance. Based on the cost assumptions used, the lifetime levelized cost of electricity generation from a PV plant using thin-film was comparable to that of a plant using crystalline PV modules, for all four of the Southeast Asian locations considered.

> "This analysis suggests that thin-film PV module technology would generally be competitive in the Southeast Asia region in terms of technical and economic performance."

While polycrystalline PV modules maintain a dominant position in the current emerging solar market, this analysis suggests that thin-film PV module technology would generally be competitive in the Southeast Asia region in terms of technical and economic performance. To select the best-performing PV module technology for a particular site, however, Mott MacDonald continues to recommend a dedicated study employing, where feasible, a combination of available climatic conditions, PV module laboratory test results, and in-field data from previously operating plants.

References

[1] EPIA 2013, "Global market outlook for photovoltaics 2013–2017" [http://www.epia.org/fileadmin/user_upload/Publications/GMO_2013_-_Final_PDF.pdf].

[2] Fraunhofer ISE 2013, "Photovoltaic Report" [http://www.ise.fraunhofer.de/en/downloads-englisch/pdf-files-englisch/photovoltaics-report-slides.pdf].

[3] Shaari, S. et al. 2009, "The temperature dependence coefficients of amorphous silicon and crystalline photovoltaic modules using Malaysian field test investigation", *Am. J. Appl. Sci.*, Vol. 6, No. 4, pp. 586–593 [http://www.iie.org.mx/PNC/energia/Files/photovoltaics%201.pdf].

[4] Napier-Moore, P. & Verojporn, S. 2012, "Gaining confidence in PV module performance through laboratory testing, factory audit and analysis of in-field data", *Renewable Energy World Asia*, October.

[5] Ipsos Business Consulting 2012, "Meeting the energy challenge in Southeast Asia" [http://w3.ipsos.com/businessconsulting/insights/whitepaper/docs/A_Paper_on_Renewable_Energy_in_South_East_Asia_July_2012.pdf].

About the Authors

Setta Verojporn is an electrical and renewable energy engineer with particular experience in engineering for solar PV plants. He specializes in detailed energy-yield assessment and is familiar with solar-related technologies in Thailand and Southeast Asia. Setta has a B.Eng. in electrical engineering and an M.Sc. in renewable energy and the environment.

Philip Napier-Moore heads Mott MacDonald's Southeast Asia renewable power team, and has provided technical support to more than 1200MW of solar PV plants. He has published a range of related technical papers. Philip is a Chartered Energy Engineer and received his Master of Engineering degree from Oxford University.

Enquiries

Mott MacDonald
19th Floor Chamnan Phenjati Building
65/159 and 65/162 Rama 9 Road
Huay Kwang
Bangkok 10310
Thailand

Tel: +66 (0) 2643 8648 ext. 202
Fax: +66 (0) 2643 8638/39
Email: setta.verojporn@thaimottmac.com
Website: www.mottmac.com

A fast solution for the optimal location of the DC combiner box in a PV array

Jian Chen, **JianGuo Chen** & **XiChen Wang**, Jiangsu Sainty Machinery Import & Export Corp., Ltd., Nanjing, P.R. China

ABSTRACT

In PV power systems the choice of an appropriate location for the installation of the PV array box (or DC combiner box) is an important undertaking. It is essential that the box be placed so that the amount of DC cabling is minimized in order to not only save cable costs but also reduce voltage losses. This paper presents a fast solution to this problem, based on a mathematical model for the minisum location of the combiner according to the Manhattan metric between the PV array and the DC combiner box. The target function and its optimal solution (i.e. the most economical amount of cabling) for this particular model were obtained, and the optimality of the solution proved by contradiction. The application of this model is illustrated by means of two typical examples, involving an odd and an even number of strings in a PV array. The proposed model is efficient and easy to apply, and as such should be of interest to PV engineers and designers.

Introduction

One of the major classical problems in operations research is the decision of optimal location, a subject of great importance in applications such as production, logistics, life in general and even military affairs. The problem has recently attracted a lot of interest in the fields of operational research, engineering science and management, as well as among computer scientists: indeed, many new problems with a practical application background are emerging as the study of the location problem becomes more profound. Among all the location research fields, facility location is one of the most important – the range of facilities may include offices, warehouses, batch plants, maintenance facilities, labour force residences and fabrication shops. The approaches and solutions to the problem of facility location mainly rely on operational research, topology, management and so on [1,2].

The choice of PV array combiner box location discussed in this paper belongs to the facility location problem; this is an important element of the whole PV system design because the decision will significantly affect cost and efficiency, as well as other aspects of the PV system. Since the cost of DC cabling is often directly proportional to the distance between the PV strings and the combiner box, the location of the combiner should be sufficiently optimal to minimize both the cost of the DC cables and the power losses in the cables, which in turn will enhance system efficiency. This paper proposes a solution to the problem of combiner location using a mathematical optimization approach based on the Manhattan metric algorithm (distance between two facilities measured along the x and y axes) [1,2]. The mathematical model for the minisum location of the combiner is established by taking the real arbitrary PV system array into consideration, and then obtaining the target function and its optimal solution. Examples of the application of the technique are presented for both an odd and an even number of PV strings.

> "The location of the combiner should be sufficiently optimal to minimize both the cost of the DC cables and the power losses in the cables"

Single-combiner location model

There is generally one combiner box in a PV array, so this is a single-facility location problem. The strings of PV modules are connected in parallel to the combiner through DC cables running along the cable trays, which are often set vertically or aligned in parallel with each other.

Assumption

The objective area for the location is continuous, and any point is a candidate for the optimal solution. In addition, for the distance between two points, rectangular distance is used, which is approximately equal to the real distance.

Problem definition

Considering a coordinate system (x, y), there exists a boundary of a planar region with given coordinate values of a number of existing points. It is desired to find the point in the coordinate system that minimizes the sum of the rectangular distances to all the existing points.

Mathematical model

Suppose there are n strings located in the PV array. A coordinate system (x, y) is established (the coordinate origin is at any position) so that the coordinates of each positive or negative output node of the strings can be measured; there are therefore $2n$ points in total. Here, suppose that (x_i, y_i) are the coordinates of the point i, while the combiner box is located at (x_p, y_p). The rectilinear, or Manhattan, distance between the point (x_i, y_i) and the combiner (x_p, y_p) is then defined as $|x_p - x_i| + |y_p - y_i|$, for $i = 1, 2, \ldots 2n$. The objective function of the combiner location can then be expressed as

$$\text{Min } L(x_p, y_p) = \sum_{i=1}^{2n} |x_p - x_i| + |y_p - y_i| \quad (1)$$

where $x_p \in [x_1, x_{2n}]$ and $y_p \in [y_1, y_{2n}]$.

Solution of the objective function

It is clear that Equation 1 is multinomial, i.e. it comprises two independent components: the distances along the x and y axes, which add to the total distance independently of each other. Hence, the objective function can also be expressed as:

$$\text{Min } L(x_p, y_p) = \sum_{i=1}^{2n} |x_p - x_i| + \sum_{i=1}^{2n} |y_p - y_i| \quad (2)$$

that is

$$\begin{aligned} L(x_p, y_p) &= \left(|x_p - x_1| + \cdots + |x_p - x_{2n}|\right) \\ &\quad + \left(|y_p - y_1| + \cdots + |y_p - y_{2n}|\right) \\ &= L(x_p) + L(y_p) \end{aligned} \quad (3)$$

Hence,

$$L(x_p) = |x_p - x_1| + \cdots + |x_p - x_{2n}| \quad (4)$$

$$L(y_p) = |y_p - y_1| + \cdots + |y_p - y_{2n}| \quad (5)$$

where $x_p \in [x_1, x_{2n}]$ and $y_p \in [y_1, y_{2n}]$.

It is clear that this task can be solved separately for the x and y coordinates and then the results merged in order to obtain

the rectangle of minimum distance points. Let x_p^* and y_p^* denote the optimal answers for

$$\text{Min} \sum_{i=1}^{2n} |x_p - x_i| \text{ and Min } \sum_{i=1}^{2n} |y_p - y_i|$$

respectively. Thus, the coordinates of the optimal point of the final solution are (x_p^*, y_p^*). A detailed induction of the optimal solution of $L(x_p)$ is given next.

Suppose we have $2n$ points ordered by x, namely $x_1, x_2, \ldots x_{2n}$, as shown in Fig. 1. It should be noted that the values of each of these may or may not be the same, which mainly depends on the position of the positive or negative outputs of the PV strings.

From Fig. 1 it is clear that x_p^* may be any of the points $x_1, x_2, \ldots x_{2n}$, or may lie in the intervals $[x_1, x_2]$, $[x_2, x_3]$, ... $[x_{2n-1}, x_{2n}]$, so the solution has $(4n-1)$ possibilities in total. Consider x_p^* to be in the interval $[x_i, x_{i+1}]$; by removing the absolute values, Equation 4 may also be written as

$$\begin{aligned} L(x_p) &= (x_p - x_1) + (x_p - x_2) \cdots + (x_p - x_i) + (x_{i+1} - x_p) + \cdots + (x_{2n} - x_p) \\ &= i * x_p - (x_1 + \cdots + x_i) + [-(2n-i)] * x_p + (x_{i+1} + \cdots + x_{2n}) \\ &= (2i - 2n) * x_p + [(x_{i+1} + \cdots + x_{2n}) - (x_1 + \cdots + x_i)] \end{aligned} \quad (6)$$

Therefore, $L(x_p)$ in any segment $[x_i, x_{i+1}]$ is given by Equation 6, where $x_p \in [x_i, x_{i+1}]$, for $i = 1, 2, \ldots 2n-1$. It is evident that Equation 6 is a piecewise function over the entire segment $[x_1, x_{2n}]$.

Similarly, $L(y_p)$ in any interval $[y_i, y_{i+1}]$ can be written as

$$L(y_p) = (2i - 2n) * y_p + [(y_{i+1} + \cdots + y_{2n}) - (y_1 + \cdots + y_i)] \quad (7)$$

where $y_p \in [y_i, y_{i+1}]$, for $i = 1, 2, \ldots 2n-1$. It is also easy to see that Equation 7 is a piecewise linear function over the entire interval $[y_1, y_{2n}]$.

As can be seen from Equation 6, $L(x_p)$ is a linear function of x_p: when $i > n$, the slope of the piecewise function is positive in any interval, whereas when $i < n$, the slope is negative. When $(2i - 2n)$ is equal to zero, the slope of the piecewise function is zero. According to the properties of a monotonic function, over the entire interval $[x_1, x_{2n}]$ the value of Min $L(x_p)$ is equal to $L(x_p)|_{i=n}$, i.e.

$$\begin{aligned} L(x_p)\big|_{i=n} &= \left[(x_{i+1} + \cdots + x_{2n}) - (x_1 + \cdots + x_i)\right]\big|_{i=n} \\ &= (x_{n+1} + \cdots + x_{2n}) - (x_1 + \cdots + x_n) \end{aligned} \quad (8)$$

so the resulting optimal solution x_p^* lies in the interval $[x_n, x_{n+1}]$.

Similarly, the optimal solution of Min $L(y_p)$ is $[y_n, y_{n+1}]$. Hence, the optimal solution of Min $L(x_p, y_p)$ is

$$\left\{(x_p, y_p) \middle| x_p = [x_n, x_{n+1}], y_p = [y_n, y_{n+1}]\right\} \quad (9)$$

> "The optimal solution x_p^* lies in the interval $[x_n, x_{n+1}]$."

Equation 9 is a fundamental solution of the functions in Equations 6 and 7. In particular, the values of x_n and x_{n+1} may or may not be the same (the same applies to y_n and y_{n+1}), depending on the numbers and positions of the PV strings, so the global optimal solution of the combiner location problem can be divided into the following four cases:

Case A: $[x_n, y_n]$ or $[x_{n+1}, y_{n+1}]$, where $x_n = x_{n+1}$, $y_n = y_{n+1}$

Case B: $\{(x_p, y_p) | x_p = x_n, y_p = [y_n, y_{n+1}]\}$, where $x_n = x_{n+1}$, $y_n \neq y_{n+1}$

Case C: $\{(x_p, y_p) | x_p = [x_n, x_{n+1}], y_p = y_n\}$, where $x_n \neq x_{n+1}$, $y_n = y_{n+1}$

Case D: $\{(x_p, y_p) | x_p = [x_n, x_{n+1}], y_p = [y_n, y_{n+1}]\}$, where $x_n \neq x_{n+1}$, $y_n \neq y_{n+1}$

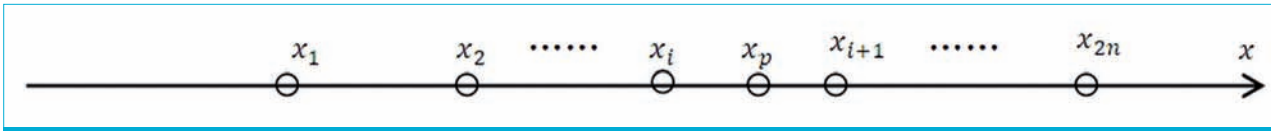

Figure 1. $2n$ points ordered by x on a line.

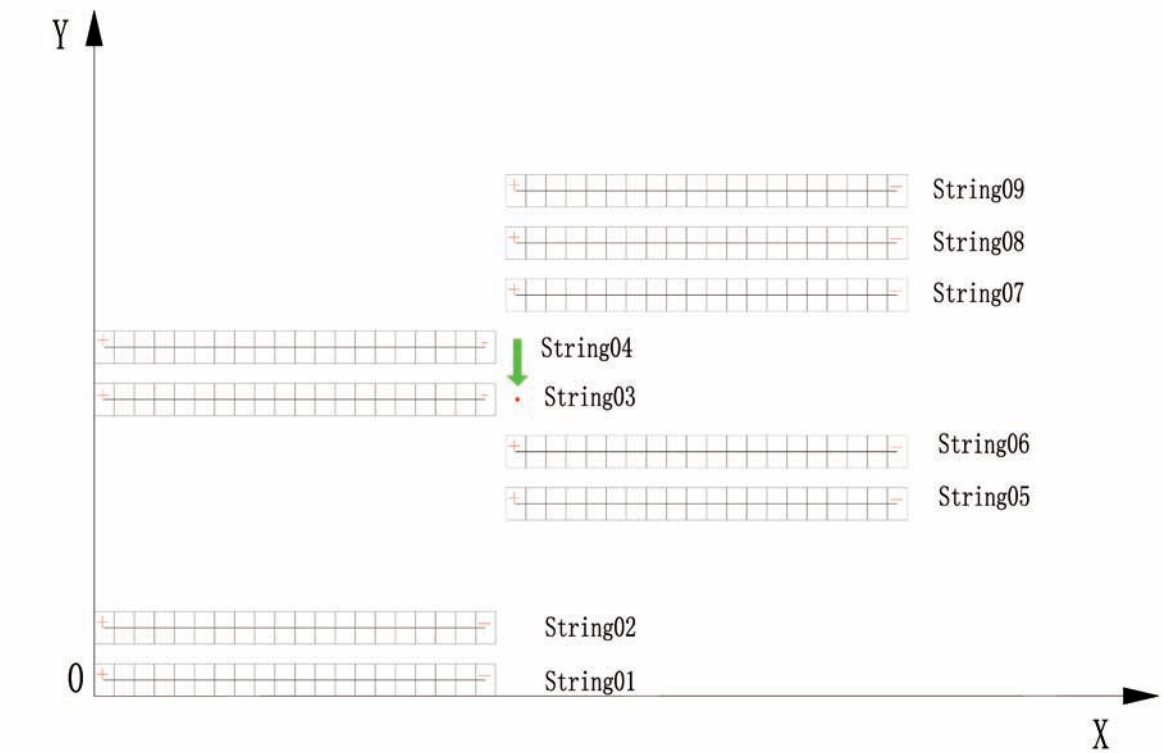

Figure 2. Case B: Optimal location of the combiner for an odd number of PV strings.

As seen above, case A represents a single point, and cases B and C denote a union of a whole segment. Case D, on the other hand, denotes a rectangular region, which means that more than one point may exist for the solution.

Verification of the optimal solution

The proof that $[x_n, x_{n+1}]$ is the optimal solution of Min $L(x_p)$ will be established by contraposition. Suppose the optimal solution lies in the interval $[x_m, x_{m+1}]$, for $i = m$ and where $m < n$ or $m > n$, so that $x_m \geq x_n$ or $x_m \leq x_n$. Thus, $L(x_p)|_{i=n} - L(x_p)|_{i=m} > 0$, where $L(x_p)|_{i=m} = (2m - 2n) * x_p + [(x_{m+1} + \ldots + x_{2n}) - (x_1 + \ldots + x_m)]$.

Proof

$$
\begin{aligned}
L(x_p)|_{i=n} - L(x_p)|_{i=m} &= (x_{n+1} + \cdots + x_{2n}) \\
&\quad - (x_1 + \cdots x_m + x_{m+1} + \cdots x_n) - (2m - 2n) * x_p \\
&\quad - [(x_{m+1} + \cdots + x_{2n}) - (x_1 + \cdots + x_m)] \\
&= (x_{n+1} + \cdots + x_{2n}) - (x_{m+1} + \cdots x_n) + 2(n - m) * x_p \\
&\quad - (x_{m+1} + \cdots + x_n) - (x_{n+1} + \cdots + x_{2n}) \\
&= 2(n - m) * x_p - 2(x_{m+1} + \cdots + x_n) \qquad (10)
\end{aligned}
$$

where $x_p \in [x_m, x_{m+1}]$.

- When n < m, $L(x_p)|_{i=n} - L(x_p)|_{i=m} < 0$, so $L(x_p)|_{i=n} < L(x_p)|_{i=m}$ (11)
- When n > m, $L(x_p)|_{i=n} - L(x_p)|_{i=m} = 2[(n - m)\, x_p - (x_{m+1} + \ldots + x_n)]$ (12)

Since $x_p \in [x_m, x_{m+1}]$, this means $x_m \leq x_p \leq x_{m+1} \leq x_{m+2} \ldots \leq x_n$. From Equations 11 and 12, $L(x_p)|_{i=n} - L(x_p)|_{i=m} \leq 0$, which is a contradiction. Thus, when $i = n$, it is proved that $[x_n, x_{n+1}]$ is the optimal solution of Min $L(x_p)$. Similarly, it can be proved that when $i = n$, then $[y_n, y_{n+1}]$ is the optimal solution of Min $L(y_p)$.

Analysis of actual cases

From a practical point of view, the number of PV strings may be odd or even, or their arrangement may be irregular. Given the values of the located points in a PV array, it is a simple task to obtain the optimal location for the combiner on the basis of the conclusion of the previous section. Two examples corresponding to the cases A and B discussed earlier will be analyzed.

Example 1: case A

Consider nine strings in a PV array and eighteen given points whose locations are as shown in Fig. 2. The numerical values of the coordinates are shown in Table 1. The origin of the coordinate system is the left corner of string number one. The coordinate value of the output of each string, in order along the x and y axes, is shown in Table 2.

According to the values provided in Tables 1 and 2, the resulting optimal solution of the combiner location problem is the point where $x_p^* \in [x_9, x_{10}]$ and $y_p^* \in [y_9, y_{10}]$. However, $x_9 = x_{10}$ and $y_9 = y_{10}$, so it follows that the optimal solution is just the point [20.5, 14.789], as shown by the red dot in Fig. 2.

Example 2: case B

Now consider ten strings in a PV array and twenty given points whose locations are as shown in Fig. 3. The numerical values of the coordinates are presented in Tables 3 and 4.

The optimal location of the combiner is the point satisfying $x_p^* \in [x_{10}, x_{11}]$ and $y_p^* \in [y_{10}, y_{11}]$, where $x_{10} = x_{11}$ and $y_{10} \neq y_{11}$. The optimal solution is therefore a segment defined by $x_p^* = 20.5$ and $y_p^* \in [14.789, 17.389]$: this is the segment between the negative outputs of the third and fourth strings of the PV array, as shown by the red line in Fig. 3.

> "The solution of the location problem can be quickly determined manually."

Conclusion

This paper has described a technique for determining the optimum location of the combiner by using a mathematical optimization function based on the Manhattan metric algorithm. The objectives of the optimization problem were to minimize both the investment in overall material cost and the system voltage losses in the cables. It was shown that the Manhattan-based optimal solution of the combiner location problem can be drawn from a finite set of candidate points (positive or negative outputs of PV strings), all of which are easy to determine. The technique was illustrated by means of two examples.

From a practical point of view, although the solution of the location problem presented in this paper cannot be obtained using computer software, it can be quickly determined manually. Moreover, the optimization model can be implemented for any size of PV array. However, if the resulting optimal location for the installation of the combiner is not feasible, the next best option is to choose the most practical placement closest to the optimal position.

String number	Coordinate of positive output of string		Coordinate of negative output of string	
	X+ [m]	Y+ [m]	X- [m]	Y- [m]
1	0.492	0.808	19.992	0.808
2	0.492	3.408	19.992	3.408
3	0.492	14.789	19.992	14.789
4	0.492	17.389	19.992	17.389
5	20.5	9.589	40.492	9.589
6	20.5	12.189	40.492	12.189
7	20.5	19.989	40.492	19.989
8	20.5	22.589	40.492	22.589
9	20.5	25.189	40.492	25.189

Table 1. Case A: Coordinate value of the output of each string.

Number	x_i [m]	y_i [m]	Number	x_i [m]	y_i [m]
1	0.492	0.808	10	20.5	14.789
2	0.492	0.808	11	20.5	17.389
3	0.492	3.408	12	20.5	17.389
4	0.492	3.408	13	20.5	19.989
5	19.992	9.589	14	40.492	19.989
6	19.992	9.589	15	40.492	22.589
7	19.992	12.189	16	40.492	22.589
8	19.992	12.189	17	40.492	25.189
9	20.5	14.789	18	40.492	25.189

Table 2. Case A: Coordinate value of the output of each string, in order along the x and y axes.

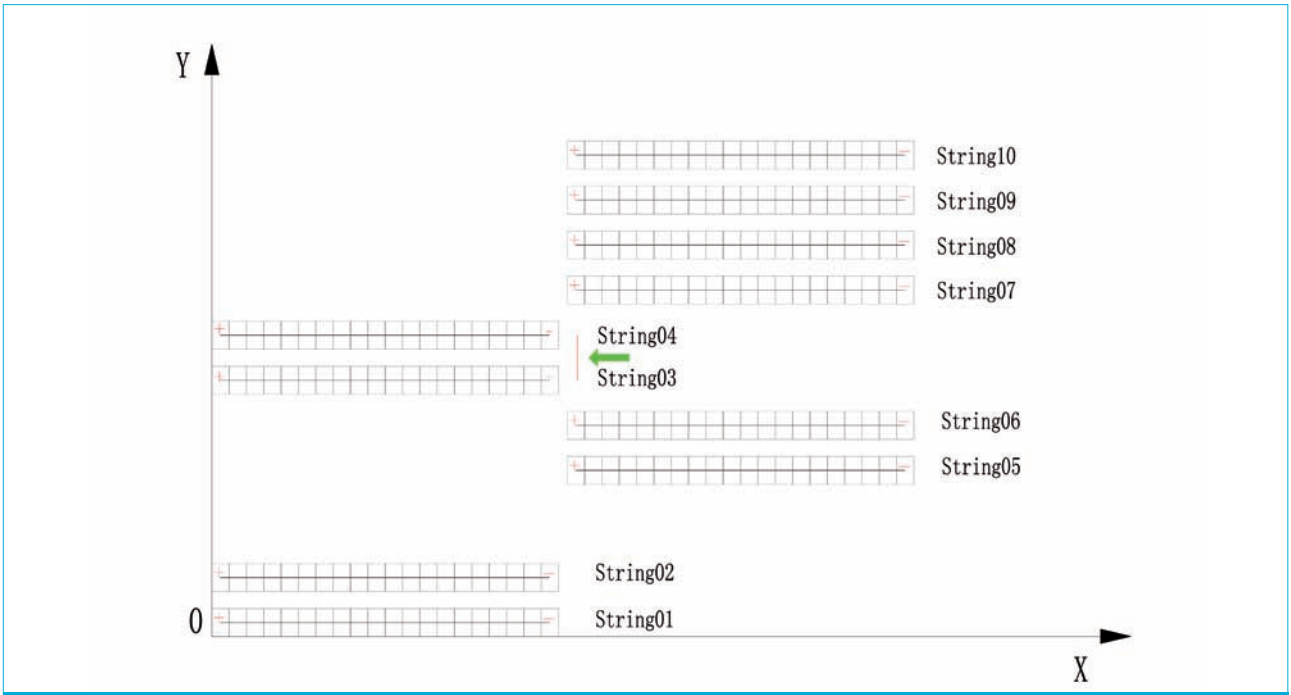

Figure 3. Optimal location of the combiner for an even number of PV strings.

String number	Coordinate of positive output of string		Coordinate of negative output of string	
	X+ [m]	Y+ [m]	X- [m]	Y- [m]
1	0.492	0.808	19.992	0.808
2	0.492	3.408	19.992	3.408
3	0.492	14.789	19.992	14.789
4	0.492	17.389	19.992	17.389
5	20.5	9.589	40.492	9.589
6	20.5	12.189	40.492	12.189
7	20.5	19.989	40.492	19.989
8	20.5	22.589	40.492	22.589
9	20.5	25.189	40.492	25.189
10	20.5	22.789	40.492	22.789

Table 3. Case B: Coordinate value of the output of each string.

Number	x_i [m]	y_i [m]	Number	x_i [m]	y_i [m]
1	0.492	0.808	11	20.5	17.389
2	0.492	0.808	12	20.5	17.389
3	0.492	3.408	13	20.5	19.989
4	0.492	3.408	14	20.5	19.989
5	19.992	9.589	15	40.492	22.589
6	19.992	9.589	16	40.492	22.589
7	19.992	12.189	17	40.492	25.189
8	19.992	12.189	18	40.492	25.189
9	20.5	14.789	19	40.492	27.789
10	20.5	14.789	20	40.492	27.789

Table 4. Case B: Coordinate value of the output of each string, in order along the x and y axes.

References

[1] Askin, R.G. & Standridge, C.R. 1993, *Modeling and Analysis of Manufacturing Systems*. New York: Wiley.

[2] Francis, R.L. & White, J.A. 1974, *Facility Layout and Location: An Analytical Approach*, 1st edn. Englewood Cliffs, NJ: Prentice-Hall.

About the Authors

Jian Chen received his bachelor's degree in mechatronics from Nanjing University of Aeronautics and Astronautics (NUAA) in 1996. He spent ten years at the Philips Centre of Research and Development, and also worked for ET Solar and Tianwei-Yingli Solar for seven years. He specializes in module and system design.

JianGuo Chen received an M.S. degree from Southeast University, Jiangsu, China, in 2009. He is currently working as a PV engineer, and his main research interests include modules, array configuration and system design in the field of PV.

XiChen Wang received her M.A.Sc. degree in mechanical engineering from the University of Windsor, Canada, in 2011. Since graduation, she has been working on PV system design and related research.

Enquiries

Jiangsu Sainty Machinery Import & Export Corp., Ltd.
Photovoltaic Division, Building C
21 Ruanjian Avenue, 210012 Nanjing
P.R. China

Photovoltaics International

Advertisers & Web Index

ADVERTISER	WEB ADDRESS	PAGE NO.
BTU International	www.btu.com	37
Ceradyne, Inc., a 3M company	www.ceradyneviox.com	19
Kipp & Zonen BV	www.kippzonen.com	107
Merck KGaA	www.merck-performance-materials.com	62
NovoPolymers	www.novopolymers.com	91
PV CYCLE aisbl	www.pvcycle.org	33
Q-Cells	www.q-cells.com	IFC
Rofin Baasel GmbH	www.rofin.com/solar	41
Spire Corporation	www.spiresolar.com	9
Technic	www.technic.com	25
Von Ardenne GmbH	www.vonardenne.biz	71

To advertise within Photovoltaics International, please contact the sales department: Tel +44 (0) 20 7871 0122

Solar PV in 2013: More diversification than consolidation, Finlay Colville

The PV industry is flying high but what business models will work in the future?

Source: Solar Impulse/Revillard/Rezo.ch

Benchmarking companies in the solar PV industry used to be straightforward. Some companies made key materials (polysilicon, wafers, cells, modules or thin-film panels); others bought and sold these locally or through the value chain. Then project developers and installers built the PV systems. Customers typically released cash up-front, owned the systems outright and could then sit back and enjoy a revenue stream linked to a government incentive.

It may sound a bit like a history lesson, but this was the solar PV industry until just a few years ago: one of several phases in going from megawatt to gigawatt. Doing benchmarking then was simple.

But the shift from a few gigawatts annually to 35GW-plus in 2013, having module pricing in the US$0.60-0.70/watt range and seeing installed system pricing fall to US$2-3/W, changed this legacy model overnight. Anyone sitting pretty before had to change.

Very few active in the industry today have a strategic roadmap that bears any great resemblance to the ones pitched to investors a few years ago. Those that clung on to module pricing's dip below the dollar per watt as being a temporary blip were finished. Installers that were contingent on local policies being maintained indefinitely were required to change business models, or get out of PV.

And new business models came on to the scene. During 2013, a wide range of short-term and long-term strategies have been unleashed on the solar PV industry. In many cases, companies previously in direct competition at one stage in the PV value-chain are barely coming across one another; rather, existing in niche application or geographic based served addressable markets. (It is worth noting as the year-end top-10 charts are counted down.)

The rate at which certain markets have grown quickly (and barriers have been placed on other markets) has been one reason for this shift. Having domestic supply or brand in a rapidly growing market definitely provides a benefit, so long as business models can adapt. Being politically connected only adds to this.

The question of whether to manufacture or not is also more visible on the radar. Indeed, in this respect, the buzzword is flexibility and having the buying power to control supply through advantageous OEM deals. Choosing to land the problem of profitable midstream wafer or cell supply on a capacity-heavy lower tier manufacturer that lacks brand or global marketing prowess is simply sound business practice, nothing else.

The opportunity exists because many Asian producers wrongly assumed that having capacity and making product available represented a sustainable working model. Shipping crates to Europe and passing the point-of-sale responsibility to distributors only had a finite shelf time. Today, the market opportunity here is rapidly dwindling.

In a nutshell, there are now many different business models that are viable across different PV regions or application segments, where you can simply guarantee what the customer (be it a homeowner, a project developer or a utility) needs to fit their budget and on their timelines.

Only a few Asian firms (with patient and well-capitalised parent-companies or majority shareholders) can bypass the need for dynamic and flexible supply and sales strategies in the PV industry over the next 12 months. Having a long-term five to 10-year strategy is a luxury not available to the masses.

Therefore, while at the macro level, talk of global grid parity and learning curves makes for good reading, the reality is an industry that has never been more fragmented in terms of supply and downstream business models, with many companies now seeking to play on both sides of the fence.

2014 is likely to see more of the same. Indeed, some are now looking at the PV industry with a blank sheet of paper, no liabilities, and free to create a new business model that is different from existing market leaders. Whether these can co-exist, offer better value to the customer, or are destined to fail before they start will only become clear over the next 12-18 months.

Whether the PV industry follows any trends seen in legacy industries (consumer electronics, telecoms, semiconductor, etc.) is also too early to call. But sitting back and waiting to see some orderly consolidation of me-too companies would appear to be rather naïve. The rollercoaster ride of the PV industry would appear to have more ups and downs ahead, before it emerges with a handful of global leaders with clearly defined business models that makes the simple task of benchmarking once more a valid exercise.

This is an edited version of a blog that originally appeared on PV-Tech.org

Finlay Colville is vice president of NPD Solarbuzz.

SOLAR ENERGY EVENTS

SOLAR ENERGY UK ROADSHOW

SOLAR ENERGY UK ROADSHOWS 2014

3 - 13 February 2014, various locations across the UK

With key challenges facing the industry, Solar Media's upcoming series of roadshows will demonstrate how the solar industry can take advantage of the policy stability and renewed governmental ambition by meeting the challenge of cutting costs and boosting profits.

http://ukroadshow.solarenergyevents.com

SOLAR & OFF-GRID RENEWABLES AFRICA

SOLAR AND OFF-GRID RENEWABLES AFRICA 2014

4 – 5 March 2014, Nairobi, Kenya

Solar and Off-Grid Renewables Africa aims to support and accelerate the deployment of solar and off-grid renewable energy in Africa, and break down the barriers to development - financial, political, technological - by bringing together key stakeholders, including investors, policy makers, developers, energy companies, financiers, NGOs, manufacturers and suppliers.

http://africa.solarenergyevents.com

SOLAR ENERGY UK

SOLAR ENERGY UK 2014

14 – 16 October 2014, The NEC, Birmingham, UK

Solar Media's most successful event to date, Solar Energy UK 2013 saw 2,404 unique visitors from 42 countries descend upon the NEC, Birmingham. The exhibition featured 173 exhibitors, two seminar areas and 88 high profile speakers. Solar Energy UK will be returning in October 2014 with demonstrations and talks on the Practical PV feature area for installers and Large Scale Solar feature area for developers and landowners. Registrations will open late June.

http://uk.solarenergyevents.com

STAY UP-TO-DATE: SOLARENERGYEVENTS.COM

EU PVSEC 2014

29th European Photovoltaic Solar Energy Conference and Exhibition

The most inspiring Platform for the global PV Solar Sector

RAI Convention & Exhibition Centre
Amsterdam, The Netherlands

Conference 22 - 26 September 2014
Exhibition 23 - 25 September 2014

www.photovoltaic-conference.com
www.photovoltaic-exhibition.com